Dietary amino acids and their contribution to *de novo* lipogenesis

Evelina Charidemou

Queens' College

University of Cambridge

November 2018

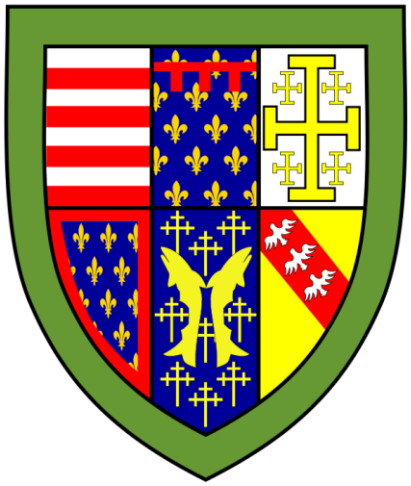

This dissertation is submitted for the degree of Doctor of Philosophy

Declarations

This dissertation is the result of my own work and includes nothing which is the outcome of work done in collaboration except as declared in the Preface and specified in the text. It is not substantially the same as any that I have submitted, or, is being concurrently submitted for a degree or diploma or other qualification at the University of Cambridge or any other University or similar institution except as declared in the Preface and specified in the text. I further state that no substantial part of my dissertation has already been submitted, or, is being concurrently submitted for any such degree, diploma or other qualification at the University of Cambridge or any other University or similar institution except as declared in the Preface and specified in the text. It does not exceed the prescribed word limit.

Abstract

Dietary amino acids and their contribution to *de novo* lipogenesis

This dissertation is submitted for the degree of Doctor of Philosophy

Evelina Charidemou

Queens' College

The alarming increase in the incidence of the metabolic syndrome is the result of the nutrition transition featuring dietary patterns high in sugars, particularly liquid carbohydrates in the form of sugary beverages, fat, and protein from red meat. The aim of this thesis was to investigate the effect of changing the solid/liquid ratio of meals on gastric emptying as well as the effect of changing meal compositions on lipid metabolism.

A 5-way crossover human study demonstrated that liquid carbohydrate was the main determinant of gastric emptying rate compared to macronutrient composition and it delayed gastric emptying of the solid fraction. In this study, the energy content of the liquid portion was not sufficient to induce *de novo* lipogenesis, however, the high protein meal, rich in glutamate increased *de novo* lipogenesis-associated triacylglycerides in plasma and liver-derived very low-density lipoprotein particles in samples from human subjects.

The underlying mechanism behind this increase in lipogenesis by dietary amino acids was investigated *in vitro*. In hepatocytes, glutamate derived carbon was incorporated into palmitate and subsequently into triacylglycerides. In addition, supplementation with glutamate, glutamine and leucine, but not lysine increased synthesised triacylglyceride content in cells and decreased glucose uptake. Glutamate, glutamine and leucine increase activation of protein kinase B, suggesting that these amino acids induce *de novo* lipogenesis via the insulin signalling cascade.

As dietary trends have shifted towards high carbohydrate/high fat consumption, and high-protein diets are popularised as healthier alternatives, the data herein suggest that this is a more complex consideration. Therefore, advocating the consumption of protein in the treatment of diabetes and obesity requires a more profound understanding of the role.

Dedication

To my beloved parents, Charis and Christiana, and brothers, Andreas and Michael

«Τα καλά κόποις χτώνται» – Aristotle

Acknowledgements

I would like to express my gratitude to my supervisor, Prof Jules Griffin, for his valuable comments, support and guidance throughout this thesis. In addition, I greatly appreciate Dr Tom Ashmore's help with cell culture work. I would also like to thank Sara Wassell, Elise Orford and Matthew Harvey for their assistance in running the human study days and Dr Xuefei Li for her help in analysing and interpreting gastric emptying data. I would like to express my great appreciation to Ben McNally, Steven Murfitt and Dr James West for helping me run the LC-MS.

Table of Contents

Abbreviations

Acaca	Mouse gene for Acetyl-CoA carboxylate
ACC	Acetyl-CoA carboxylate
ACL	ATP-citrate lyase
Acly	Mouse gene for ATP-citrate lyase
ACN	Acetonitrile
ACP	Acyl-carrier protein
ADI	Acceptable daily intake
AGEs	Advanced glycosylation end products
AGPAT	Acylglycerol-phosphate acyl transferase
AML 12	Alpha mouse liver 12
AMPK	AMP-activated protein kinase
ANOVA	Analysis of variance
Apo	Apolipoprotein
ApoCIII	Apolipoprotein CIII
Apoc3	Mouse gene for apolipoprotein CIII
ATCC	American Type Culture Collection
AUC	Area under the curve
BCA	Bicinchoninic acid
BCAAs	Branched-chain amino acids
BSA	Bovine serum albumin
C	Control
CB	Control with bread
CCK	Cholecystokinin
cDNA	Complimentary DNA
CF	Continuous flow
ChoRE	Carbohydrate response element

ChREBP	Carbohydrate response element binding protein
CiC	Citrate carrier
CoA	Coenzyme A
CPT1	Carnitine palmitoyl transferase 1
CS	Citrate synthase
CV	Coefficient of variation
CVD	Cardiovascular disease
CV-ANOVA	Cross validated residuals analysis of variance
DAG	Diacylglycerol
DCM	Dichloromethane
DGAT	Diacylglycerol acyl transferase
Dgat2	Mouse gene for diacylglycerol acyl transferase 2
DH	Dehydratase
DHAP	Dihydroxyacetone phosphate
DNA	Deoxyribonucleic acid
DNL	*De novo* lipogenesis
DRVs	Dietary Reference Values
EFSA	European Food Safety Authority
EIC	Extracted ion chromatogram
ELOVL6	Elongation of very long chain fatty acids protein 6
Elovl6	Mouse gene for elongation of very long chain fatty acids protein 6
ER	Endoplasmic reticulum
ESI	Electrospray ionisation
Fas	Fatty acids
FAS	Fatty acid synthase
Fasn	Mouse gene for Fatty acid synthase
FBS	Fetal bovine serum
FFA	Free fatty acid

GAP	GTPase activating protein
G3P	Glyceraldehyde 3-phosphate
GEF	Guanine nucleotide exchange factor
GIP	Gastric inhibitory polypeptide
GLP-1	Glucagon like peptide-1
GLUT4	Glucose transporter type 4
GPAT	Glycerol-3-phosphate acyltransferase
GTP	Guanosine-5-triphosphate
HC	High carbohydrate
HDL	High density lipoprotein
HF	High fat
HP	High protein
IDH	Isocitrate dehydrogenase
IL-1	Interleukin-1
IPA	Isopropanol
IRS	Insulin receptor substrate
ITS	Insulin-Transferrin-Selenium
KR	β-Ketoacyl reductase
KS	β-ketoacyl synthase
LC-MS	Liquid chromatography mass spectrometry
LDL	Low-density lipoprotein
LG	Low glucose
LPA	Lysophosphatidic acid
LPK	Pyruvate kinase
LPL	Lipoprotein lipase
LXRα	Liver X receptor α
MAT	Malonyl/acetyl transferase
mLST8	Mammalian lethal with SEC13 protein 8

MPA	Median peak area
mSIN1	Mammalian stress-activated protein kinase interacting protein 1
mTOR	Mammalian target of rapamycin
mTORC1	Mammalian target of rapamycin complex 1
mTORC2	Mammalian target of rapamycin complex 2
MTP	Microsomal transfer protein
Mttp	Mouse gene for microsomal transfer protein
NAD^+	Oxidised nicotinamide
NADH	Reduced nicotinamide
$NADP^+$	Oxidised nicotinamide phosphate
NADPH	Reduced nicotinamide phosphate
NADPH-ER	NADPH-dependent enoyl reductase
NAFLD	Non-alcoholic fatty liver disease
NASH	Non-alcoholic steatohepatitis
NCDs	Non-communicable diseases
NEFAs	Non-esterified fatty acids
OBT	Octanoic acid breath test
OD	Optical density
OPLS-DA	Orthogonal projections to latent structure-discriminant analysis
$p70^{S6K1}$	Ribosomal protein S6 kinase beta-1
PA	Phosphatidic acid
PAP	Phosphatidic acid phosphorylase
PBS	Phosphate buffered saline
PCA	Principal component analysis
PDB	Pee Dee Belemnite
PDK-1	3-phosphoinositide-dependent protein kinase-1
PEFAs	Picolinyl esters of fatty acids
PEP	Phosphoenolpyruvate

PI3K	Phosphatidylinositol 3-kinase
PIP_2	Phosphatidylinositol-4, 5-bisphosphate
PIP_3	Phosphatidylinositol-3, 4, 5-triphosphate
PKA	Protein kinase A
PKB	Protein Kinase B
PP2A	Protein phosphatase 2A
PRI	Population reference intake
PYY	Peptide tyrosine-tyrosine
QA	Quality assurance
QC	Quality control
qPCR	Quantitative polymerase chain reaction
Raptor	Regulatory-associated protein of mTOR
Rheb	Ras homolog enriched in brain
RICTOR	Rapamycin-insensitive companion of mTOR
RNA	Ribonucleic acid
RNI	Reference nutrient intake
RSD	Relative standard deviation
RXR	Retinoid X receptor
S1P	Site 1 protease
S2P	Site 2 protease
SCAP	SREBP cleavage activating protein
SCD1	Stearoyl-CoA desaturase-1
SCD1	Human gene for Stearoyl-CoA desaturase-1
ScTAGs	Shorter chain TAGs
SEM	Standard error of the mean
SREBP-1c	Sterol regulatory binding protein 1c
SRE	Sterol regulatory element
T1DM	Type 1 diabetes mellitus

T2DM	Type 2 diabetes mellitus
TAGs	Triacylglycerides
TCA	Tricarboxylic acid
TE	Thioesterase
T_{half}	Half-emptying time
$T_{half(in)}$	Self-corrected half emptying time
TIC	Total ion chromatogram
T_{lag}	Lag phase time
$Tl_{ag(in)}$	Self-corrected lag phase time
TSC1/2	Tuberous sclerosis complex
TNF- α	Tumour necrosis factor α
UHPLC	Ultra-high performance liquid chromatography
UV	Univariate
v-ATPase	Vacuolar-type H^+- ATPase
VIP	Variable importance in projection
VLDL	Very low-density lipoprotein
WHO	World Health Organisation

Chapter 1. Introduction

1.1 The nutrition transition and obesity epidemic

Human dietary habits, in all their diversity, significantly delineate people's health, growth and development. Since the Palaeolithic era when humans appeared on the Earth, a series of dietary changes have coincided with modernisation, urbanisation, economic development, and increased wealth. These changes are reflected in average stature and body composition and are accompanied by major changes in health status; i.e. broad patterns in food use and corresponding nutrition-related disease (Misra and Khurana, 2008). Currently, research focuses on the most recent nutritional shifts as they reflect the global population today. The latest transitions include the shift from traditional diets (high in cereal and fibre) to Western-style diets (high in sugars, fat, and animal-derived food), which is a key contributor to the obesity epidemic and increased incidence of non-communicable diseases (NCDs) in developing countries (Popkin, 2006).

The World Health Organisation (WHO) defines obesity as the abnormal or excessive accumulation of fat with ectopic fat deposition, which may impair health. Ectopic fat deposition is described as the storage of lipids in tissues other than adipose tissue, such as liver, skeletal muscle, heart and the pancreas. Ectopic fat may interfere with cellular functions leading to insulin resistance (Snel et al., 2012). Over-nutrition and a sedentary lifestyle are the major factors contributing to obesity (Hruby and Hu, 2015). Persistent obesity dysregulates a variety of metabolic processes, including the action of insulin. Insulin, a peptide hormone, is responsible for the regulation of glucose and lipid metabolism. Impaired insulin activity can disrupt processes controlling blood glucose, blood pressure, and lipids, and consequently, precipitate a number of conditions such as dysglycaemia, dyslipidaemia, and hypertension. The aforementioned conditions constitute the most dangerous heart attack risk factors and are associated with the 'metabolic syndrome' (Alberti et al., 2006). Being overweight or obese, and having the metabolic syndrome are precursors to the development of Type 2 Diabetes Mellitus (T2DM) and cardiovascular disease (CVD). Both of these diseases are examples of chronic

NCDs which are increasing in developed and developing countries (Popkin, 2006) and are of protracted duration and slow development.

1.2 The metabolic syndrome

A constellation of metabolic disorders, including hypertension, hyperglycaemia and hyperuricaemia, were observed in a number of patients back in 1923 by Kylin (Kylin, 1923). After Kylin's observations, Revean noticed that often a person with impaired glucose tolerance will have at least one CVD risk factor. He then described this cluster of metabolic abnormalities as syndrome X (Reaven, 2001). Initially, central obesity was not included in the term syndrome X, and the term metabolic syndrome was coined to include central obesity as a collection of interacting risk factors. Even though the concept of the metabolic syndrome was accepted in the early 1920s, it was not until 1998, that researchers attempted to develop an internationally recognised definition to provide a tool for clinicians and researchers.

In 1999, the WHO defined the metabolic syndrome as glucose intolerance, impaired glucose tolerance or diabetes mellitus and/or insulin resistance together with two or more risk factors listed below (Alberti et al., 2006):

(1) Raised arterial pressure ≥ 140/90 mmHg

(2) Raised plasma triacylglycerides (TAGs ≥ 1.7 mmol/L) and or low high-density lipoprotein (HDL)-cholesterol (< 0.9 mmol/L in men and < 1.0 mmol/L in women)

(3) Central obesity (waist to hip ratio > 0.90 in males and > 0.85 in females) and or BMI > 30 kg/m^2

(4) Microalbuminuria (urinary albumin excretion rate ≥ 20 μg/min or albumin: creatinine ratio ≥ 30 mg/g)

Each component of the metabolic syndrome contributes to increased CVD risk, but combinations of two or more represent an increased risk compared to the individual factors alone (i.e. they are not merely additive). However, people might experience hyperglycaemia for up to 10 years before they develop glycaemic disorders (Martín-Timón et al., 2014).

Therefore, early management of the metabolic syndrome might have a significant impact on both diabetes and CVD, preventing the syndrome to develop into overt disease.

1.2.1 Metabolic syndrome and cardiovascular disease

Variable characteristics of the metabolic syndrome, including hyperglycaemia, hypertension, insulin resistance, a proinflammatory and prothrombotic state increase the risk of CVD. People with the metabolic syndrome have at least 2-fold increased risk of CVD compared to people without (Kaur, 2014). Elevated levels of TAGs, low-density lipoprotein (LDL) in the circulation and low levels of HDL-C, known as atherogenic dyslipidaemia, contribute to the formation of plaques in the artery wall (Grundy, 2004). The onset of diabetes is accompanied with CVD risk, suggesting that hyperglycaemia is atherogenic. However, there are limited data on the molecular basis of hyperglycaemia inducing atherosclerosis in part reflecting the difficulty in modelling long term chronic diseases. A plausible mechanism proposed is the non-enzymatic glycosylation of lipoproteins and proteins within the arterial walls (Aronson and Rayfield, 2002). Advanced glycosylation end products (AGEs) have been shown to trap LDL in the subendothelium as well as reduce LDL recognition by the LDL receptors (Brownlee et al., 1985) and promote collagen cross-linking (Brownlee et al., 1986). AGEs have also been shown to induce the secretion of cytokines such as tumour necrosis factor α (TNF-α) and interleukin-1 (IL-1) to promote inflammation (Brownlee et al., 1986). The basic concept of atherogenesis is the lipid-induced injury within the arteries that induces inflammation followed by the proliferation of smooth muscle cells.

1.2.2 Metabolic syndrome and T2DM

Glucose transporters, such as glucose transporter type 4 (GLUT4), stimulate glucose transport in response to insulin. An increase in postprandial glucose is sensed by the β-cells of the pancreatic islets of Langerhans, adjusting insulin secretion to control blood glucose levels. The insulin signalling cascade results in the translocation of GLUT4 storage vesicles to the plasma membrane to mediate glucose uptake. Impairment of any of the aforementioned steps leads

to insulin resistance. Insulin resistance is a major component of the metabolic syndrome. In T2DM, cells within the body become insulin resistant (i.e. they no longer take up glucose in response to insulin or uptake is impaired) and as the condition progresses, the pancreas decreases insulin production following a period of hyperinsulinaemia. The levels of GLUT4 are decreased in type 2 diabetic patients (Kampmann et al., 2011). T2DM accounts for ~90% of all cases of diabetes and is often associated with obesity (Wu et al., 2014). Lipoprotein metabolism is altered in T2DM, characterised by an overproduction of very low-density lipoprotein (VLDL) rich in TAGs and a decrease in the production and circulation of HDL (Adiels et al., 2008). Furthermore, levels of lipoprotein lipase (LPL) expression and activity of hormone sensitive LPL, are decreased, slowing removal of TAGs from VLDL (Verges, 2015). In addition, insulin resistant subjects fail to suppress gluconeogenesis, further increasing the levels of glucose but continue to activate lipogenesis (Brown and Goldstein, 2008). As in type 1 diabetes mellitus (T1DM), an impaired response to insulin produces increased blood glucose, resulting in a variety of long-term problems, including diabetic retinopathy (Duh et al., 2017) and diabetic gastroparesis (Reddy et al., 2010).

1.2.2.1 Diabetic gastroparesis

Diabetic gastroparesis (meaning partial stomach paralysis) refers to a chronic condition of delayed gastric emptying experienced by people with both T1DM and T2DM (Halland and Bharucha, 2016). In health, the vagus nerve provides a channel for bidirectional interaction between the brain and the gut (Bonaz et al., 2018). Vagal axons associate with the interstitial cells of Cajal, which generate electrical slow waves to regulate the strength and frequency of the contractions of the gastrointestinal muscles between the stomach and the duodenum (Ordog et al., 1999). Firstly, the proximal stomach relaxes to accommodate large volumes of food, the antrum grinds food to small particles and the chyme is pumped, in peristaltic waves, across the pylorus. In diabetes, prolonged hyperglycaemia damages peripheral nerve fibres as well as the interstitial cells of Cajal (Yagihashi et al., 2011). Therefore, the stomach cannot contract correctly, and the emptying of its contents to the duodenum is delayed (Marathe et

al., 2013). More recently, it has been proposed that macrophages and mast cells are responsible for the pathogenesis of delayed gastric emptying (Srinivasan, 2016). It has been shown that in diabetes, increased numbers of macrophages correlate with a decrease in the number of interstitial cells of Cajal (Mikkelsen, 2010). Diabetic mice lacking macrophages ($Csf1^{op/op}$) in the muscle layer of the small intestine do not lose the interstitial cells of Cajal and do not develop delayed gastric emptying (Srinivasan, 2016). Prolonged gastroparesis has been associated with increased small intestinal bacterial overgrowth (Reddymasu and McCallum, 2010). In addition, gastroparesis may result in the formation of bezoars, which are aggregates of undigested food in the stomach that form into a harden solid mass and they can potentially block food passing to the intestine (Eng and Kay, 2012). The rate of gastric emptying is crucial for the homeostasis of postprandial blood glucose levels. Therefore, prolonged gastroparesis may result in poor glycaemic control (Phillips et al., 2015). It is therefore important to control the rate of gastric emptying.

1.2.2.2 Regulation of gastric emptying

The rate of gastric emptying is crucial for glucose homeostasis. There is a bidirectional communication between glucose and gastric emptying (Marathe et al., 2013). Exposure of nutrients to the duodenum induces a negative feedback loop, decreasing gastric emptying. The intestine releases cholecystokinin (CCK), peptide tyrosine-tyrosine (PYY), and glucagon like peptide-1 (GLP-1) to mediate the ileal brake, i.e. decrease the contractions of the stomach to delay the transit of chyme through the gastrointestinal track. The interaction of nutrients with the small intestine mucosa induces the release of gastric inhibitory polypeptide (GIP) and GLP-1 from K cells and L cells, respectively (Baggio and Drucker, 2007). Both GIP and GLP-1 stimulate glucose-dependent insulinotropic effects. However, GLP-1 is also responsible for inhibiting the secretion of glucagon to modulate postprandial glycaemic excursions. Insulin and amylin are co-secreted from the pancreas to control glucose uptake and inhibit gastric emptying (Phillips et al., 2015).

1.2.2.3 Factors affecting gastric emptying

There are a variety of factors that affect gastric emptying including: meal energy content, meal weight, volume, macronutrient composition, fibre content, pH and temperature (Chaw et al., 2001; Clegg and Shafat, 2010). Since the obesity epidemic, research has focused on the effect of high energy dense food on gastric emptying (Xing and Chen, 2004). Studies have showed that high fat meals delay gastric emptying compared to low fat meals (Clegg and Shafat, 2010). In addition, high-carbohydrate meals have slower emptying times (Marciani et al., 2015). However, data from a previous study at the Medical Research Council-Elsie Widdowson Laboratory (MRC-EWL; Bluck, Griffin & Li personal communication) contradicts this. High fat, high carbohydrate and, high protein meals had a rapid gastric emptying rate compared to the control meal with no significant differences in gastric emptying between the three altered meals. The difference between the control meal and the modified meal was that the carbohydrate content was in liquid form in the control meal. This might suggest that liquid carbohydrate empties the stomach faster and induces slower emptying of the solid portion via negative feedback control. This also suggests that liquid carbohydrate is the main driver of gastric emptying rates compared to macronutrient compositions. As mentioned above, delayed gastric emptying changes the control of glycaemia and might therefore change glucose and lipid metabolism, predisposing an individual to insulin resistance. This warrants further investigation and forms the basis of this thesis.

1.2.3 Metabolic syndrome and non-alcoholic fatty liver disease

Non-alcoholic fatty liver disease (NAFLD) is an umbrella term describing a range of liver conditions that arise from fat accumulation without any excessive alcohol consumption. It is the most common cause of chronic liver disease in western society and is predicted to be the major reason for liver transplantation by 2030 (Byrne and Targher, 2015). There are two pathological forms: steatosis and non-alcoholic steatohepatitis (NASH). Isolated steatosis is considered a benign condition, however fat accumulation induces inflammation and may eventually cause NASH. Persistent inflammation results in the formation of scar tissue (fibrosis) and subsequent cirrhosis (Pais et al., 2011). NALFD is strongly correlated with the metabolic syndrome, though their relationship is complex and may be bidirectional. Approximately 90% of NAFLD patients fulfil one of the metabolic syndrome conditions whilst 33% patients fulfil three conditions and therefore are defined as suffering from the metabolic syndrome as well (Marchesini et al., 2003). In addition, NAFLD is highly prevalent among T2DM patients; approximately 85% of NALFD patients have pre-diabetes or T2DM (Gaggini et al., 2013). In addition a hallmark for NAFLD and T2DM is increased hepatic *de novo* lipogenesis (DNL) which may further contribute to NAFLD (Sanders and Griffin, 2016).

1.2.3.1 The biochemical process of DNL

Hepatic DNL is the biochemical pathway by which fatty acids (FAs) are synthesised from acetyl-coenzyme A (CoA) subunits in the liver. Fatty acids are incorporated into a plethora of lipid species. Even though lipid species have several biological functions, accumulation of lipids, in cases of increased DNL, may be deleterious (Ress and Kaser, 2016). As mentioned above, increased DNL has been reported to contribute in the development of NAFLD, a condition linked to the metabolic syndrome and T2DM (Paschos and Paletas, 2009). Moreover, DNL levels are elevated in insulin resistance, indicating that the levels of DNL might be an important metric for pre-diabetes (Ameer et al., 2014). It is therefore crucial to understand the biochemical pathways of DNL and how it is induced.

When there is excess energy, reflected by increased levels of the reducing agent NADH, the tricarboxylic acid (TCA) cycle is inhibited and results in the accumulation of acetyl-CoA in the mitochondrion (Shi and Tu, 2015). Acetyl-CoA is then combined with oxaloacetate to synthesise citrate via citrate synthase (CS). Citrate is then exported to the cytosol through the citrate carrier (CiC) protein, also known as the citrate transport protein (Ferramosca and Zara, 2014). In the cytosol, citrate is lysed to acetyl-CoA by ATP-citrate lyase (ACL) to initiate DNL. Acetyl-CoA is then carboxylated to malonyl-CoA by acetyl-CoA carboxylase (ACC; Bianchi et al., 1990). Malonyl-CoA is the elongation unit of the multi-functional enzyme fatty acid synthase (FAS). Eukaryotic FAS (Type I FAS) is a multi-protein complex with multiple functional polypeptides at different regions. It harbours catalytic domains for all the reactions required for fatty acid synthesis as well as acyl-carrier protein (ACP; Smith et al., 2003). The phosphopantetheine prosthetic arm of ACP shuttles the elongating acyl-chain to various catalytic sites of FAS, which rotates to aid in synthesis (Maier et al., 2008). The process is initiated by the transfer of acetyl-CoA and malonyl-CoA to the ACP generating acetyl-ACP and malonyl-ACP, respectively (Figure 1A). This reaction is catalysed by the malonyl/acetyl transferase (MAT) region of FAS (Mikkelsen et al., 1985).

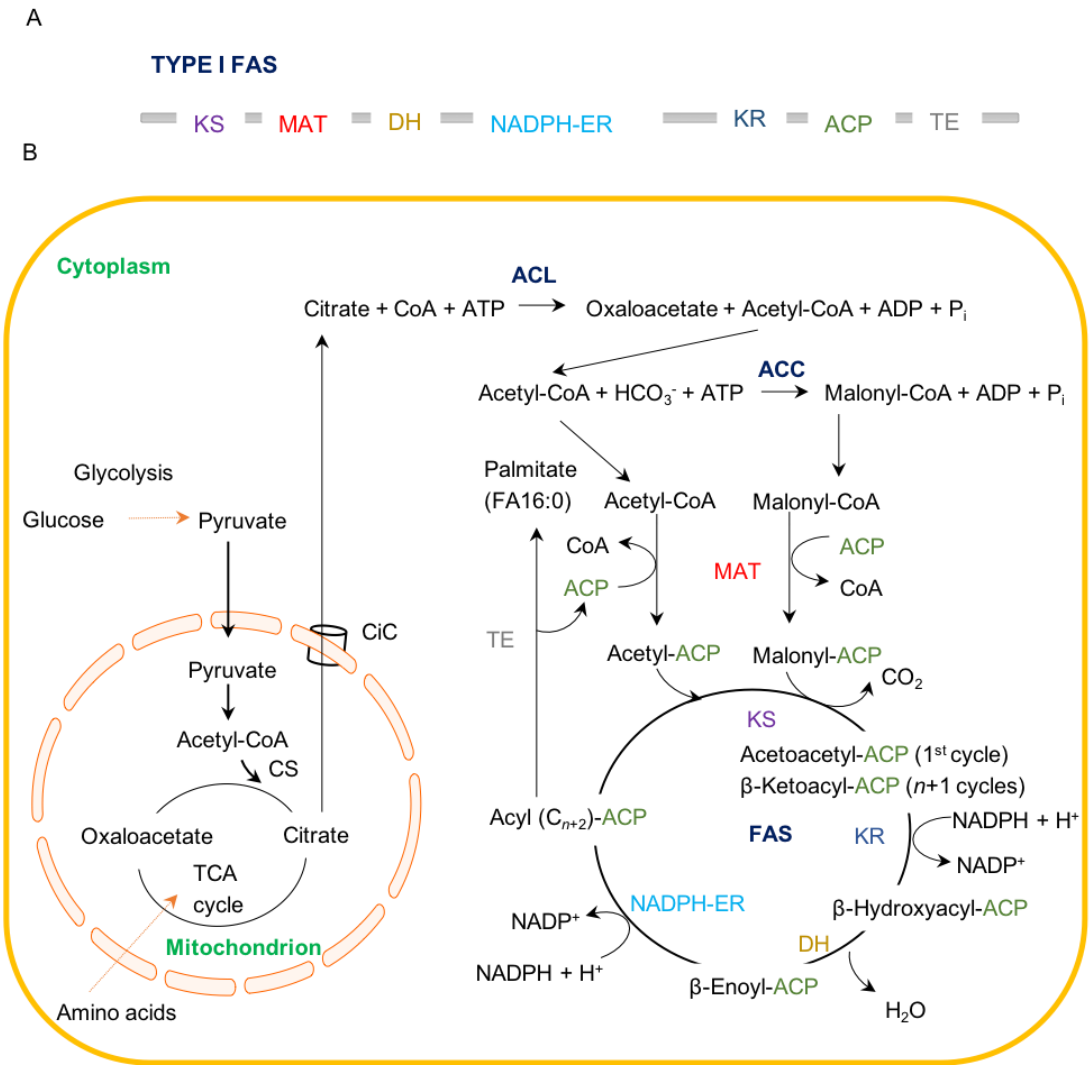

Figure 1. Schematic representation of the organisation of FAS domains and its catalytic cycle. (**A**) Linear organisation of the mammalian FAS domains. (**B**) High energy balance causes citrate to be exported from the mitochondrion to the cytoplasm. In the cytoplasm, citrate is lysed to acetyl-CoA by ACL. Acetyl-CoA is then carboxylated to malonyl-CoA by ACC. Acetyl-CoA and malonyl-CoA are transferred to ACP by MAT (red). Acetyl-ACP and malonyl-ACP are condensed by KS (purple) to synthesise acetoacetyl-ACP in the first cycle of synthesis. In following cycles malonyl-ACP condenses with acyl (C_{n+2})-ACP to synthesise β-ketoacyl-ACP. The β-ketoacyl-ACP intermediate is then reduced to β-hydroxyacyl-ACP by KR (blue), dehydrated to β-enoyl-ACP by DH (yellow) and reduced again to synthesise a four-carbon acyl-substrate for further elongation cycles by NADPH-ER (light blue). Once an acyl chain of 16 carbons is formed, the reaction is terminated by the action of TE (grey), which cleaves the fatty acid from ACP. ACL, ATP-citrate lyase; ACC; acetyl-CoA carboxylase; KS, β-ketoacyl synthase; KR, β-ketoacyl reductase; DH, dehydratase; NADPH-ER, NADPH-dependent enoyl reductase. Adapted from Maier, Jenni and Ban, 2006.

The β-ketoacyl synthase (KS) domain then catalyses the decarboxylative condensation of malonyl-ACP and acetyl-ACP to acetoacetyl-ACP in the first cycle or of the acyl (n+2)-ACP intermediate and malonyl-ACP to β-ketoaceyl-ACP in the next cycles. The β carbon of the ketone is reduced to a hydroxyl group by the β-ketoacyl reductase (KR) domain. The resulting β-hydroxyacyl-ACP is dehydrated by the dehydratase (DH) active site to β-enoyl-ACP, which is then reduced by an NADPH-dependent enoyl reductase (NADPH-ER; Chang and Hammes, 1990). This yields a four-carbon acyl-substrate for further elongation cycles. Each time the acyl-chain is elongated by 2-carbon units derived from malonyl-CoA. The end result is usually the 16-carbon palmitate which is released from ACP by the action of the thioesterase (TE) active site of FAS (Figure 1B; Maier, Jenni and Ban, 2006). Typically, the activity of thioesterase is lower for acyl chains shorter than 14 carbon and longer than 18 carbons as these might not be accommodated by the binding groove of the thioesterase (Chakravarty et al., 2004). Moreover, the longer acyl chains are not readily transferred to the thiol of the cysteine in the KS active site (Witkowski et al., 1997).

1.2.3.2 Transcriptional control of hepatic *de novo* lipogenesis

In an effort to maintain metabolic homeostasis, cells employ a variety of biochemical reactions. During fasting, hepatocytes and adipocytes stimulate β-oxidation of fatty acids (breakdown of fatty acids) to generate energy, whilst during feeding they induce the synthesis of fatty acids, requiring energy (Rui, 2014). The two processes are tightly controlled to avoid any metabolic perturbations, which may lead to a variety of diseases. The process of β-oxidation more specifically is regulated by the transcriptional control of the carnitine palmitoyl transferase 1 (*CPT1*) gene. CPT1 is responsible for the transport of fatty acids from the cytosol to the mitochondrion where they are oxidised. When the energy balance is high, malonyl-CoA inhibits CPT1, preventing the import of fatty acids into the mitochondrion and is itself the substrate for fatty acid synthesis (Torchon et al., 2017). This latter mechanism is the main control process for fatty acid oxidation following uptake of fatty acids into the cell.

Both metabolic and hormonal stimuli, such as glucose and insulin, regulate lipogenesis. There are two major transcription factors responsible for the control of hepatic lipogenesis: carbohydrate response element binding protein (ChREBP) and sterol regulatory binding protein 1c (SREBP-1c). Glucose activates ChREBP whilst insulin activates SREBP-1c.

(1) ChREBP

During starvation, high glucagon levels increase cAMP and activate protein kinase A (PKA), which phosphorylates ChREBP. Phosphorylation at serine residue 196 (Ser196) inactivates nuclear export and phosphorylation at threonine 666 (Thr666) inhibits deoxyribonucleic acid (DNA) binding of ChREBP (Kawaguchi et al., 2001). In addition, ATP depletion and fatty acid oxidation activate AMP-activated protein kinase (AMPK), via increased AMP levels, which also phosphorylates and in turn inhibits ChREBP (Kawaguchi et al., 2002). In contrast, glucose and high carbohydrate feeding activate ChREBP via an incompletely elucidated mechanism. Data suggest that glucose is converted to xylulose-5-phosphate in the pentose phosphate pathway to activate protein phosphatase 2A (PP2A). PP2A dephosphorylates ChREBP allowing its nuclear translocation (Kabashima et al., 2003). Xylulose-5-phosphate-mediated PP2A activation has also been observed when fructose-2,6-bisphosphatase is activated, a key enzyme in glycolysis and gluconeogenesis (Nishimura and Uyeda, 1995). In the nucleus ChREBP binds to the carbohydrate response element (ChoRE) to induce the expression of genes such as FAS and ACC, as well as liver pyruvate kinase (LPK), which converts phosphoenolpyruvate (PEP) to pyruvate (Figure 2; Towle et al., 1997). Xyluose-5-phosphate is an important mediator for activating glycolysis and lipogenesis in parallel, via ChREBP. During glycolysis, glucose generates pyruvate which is oxidised to acetyl-CoA. Acetyl-CoA then condenses with oxaloacetate to synthesise citrate. In parallel, glucose is shuttled though the pentose phosphate shunt to generate NADPH. Accumulation of citrate in the mitochondrion induces its export to the cytosol. Both cytosolic citrate and NADPH are then used for the synthesis of fatty acids (Iizuka and Horikawa, 2008).

The levels of ChREBP are significantly increased in the liver of ob/ob mice and liver specific inhibition of ChREBP in these mice improves hepatic steatosis by decreasing the activity of DNL (Dentin et al., 2006).

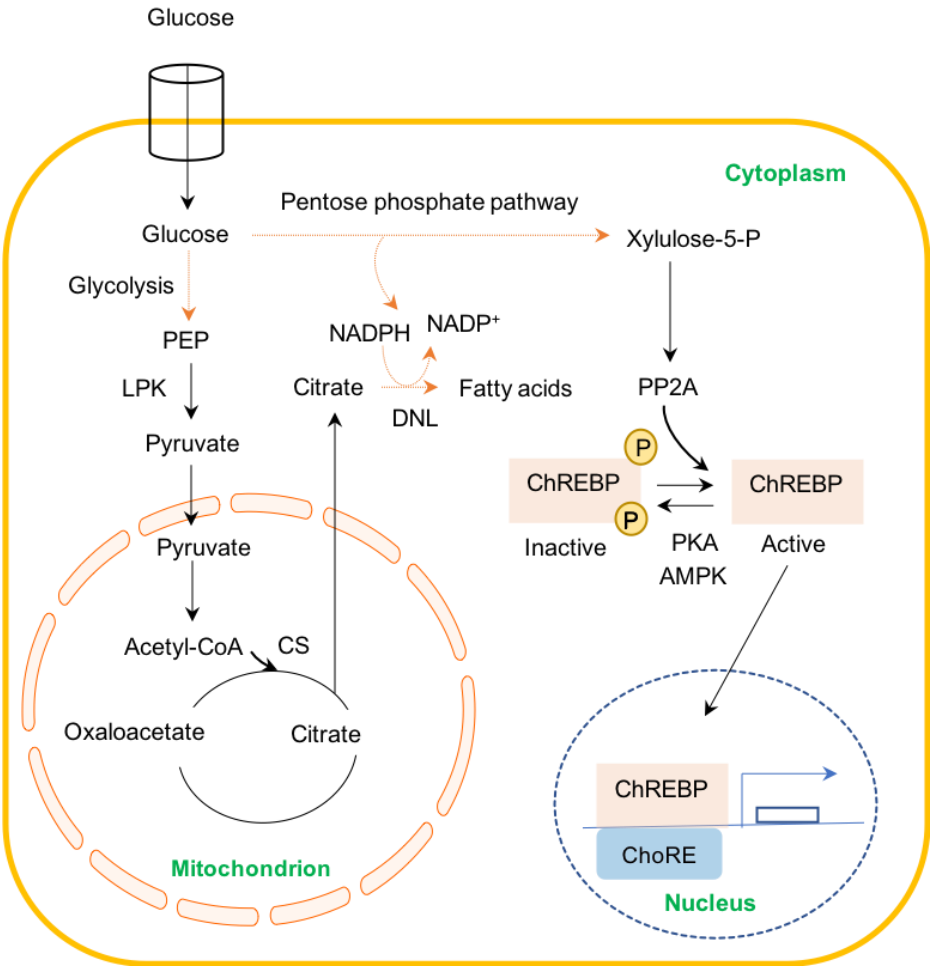

Figure 2. Schematic representation of hepatic activation of DNL gene expression by ChREBP. An increase in postprandial glucose triggers glucose uptake through the transporter GLUT2. Glucose is shuttled to glycolysis and the pentose phosphate pathway to provide substrate and the cofactor NADPH for DNL, respectively. Xylulose-5-phosphate, an intermediate of the pentose phosphate pathway, activates the phosphatase PP2A, which dephosphorylates ChREBP. Dephosphorylation of ChREBP activates the transcription factor and allows its translocation to the nucleus where it binds to the ChoRE consensus sequence to increase the expression of genes required for DNL. GLUT2, glucose transporter 2; PP2A, protein phosphatase 2A; ChREBP, carbohydrate response element binding protein; CHoRE, carbohydrate response element.

(2) SREBP-1c

As mentioned above, SREBP-1c responds to insulin stimuli to induce the expression of genes required for DNL. The SREBP family consists of SREBP-1a, SREBP-1c and SREBP2. SREBP-1a and SREBP-1c are encoded by one gene but transcribed by initiation from two different promoters. SREBP-1c is mostly expressed in the liver whilst SREBP-1a is abundant in immune cells. SREBP-1c is responsible for the expression of lipogenic genes whilst SREBP-2 is responsible for activating cholesterol-metabolism genes. SREBPs bind to sterol regulatory element (SREs) sequences found on promoters of their target genes (Eberlé et al., 2004).

SREBPs are embedded in the endoplasmic reticulum (ER) membrane as inactive precursors by associating with the SREBP cleavage activating protein (SCAP) and ER retention protein Insig (Figure 3). In order to be activated, the SCAP-SREBP complex should be dissociated from Insig in the ER and associate with COPII-coated vesicles that then migrate to the Golgi apparatus. There, SREBPs are cleaved by site 1 and site 2 proteases (S1P and S2P, respectively), releasing the N-terminal cytosolic portion of the protein that migrates in the nucleus and acts as a mature transcription factor (Xu et al., 2013).

In the liver, insulin signalling, through the phosphatidylinositol 3-kinase (PI3K), both activates and increases the levels of the nuclear SREBP-1c protein. Insulin signalling via the insulin receptor induces the phosphorylation and activation of the insulin receptor substrate (IRS). Activated IRS recruits PI3K to the membrane where it phosphorylates phosphatidylinositol-4, 5-bisphosphate (PIP_2) to phosphatidylinositol-3, 4, 5-triphosphate (PIP_3), which acts as a secondary messenger for the mammalian target of rapamycin complex 2 (mTORC2) and 3-phosphoinositide-dependent protein kinase-1 (PDK1). Both phosphorylate and activate AKT2 (Protein Kinase B/PKB). PhosphoAKT in turn activates the mammalian target of rapamycin complex 1 (mTORC1). The kinase mTORC1 stimulates the nuclear translocation of the liver X receptor α (LXRα), where it heterodimerises with the retinoid X receptor (RXR; Kawano and Cohen, 2013). The heterodimer then induces the expression of lipogenic genes including that of SREBP-1c. The full maturation of SREBP-1c protein is mediated through the inhibition of lipin-1 by mTORC1, allowing its entry to the nucleus (Peterson et al., 2011). Suppression of

mTORC1 by rapamycin inhibits the expression of SREBP-1c in mice fed with a high carbohydrate diet (Li et al., 2010).

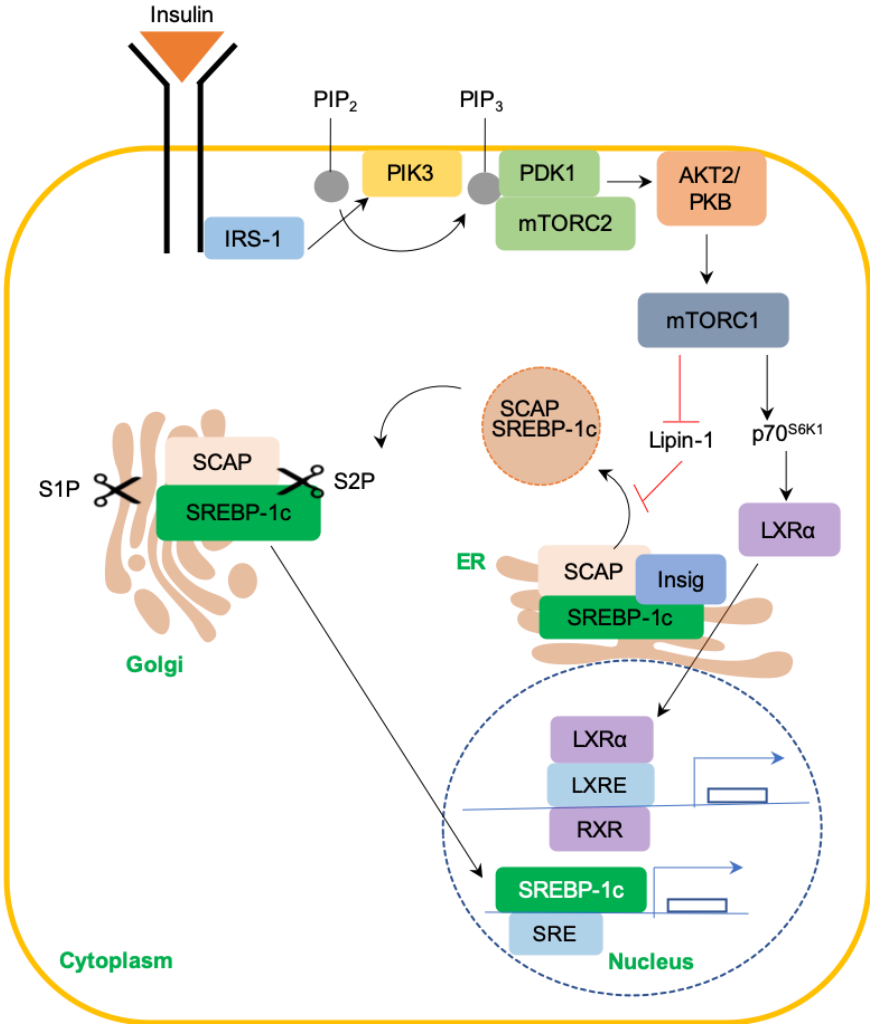

Figure 3. Schematic representation of hepatic activation of DNL gene expression by SREBP-1c. Insulin interaction with the insulin receptor mediates the recruitment of the IRS to the receptor. The IRS recruits PI3K to the membrane, where it phosphorylates PIP_2 to PIP_3. The secondary signalling molecule PIP_3 recruits mTORC2 and PDK1 to the membrane. Both kinases phosphorylate and activate AKT2. In turn, AKT2 activates mTORC1, which has a variety of targets. One such target is the kinase $p70^{S6K1}$, which induces the nuclear translocation of LXRα. In the nucleus, LXRα dimerises with RXR and the complex binds to the LXRE motif to induce the expression of SREBP-1c and other lipogenic genes. Translocation of mature SREBP-1c to the nucleus, where it binds to the SRE motif, induces the expression of genes required for DNL. IRS, insulin receptor substrate; PI3K; phosphatidylinositol 3-kinase; PIP_2, phosphatidylinositol-4, 5-bisphosphate; PIP_3, phosphatidylinositol-3, 4, 5-triphosphate; mTORC1, mammalian target of rapamycin complex 1; $p70^{S6K1}$, ribosomal protein S6 kinase beta-1; LXRα, the liver X receptor α; RXR, retinoid X receptor; LXRE, liver X receptor regulatory element; SREBP-1c, sterol regulatory binding protein 1c; SRE, sterol regulatory element.

1.2.3.3 Fatty acid synthesis, processing and packaging

Both ChREBP and SREBP-1c increase the expression of genes required for fatty acid synthesis as well as processing. This includes ATP citrate lyase (*ACLY*), acetyl-CoA carboxylase α (*ACACA*), fatty acid synthase (*FASN*), stearoyl-CoA desaturase-1 (*SCD1*) and elongation of very long chain fatty acids protein 6 (*ELOVL6*; Strable and Ntambi, 2010).

The synthesis of fatty acids is initiated by the carboxylation of acetyl-CoA to malonyl-CoA, which undergoes multiple rounds of elongation to generate palmitate (Figure 4, inset 1). Once synthesised, palmitate may be desaturated and/or elongated to palmitoleate and stearate by SCD1 and ELOVL6, respectively (Figure 4, inset 2).

Fatty acyl-CoAs are in turn used for *de novo* synthesis of TAGs. The reaction is initiated by the transfer of a fatty acyl-CoA onto glycerol-3-phosphate, generating a lysophosphatidic acid (LPA) by glycerol-3-phosphate acyltransferase (GPAT). The LPA is further acetylated to phosphatidic acid (PA) by acylglycerol-phosphate acyl transferase (AGPAT). The phosphate group is then removed from the PA by the action of phosphatidic acid phosphorylase (PAP), generating a diacylglycerol (DAG; Coleman and Lee, 2004). The DAG is finally acylated to a TAG by the action of diacylglycerol acyl transferase (DGAT; Shi and Cheng, 2009; Figure 4 inset 3).

TAGs are stored in the cytosol in the form of lipid droplets. These lipid droplets are used for the assembly of VLDL, which act as the major transport vehicle of lipids from the liver to other organs. VLDL particles are made of an external phospholipid layer with cholesterol as well as apolipoproteins (apo) while the internal neutral lipid core is formed mainly of TAGs (Sundaram and Yao, 2010). VLDL particles are assembled in 2 steps (Rustaeus et al., 1999). The first step is the co- and post-translational lipidation of apoB100 by the microsomal transfer protein (MTP) to prevent its degradation in the ER (Pan et al., 2002). This generates a precursor-VLDL particle which is further lipidated by TAGs in the second step. ApoCIII is also an important apolipoprotein for the stabilisation of neutral lipid droplets (Qin et al., 2011). These VLDL particles are transported to the Golgi via specialised VLDL transport vesicles. In the Golgi, apoB100 is glycosylated and phosphorylated generating a mature VLDL (Swift, 1996). Mature

VLDL particles are then trafficked to the membrane via transport vesicles. These vesicles fuse with the membrane releasing mature VLDL particles into the circulation (Figure 4 inset 4).

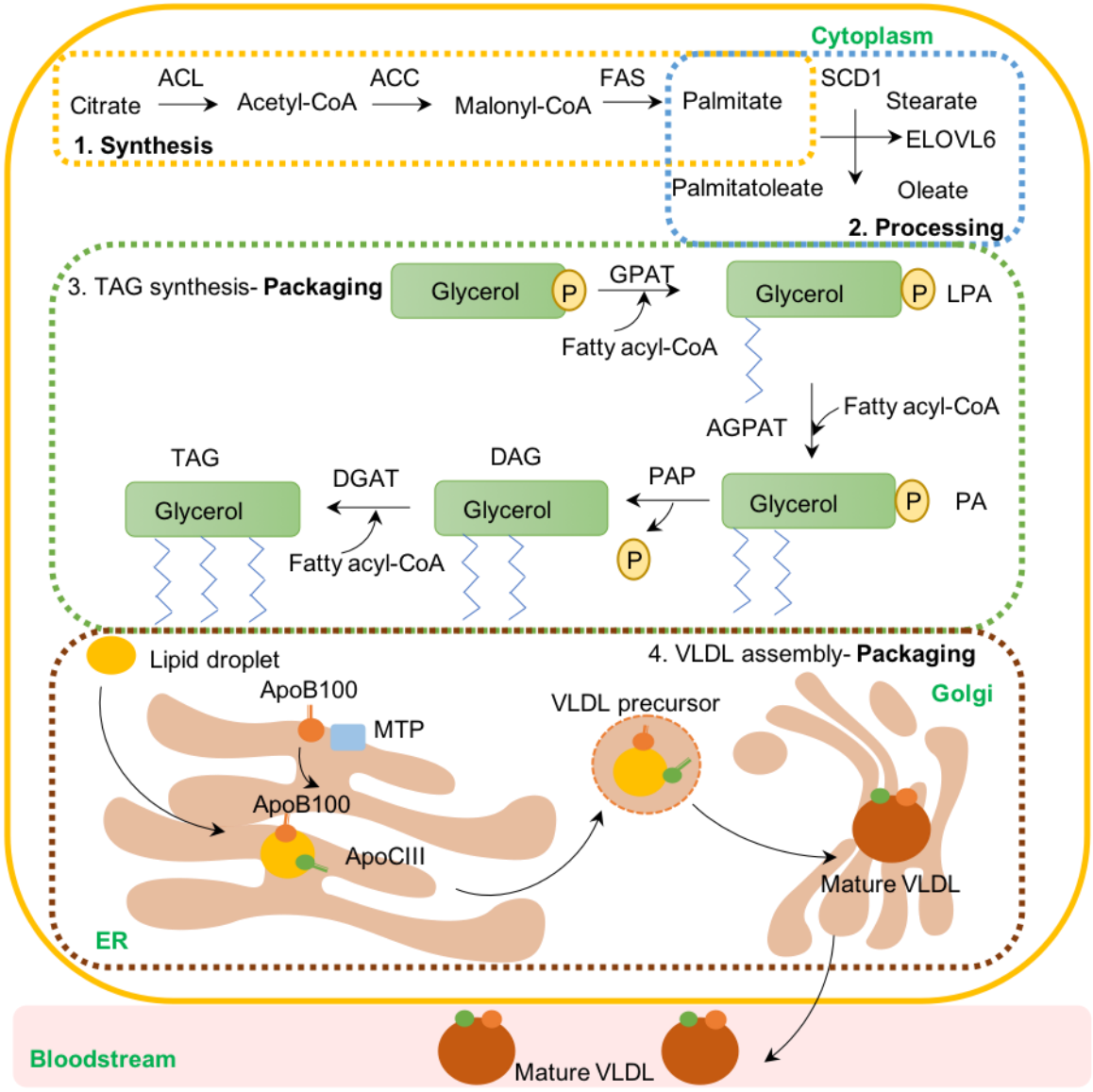

Figure 4. Schematic representation of fatty acid synthesis processing and packaging. Fatty acid synthesis commences with the lysis of citrate to acetyl-CoA (1). Acetyl-CoA is carboxylated to malonyl-CoA. After elongation, FAS generates palmitate, a 16-carbon fatty acid. Palmitate may be desaturated and/or elongated (2) and then used for TAG synthesis (3). TAGs are packaged into lipid droplets within the cytosol and are used for the assembly of VLDL particles in the ER. Subsequent transport through the Golgi generates a mature VLDL particle, which is transported to the membrane for export into the circulation (4). FAS, fatty acid synthase; TAGs, triacylglycerides; VLDL, very low-density lipoprotein; ER, endoplasmic reticulum.

1.2.3.4 Markers of *de novo* lipogenesis

Increased hepatic DNL has been shown to contribute to lipid accumulation in patients with insulin resistance and NALFD (Bhat et al., 2012). Labelled palmitate studies demonstrate that around 5% of TAGs in the liver of healthy subjects are derived from DNL. Feeding healthy subjects with a high carbohydrate meal is sufficient to increase DNL derived TAG content to 23% (Timlin and Parks, 2005). In hyperinsulinaemic individuals with NALFD, DNL derived TAG content increases to 26% (Donnelly et al., 2005). Patients with lipodystrophy also present elevated levels of DNL and hepatic lipid accumulation (Semple et al., 2009). They possess a significant increase in VLDL particles containing TAG 46:1, TAG 48:0 and TAG 48:1 compared to controls, suggesting a possible link between DNL and this group of TAGs (Lee et al., 2015). Indeed, the monounsaturated fatty acid, palmitoleate in VLDL-TAGs has been characterised as a marker of increased DNL and NAFLD (Eiden et al., 2015). Moreover, in the Fenland cohort, a group of shorter chain saturated TAGs (scTAGS; containing FA 16:0, 16:1, 18:0, 18:1) are linked with DNL and steatosis (Sanders et al., 2018). In the same cohort, palmitate synthesis is directly correlated to each of these TAGs. The same group of TAGs have been correlated with insulin resistance (Rhee et al., 2011) as well as cardiovascular disease (Stegemann et al., 2014).

1.2.3.5 Substrates of *de novo* lipogenesis

Despite the fact that DNL has been linked with overnutrition and the metabolic syndrome (Grundy, 2016), our knowledge on acetyl-CoA substrates that fuel the process might be limited. A number of studies have been focused on glucose and fructose as ‘lipogenic’ nutrients that contribute to the acetyl-CoA pool (Moore et al., 2014). However, the liver can use a variety of nutrients to generate acetyl-CoA, including amino acids.

(1) Glucose

A well-characterised substrate for DNL is glucose. Once in the cell, glucose undergoes glycolysis generating pyruvate. Pyruvate can either undergo complete oxidation through the TCA cycle to generate energy or provide a carbon source for lipid synthesis when there is excess energy. While there is a limited capacity to store glycogen from excess glucose, it is near limitless for fat. Once pyruvate is in the mitochondrion, it is oxidised to acetyl-CoA, which condenses with oxaloacetate to generate citrate. Accumulation of citrate within the mitochondrion induces its export to the cytosol, where it is used to synthesise fatty acids (Figure 5 inset 1). A high carbohydrate diet increases the rate of DNL by loading the system with a large substrate pool (Marques-lopes et al., 2001), exacerbated by the relatively small capacity for storing carbohydrates when compared with fats. In addition, carbohydrate overfeeding increased scTAG content of secreted VLDL from 5% (basal DNL) to 20% (Aarsland et al., 1996) reflecting the dominant products of DNL.

(2) Fructose

Besides glucose, fructose has also been characterised as a lipogenic substrate (Dekker et al., 2010). In the liver, fructose is phosphorylated to fructose-1-phosphate by a fructokinase. Fructose-1-phosphate is then cleaved by an aldolase to generate dihydroxyacetone phosphate (DHAP) and glyceraldehyde, both of which feed into glycolysis via glyceraldehyde 3-phosphate (G3P). DHAP is converted to G3P by triose phosphate isomerase, whilst glyceraldehyde is phosphorylated to G3P by a triose kinase (Figure 5 inset 2). Fructose consumption in healthy humans increased the rates of DNL 2-fold compared to no fructose consumption (Parks et al., 2008). This might explain the fact that fructose consumption correlates with increased levels of obesity, NAFLD and T2DM.

(3) Amino acids

Although amino acids may also provide a potential source of lipogenic acetyl-CoA, studies on how amino acids affect DNL are limited. Catabolism of amino acids feeds into the TCA cycle at different entry points depending on the amino acid. Therefore, in theory amino acids may provide carbon for fatty acid synthesis. However, it is not known whether specific amino acids in excess or high protein feeding can induce DNL in a comparable fashion to carbohydrates. It is well characterised that glutamine and glutamate provide a carbon source for fatty acid synthesis in the context of oncometabolism. Under hypoxic conditions, glutamine undergoes reductive carboxylation to generate citrate for fatty acid synthesis (Metallo et al., 2011). However, it is still unknown whether glutamate can provide a carbon source for fatty acids under physiological conditions. It has more recently emerged that elevated branched chain amino acids (BCAAs) contribute to 25% of lipogenic acetyl-CoA in adipocytes (Figure 5 inset 3; Crown et al., 2015). The BCAAs, leucine, isoleucine and valine, are essential amino acids and account for 20% of protein intake. Increased BCAA levels in the bloodstream have been correlated with insulin resistance and T2DM in humans (Würtz et al., 2012). Deprivation of BCAAs from the diet whilst maintaining levels of other amino acids is sufficient to improve glycaemic control (Xiao et al., 2014). Despite this, high protein/low carbohydrate diets are popular regimes for weight loss in humans and dietary protein has been shown to decrease hepatic lipid accumulation in rodents (Schwarz et al., 2012). Presently, the precise amino acid components that are responsible for these effects, and the extent to which amino acids are able to induce DNL and VLDL secretion are not known.

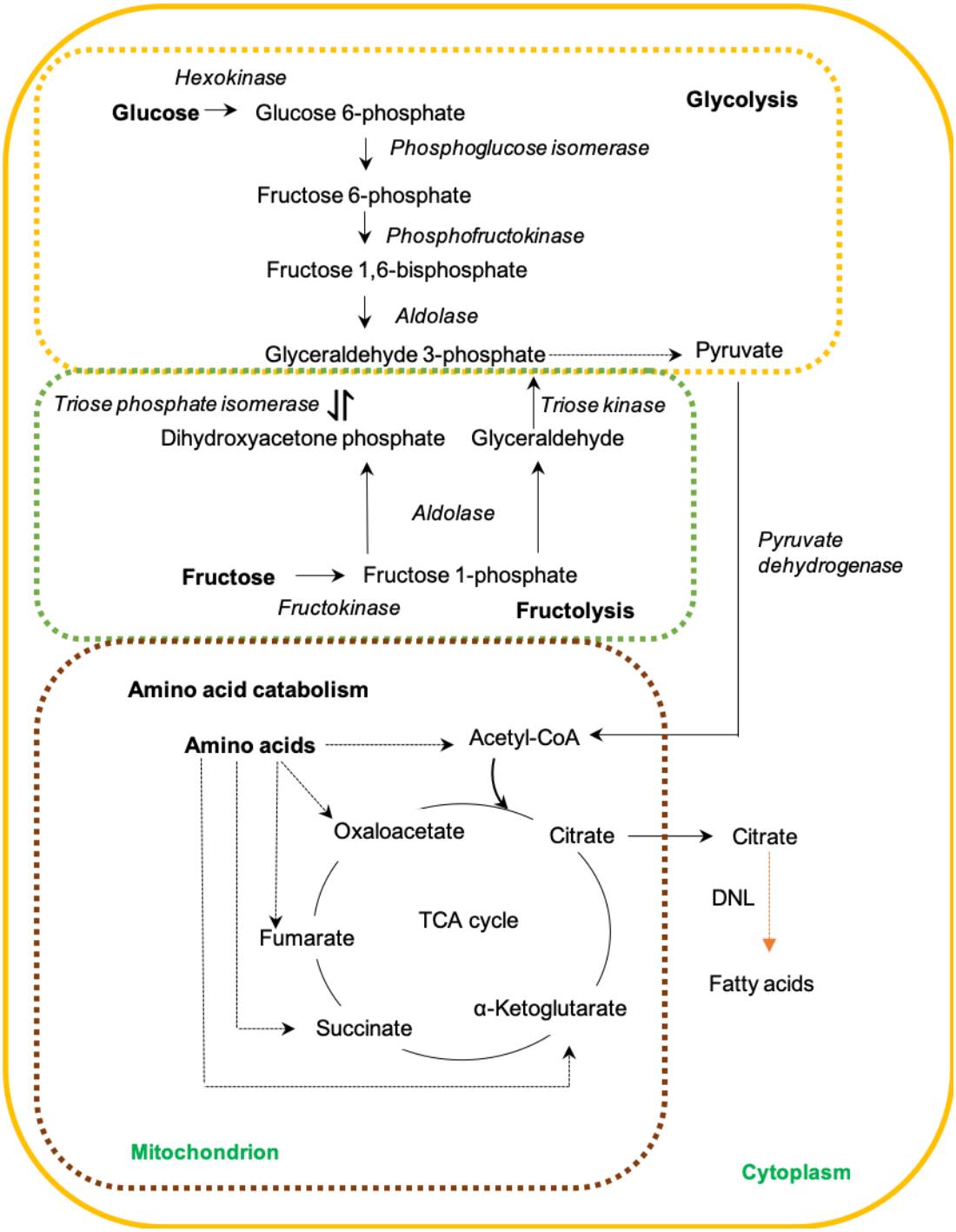

Figure 5. Substrates of *de novo* lipogenesis. (**1**) Glucose undergoes glycolysis to generate pyruvate. Pyruvate enters the mitochondrion to undergo reduction to acetyl-CoA by pyruvate dehydrogenase. (**2**) Fructose feeds the glycolytic pathway at the level of dihydroxyacetone phosphate and glyceraldehyde, both may be converted to glyceraldehyde 3-phosphate by the triose phosphate isomerase and triose kinase respectively. Glyceraldehyde phosphate is then converted to pyruvate through multiple glycolytic reactions. (**3**) Amino acid catabolism feeds into different points in the TCA cycle. During excess macronutrient intake, carbon from glucose, fructose and BCAAs (the contribution is still largely unknown for other amino acids) is incorporated into fatty acids, through the generation of cytosolic acetyl-CoA. TCA cycle, tricarboxylic acid cycle; BCAA, branched-chain amino acids.

1.3 Amino acids and the mammalian target of rapamycin

The mammalian target of rapamycin (mTOR) is a kinase encoded by the *MTOR* gene in humans and is the catalytic subunit of two distinct complexes: mTORC1 and mTORC2. mTORC1 is composed of mTOR, regulatory-associated protein of mTOR (Raptor) and mammalian lethal with SEC13 protein 8 (mLST8) whilst mTORC2 is composed of mTOR, rapamycin-insensitive companion of mTOR (RICTOR) and mammalian stress-activated protein kinase interacting protein 1 (mSIN1; Foster and Fingar, 2010). The mTORC1 kinase has been described as the master regulator of cell growth by sensing nutrients, in particular amino acids (Bar-Peled and Sabatini, 2014). The mechanism of sensing amino acids is complex and still not completely characterised. Amino acids in the lysosomal lumen are sensed by a vacuolar-type H^+- ATPase (v-ATPase; Zoncu et al., 2011). This induces a conformational change in V-ATPase and Ragulator, releasing the guanine nucleotide exchange factor (GEF) activity of Ragulator (Bar-Peled et al., 2012). This results in the conversion of RagA/B into the guanosine-5-triphosphate (GTP)-bound form that recruits mTORC1 to the lysosome, where it interacts with and is activated by Ras homolog, which is enriched in the brain (Rheb; Yao et al., 2017; Figure 6).

The mTORC1 signalling cascade integrates insulin signalling, via its activation by AKT2. The kinase AKT2 regulates the tuberous sclerosis complex (TSC1/2) by phosphorylating TSC2 at multiple sites. This phosphorylation relieves the inhibitory effect of the TSC1/2 complex on Rheb allowing it to activate mTORC1. Phosphorylation of TSC2 impairs the ability of the TSC1/2 complex to act as a GTPase activating protein (GAP) on the GTPase Rheb, therefore allowing GTP-Rheb to activate mTORC1 (Huang and Manning, 2010). Besides mTORC1 being a well characterised amino acid sensor, there is some evidence that mTORC2 is also activated by amino acids (Tato et al., 2011). mTORC2 is also activated by the insulin signalling pathway and in turn activates AKT2. Activation of mTORC1 results in the stimulation of ribosomal protein S6 kinase beta-1 ($p70^{S6K1}$), resulting to the nuclear translocation of LXRα and its heterodimerisation with RXR. The LRXα-RXR complex induces the transcription of

lipogenic genes including SREBP-1c. The mTORC1 kinase also mediates the full maturation of SREBP-1c. Activated $p70^{S6K1}$ also phosphorylates the insulin receptor substrate at multiple serine/threonine residues and directs its degradation. This acts as a negative feedback loop, whereby active $p70^{S6K1}$ attenuates any further activation of the insulin signalling pathway, reducing glucose uptake. Persistent activation of $p70^{S6K1}$ by excessive amino acid concentrations may therefore lead to insulin resistance (Tremblay and Marette, 2001).

These effects have been proved for BCAAs and underlie the molecular basis of insulin resistance and elevated levels of BCAAs. However, the precise effects of other amino acids on DNL and glucose uptake via the mTOR pathway are yet to be fully elucidated.

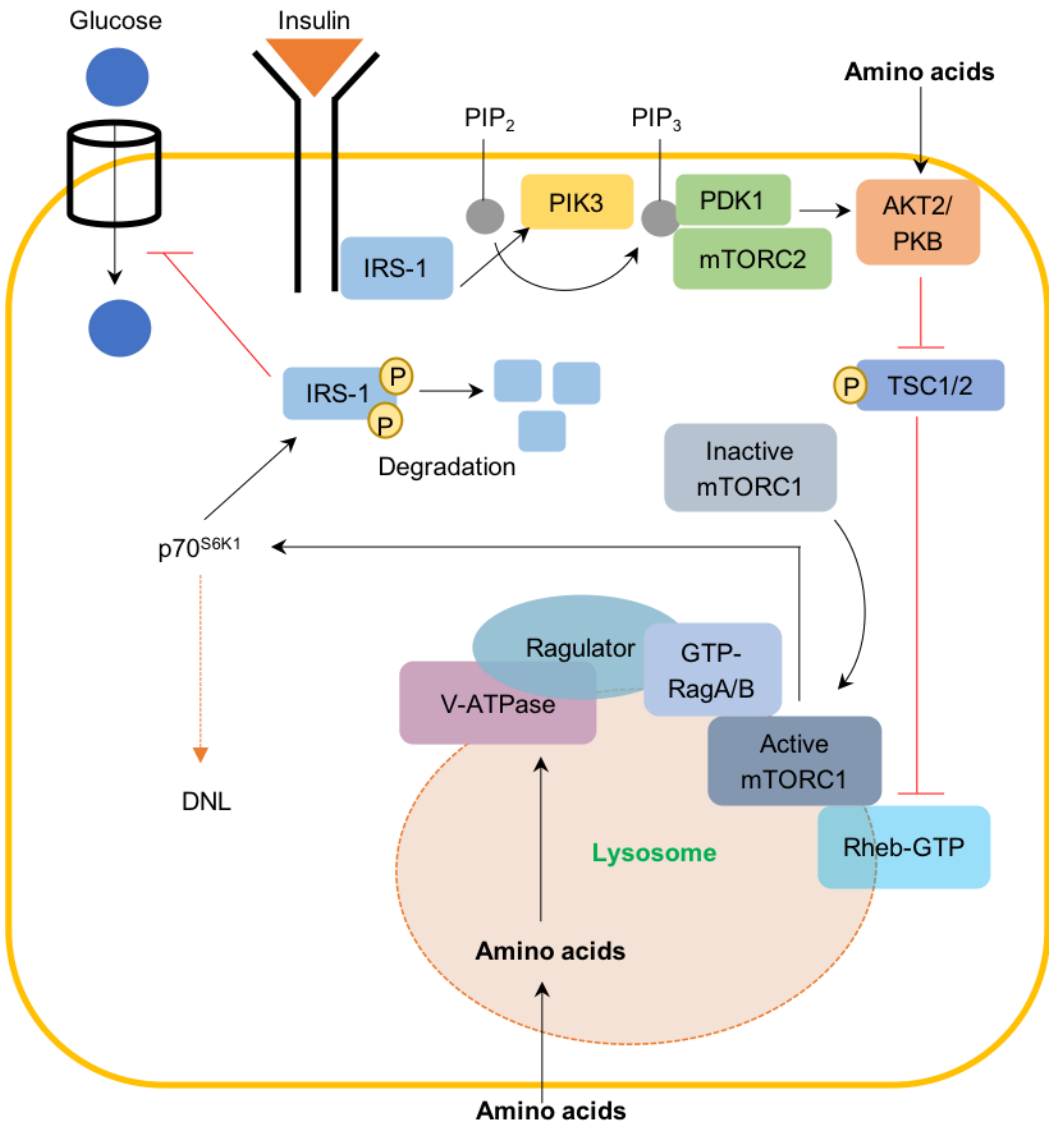

Figure 6. Schematic representation of amino acid activation of mTOR. Amino acids are sensed by V-ATPase in the lysosome, inducing a conformational change in V-ATPase and Ragulator. The GEF activity of Ragulator results in a GTP-bound RagA, which recruits mTORC1 to the lysosomal membrane where it is activated by Rheb. Amino acids may also activate AKT2, which phosphorylate and relieves the inhibition of the TSC1/2 complex on Rheb, allowing Rheb to activate mTORC1. Activated mTORC1, induces the kinase $p70^{S6K1}$, which results in the induction of the expression of genes required for DNL. Activated $p70^{S6K1}$ also phosphorylates IRS-1 at multiple serine residues targeting it to degradation and therefore decreasing glucose uptake. v-ATPase, vacuolar-type H^+-ATPase; Rheb, Ras homolog enriched in brain; TSC1/2, tuberous sclerosis complex; mTORC1, mammalian target of rapamycin complex 1; $p70^{S6K1}$, ribosomal protein S6 kinase beta-1; IRS-1, insulin receptor substrate 1.

1.4 Thesis aims and overview

The latest nutrition transition from traditional diets to Western-style diets, high in sugars, fats and protein from red meat, have led to the growing prevalence of obesity and the metabolic syndrome (Popkin, 2006). In particular, the increasing consumption of liquid carbohydrate in the form of sugary beverages coincides with the increasing incidence of the metabolic syndrome over the last 20 years (Sartorius et al., 2016). Based on a previous study performed in our group, it is hypothesised that liquid carbohydrate reaches chemoreceptors in the intestine faster, inducing a postprandial neurohormonal delay in the gastrointestinal motility of the solid phase. In addition, this increased load of carbohydrate might induce lipogenesis and therefore provide a possible mechanism to explain how liquid carbohydrate links with the metabolic syndrome.

In chapter 3, a human intervention study is used to characterise the effect of changing solid/liquid ratio of isoenergetic meals on gastric emptying and how different macronutrient compositions affect DNL. Nine subjects consumed the five randomised meals (containing ^{13}C-octanoic acid in the solid phase of the meal): Control with Bread (CB) and four other meals in which carbohydrate was solely from orange juice - Control (C, without bread), High Fat (HF), High Carbohydrate (HC) and High Protein (HP), in a randomised order. The ^{13}C-enrichment in breath exhalates was measured by isotope ratio-mass spectrometry to determine the gastric emptying rate of each individual after every meal. In addition, the plasma profile of each subject was analysed by liquid chromatography mass spectrometry (LC-MS) to determine how different macronutrient compositions affect DNL, using the metric of the scTAG cluster.

Chapter 4 investigates the underlying mechanism of the increase in lipogenic triacylglycerides caused by a high protein meal rich in glutamate. As liver is the primary site of DNL, Alpha mouse liver 12 (AML12) hepatocytes were utilised to examine whether glutamate may (1) provide carbon for fatty acid synthesis and (2) induce DNL. Under normal physiological conditions carbohydrates act as the canonical source of substrate for DNL. However, the

contribution of amino acids, derived from protein-rich diets, is less well understood beyond the context of oncometabolism. To determine whether glutamate can act as a substrate for DNL under conditions of typical carbohydrate supply, AML 12 hepatocytes were supplemented with $^{13}C_5$-labelled glutamate, one of the most abundant dietary amino acids, to trace its metabolic fate. In addition, AML 12 hepatocytes were supplemented with increasing doses of the glucogenic amino acid, glutamate, to assess whether it can activate AKT2 and $p70^{SK61}$, key kinases of the insulin signalling cascade. This leads to the expression of SREBP-1c to induce the expression of genes required for DNL and therefore increase fatty acid synthesis.

The final chapter examines the extent to which this induction in DNL is a response of a general amino acid increase or whether it is amino acid specific. Studies have previously demonstrated that a higher protein/lower carbohydrate diet downregulates DNL, typically in longer-term dietary interventions (Schwarz et al., 2012). In this chapter, hepatocytes are supplemented with glucogenic, ketogenic and BCAAs to investigate whether they can induce DNL at a gene expression, protein translation/activity and metabolic level, making use of the scTAG cluster as an indicator of rates of DNL.

Chapter 2. General methods and materials

The methods described in the present chapter are used throughout the thesis. Methods specific to Chapters 3, 4 and 5, may be found in the appropriate section of each chapter. The supplier of the materials used is specified in the relevant section.

2.1 Measurement of metabolite levels by mass spectrometry

2.1.1 Metabolite extractions

Metabolites were extracted from blood plasma or cells using a modified method of Folch and colleagues (Folch et al., 1957). Briefly, 15 µL of blood plasma or pelleted cells were mixed with chloroform/methanol (2:1, v/v, 750 µL); including a mixture of deuterated internal standards (Table 1). Samples were sonicated for 15 min and water was added (300 µL). Samples were then centrifuged at 13,000 x g for 20 min. The organic (upper layer) and aqueous (lower layer) phases were separated. The organic phase extracts containing lipids were dried under a stream of nitrogen gas whilst the aqueous samples were dried in a CentriVap Centrifugal Concentrator with attached cold trap (78100 series, Labconco Co, Kansas City, USA).

Table 1. Internal standards used for LC-MS of the organic phase.

Internal Standard	Supplier
18:0-d6 CE	QMX
C16-d31 Ceramide	AVANTI
15:0-d29 FA	QMX
17:0-d33 FA	QMX
20:0-d39 FA	QMX
14:0-d29 LPC-d13	QMX
16:0-d31-18:1 PA	AVANTI
16:0-d31-18:1 PC	AVANTI
16:0-d31-18:1 PE	AVANTI
16:0-d31-18:1 PG	AVANTI
14:0 PS-d54	AVANTI
16:0-d31 SM	AVANTI
45:0-d29 TAG	QMX
48:0-d31 TAG	QMX
54:0-d35 TAG	QMX

2.1.2 Analysis of intact lipids using orbitrap mass spectrometry

The organic fraction was reconstituted in 100 µL chloroform/methanol (1:1, v/v), and 10 µL of the resulting solution added to 90 µL isopropanol (IPA)/acetonitrile (ACN)/water (2:1:1, v/v). Analysis of the fractions was performed using an LTQ Orbitrap Elite Mass Spectrometer (Thermo Scientific, Hemel Hempstead, UK). In positive mode, 5 µL of sample were injected onto a C18 CSH column, 1.7 µM pore size, 2.1 mm x 50 mm, (Cat # 186005296, Waters Ltd, Manchester, UK) which was held at 55°C in a Dionex Ultimate 3000 ultra-high performance liquid chromatography system (UHPLC; Thermo Scientific). A gradient (flow rate 0.5 mL/min) of mobile phase A (ACN/water 60:40, 10 mmol/L ammonium formate) and B (LC–MS-grade ACN/IPA 10:90, 10 mmol/L ammonium formate) was used. In negative ion mode, 10 µL of the sample was injected and 10 mmol/L ammonium acetate was used as the additive to aid ionisation. In both positive and negative ion mode, the gradient began at 40% B, increased to 43% B at 0.8 min, 50% B at 0.9 min, 54% B at 4.8 min, 70% B at 4.9 min, 81% B at 5.8 min, peaked at 99% B at 8 min for 0.5 min, and subsequently returned to the starting conditions for another 1.5 min to re-equilibrate the column. The UHPLC was coupled to an electrospray ionisation (ESI) source which ionised the analytes before entering the mass spectrometer. Data were collected in both positive and negative ion mode with a mass range of 110–2000 *m/z*. Default instrument-generated optimisation parameters were used (Table 2). Tandem MS was performed, using normalised collision energy, to fragment intact lipids listed in Table 3, in order to identify the fatty acyl chains contained within. Xcalibur Software (Thermo Scientific) was used to identify peaks and process mass spectra.

Table 2. Mass spectrometer optimised settings for intact lipids.

Instrument Optimisation Parameters	
Method Duration (min)	10
Ion Source Type	H-ESI
Ion Spray Voltage: Positive Ion (V)	3500
Ion Spray Voltage: Negative Ion (V)	2500
Sheath Gas (Arb)	20
Sweep Gas (Arb)	5
Capillary Temperature (°C)	380
Source Heater Temperature (°C)	420
Column Temperature (°C)	55

Table 3. scTAG species. These TAGs contain main products of DNL including, FA 16:0, 16:1, 18:0 and 18:1.

Triglyceride	Product ion $[M+NH_4]^+$
TAG 46:2	792.7076
TAG 46:1	794.7232
TAG 46:0	796.7389
TAG 48:2	820. 7389
TAG 48:1	822.7545
TAG 48:0	824.7702
TAG 49:2	834.7545
TAG 49:1	836.7702
TAG 49:0	838.7858

A typical total ion chromatogram (TIC) obtained by this method is illustrated by Figure 1. TAGs eluted with a long retention time because they contain three fatty acids, making them less polar compared to phospholipids or lysophospholipids that have 2 and 1 fatty acid chains, respectively, as well as a more polar head group. scTAGs (Figure 2) were selected for fragmentation. This was achieved by applying collision energy to the mass of the selected precursors listed in Table 3. The fragments were used for identification. For instance, *m/z* 551.49 is a DAG fragment specific to TAG 48:0 containing three palmitic acids (Figure 3).

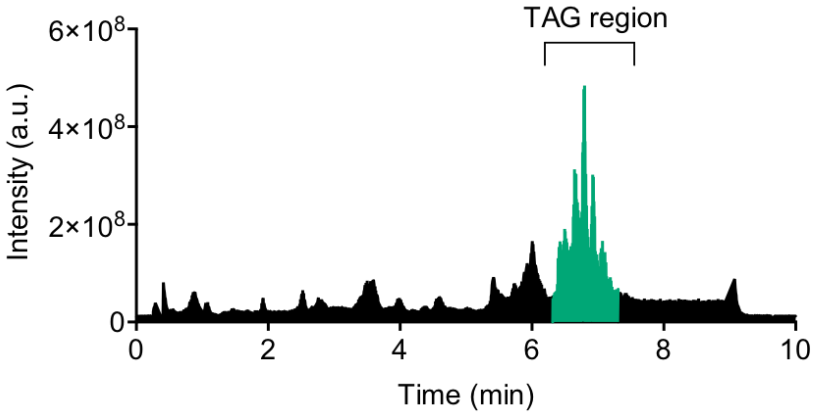

Figure 1. TIC of the intact lipids detected using UHPLC. Different lipid classes elute at different time points based on their polarity. In reverse phase chromatography, polar metabolites retain less on the stationary phase of the column because of the polarity of the starting solution, and therefore elute first. In green is the TAG region which was analysed.

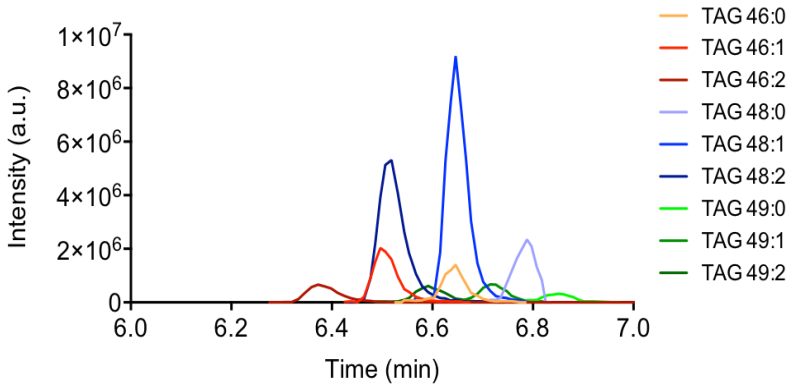

Figure 2. Extracted ion chromatogram (EIC) of scTAGs. TAGs with longer fatty acids eluted later, while TAGs with double bonds eluted earlier.

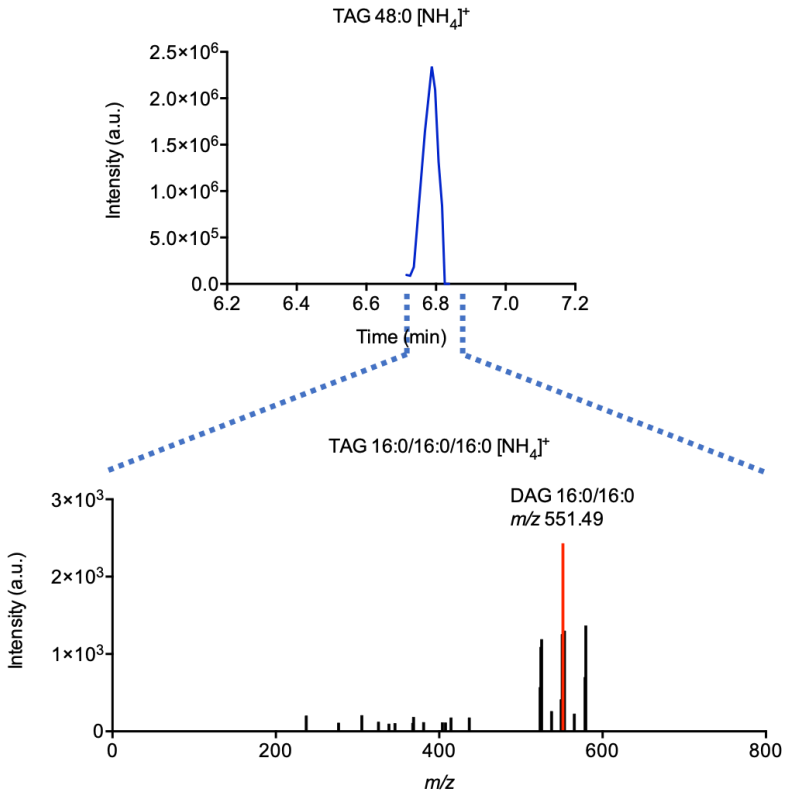

Figure 3. Collision-induced dissociation mass spectrum. The identification mass spectrum was acquired by applying collision energy to the mass of the selected precursors (listed in Table 3). This specific example illustrates the fragmentation pattern of TAG 48:0 at *m/z* 824.7702. The precursor was fragmented to give the DAG fragment at *m/z* 551.49, which is typical of a TAG containing three palmitic acids.

2.1.3 Picolinyl esters of fatty acids (PEFA) derivatisation for LC-MS

The derivatisation procedure was modified from Li and Franke, 2011. To each dried organic extract 200 µL of 10 µmol/L deuterated internal standard mix were added and dried completely under nitrogen. Each sample was resuspended in 200 µL of 2 mol/L oxalyl chloride in dichloromethane (DCM; Cat. # 310670, Sigma), capped securely, and then incubated at 65°C in a heating block for 10 min; achieving cleavage of fatty acids from complex lipids and activating the carboxylic group. Samples were then dried under nitrogen and washed with 200 µL DCM (Cat. # 270997, Sigma) and re-dried. Each dried residue was then resuspended in 150 µL of 1% 3-hydroxymethylpyridine (Cat. # P66807, Sigma) in ACN and incubated at room temperature for 5 min to give derivatised fatty acids. Samples were dried under nitrogen,

washed with 200 µL dichloromethane to ensure unreacted 3-hydroxymethylpyridine was evaporated, dried under nitrogen once more and stored at -80 °C until analysis.

2.1.4 Analysis of total fatty acids by triple quadrupolar mass spectrometry

PEFAs were reconstituted in 100 µL 2:1 (v/v) methanol:water and sonicated for 15 min. Samples were then centrifuged for 15 min at 13,000 x g to pellet any remaining debris. A 2 µL injection volume of the resulting solution was analysed on a TSQ Quantiva™ Triple Quadrupole mass spectrometer attached to a Vanquish UHPLC system (Thermo Scientific). Chromatographic separation was achieved on an Acquity UPLC BEH C18 1.7 µm x 2.1 mm x 50 mm column (Cat # 186002350, Waters). Mobile phase A was 100% water with 0.1% formic acid and mobile phase B was 50:50 ACN:IPA with 0.1% formic acid. The chromatography gradient started at 30% B for 2.33 min, increased to 100% B over 1.34 min and decreased to 30% B for 1.23 min (to re-equilibrate the column) at a flow rate of 0.735 mL/min. Default instrument-generated optimisation parameters were used (Table 4). Xcalibur Software (Thermo Scientific) was used to identify peaks, process mass spectra and normalise data to the closest-eluting internal standard. A typical TIC of PEFAs obtained by the above method is shown in Figure 4A. The TIC was used to extract fatty acids: 16:0 and 16:1 (Figure 4B) as well as 18:0, 18:1 and 18:2 (Figure 4C).

Table 4. Mass spectrometer optimised settings for PEFAs.

Instrument Optimisation Parameters	
Method Duration (min) Ion Source Type Ion Spray Voltage: Positive Ion (V) Sheath Gas (Arb) Sweep Gas (Arb) Ion Transfer Tube Temperature (°C) Vaporiser Temperature (°C) Column Temperature (°C)	5 H-ESI 3500 55 2 356 365 55
Needle Wash	1:1 (v:v) IPA:CAN
Seal Wash	4:1 (v:v) IPA:Water with 0.1% formic acid

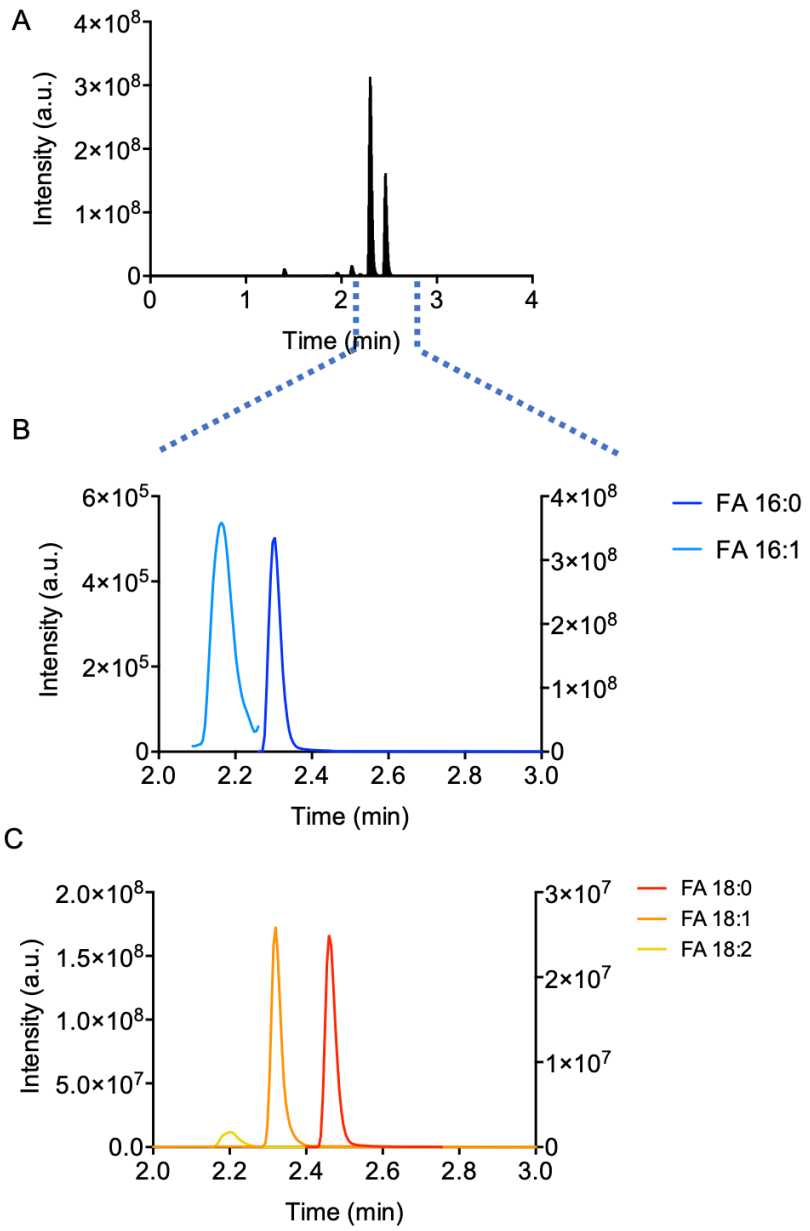

Figure 4. TIC and EIC for PEFAs. (**A**) The TIC of all PEFAs detected by LC-MS. (**B**) The EIC for the peaks at *m/z* 348.36 (FA 16:0) and 346.33 (FA 16:1). FA 16:1 is plotted on the left y-axis and FA 16:0 is plotted on the right. (**C**) The EIC for the peaks at *m/z* 376.40 (FA 18:0), 374.36 (FA 18:1) and 372.33 (FA 18:2). FA 18:1 and FA 18:2 are plotted on the left y-axis and FA 18:0 is plotted on the right. All peaks had a daughter ion at *m/z* 92.11, corresponding to a loss of the group added by derivatisation.

2.2 Statistical analysis

2.2.1 Univariate statistics

Data were visualised using GraphPad (GraphPad Prism 5.2; GraphPad Software, San Diego, CA, USA). All data are expressed as means ± the standard error of the mean (SEM). In GraphPad, one-, two-way analysis of variance (ANOVA) or two-tailed t-test were performed where appropriate to determine significant differences between experimental groups. For one-way ANOVA, Tukey's *post-hoc* multiple comparison test was performed, whilst for two-way ANOVA, Sidak's *post-hoc* multiple comparison test was used. For the human study analyses were paired whilst for the cell culture studies, analyses were unpaired. Differences between experimental groups were considered to be statistically significant when $p \leq 0.05$.

Chapter 3. The effects of diet on gastric emptying and the blood lipidome

Abstract

Abnormally delayed gastric emptying in the absence of mechanical impediment is common among patients with longstanding type 2 diabetes mellitus. Hyperglycaemia, increased blood glucose levels, damages the vagus nerve and results in dysregulated gastric emptying that can further affect glucose and lipid metabolism. The present study aimed to define, in healthy human males, how solid/liquid ratios of meals and macronutrient compositions affect gastric emptying and lipid metabolism. After a 12-hour fast, subjects (n=9) consumed each of five randomised meals containing ^{13}C-octanoic acid in the solid phase. A standardised 2 MJ control meal with bread was modified to contain purely liquid carbohydrate. This was further altered to provide isoenergetic meals high in fat, protein and carbohydrate. ^{13}C-enrichment in breath exhalates, measured by isotope ratio-mass spectrometry, demonstrated that liquid carbohydrate was the main determinant of gastric emptying and it delayed the motility of the solid phase of the food. The liquid carbohydrate meal was not sufficient to induce *de novo* lipogenesis. However, the high protein meal, rich in glutamate, increased plasma triacylglycerides (measured by liquid chromatography-mass spectrometry) associated with *de novo* lipogenesis and in liver-secreted lipoproteins. This may implicate glutamate, and/or other amino acids, which are not obvious precursors of fat, in the process of *de novo* lipogenesis under physiological conditions following a high protein meal.

3.1 Introduction

3.1.1 Gastric emptying

Approximately 50-75% of diabetic patients suffer from diabetic dyslipidaemia related to diabetic hyperglycaemia and insulin resistance. Diabetic dyslipidaemia is characterised by increased levels of TAGs, VLDL and decreased levels of HDL (Goldberg, 2001). In addition, approximately 30-50% of diabetics experience delayed gastric emptying, known as gastroparesis diabeticorum (Samsom et al., 2009). This patient group may reflect the possible relationship between lipids, lipoprotein metabolism and gastric emptying (Horowitz et al., 2002).

Gastric emptying is the complex process by which food leaves the stomach and enters the duodenum, the first part of the small intestine. Firstly, the proximal stomach (comprising the first three parts of the stomach; cardia, fundus, and body) relaxes to accommodate large volumes of food. Food then arrives in the antrum, the first part of the distal stomach, where it is mixed with gastric juices to aid digestion. The chyme, containing gastric juices and semi-digested food, is then pumped by peristaltic pulses across the pylorus, the last part of the distal stomach. Subsequently, the pyloric sphincter opens allowing the chyme to enter the duodenum (Marathe et al., 2013).

Gastric emptying is organised by the motor activity of both the stomach and small intestine, which are determined by spontaneous electrical slow waves generated by the interstitial cells of Cajal. These activities are thought to be regulated by a feedback mechanism whereby the nutrient density is sensed by receptors in the small intestine, inducing the release of neuronal and hormonal signals back to the stomach to control gastric emptying (Williams et al., 2016). These signals consist of the stimulation of the vagus nerve and secretion of gut hormones, such as GLP-1, CCK and PYY (Ronveaux et al., 2015). Other factors that influence gastric emptying include the total meal energy content, meal weight, volume, macronutrient

composition (the percentage of fat, carbohydrate and protein), fibre content, pH and temperature (Chaw et al., 2001; Clegg and Shafat, 2010).

3.1.2 Liquid carbohydrate and gastric emptying

A variety of studies examining the effect of macronutrient composition on the rate of gastric emptying conclude that high fat and high carbohydrate diets delay gastric emptying. There is evidence that high fat diets induce this via the redistribution of stomach contents from the distal stomach back into the proximal stomach (Houghton et al., 1990). It is also reported that as the carbohydrate content increases, gastric emptying of the meal slows (Calbet and MacLean, 1997). However, unpublished data collected at the MRC-EWL unit appears contradictory in this regard (Bluck, Griffin & Li personal communication). A C meal (15% protein, 40% fat, 45% carbohydrate) was altered to create HF, HC and HP meals. All three meals had a more rapid gastric emptying rate compared to C with no significant differences in gastric emptying between the three altered meals (Figure 1). The possible reason for this disagreement is that the carbohydrate content of the C meal was in liquid form (624 kJ in the form of orange juice, compared with 85-430 kJ in the others). Therefore, it is conceivable that the liquid form of carbohydrate (above ~500 kJ in this phase) might empty from the stomach more rapidly, reaching chemoreceptors in the small intestine inducing the release of signals back to the stomach to delay the motility of the solid phase. Other data is also supportive in that increasing the amount of carbohydrate, especially glucose in a liquid meal, inhibits gastric emptying (Brener et al., 1983). Delayed gastric emptying may alter nutrient absorption and induce changes in glucose and lipid metabolism. These changes can potentially predispose individuals to insulin resistance, dyslipidaemia and diabetes.

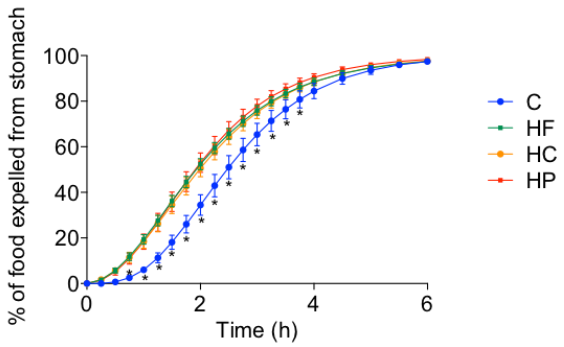

Figure 1. Gastric emptying rate is delayed in C. Gastric emptying rate as a percentage of food expelled from stomach over 6 h after C (blue), HF (green), HC (orange) and HP (red) meal. Data are presented as mean ± SEM and analysed by two-way repeated measures ANOVA with *post-hoc* Sidak's multiple comparisons test; * = $p \leq 0.05$, n=12/group (Bluck, Griffin & Li unpublished data).

3.1.3 Carbohydrate and *de novo* lipogenesis

In the liver, energy balance is maintained by the dynamic partitioning of carbon units between carbohydrate, lipid synthesis and oxidation. During fasting, there is an increase in fatty acid β-oxidation. These fatty acids are supplied by the process of lipolysis in white adipose tissue, in the form of non-esterified fatty acids (NEFAs). Fatty acid oxidation generates ATP and reducing intermediates, which may be oxidised further or utilised in the generation of glucose via gluconeogenesis. Acetyl-CoA, generated from β-oxidation, may be used in the TCA cycle to regenerate citrate, or instead to produce ketone bodies (Jones, 2016; Jones et al., 2001). However, during feeding, the liver receives a plethora of macronutrients (glucose, amino acids and fatty acids), via the portal vein. The portal vein transports approximately 15-30% of glucose from the digestive tract to the liver. Glucose undergoes glycolysis, and results in increased acetyl-CoA, the primary substrate of DNL (Guo et al., 2012). Dietary glucose as well as fructose stimulate DNL, through increased availability of acetyl-CoA. Consequently, liquid carbohydrate that empties the stomach faster (approximately 80% of the liquid fraction is emptied before the solid fraction; Phillips et al., 2015) might increase the rate of DNL. The initial reaction for the production of fatty acids from acetyl-CoA is its condensation with oxaloacetate to produce citrate, catalysed by CS in the mitochondria (Tappy and Lê, 2012). Citrate is then shuttled from the mitochondrial matrix to the cytosol, whereupon it is cleaved by ACL in the reverse reaction,

regenerating oxaloacetate and acetyl-CoA. Acetyl-CoA is carboxylated by cytosolic ACC, itself allosterically activated by high concentrations of citrate found during positive energy balance. Malonyl-CoA, the product of this reaction, is the subunit from which FAS may generate new fatty acids. Malonyl-CoA is also a highly potent inhibitor of CPT1, the enzyme which facilitates the entry of fatty acids into the mitochondrion to undergo β-oxidation. In this manner, malonyl-CoA prevents the futile metabolic cycle of newly generated fatty acids being utilised to produce acetyl-CoA via β-oxidation. The fatty acids produced by FAS (typically the 16-carbon palmitic acid) may then be modified by the elongase, ELOVL6 and/or desaturated by SCD1). The processed fatty acids are subsequently esterified to glycerol to produce TAGs and incorporated into VLDL for export (Berg, Tymoczko and Stryer, 2002; Figure 2).

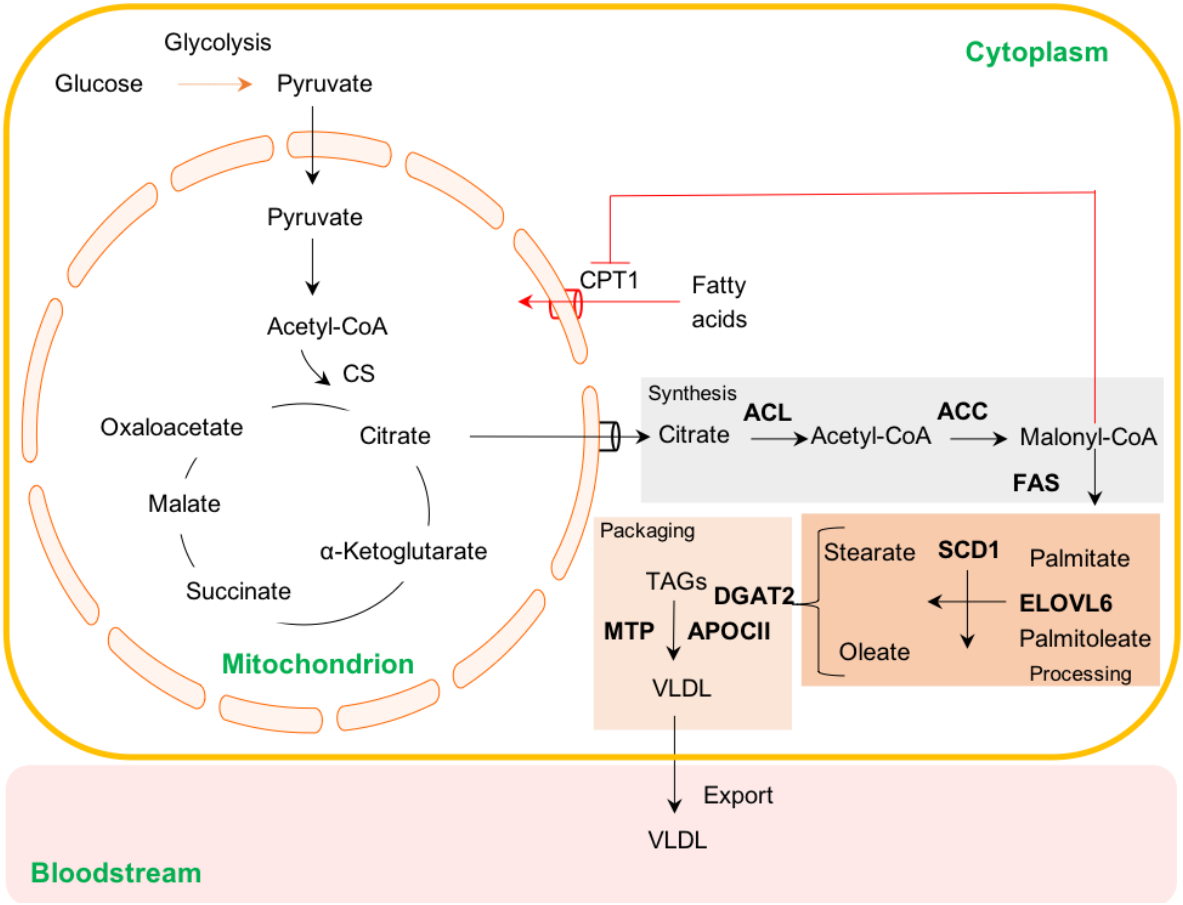

Figure 2. Schematic representation of DNL induction by glucose. Pyruvate from glucose, generated via glycolysis, enters the TCA cycle in the mitochondrion. There, pyruvate is oxidised to acetyl-CoA. Acetyl-CoA and oxaloacetate condense to make citrate, via CS. Citrate is then shuttled to the cytosol where it is cleaved by ACL to generate cytosolic acetyl-CoA. Cytosolic acetyl-CoA is then carboxylated by ACC to malonyl-CoA. Malonyl-CoA is the working unit of FAS that synthesises palmitate. Palmitate may then be desaturated or elongated by SCD1 or ELOVL6 respectively. Fatty acids are esterified to glycerol to form TAGs in a series of reactions with the last one catalysed by DGAT2. TAGs are transported through the intracellular membranes by the MTP and associate with ApoCIII to form VLDL. VLDL particles are then exported into the circulation for transport to other cells.

3.1.4 Specific TAGs and DNL

Increased hepatic DNL contributes to lipid accumulation in patients with insulin resistance and NAFLD (Bhat et al., 2012). Patients with lipodystrophy also present elevated levels of DNL and hepatic lipid accumulation. In addition, this group of patients demonstrate a significant increase in VLDL particles containing TAG 46:1, TAG 48:0 and TAG 48:1 compared to controls, suggesting a possible link between DNL and this group of TAGs (Lee et al., 2015). Indeed, the monounsaturated fatty acid palmitoleate in VLDL-TAGs has been characterised as a marker of increased DNL and NAFLD (Eiden et al., 2015). In the AusDiab cohort, the metabolic phenotype of 11,247 people was assessed biomedically and with anthropometric measurements. Around 6500 of these people came back for a follow up to track the changes of the incidence and progression of diabetes. TAGs containing monounsaturated fatty acids correlated with pre-diabetes in the AusDiab cohort (Wong et al., 2013). Moreover, in the Fenland cohort, whereby the metabolic health, diet, other lifestyle factors, body composition and physical activity of approximately 12,500 people were assessed, a group of scTAGs containing FA 16:0, 16:1, 18:0 and 18:1 were linked with DNL and steatosis (Sanders et al., 2018). In healthy humans, the amount of *de novo*-produced TAG incorporated in VLDL is minimal (below 5%; Timlin and Parks, 2005). However, in hyperinsulinaemic individuals with NALFD, DNL derived TAG content increases to 26% (Donnelly et al., 2005). Furthermore, in healthy human subjects, feeding with a high carbohydrate meal is sufficient to increase DNL derived TAG content to 23% (Timlin and Parks, 2005).

3.2 Chapter aims

In this chapter a human dietary intervention study is used to test the hypothesis that carbohydrate in the liquid form delays gastric emptying and induces DNL in healthy adult males. In this study, we use the non-invasive ^{13}C-octanoic acid breath test (OBT) to measure gastric emptying, and LC-MS to characterise the plasma TAG profile. Moreover, the study aims to define the main determinant of gastric emptying in relation to the solid/liquid ratio and macronutrient composition, as well as to characterise the contribution of macronutrients to DNL, using the metric of the scTAG cluster as a measure of DNL activity.

3.3 Materials and methods

3.3.1 Clinical protocol

General design

The protocol of the present study was approved by both the internal research review board of MRC-EWL and the Cambridge South Local Research Ethics Committee, UK (Ref no.: 15/EE/0232). The study was divided into the following sections: (1) recruitment (2) pre-screening questionnaire and screening visit and (3) five separate study days (Figure 3). Nine participants took part in a randomised, five-way crossover study. Each participant had a screening visit, followed by five trial visits separated by at least a two-week washout period. Twenty-four hours before each trial day, the diet and activity of each participant was monitored. On the trial day, participants attended MRC-EWL for 7 h and received one of the five isoenergetic mixed meals in a randomised order. The five isoenergetic meals comprised of: Control with Bread (CB) and four other meals in which carbohydrate was solely from orange juice - Control (C, without bread), High Fat (HF), High Carbohydrate (HC) and High Protein (HP).

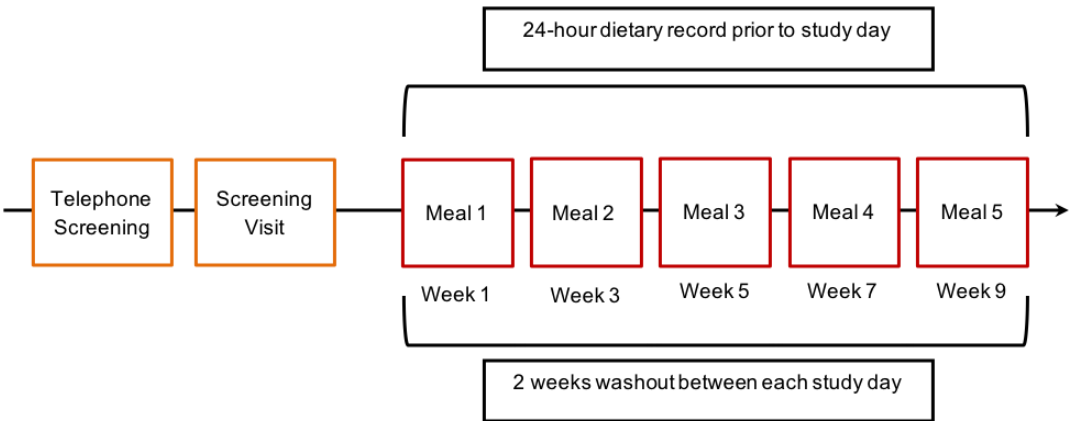

Figure 3. General study design. The study was divided into three sections: recruitment, screening (orange boxes) and five separate study days (red boxes). There was a minimum of two-week washout between each study day. The diet and activity of each volunteer was monitored.

Volunteer recruitment and screening

Nine healthy, non-smoking men aged 19 to 29 years with a BMI between 18.9 and 27.5 kg/m^2 were recruited. The sample size calculation is summarised in Appendix I A. Only men were recruited due to the large difference between the lipid profiles of men and pre-menopausal women arising from different sex hormones, which are important regulators of lipid metabolism (Varlamov et al., 2015). All participants were recruited through contact with companies, universities and colleges via letters and email, distributing leaflets in offices, shops and local residential areas, displaying posters on local community notice boards and from the volunteer database held at MRC-EWL. An information sheet was provided to men who were interested in participating. Subjects who showed interest were assessed by the pre-screening questionnaire in the first instance. Volunteers that fulfilled the inclusion criteria were invited to the MRC-EWL suite for the screening visit.

Screening visit

Participants were requested to complete a 24-hour food diary. After an overnight 12-hour fast, participants attended MRC-EWL. During the screening visit, the study process was described to the participant, giving them the opportunity to ask any questions. Participants were requested to read and sign the informed consent form. Subsequently, anthropometric measurements (weight, height, blood pressure) and a fasting blood sample were taken. The fasting blood sample was taken by venepuncture for analysis of full blood count, liver function, glucose, insulin and lipid profile, including total cholesterol, HDL, LDL and triacylglycerides. These measurements were used to determine whether participants met the inclusion criteria (Appendix I B) of the study.

Study day protocol

Participants arrived at the MRC-EWL Volunteer Suite in the morning after a 12-hour overnight fast. The 24-hour food diary for the day before was requested from the volunteers. Upon arrival, participants were cannulated via the antecubital vein of one arm and two basal breath and blood samples were collected, 10 min apart. Participants then consumed, within 15 min of onset of eating, one of the five isoenergetic mixed meals containing 100 µL [1-^{13}C]-octanoic acid (Figure 4, 0 h). Subsequently, blood and breath samples were collected over a six-hour period. During the six-hour period, food consumption was not allowed, and only water was permitted ad libitum after 3 h had elapsed. Breath samples (22 samples per participant; blue arrows) were collected every 15 min in the first 4 h and every 30 min in the following 2 h (Figure 4). Blood samples were collected at 12 time points at various intervals throughout the 6-hour period (238 mL blood in total; red arrows). The cannula was cleared with 2 mL isotonic saline (0.9% NaCl) after every blood sample. Finally, the cannula was removed from the participant after all blood samples were collected, allowing them to depart. Blood sample collection was performed by Matthew Harvey.

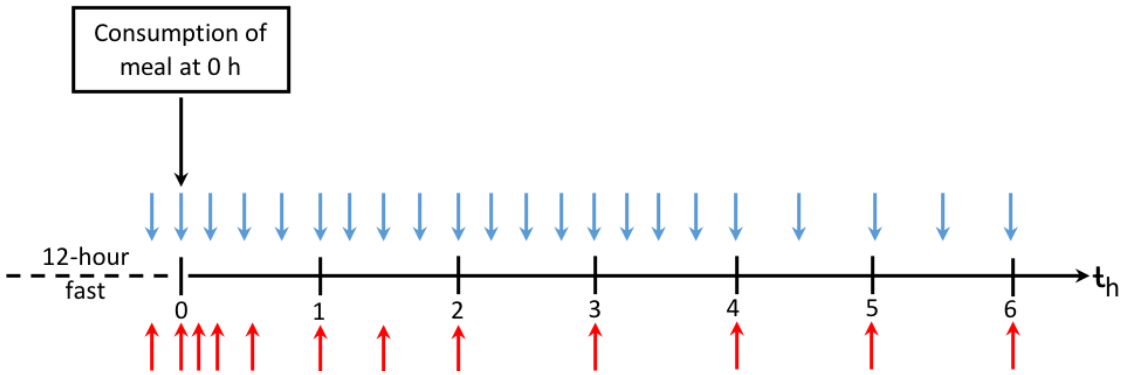

Figure 4. Breath and blood sampling time points. The blue arrows indicate the breath sampling points and the red arrows indicate the blood sampling points. At t=0 h the participants consumed one of the five isoenergetic mixed meals containing 100 µL ^{13}C-octanoic acid.

3.3.2 Analytical protocol

Test meals

All test meals consisted of eggs, butter and orange juice. The CB meal also had white bread, while soy protein powder (rich in glutamate) was added to obtain the HP meal. The detailed meal compositions are shown in Appendix II A. The egg yolk was labelled with 100 µL [1-^{13}C]-octanoic acid (C/D/N Isotopes Inc., Quebec, Canada). A detailed procedure of the food preparation is described in Appendix II B. The ingredient compositions were modified so that on each study day the volunteer consumed a 2 MJ meal (Table 1). The detailed fatty acid and amino acid composition of meals are shown in Appendix II C and II D respectively. The compositions of the meals are compared to the Dietary reference values (DRVs) of the UK Department of Health and European Food Safety Authority (EFSA) as well as to previous studies (Appendix II E).

Table 1. Test Meal Compositions.

	Protein (%)	Fat (%)	Carbohydrate (%)	Volume (Orange juice/mL)
Control with bread (CB)	15	40	45	365
Control without bread (C)	15	40	45	556
High Fat (HF)	14	62	24	271
High Carbohydrate (HC)	14	26	60	681
High Protein (HP)	32	33	35	414

^{13}C-Breath test (sample collection and analysis)

Isotopic enrichment of ^{13}C in breath samples was analysed by continuous flow (CF) isotope ratio mass spectrometry (IRMS; AP2003 IRMS, Analytical Precision Ltd, Northwich, Cheshire, UK). The CF-IRMS was calibrated against a reference gas and the results were expressed as a percentage relative to the primary standard, Pee Dee Belemnite (PDB). The baseline-

corrected ^{13}C-enrichment values were fitted to an established gastric emptying model to derive the lag time (T_{lag}, the time taken to maximal $^{13}CO_2$ excretion), and half excretion time (T_{half}, time taken for 50 % of the total ^{13}C excreted to appear in the breath). This analysis was performed by Elise Orford at the MRC EWL.

Blood sampling

Samples collected during the screening visits were analysed by the Pathology Partnership (Addenbrooke's Hospital, Cambridge, UK). Glucose and insulin concentrations were quantified, and a full blood count, full lipid profile and liver function tests were performed. On the study days, fresh blood was drawn into a vacutainer serum separator tube containing either K_2-EDTA or lithium heparin, depending on the analysis to be performed (Table 2). Samples in K_2-EDTA were centrifuged immediately after collection at 4°C at 8000 x g for 20 min whilst samples in lithium heparin were kept on ice for 30 min before centrifugation in the same conditions.

Table 2. Human samples analyses.

Vacutainer serum separator tube type	Analysis
K_2-EDTA	Lipidomics and VLDL/LDL
Lithium heparin	Insulin concentration

Insulin quantification

Insulin levels were measured using chemiluminescence immunoassay on a Diasorin Liaison XL AutoAnalyser (Diasorin S.p.A, Saluggia, Italy) by the Pathology Partnership (Addenbrooke's Hospital, Cambridge, UK). The working range of the assay was 3 - 3000 pmol/L (fasting adult 'normal range' for insulin is up to 80 pmol/L).

LDL/VLDL purification

Purified LDL/VLDL fractions were obtained using an LDL/VLDL Purification kit (Ultracentrifugation free; Cell Biolabs, Inc.). To 200 µL of plasma on ice, 10 µL of dextran solution and 100 µL of precipitation solution A were added. The samples were incubated for 5 min on ice before centrifuging (6000 x g) for 10 min at 4°C. The remaining pellet (containing LDL/VLDL) was resuspended in 80 µL of bicarbonate solution and centrifuged (6000 x g) for 10 min at 4°C. The supernatant was transferred to a new tube and mixed thoroughly with 1 mL of 1X precipitation solution B and centrifuged (6000 x g) for 10 min at 4°C. The pellet was resuspended in 40 µL of 5% sodium chloride solution, mixed thoroughly with 1 mL of 1X precipitation solution C and centrifuged (6000 x g) for 10 min at 4°C. The above step was repeated, and the pellet resuspended in 100 µL of sodium chloride solution. To the mixture 16 µL was added of dextran removal solution before incubating for 1 h at 4°C and then centrifuging (6000 x g) for 10 min at 4°C. The supernatant (containing purified LDL/VLDL) was recovered and stored at -80°C. After acquiring the purified LDL/VLDL fractions, metabolites were extracted from these fractions as described below and analysed by LC-MS of the lipid fraction.

Metabolite extractions

Metabolites were extracted as described in Chapter 2, Section 2.1.1.

Analysis of intact lipids using orbitrap mass spectrometry

The organic fraction was analysed by the method described in Chapter 2, Section 2.1.2.

PEFA derivatisation of organic fractions for LC-MS and analysis of total fatty acids by triple quadrupole mass spectrometry

Each dried organic extract was derivatised by the method described in Chapter 2, Section 2.1.3 and analysed by the method described in Chapter 2, Section 2.1.4

Measurement of glutamate using triple quadrupole mass spectrometry

After inferring the effect of high protein feeding, rich in glutamate, on fatty acid synthesis, the levels of glutamate were measured in plasma. Aqueous extracts were reconstituted in 100 µL of 7:3 (v/v) ACN:water with 0.1% ammonium carbonate before glutamate was separated using reverse phase liquid chromatography using a Vanquish UHPLC attached to a TSQ Quantiva triple quadrupole mass spectrometer (Thermo Scientific). Multiple reaction monitoring was used in conjunction with positive/negative ion mode switching. For each sample, 5 µL was injected onto an Acquity UHPLC BEH amide column 100 mm x 2.1 mm, 1.8 µm (Waters, Corp.) at a flow rate of 0.6 mL/min. For chromatography on the UHPLC system, mobile phase (A) was water with 10 mmol/L ammonium carbonate and mobile phase (B) was ACN. The gradient started at 80% (B), decreased to 40% (B) at 4 min for 1 min and returned to the starting conditions for another 3 min to re-equilibrate the column. The mass transition for glutamate was 148.0 > 84.2. Collision energies and RF lens voltages were generated for each species using the TSQ Quantiva optimisation function. Instrument optimisation parameters are detailed in Table 3. Xcalibur Software (Thermo Scientific) was used to identify peaks, process mass spectra and normalise data to the closest-eluting internal standard.

Table 3. Mass spectrometer optimised settings for aqueous LC-MS.

Instrument Optimisation Parameters	
Method Duration (min)	7
Ion Source Type	H-ESI
Ion Spray Voltage: Positive Ion (V)	3500
Ion Spray Voltage: Negative Ion (V)	2500
Sheath Gas (Arb)	54
Sweep Gas (Arb)	2
Ion Transfer Tube Temperature (°C)	362
Vaporiser Temperature (°C)	440
Column Temperature (°C)	30
Needle wash	1:1 (v:v) water:CAN
Seal wash	4:1 (v:v) IPA:Water with 0.1% formic acid

A TIC of aqueous metabolites in human blood plasma obtained by the above method is shown in Figure 5A. From the TIC glutamate (*m/z* 148.0 > 84.2) and glutamine (*m/z* 147.1 > 84.2) were extracted (Figure 5B).

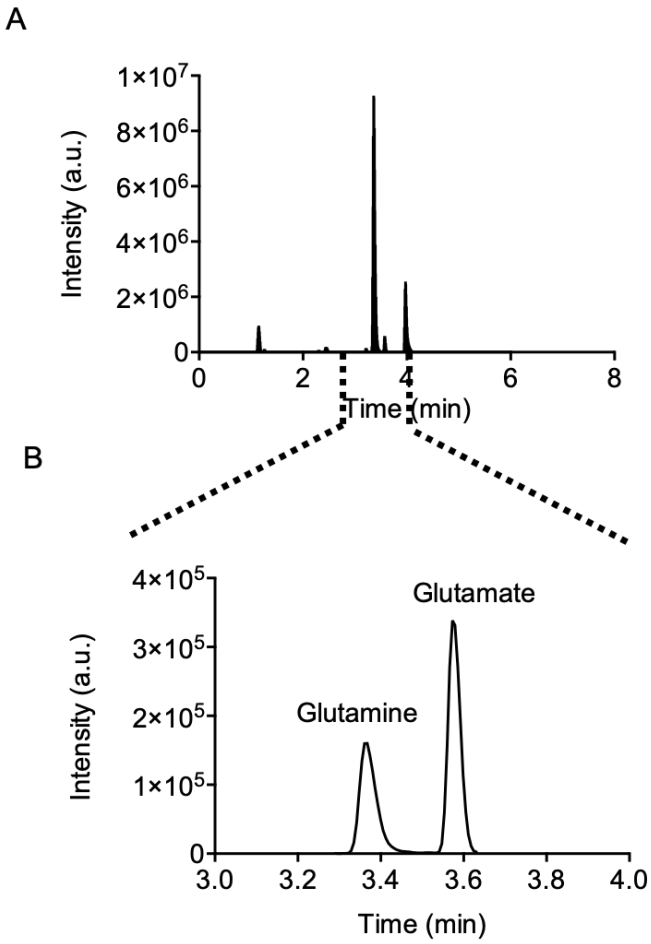

Figure 5. TIC and EICs for glutamate and glutamine. (**A**) The TIC of aqueous metabolites in human blood plasma detected by LC-MS. (**B**) EIC for the peaks at *m/z* 148.0 (glutamate) and 147.1 (glutamine). Both peaks had a daughter ion at *m/z* 84.2.

3.3.3 Data analysis

WinBUGS analysis of gastric emptying

Breath test data was collected in the form of isotope molar fractions (1) and fitted to curves according to (2) based on a Bayesian model as described previously by Ghoos et al., 1993 using the package WinBUGS. The fitted parameters k(n) and β(n) where assumed to be uniformly distributed and were assigned vague informative priors based on previous breath test data collected. From these fitted parameters, T_{lag} (3) and T_{half} (4) were calculated. T_{lag} described the peak emptying of the label and T_{half}, the time when half of the label was excreted in the breath. ^{13}C released from metabolism of labelled octanoic acid was sequestered initially in the citric acid cycle, and subsequently, as $^{13}CO_2$ in the bicarbonate pool. Thus, a further equation was derived considering the incorporation of the label into the bicarbonate pool, giving rise to the cumulative "self-corrected" data used herein (5). From this equation the self-corrected parameters Tlag ($T_{lag(in)}$) and Thalf ($T_{half(in)}$) were derived. This analysis was performed by Xuefei Li.

The calculations performed were as follows:

$$\mathrm{CO_2\ production\ rate}\ \left(\frac{\mathrm{mol}}{\mathrm{h}}\right), F_{CO_2} = 0.04518W^{0.5378}H^{0.3964}$$

$$\delta^{13}\mathrm{C} = \left(\frac{\left(\frac{^{13}C}{^{12}C}\right)_{sample}}{\left(\frac{^{13}C}{^{12}C}\right)_{standard}} - 1\right) \times 1000\ ‰ \quad (1)$$

$$\delta(n,t) = \delta_b(n) + \frac{1000 \cdot d}{(PDB) \cdot F_{CO_2}(n)} F_\infty(n) k(n) \beta(n) (1 - e^{-k(n)t})^{\beta(n)-1} \cdot e^{-k(n)t} \quad (2)$$

$$T_{lag}(n) = \frac{\ln \beta(n)}{k(n)} \quad (3)$$

$$T_{half}\ (n) = \frac{-\ln\left(1-2^{\frac{-1}{\beta(n)}}\right)}{k(n)} \quad (4)$$

$$G(n,t) = \beta(n)(1 - e^{-k(n)t})^{\beta(n)-1} - (\beta(n) - 1)(1 - e^{-k(n)t})^{\beta(n)} \quad (5)$$

Where the $\mathrm{CO_2\ production\ rate}$ is defined as $F_{CO_2} = 0.04518W^{0.5378}H^{0.3964}$ (W is weight in kg and H is height in m), F∞ (n) is the fraction of the dose recoverable in breath, d is the isotope dose given, PDB is the isotopic composition of the international standard of fixed carbon isotope ratio (calcium carbonate from belemnite from the Pee Dee formation in South

Carolina; $\frac{^{13}C}{^{12}C} = 0.0112$), $\delta_b(n,t)$ and $\delta_b(n)$ (‰) the measured isotopic compositions with respect to PDB for each of the breath tests at time t and in the basal state, respectively.

KNIME pipeline for the analysis of lipidomic data

Samples obtained from human subjects were acquired in two analytical batches using the analytical method described above, along with a set of quality controls (QCs, obtained by pooling 15 μL of all samples). The resulting raw data files were converted into mzML format using the tool MSConvert of the ProteoWizard software package (Holman et al., 2014; Kessner et al., 2008). Further processing occurred within the R environment (R Core Team, 2017) with the libraries IPO, XCMS and CAMERA (Kuhl et al., 2012; Libiseller et al., 2015; Smith et al., 2006) to perform parameter optimisation based on the QC samples, peak extraction, grouping, retention time correction, and annotation of adducts and isotopes. The output from these pre-processing steps was exported as a .csv file and imported into an adapted implementation of the KniMet pipeline (Liggi et al., 2018) for post-processing. The nonlinear local polynomial regression (LOESS) batch correction utility was used to normalise for differences among the two analytical batches (based on QCs for intra-batch correction, and on all samples for inter-batch correction). Features were filtered firstly based on their presence in the QC samples on the two separate batches with the QC-based feature filtering functionality (thresholds for missing values and relative standard deviation were 50% and 20%, respectively), whilst median peak area comparison, as previously described by Dunn and co-workers (Dunn et al., 2011), was used on the merged dataset. Metabolites were annotated based on accurate mass using a library built with the LIPID MAPS mass spectrometry combinatorial expansion package (Sud et al., 2012). Finally, the data matrix to be utilised for multivariate statistical analysis was subjected to missing values imputation with the KniMet MVI-KNN tool. This analysis was performed by Sonia Liggi. The quality assurance of the method is detailed in Appendix III.

3.3.4 Statistical analysis

Multivariate statistics

Multivariate statistical analyses were performed in SIMCA-P software, Version 13.0 (Umetrics, Sweden). All variables were univariate (UV) scaled and subjected to principal components analysis (PCA) coupled with Hotelling's T2 test to evaluate the distribution of the observations and identify any possible outliers. Subsequently, samples were classified based on the diet and a supervised Orthogonal Projections to Latent Structures Discriminant Analysis (OPLS-DA) model was developed to maximise separation between the different classes. The models were validated by a permutation test (n=100) and their significance ($p \leq 0.05$) was assessed by submitting the scores of the models to a cross-validated analysis of variance (CV-ANOVA) test. Loadings plots and the variable importance in projection (VIP) were acquired for each model to determine which variables drove the separation between classes (threshold limit > 1.0). These variables were subsequently visualised using univariate statistics. The extent to which the model fits and predicts the data is supplied by R^2X and Q^2X, respectively. R^2X, the "goodness of fit", varies between 0 and 1, where 1 is a perfectly fitted model. However, with increasing complexity, (i.e. increased numbers of parameters and components), R^2X will tend towards 1, and so Q^2X, the "goodness of prediction" is used as a supplementary measure, with a value greater than 0.4 considered significantly predictive.

Univariate statistics

Data were visualised using GraphPad (GraphPad Prism 5.2; GraphPad Software, San Diego, CA, USA). All data are expressed as means ± the SEM. In GraphPad, repeated measures one-, two-way ANOVA or paired two-tailed t-test were performed where appropriate to determine significant differences between experimental groups. For one-way ANOVA, Tukey's *post-hoc* multiple comparison test was performed, whilst for two-way ANOVA, Sidak's *post-hoc* multiple comparison test was used. Differences between experimental groups were considered to be statistically significant when $p \leq 0.05$.

3.4 Results

3.4.1. Participant characteristics

The nine participants' screening results adhered to the inclusion criteria of the study. The anthropometric, haematological and biochemical characteristics of the participants that met the inclusion criteria are detailed in Table 4. Their age and BMI ranged from 19-29 years old and 18.9-27.5 kg/m^2, respectively. Their haematological characteristics, including arterial blood pressure and full blood count were within the healthy range. Moreover, their fasting lipid profile, blood insulin and glucose as well as liver function test were all within the defined healthy range.

3.4.2 Gastric emptying rates and parameters

The breath test kinetics, measured by ^{13}C-OBT to characterise gastric emptying, are detailed in Table 5. Each parameter, T_{half} (Table 5A) and T_{lag} (Table 5B) as well as $T_{half(in)}$ (Table 5C) and $T_{lag(in)}$ (Table 5D), were analysed between each group using repeated measures one-way ANOVA with *post-hoc* Tukey's multiple comparisons test. The percentage of the solid food fraction expelled from stomach was not significantly different between HF and CB, HP and C, HP and HC as well as C and HC. The results that were significant for both $T_{half(in)}$ and $T_{lag(in)}$ (red box) will be shown in more detail below.

Gastric emptying rate was faster in HF group compared to the HP, C or HC group

Volunteers that consumed a HF meal experienced a significantly faster gastric emptying rate compared to the same volunteers consuming a HP (Figure 6A), C (Figure 6B) and HC meal (Figure 6C). $T_{half(in)}$ was significantly faster in the HF group than the HP (by 25.2%; Figure 7A), C (by 28.7%; Figure 7B) and HC group (by 28.1%; Figure 7C). $T_{lag(in)}$ was significantly faster in the HF group than the HP (by 31.3%; Figure 7D), C (by 42.7%; Figure 7E) and HC group (by 42.0%; Figure 7F).

Gastric emptying rate was faster in CB group compared to the HP, C or HC group

Volunteers that consumed a CB meal experienced a significantly faster gastric emptying rate compared to the same volunteers consuming a HP (Figure 8A), C (Figure 8B) and HC meal (Figure 8C). $T_{half(in)}$ was significantly faster in the CB group than the HP (by 11.5%; Figure 9A), C (by 14.6%; Figure 9B) and HC group (by 14.1%; Figure 9C). $T_{lag(in)}$ was significantly faster in the CB group than the HP (by 12.4%; Figure 9D), C (by 22.2%; Figure 9E) and HC group (by 21.6%; Figure 9F).

Table 4. Participant characteristics. Table detailing anthropometric, haematological and biochemical characteristics of the volunteers.

Anthropometric Parameter	Units	Mean	Standard Deviation	Range
Age	years	24.7	4.24	19-29
Weight	kg	72.4	7.38	65.5-88.7
Height	cm	179	7.74	168-192
BMI	kg/m^2	22.7	2.58	18.9-27.5
Systolic BP	mmHg	123	8.41	100-140
Diastolic BP	mmHg	71.1	8.54	50-85
Haematology				
White blood cell (WBC)count	$10^9/L$	5.03	0.542	3.90-10.2
Red blood cell (RBC) count	$10^{12}/L$	5.10	0.312	4.30-5.75
Haemoglobin (Hb)	g/L	147	4.70	135-172
Haematocrit (Hct)	L/L	0.445	0.0197	0.395-0.505
Mean cell volume (MCV)	fL	87.4	5.63	80.0-99.0
Mean cell haemoglobin(MCH)	pg	28.8	2.08	27.0-33.5
Red cell distribution width (RDW)	%	13.1	0.791	11.0-16.0
Platelet (PLT) count	$10^9/L$	230	28.1	150-370
Platelet Haematocrit (PCT)	L/L	0.199	0.0215	0.19-0.29
Mean Platelet Volume (MPV)	fL	8.67	0.870	
Neutrophil count	$10^9/L$	2.74	0.576	1.50-7.70
Lymphocyte count	$10^9/L$	1.48	0.337	1.10-4.50
Monocyte count	$10^9/L$	0.346	0.110	0.10-0.90
Eosinophil count	$10^9/L$	0.0944	0.0436	0.02-0.50
Basophil count	$10^9/L$	0.0322	0.0172	0.00-0.20
Lipid profile, insulin and glucose				
Cholesterol	mmol/L	4.16	0.688	< 5
Triglyceride	mmol/L	0.878	0.342	0.3-1.80
HDL Cholesterol	mmol/L	1.39	0.170	> 1
LDL Cholesterol	mmol/L	2.37	0.582	< 2.59
Cholesterol/HDL Ratio		3.02	0.696	< 3.5
Non HDL Cholesterol	mmol/L	2.77	0.702	<2.95
Insulin	pmol/l	36.3	19.6	0-80
Serum Glucose	mmol/L	4.47	0.415	3.9-5.5
Liver function				
Albumin	g/L	42.8	2.95	35-50
Total Bilirubin	µmol/L	15.0	4.66	0-20
Alkaline Phosphatase	U/L	65.3	12.2	30-130
Alanine Transaminase	U/L	20.5	6.78	7-40
Gamma Glutamyltransferase	U/L	16.1	4.99	0-72

Table 5A. T_{half} represented as a mean ± SEM. T_{half} comparisons between meals were analysed by one-way repeated measures ANOVA with *post-hoc* Tukey's multiple comparisons test; * = $p \leq 0.05$, n = 9/group.

T_{half} (h)	HF	CB	HP	C	HC
Mean ± SEM	3.15 ± 0.63	3.32 ± 0.64	3.68 ± 0.68	3.51 ± 0.66	3.48 ± 0.66
HF vs. CB	ns (p = 0.4)				
HF vs. HP	*(p = 0.002)				
HF vs. C	* (p = 0.02)				
HF vs. HC	ns (p = 0.2)				
CB vs. HP		* (p = 0.01)			
CB vs. C		ns (p = 0.09)			
CB vs. HC		ns (p = 0.5)			
HP vs. C			ns (p = 0.1)		
HP vs. HC			ns (p = 0.3)		
C vs. HC				Ns (p = 1)	

Table 5B. T_{lag} represented as a mean ± SEM. T_{lag} comparisons between meals were analysed by one-way repeated measures ANOVA with *post-hoc* Tukey's multiple comparisons test; * = $p \leq 0.05$, n = 9/group.

Tl_{ag} (h)	HF	CB	HP	C	HC
Mean ± SEM	2.42 ± 0.55	2.63 ± 0.57	2.91 ± 0.60	2.89 ± 0.60	2.86 ± 0.60
HF vs. CB	ns (p = 0.2				
HF vs. HP	* (p = 0.003)				
HF vs. C	* (p = 0.008)				
HF vs. HC	ns (p = 0.05)				
CB vs. HP		* (p = 0.005)			
CB vs. C		* (p = 0.003)			
CB vs. HC		ns (p = 0.003)			
HP vs. C			ns (p = 0.08)		
HP vs. HC			ns (p = 0.3)		
C vs. HC				ns (p = 1)	

Table 5C. $T_{half(in)}$ represented as a mean ± SEM. $T_{half(in)}$ comparisons between meals were analysed by one-way repeated measures ANOVA with *post-hoc* Tukey's multiple comparisons test; * = $p \leq 0.05$, n = 9/group.

$T_{half(in)}$ (h)	HF	CB	HP	C	HC
Mean ± SEM	1.71 ± 0.46	1.92 ± 0.49	2.14 ± 0.52	2.20 ± 0.52	2.19 ± 0.52
HF vs. CB	ns (p = 0.2)				
HF vs. HP	* (p = 0.003)				
HF vs. C	* (p = 0.006)				
HF vs. HC	* (p = 0.03)				
CB vs. HP		* (p = 0.003)			
CB vs. C		* (p = 0.0002)			
CB vs. HC		* (p = 0.02)			
HP vs. C			ns (p = 0.6)		
HP vs. HC			ns (p = 0.9)		
C vs. HC				ns (p = 1)	

Table 5D. $T_{lag(in)}$ represented as a mean ± SEM. $Tl_{ag(in)}$ mean comparisons between meals were analysed by one-way repeated measures ANOVA with *post-hoc* Tukey's multiple comparisons test; * = $p \leq 0.05$, n = 9/group.

$T_{lag(in)}$ (h)	HF	CB	HP	C	HC
Mean ± SEM	1.31 ± 0.40	1.53 ± 0.44	1.72 ± 0.46	1.87 ± 0.48	1.86 ± 0.48
HF vs. CB	ns (p = 0.1)				
HF vs. HP	* (p = 0.005)				
HF vs. C	* (p = 0.005)				
HF vs. HC	* (p = 0.02)				
CB vs. HP		* (p = 0.002)			
CB vs. C		* (p = 0.0002)			
CB vs. HC		* (p = 0.009)			
HP vs. C			ns (p = 0.06)		
HP vs. HC			ns (p = 0.4)		
C vs. HC				ns (p = 1)	

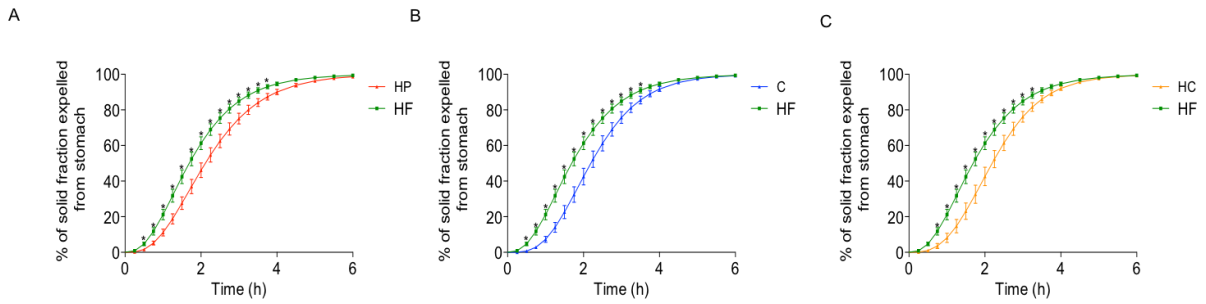

Figure 6. Gastric emptying rate was faster after consuming the HF meal compared with the HP, C and HC meal. (**A**) Gastric emptying rate as a percentage of food expelled from stomach over 6 h after HF (green) and HP (red) meals. (**B**) Gastric emptying rate as a percentage of food expelled from stomach over 6 h after HF (green) and C (blue) meals. (**C**) Gastric emptying rate as a percentage of food expelled from stomach over 6 h after HF (green) and HC (orange) meals. Data are presented as mean ± SEM and analysed by two-way repeated measures ANOVA with *post-hoc* Sidak's multiple comparisons test; * = $p \leq 0.05$, n = 9/group.

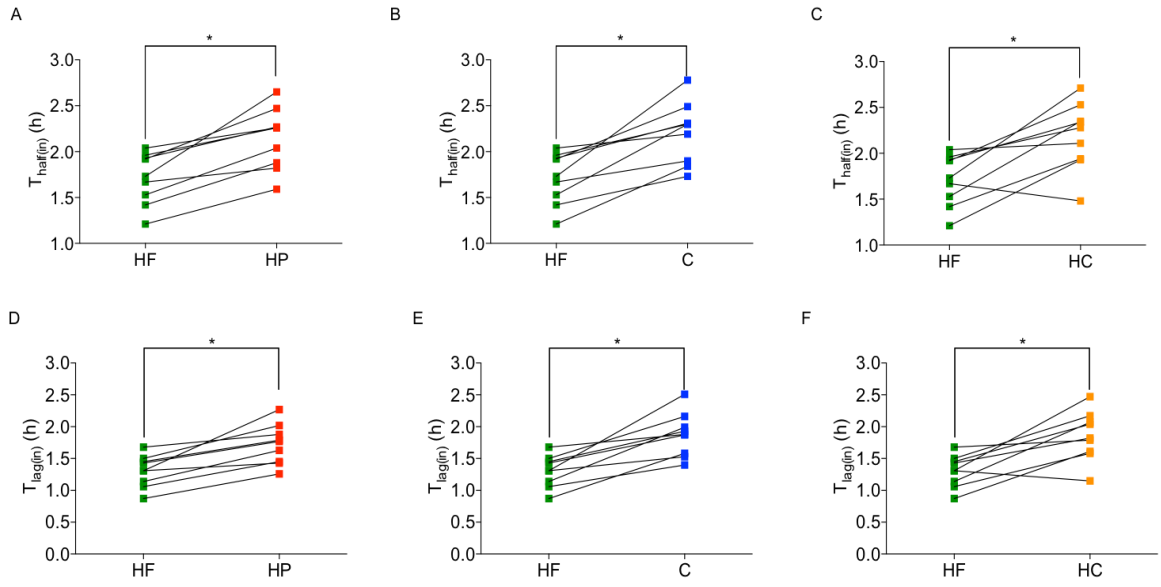

Figure 7. $T_{half(in)}$ and $T_{lag(in)}$ were faster after consuming the HF meal compared with the HP, C and HC meal. (**A**) $T_{half(in)}$ after HF (green) and HP meals (red). (**B**) $T_{half(in)}$ after HF (green) and C meals (blue). (**C**) $T_{half(in)}$ after HF (green) and HC meals (orange). (**D**) $T_{lag(in)}$ after HF (green) and HP meals (red). (**E**) $T_{lag(in)}$ after HF (green) and C meals (blue). (**F**) $T_{lag(in)}$ after HF (green) and HC meals (orange). Data are presented as individual values and analysed by paired two-tailed t-Test; * = $p \leq 0.05$, n = 9/group.

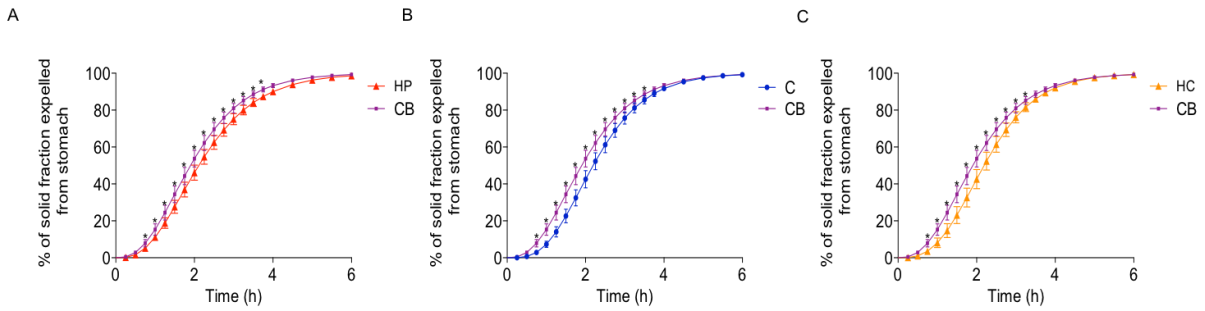

Figure 8. Gastric emptying rate was faster after consuming the CB meal compared with the HP, C and HC meal. (**A**) Gastric emptying rate as a percentage of food expelled from stomach over 6 h after CB (purple) and HP (red) meals. (**B**) Gastric emptying rate as a percentage of food expelled from stomach over 6 h after CB (purple) and C (blue) meals. (**C**) Gastric emptying rate as a percentage of food expelled from stomach over 6 h after CB (purple) and HC (orange) meals. Data are presented as mean ± SEM and analysed by two-way repeated measures ANOVA with *post-hoc* Sidak's multiple comparisons test; * = $p \leq 0.05$, n = 9/group.

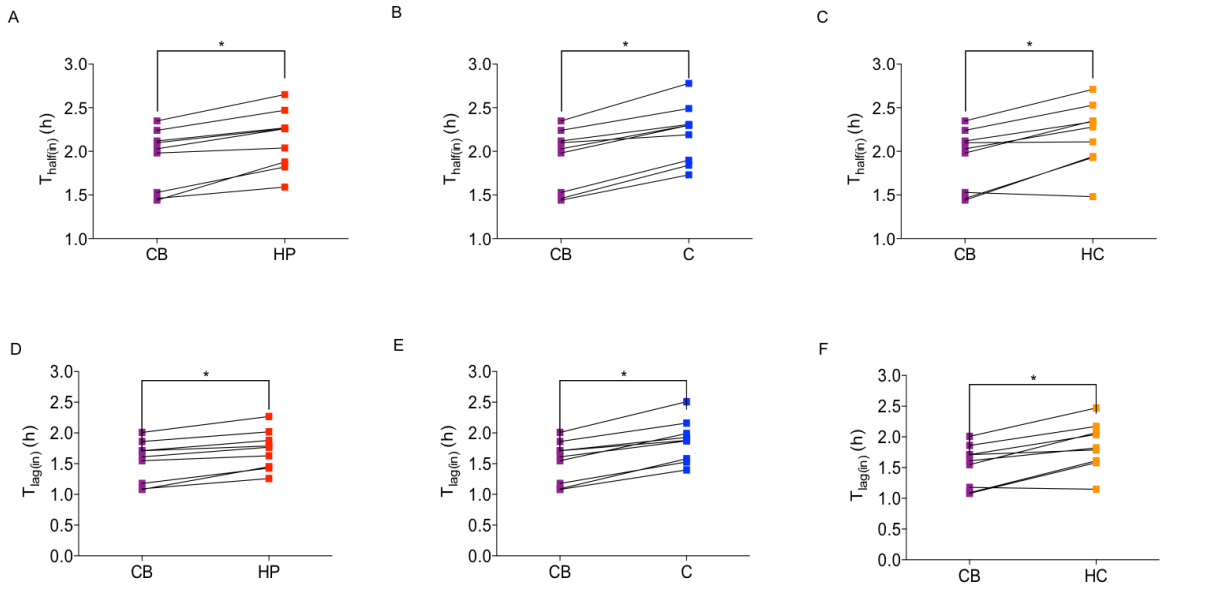

Figure 9. $T_{half(in)}$ and $T_{lag(in)}$ were faster after consuming the HF meal compared with the HP, C and HC meal. (**A**) $T_{half(in)}$ after CB (purple) and HP meals (red). (**B**) $T_{half(in)}$ after CB (purple) and C meals (blue). (**C**) $T_{half(in)}$ after CB (purple) and HC meals (orange). (**D**) $T_{lag(in)}$ after CB (purple) and HP meals (red). (**E**) $T_{lag(in)}$ after CB (purple) and C meals (blue). (**F**) $T_{lag(in)}$ after CB (purple) and HC meals (orange). Data are presented as individual values and analysed by paired two-tailed t-Test; * = $p \leq 0.05$, n = 9/group.

3.4.3 Gastric emptying parameter correlations

Gastric emptying parameters weakly correlated with dietary fat and carbohydrate but did not correlate with protein intake

Gastric emptying parameters, $T_{half(in)}$ and $T_{lag(in)}$, were weakly associated with fat (Figure 10) and carbohydrate content (Figure 11) but did not correlate with protein (Figure 12) content. Pearson correlation analysis did not reveal any statistically significant correlation coefficients (r). The data were then fitted into a linear regression model. The coefficients of determination, r^2, for all models were low, indicating weak models.

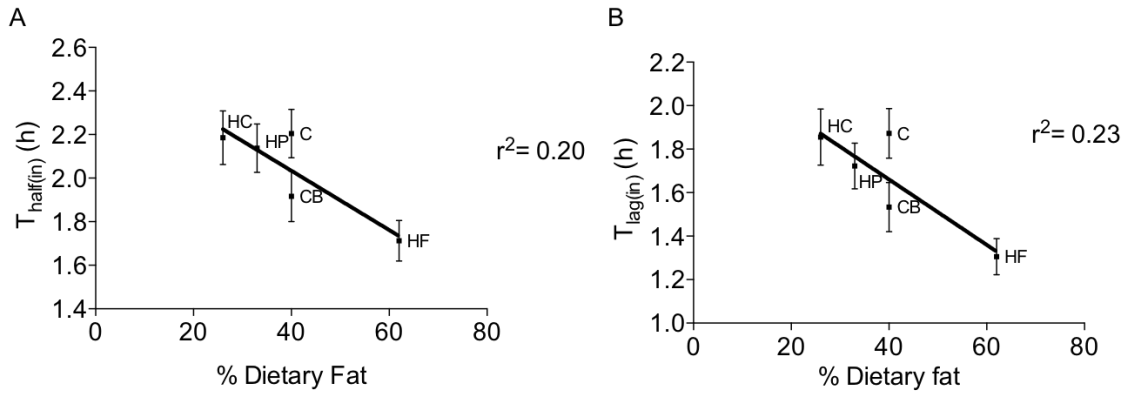

Figure 10. Gastric emptying weakly correlated with fat content. (**A**) Linear regression model showing $T_{half(in)}$ as a function of fat content (r^2=0.20; *p*=0.002). (**B**) Linear regression model showing $T_{lag(in)}$ as a function of fat content (r^2=0.23; *p*=0.0008). Data are presented as mean ± SEM; *n* = 9/group.

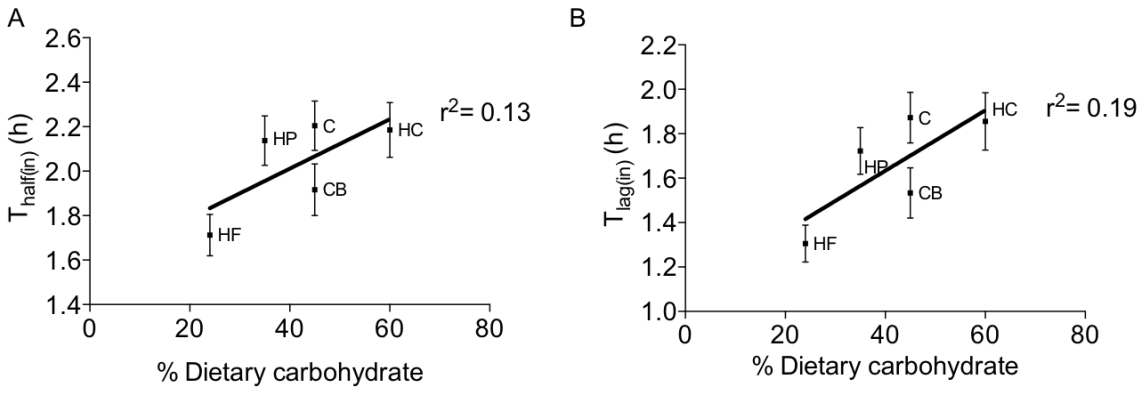

Figure 11. Gastric emptying weakly correlated with carbohydrate content. (**A**) Linear regression model showing $T_{half(in)}$ as a function of carbohydrate content (r^2=0.13; *p*=0.02). (**B**) Linear regression model showing $T_{lag(in)}$ as a function of carbohydrate content (r^2=0.19; *p*=0.003). Data are presented as mean ± SEM; *n* = 9/group.

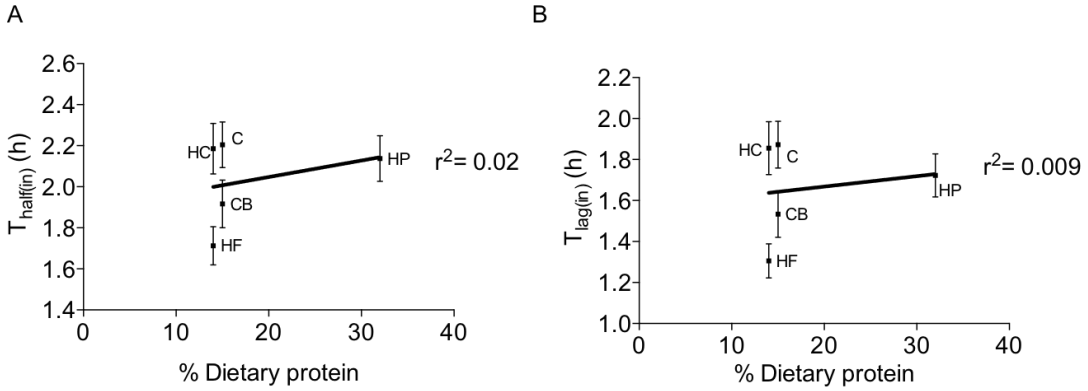

Figure 12. Gastric emptying did not correlate with protein content. (**A**) Linear regression model showing $T_{half(in)}$ as a function of protein content (r^2=0.02; *p*=0.3). (**B**) Linear regression model showing $T_{lag(in)}$ as a function of protein content (r^2=0.009; *p*=0.5). Data are presented as mean ± SEM; *n* = 9/group.

The fact that the C and the CB meals have the same fat, carbohydrate and protein content but they consistently do not fall on the same point on the line, suggests that there is another factor affecting gastric emptying.

Gastric emptying rate parameters were delayed with increasing liquid carbohydrate

Even though total carbohydrate content and other macronutrients did not correlate with gastric emptying parameters, liquid carbohydrate delayed gastric emptying as determined by the increases in the parameters, $T_{half(in)}$ (Figure 13A) and $T_{lag(in)}$ (Figure 13B). The effect of liquid carbohydrate content of the meal on gastric emptying rates was only apparent up to 50% of the total meal composition and $T_{half(in)}$ plateaued at this stage.

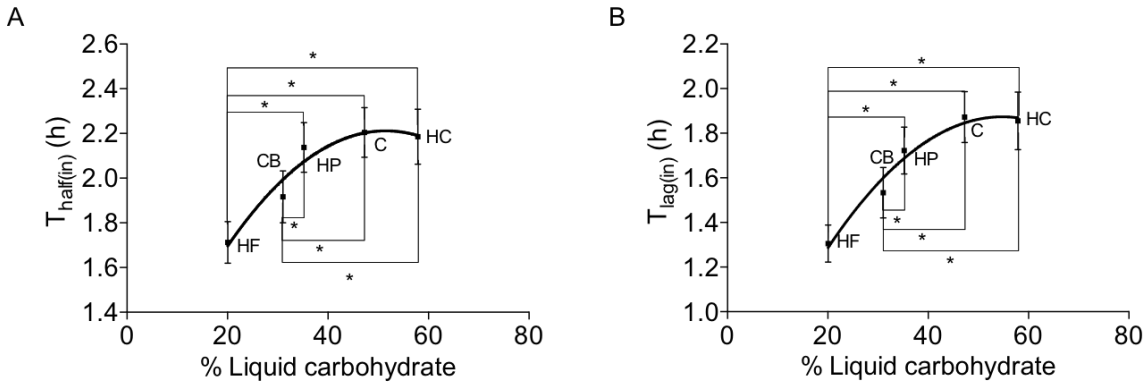

Figure 13. Gastric emptying was delayed with increasing liquid carbohydrate intake. (**A**) Second order polynomial equation describing $T_{half(in)}$ as a function of liquid carbohydrate content (**B**) Second order polynomial equation $T_{lag(in)}$ as a function of liquid carbohydrate content. Data are presented as mean ± SEM and analysed by two-way repeated measures ANOVA with *post-hoc* Sidak's multiple comparisons test; * = $p \leq 0.05$, n = 9/group.

Fat fraction expelled from stomach positively correlated with the total amount of lipids in plasma

The amount of fat expelled from the stomach was calculated by multiplying gastric emptying by total fat intake per meal (Figure 14A) at each time point. The area under the curve (AUC; Figure 14B) was calculated to provide an estimate of the total amount of fat expelled from the stomach over the course of 6 h. The total amount of fat expelled from stomach after consuming the HC or HP meals was significantly lower compared to the C meal. However, the total amount of fat expelled from the stomach after consuming the CB or HF meals was significantly higher compared to the C meal.

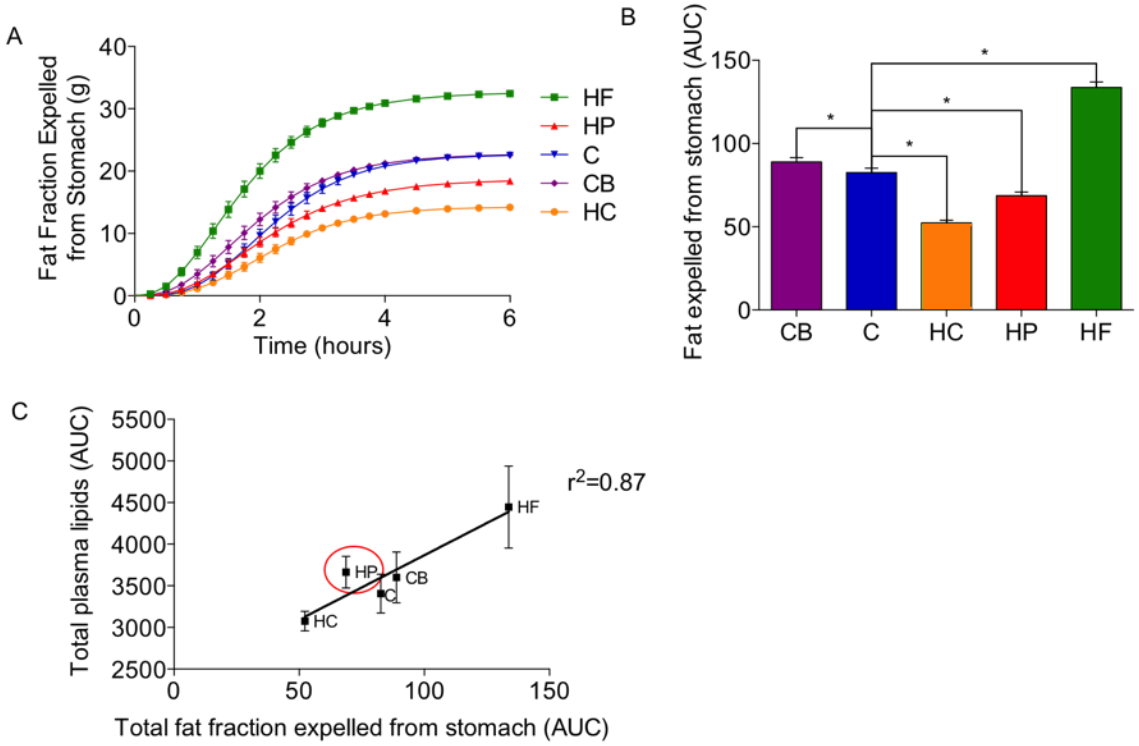

Figure 14. Total plasma lipids positively correlated with total fat fraction expelled from stomach. (**A**) Fat fraction expelled from the stomach, after consuming HF (green), HP (red), C (blue), CB (purple) and HC (orange) meals over 6 h. (**B**) Total amount of fat expelled from the stomach after consuming HF (green), HP (red), C (blue), CB (purple) and HC (orange) meal. (**C**) Linear regression model of fat total plasma lipids as a function of total fat fraction expelled from the stomach. HP meal resulted in more plasma lipids than expected from the linear trend (red circle). Data are presented as mean ± SEM and analysed by one-way repeated measures ANOVA with *post-hoc* Tukey's multiple comparisons test; * = $p \leq 0.05$, n = 9/group.

Linear regression analysis of total plasma lipids, reflected by the TIC of mass spectra, as a function of fat fraction expelled from stomach gave a positive linear relationship (Figure 14C). The coefficient of determination, r^2, was 0.87 (close to 1), indicating a good fit of data into a linear model (p=0.02). The exception to this good linear model was the HP group. The total amount of lipids detected in plasma after consuming the HP meal was greater than the amount of fat fraction expelled from the stomach after consuming the same meal (red circle, Figure 14C).

3.4.4 Open profile lipidomics and fatty acid analysis of plasma and liver-derived lipoproteins

ScTAGs were the major discriminant variables between high protein- and control-fed healthy male subjects

To assess changes in the plasma triglyceride profiles obtained by LC-MS, spectra were processed to construct PCA models to identify the distribution of the variables and remove any outliers detected by the Hotelling's T2 test. Subsequently, OPLS-DA models were created to discriminate between the two groups. In the OPLS-DA models, time points T3, T4 and T5 were utilised as this provided sufficient time for ingested macronutrients to reach the extrahepatic blood (Samson et al., 2012). OPLS-DA readily separated the HP group from the C group (R^2X = 0.84, Q^2 = 0.47; Figure 15A). The model was validated using a permutation test, yielding R^2X and Q^2 values [R^2 = (0.0, 0.56), Q^2= (0.0, -0.63)] lower than the original, indicating a stable and non-random model (Figure 15B). CV-ANOVA also showed a significant p-value for the model (*p*=0.0063).

The loadings plot of the model, C versus HP, was then used to determine the metabolite features that differ between the groups (Figure 15C). VIP was utilised to filter important metabolites in the model. The vectors in the projection were regularised such that, if all variables were of equal importance, their values would be equal to 1. Therefore, any variable with a VIP value greater than 1 was considered to be a potential discriminant. TAGs containing shorter and more saturated fatty acids, scTAGs, (red circles; Figure 15C) were the VIPs most elevated in the HP group (Figure 15D).

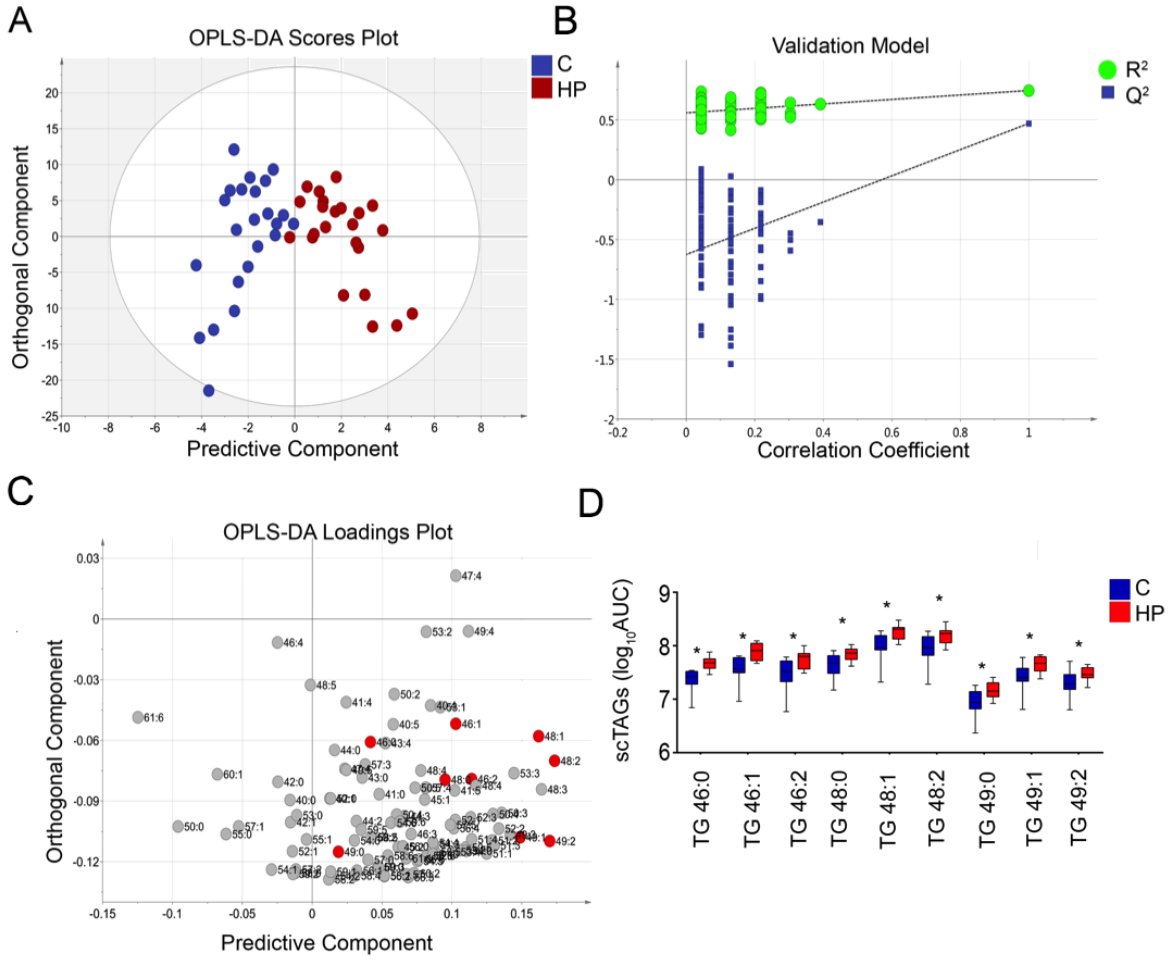

Figure 15. Multivariate data analysis of C- and HP-fed healthy human subjects. (**A**) OPLSA-DA scores plot discriminating TAG profiles in plasma of C- and HP-fed individuals after 3, 4 and 5 h. Each blue circle represents a single C-fed individual, whilst red represents HP-fed individuals (R^2X = 0.84, Q^2 = 0.47). (**B**) Cross validation of (A) acquired through 100 permutation tests; y-axis intercepts: R^2 = (0.0, 0.56), Q^2= (0.0, -0.63). (**C**) OPLS-DA loadings plot of TAG influence on the separation between the HP and C groups. TAGs elevated in HP are displayed on the positive side of the predictive component, whilst TAGs elevated in C are displayed on the negative. Red circles scTAGs. (**D**) Box plots showing the range of scTAGs in C- (blue) and HP-fed (red) individuals. Data are presented as mean ± SEM and analysed by two-way repeated measures ANOVA with *post-hoc* Sidak's multiple comparisons test; * = $p \leq 0.05$, n = 9/group.

HP feeding in healthy male subjects revealed discrete clusters of TAGs in blood plasma

The TAG profiles were further analysed by hierarchical clustering, and heatmap representations were obtained from the Spearman correlation matrix among metabolites. One of the clusters contained scTAGs, indicating that changes in TAG levels were consistent within members of the cluster, and these have been previously correlated with DNL and steatosis (Figure 16).

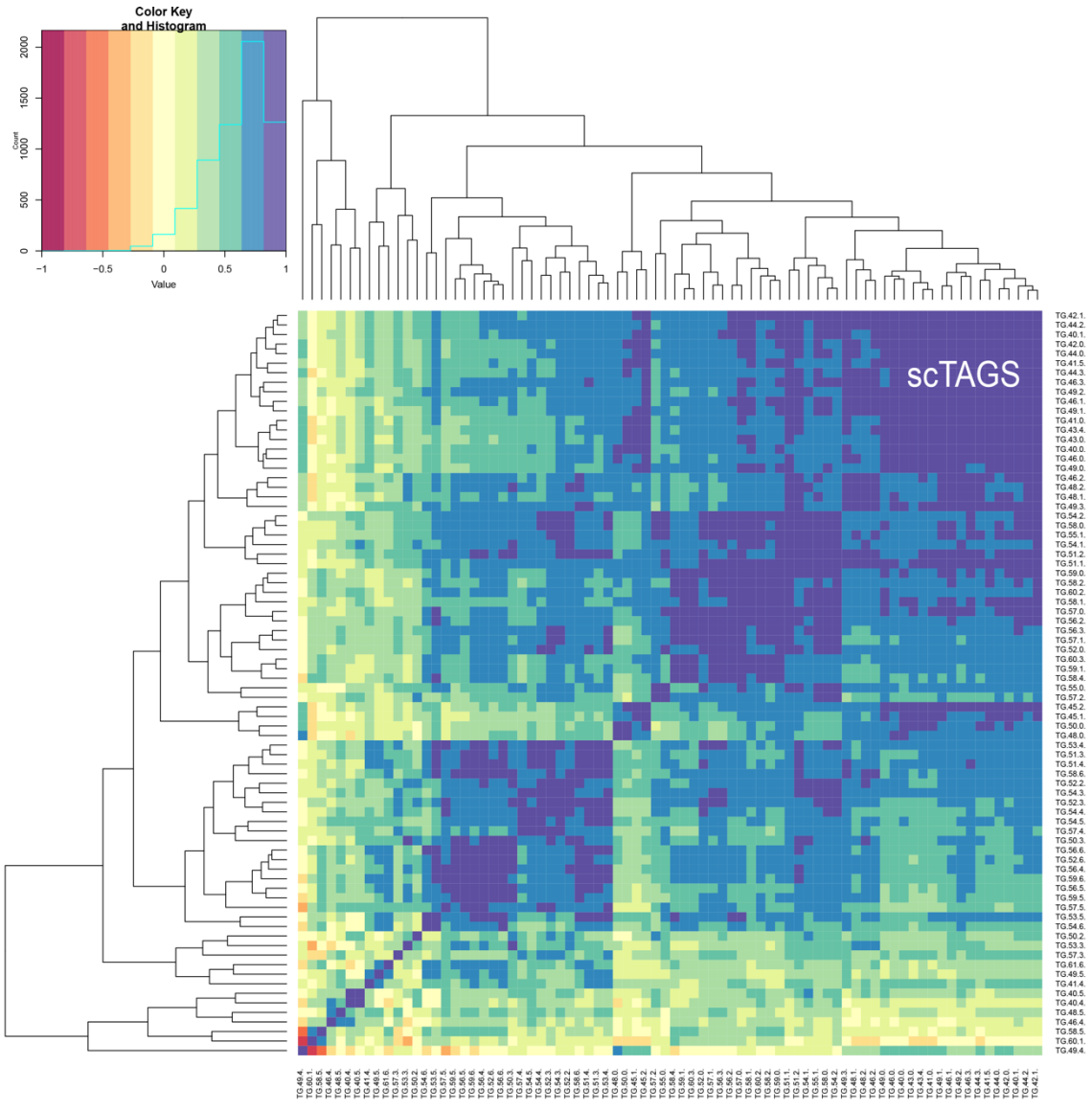

Figure 16. scTAGs form a distinct cluster. Hierarchical Cluster Analysis with Spearman correlation among the TAG profiles measured by LC-MS of all individuals after a HP meal; *n* = 9.

HP feeding in healthy male subjects increased scTAGs in blood plasma

The total amount of triacylglycerides was not significantly different between all five meals (Figure 17A). However, scTAGs were significantly elevated after a HP meal at 3 and 4 h compared to the same individuals fed with C, CB, HF or HC meals (Figure 17B). scTAG content in CB, HC, and HF was not significantly different when compared to C (Figure 17B).

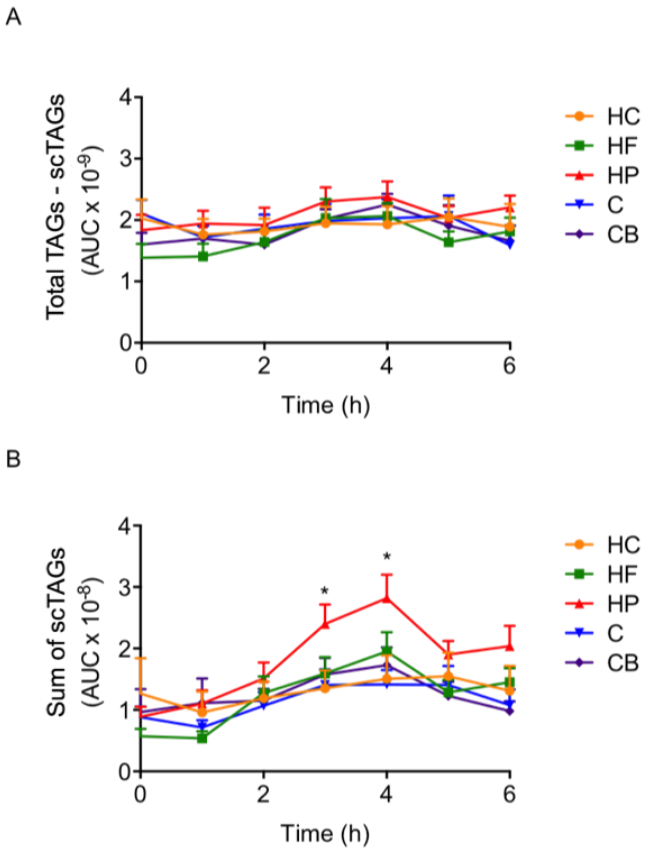

Figure 17. scTAGs were elevated in plasma after a HP meal in healthy human subjects. (**A**) Fasting (baseline; 0 h) and postprandial total TAG abundance in plasma after CB (purple), C (blue), HP (red), HF (green) and HC (orange) meals measured by LC-MS in samples drawn over 6 h. (**B**) Fasting (baseline; 0 h) and postprandial sum of scTAG abundance in plasma CB (purple), C (blue), HP (red), HF (green) and HC (orange) meals measured by LC-MS in samples drawn over 6 h. Data are presented as mean ± SEM and analysed by two-way repeated measures ANOVA with *post-hoc* Sidak's multiple comparisons test; * = $p \leq 0.05$, n = 9/group.

HP feeding in healthy male subjects increased scTAGs in the LDL/VLDL fraction

The total triglyceride content was not significantly different between the C and HP groups (Figure 18A). However, total scTAGs were markedly elevated in HP-fed subjects 3 h post-feeding compared with the same individuals fed with the C meal (Figure 18B). After an overnight fast and subsequent feeding with the HP meal, there was an increase in scTAGs up to 4 h compared with baseline (Figure 18B). There were no significant differences in scTAGs between the baseline and hourly samples in C-fed subjects (Figure 18B). To determine whether these TAGs were produced by the liver and not the intestine or adipose tissue, LDL/VLDL particles were extracted from plasma, by a series of precipitation and low centrifugation steps, and their TAG profiles analysed. In line with changes in plasma, the sum of scTAGs in the LDL/VLDL fraction was higher in HP-fed subjects than C-fed subjects after 3 h (Figure 18C).

Fatty acids from the meal as well as free fatty acid (FFA) are major precursors of lipoprotein TAGs. The C and HP meals did not have any differences in meal fatty acid compositions (Appendix II C) nor in the plasma FFA content (Appendix IV), indicating that these TAGs were synthesised *de novo*.

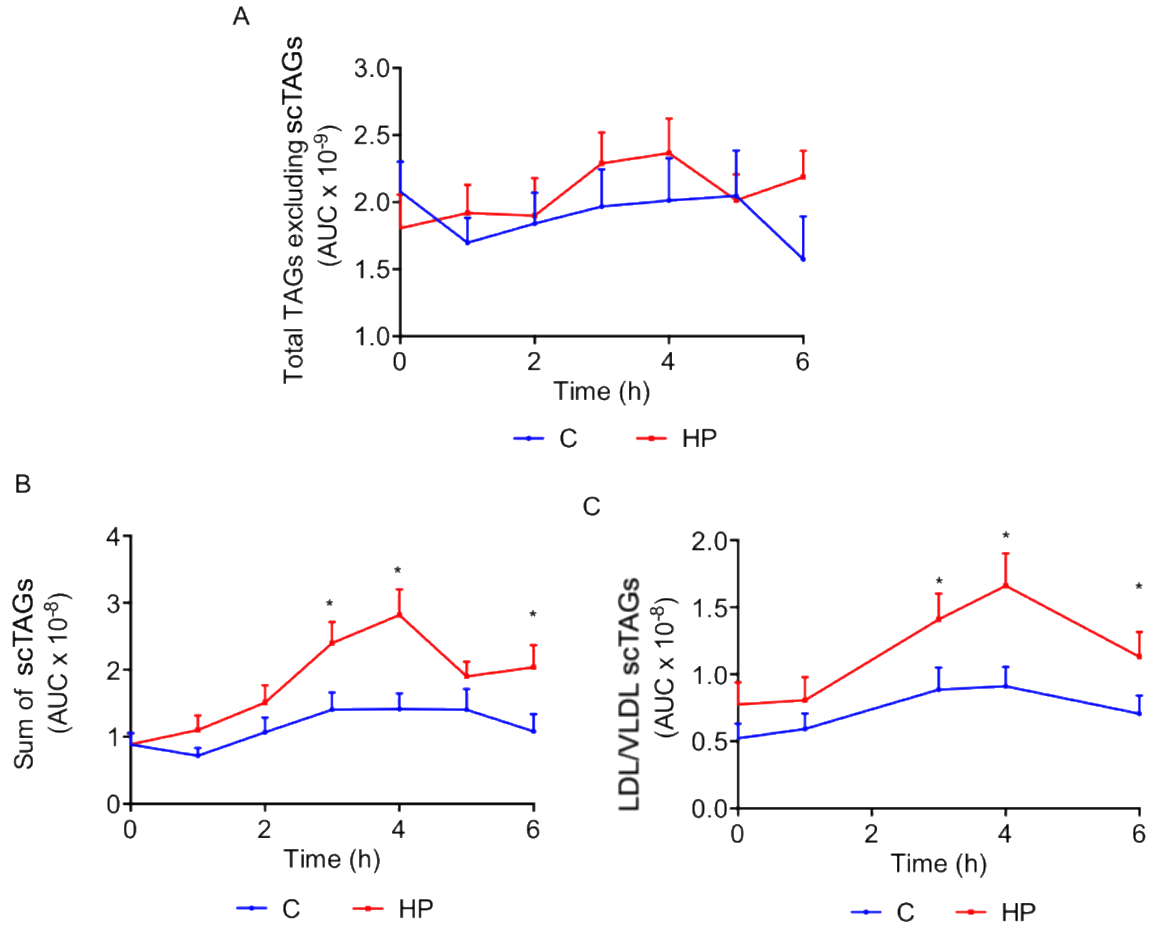

Figure 18. scTAGs were elevated in plasma and plasma LDL/VLDL fraction after a HP meal in healthy human subjects. (**A**) Fasting (baseline; 0 h) and postprandial total TAG abundance in plasma after C (blue) and HP (red) meal measured by LC-MS in samples drawn over 6 h. (**B**) Fasting (baseline; 0 h) and postprandial sum of scTAG abundance in plasma after C (blue) and HP (red) meal measured by LC-MS in samples drawn over 6 h. (**C**) Fasting (baseline; 0 h) and postprandial LDL/VLDL TAG abundance in plasma after C (blue) and HP (red) meals measured by LC-MS in samples drawn over 6 h. Data are presented as mean ± SEM and analysed by two-way repeated measures ANOVA with *post-hoc* Sidak's multiple comparisons test; * = $p \leq 0.05$, n = 9/group.

Fatty acid analysis indicated an increase in the DNL index after consuming HP meal

The plasma 16:0/18:2n-6 ratio was calculated as an index of DNL, as during DNL, plasma TAGs are enriched with 16:0, the primary product of FAS, and depleted in 18:2n-6, an essential fatty acid. At 4 h, where the biggest increase in scTAGs was observed, the 16:0/ 18:2n-6 ratio was significantly greater after the HP meal than after the C meal (Figure 19).

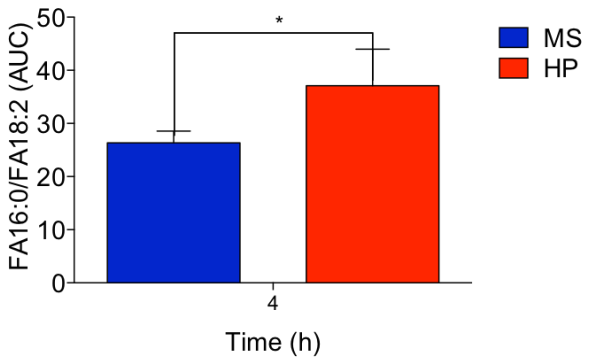

Figure 19. DNL index increased after a HP meal in healthy human subjects. DNL index reflected by the ratio of FA 16:0 to FA 18:2n-6 after C (blue) and HP (red) meals at 4 h. Data are presented as mean ± SEM and analysed by a paired t-Test (E); * = $p \leq 0.05$, n = 9/group.

3.4.5 Plasma glutamate levels

High protein meal increased plasma glutamate levels

High protein feeding, using a soy protein intervention rich in glutamate, resulted in increased levels of scTAGs and VLDL-associated scTAGs in plasma of human subjects. To characterise what was driving this increase in DNL, glutamate levels in plasma were analysed. At 3 h (one hour before maximum DNL levels), the plasma glutamate levels were significantly higher in subjects that consumed the HP meal compared to the same subjects fed with the C meal. However, at 4h there was a decrease in plasma glutamate levels after the HP meal, possibly indicating uptake by the liver (Figure 20).

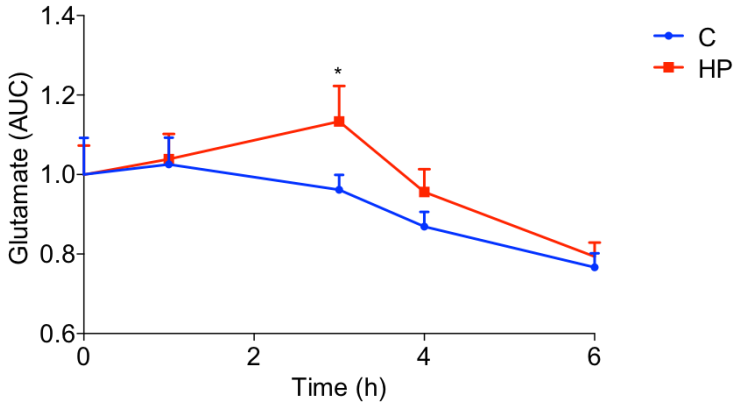

Figure 20. HP-feeding increased plasma glutamate levels in human subjects. Fasting (baseline; 0 h) and postprandial glutamate abundance in plasma after C (blue) and HP (red) meal measured by LC-MS in samples drawn over 6 h. Data are presented as mean ± SEM and analysed by two-way repeated measures ANOVA with *post-hoc* Sidak's multiple comparisons test; * = $p \leq 0.05$, n = 9/group.

3.4.6 Liquid carbohydrate and DNL

Liquid carbohydrate did not correlate with DNL

scTAGs that were used as markers of DNL were not dependent on the amount of liquid carbohydrate (Figure 21). Pearson correlation analysis did not give any statistically significant correlation coefficients (r) and the data did not fit into a linear regression model. The coefficient of determination, r^2, for the model was 0.01 indicating no correlation.

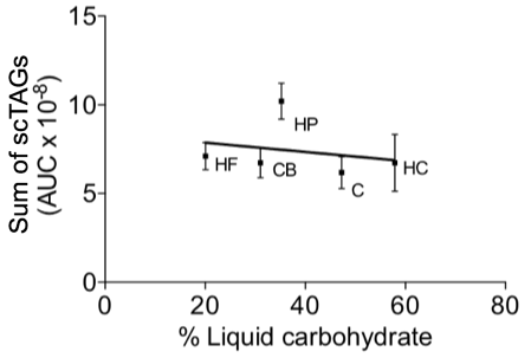

Figure 21. scTAGs did not correlate with liquid carbohydrate content. Linear regression model showing Sum of scTAGs as a function of liquid carbohydrate content (r^2=0.01; p=0.5). Data are presented as mean ± SEM; n = 9/group.

3.4.7 Plasma insulin levels

Insulin levels correlated with dietary carbohydrate and protein

Blood insulin concentration was positively associated with carbohydrate and protein content of the meals (Figure 22). Pearson correlation analysis did not give statistically significant correlation coefficient (r) between insulin and carbohydrate only (r=0.86; *p*=0.06). However, insulin as a function of carbohydrate and protein content together gave a significant correlation coefficient (r=0.96; *p*=0.007). The data were then fitted into linear regression models. The coefficient of determination, r^2, for insulin versus carbohydrate only was not significant (r^2=0.74; *p*=0.06; Figure 22A). For insulin versus carbohydrate and protein, r^2 was significant and higher than that of insulin versus carbohydrate indicating a stronger relationship (r^2=0.94; *p*=0.007; Figure 22B).

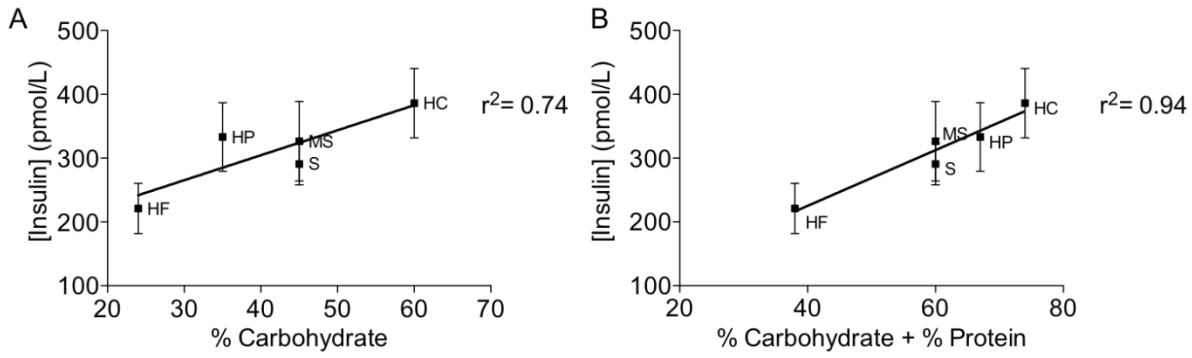

Figure 22. Plasma insulin concentration correlated with carbohydrate and protein. (**A**) Linear regression model showing insulin concentration (pmol/L) a function carbohydrate content (r^2 = 0.74; *p*=0.06). (**B**) Linear regression model showing insulin concentration (pmol/L) as a function of carbohydrate and protein content (r^2=0.94; *p*=0.007). Data are presented as mean ± SEM; *n* = 9/group.

Insulin levels were not different between the C and HP groups

Differences in insulin levels may be a more plausible explanation for the increase in lipogenesis during high protein (Boden et al., 2013). Even though insulin correlated better with carbohydrate and protein rather than carbohydrate only, there were no significant differences in the plasma insulin levels (Figure 23A) as well as the total amount of insulin released between the C and HP groups (Figure 23B).

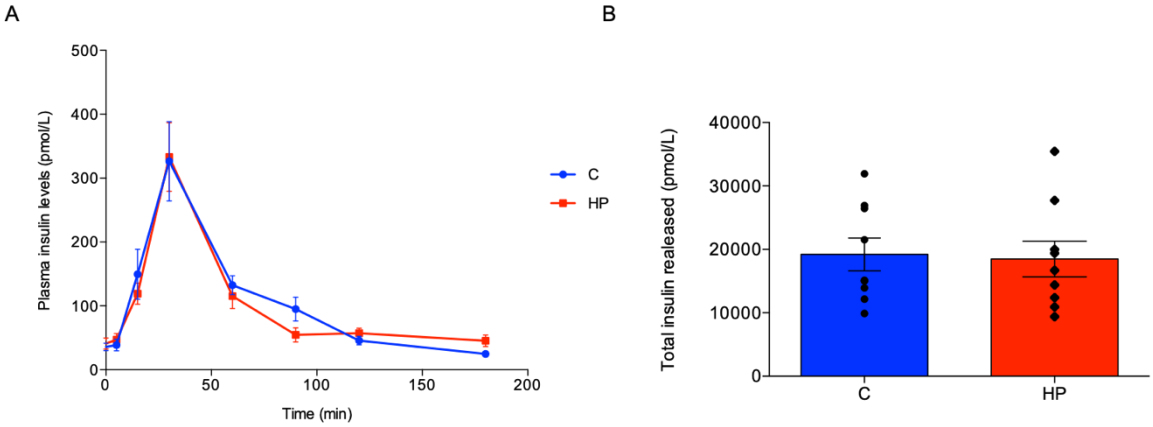

Figure 23. Plasma insulin levels. (**A**) Plasma insulin released after consuming a C (blue), HP (red) and a HF (green) meal. (**B**) Total plasma insulin released after consuming a C (blue), HP (red) and a HF (green) meal over 3 hours. Data are presented as mean ± SEM and analysed by two-way repeated measures ANOVA with *post-hoc* Sidak's multiple comparisons test (**A**); or by a paired two-tailed t-test **(B)**; * = $p \leq 0.05$, n = 9/group.

3.5 Discussion

Gastroparesis, defined as abnormally delayed gastric emptying is prevalent amongst patients with longstanding T2DM. Persistent hyperglycaemia damages the vagus nerve and leads to uncontrolled emptying of the stomach (Wilcox, 2005.). A range of studies have previously characterised how different macronutrient compositions, energy, meal texture, volumes, temperatures and pH affect gastric emptying (Leiper, 2015). However, there is limited data on which factor is the main determinant of gastric emptying and how this in turn affects lipid metabolism. In this chapter, liquid carbohydrate was shown to be the main determinant of gastric emptying, which delayed the emptying of the solid fraction. Moreover, DNL was not affected by liquid carbohydrate in the present study. However, the HP meal increased scTAGs in healthy males, a set of TAGs previously associated with DNL.

Previous studies into the effects of macronutrient composition of gastric emptying have concluded that high fat and carbohydrate meals delay gastric emptying in liquids or semi-solid meals (Gentilcore et al., 2006; Hellström et al., 2017; Mushref and Srinivasan, 2013). The results of this study indicate that liquid carbohydrate was the primary determinant of gastric emptying rather than macronutrient compositions. The delay caused by carbohydrate in the liquid phase occurred only up to a liquid carbohydrate content of 50%, at which point, increasing levels of liquid carbohydrate no longer slowed gastric emptying rates in the present study. Liquid gastric emptying is faster than solid gastric emptying and therefore in the C and HC meals (containing a greater proportion of the meal in liquid form), the rate of early carbohydrate delivery to the duodenum was higher than in the HF, CB and HP meals. This agrees with the hypothesis that early delivery of carbohydrate to the duodenum is sensed by receptors in the small intestine to delay the emptying of the solid portion, where the supplied ^{13}C-octanoic acid is bound. This hypothesis is also supported by Collins et al., wherein a delay in gastric emptying was induced by dextrose following a mixed meal (Collins et al., 1991). The extent to which the gastric emptying response was partly due to volume, or composition of the

liquid is unknown. Water (liquid without carbohydrate) might be having an effect in this delay and therefore is should be further investigated to fully characterise what induces this delay.

It has previously been demonstrated that high carbohydrate diets induce DNL (Tappy and Lê, 2012; Timlin and Parks, 2005). This was elicited by postprandial glucose activation of the transcription factor, ChREBP by glucose (Iizuka and Horikawa, 2008). Rapidly increased hepatic glucose levels induce glycolysis, and a number of glycolytic intermediates, including glucose-6-phosphate and fructose-2,6-bisphosphate, have been shown to increase the activity of ChREBP (Otero et al., 2014). This transcription factor then upregulates the expression of DNL genes encoding ACL, ACC and FAS. It also induces the expression of pyruvate kinase that generates pyruvate, which is in turn de-carboxylated to acetyl-CoA to provide an alternative source of the DNL substrate (Ma et al., 2005). Mice deficient in ChREBP also present with decreased levels of DNL (Iizuka et al., 2004). It is conceivable that liquid carbohydrate, which empties from the stomach and reaches the liver rapidly (Phillips et al., 2015), induces DNL. However, the HC meal, containing the highest amount of liquid carbohydrate in this study did not increase the levels of typical scTAGs. Moreover, scTAG content was not different between the two meals that contained the same carbohydrate content whilst the form of carbohydrate was different (solid compared with liquid), suggesting that liquid carbohydrate did not induce DNL in this study. This may be explained by the fact feeding was preceded by a 12 h fast which typically suppresses DNL and increases gluconeogenesis. Refeeding with a 2 MJ high carbohydrate meal may not have been sufficient in this case to replenish the glycogen stores and induce DNL. In studies demonstrating an increase in DNL after high carbohydrate feeding, the meals were above 3 MJ (Marques-lopes et al., 2001) and in some, subjects were fed multiple times (Timlin and Parks, 2005).

Besides glucose, insulin can also induce DNL, through activation of the sterol responsive SREBP-1c transcription factor and subsequent activation of DNL gene transcription (Boden et al., 2013). They both involve PI3K/PKB, which can result in the phosphorylation and activation of SREBP1c or LXRα; (Kawano and Cohen, 2013). Important nodes of the insulin signalling

cascade are the mTOR complexes that are activated by amino acids (Bar-Peled and Sabatini, 2014). In this study, insulin concentration correlated better with dietary carbohydrate and protein together rather than solely carbohydrate content. This may suggest that dietary protein might also induce the release of insulin to activate DNL.

Interestingly, the HP meal had more plasma lipid than that expelled from the stomach, when estimated by calculating the AUCs. The HP meal, rich in glutamate, specifically increased scTAGs in plasma (rather than a global increase in TAGs) as well as in the LDL/VLDL fraction in healthy human males. A previous study reported that DNL peaks at 4 hours after feeding (Timlin and Parks, 2005), which aligns with the peak concentration of scTAGs in plasma and the LDL/VLDL fraction. Plasma glutamate concentration peaked at 3 h and decreased at 4 h when DNL peaked. This may suggest that glutamate was utilised by the liver to induce DNL, or possibly that its uptake was driving the increase in DNL. This agrees with the finding that glutamate, like citrate, is an allosteric activator of ACC (Boone et al., 2000). It is postulated that glutamate induces the polymerisation of ACC1 (the isoform that is present in lipogenic tissues) and thereby increases its activity (Boone et al., 2000). Even though glutamate is not typically viewed as a lipogenic precursor, carbon from glutamate/glutamine has been shown to be incorporated into fatty acids in cells with increased isocitrate dehydrogenase 1/2 (IDH1/2) activity. These cells are usually functioning under hypoxic conditions in the cancerous state (Metallo et al., 2011). However, wild-type brown adipocytes have been showed to have increased in vivo activity of IDH1 (Yoo et al., 2008). IDH1/2 converts α-ketoglutarate to citrate via reductive carboxylation under a high mitochondrial reduced nicotinamide (NADH) oxidised nicotinamide (NAD^+) ratio (Koh et al., 2004). Increases in energy balance, reflected by a high mitochondrial NADH/NAD^+ ratio, increase the activity of IDH1/2 to induce reductive carboxylation and generate citrate from glutamate. The extent to which glutamate surplus affects the NADH/NAD^+ ratio and is itself incorporated into lipids in hepatocytes will be examined in the next chapter.

The data also support the fact that BCAAs, leucine, isoleucine and valine correlate with insulin resistance and T2DM in humans (Würtz et al., 2012). It has been demonstrated that

deprivation of BCAAs from the diet whilst maintaining levels of other amino acids is sufficient to improve glycaemic control (Xiao et al., 2014). Increased circulating BCAAs are sensed by mTOR and subsequently promote DNL and may explain the effects of BCAAs (Crown et al., 2015). The effects seen in this study were following a 12-hour fast, which typically supresses DNL (Nieminen et al., 2016), and may therefore have general implications for high-protein diets and T2DM. Studies have previously demonstrated that a higher protein/lower carbohydrate diet downregulates DNL (Garcia-Caraballo et al., 2013; Margolis et al., 2016), typically in longer-term dietary interventions. However, the precise amino acid composition of high protein diets used in many studies is not often reported in publications. The detailed metabolic parameters of amino acid-driven DNL will be investigated in subsequent chapters.

3.6 Conclusions

In this human intervention study, liquid carbohydrate was the main determinant of gastric emptying rate, not macronutrient composition. Indeed, the energy contained within the liquid carbohydrate component of the meal delayed gastric emptying of the solid component up to approximately 1000 KJ, with no further delay being observed with increasing liquid carbohydrate energy content beyond that value. This suggests that liquid carbohydrate reaches chemoreceptors in the intestine faster, inducing a postprandial neurohormonal delay in the gastrointestinal motility of the solid phase. The energy content of the liquid portion was not sufficient to induce DNL, as liquid carbohydrate did not correlate with the amount of scTAGs. However, the HP meal, rich in glutamate, increased scTAGs in plasma and the liver-derived lipoprotein, VLDL. The data suggest that glutamate may be responsible for inducing DNL. The effects of glutamate on DNL will be examined in the next chapter.

Chapter 4. Glutamate is a substrate of fatty acid synthesis and induces *de novo* lipogenesis in hepatocytes

Abstract

Glutamate is one of the most abundant amino acid in foods. In the previous chapter, a meal rich in glutamate increased the levels of triacylglycerides associated with *de novo* lipogenesis in plasma and liver-derived lipoproteins. The studies contained in this chapter investigate the underlying mechanism of the increase in lipogenic triacylglycerides caused by a meal containing high levels of glutamate. Carbon from glutamate was incorporated into fatty acids and palmitate-containing triacylglycerides, through an increase in cellular energy balance. In addition, glutamate increased the levels of lipogenic triacylglycerides in hepatocytes, through the activation of the protein kinase B pathway. The expression of lipogenic genes under the control of protein kinase B were increased with glutamate treatment. The induction of *de novo* lipogenesis by glutamate was dependent on insulin. The levels of lipogenic triacylglycerides and expression of genes were not increased in insulin starved cells. Though glutamate is not considered a canonical precursor of lipogenesis, the data suggest that the levels of incorporation of glutamate-derived carbon into fats are appreciable even under physiological glucose concentrations. In addition, glutamate supplementation was sufficient to induce *de novo* lipogenesis in wild-type hepatocytes, suggesting that the use of diets rich in glutamate, and by extension high protein, for the treatment of metabolic dysregulation requires greater consideration.

4.1 Introduction

4.1.1 DNL substrates

DNL is the pathway that converts acetyl-CoA to fatty acids primarily in the liver (Diraison et al., 2003) and may be considered as a pathway for the storage of excess carbon from nutrients into fatty acids and energy-dense TAGs, which can be later mobilised to provide energy as needed. Abnormal rates of DNL may represent an early stage in the development of fatty liver and diabetes as increased lipid accumulation is a common feature of both disorders (Paglialunga and Dehn, 2016). Despite the fact that DNL has been linked with overnutrition and the metabolic syndrome (Grundy, 2016), our knowledge of substrates that fuel the process is limited. A significant number of studies have focused on glucose and fructose as 'lipogenic' nutrients that contribute to the acetyl-CoA pool (Moore, Gunn and Fielding, 2014). However, the liver is capable of utilising a variety of molecules to generate acetyl-CoA, including amino acids. In particular, glutamate has been shown to be incorporated into fatty acids under hypoxic conditions (Brose, Marquardt and Golovko, 2015).

4.1.2 Glutamate and hypoxia

Hypoxia is a status prevalent in many disorders including cancer, heart disease, atherosclerosis, brain injury, neurological disorders, and aging (Clambey et al., 2012; Kirby et al., 2012; Raymond et al., 2011). Biological hypoxia is defined as sub-physiological partial pressure of oxygen, or pO_2. In the case of cancer, cell proliferation outpaces blood supply by vascularisation, thus depleting large regions of tumour tissue of oxygen (Muz and Azab, 2015). One major adaptation to anaerobic conditions is the increased levels of glutamate consumption, at levels exceeding protein synthesis requirements (Eales et al., 2016). Indeed, it has been reported that glutamate increases lipid synthesis under hypoxia, via its contribution to lipogenic acetyl-CoA (Brose et al., 2015).

4.1.3 Glutaminolysis and reductive carboxylation

There are two pathways by which glutamate can generate acetyl-CoA: glutaminolysis and reductive carboxylation. In glutaminolysis, glutamate is converted to α-ketoglutarate, an intermediate of the TCA cycle. α-ketoglutarate is oxidised in the TCA cycle to malate, which can be converted to pyruvate via malic enzyme. Pyruvate then undergoes oxidative decarboxylation to generate acetyl-CoA (Kim et al., 2017). This is then combined with oxaloacetate, via CS, to generate citrate (Figure 1A). Alternatively, operating in reverse of the typical flow of the TCA cycle, α-ketoglutarate can be converted to citrate via IDH1/2 in the process of reductive carboxylation (Figure 1B).

Citrate produced by both pathways is transported to the cytosol and lysed to lipogenic acetyl-CoA. In the context of oncometabolism, both glutaminolysis and reductive carboxylation have been demonstrated in rapidly dividing cancer cells (Fendt et al., 2013). However, it has not yet been determined whether glutamate can be incorporated into fatty acids under physiological conditions.

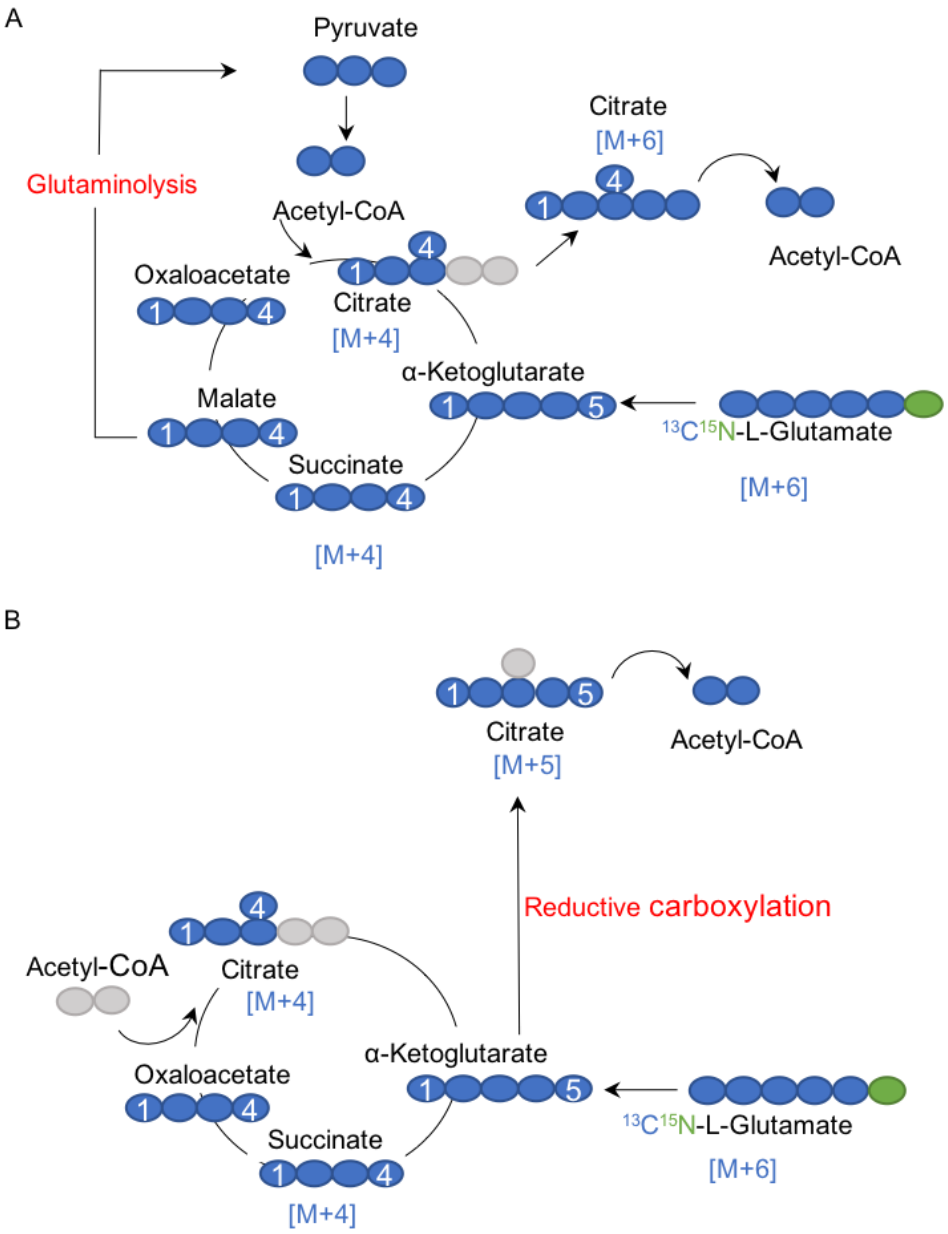

Figure 1. Schematic representation of the production of lipogenic acetyl-CoA from $^{13}C_5{}^{15}N$-L-glutamate. (**A**) Label from glutamate is routed to lipids via glutaminolysis; malic enzyme produces fully labelled pyruvate [M+3] from malate [M+4], and pyruvate is then decarboxylated to acetyl-CoA [M+2]. Fully labelled oxaloacetate [M+4] then combines with labelled acetyl-CoA [M+2], via citrate synthase, to generate fully labelled citrate [M+6]. Citrate is then lysed to generate fully labelled acetyl-CoA [M+2]. (**B**) Label from glutamate is routed to lipids via reductive decarboxylation; fully labelled α-ketoglutarate [M+5] is carboxylated to labelled isocitrate and citrate [M+5]. Citrate is then lysed by ACL to generate fully labelled acetyl-CoA [M+2]. In both cases carbon from acetyl-CoA may be shuttled to lipids. Adapted from Kim et al., 2017.

4.1.4 NAD^+ to NADH ratio and DNL

The ratio of oxidised to reduced nicotinamide nucleotides (redox state) affects the activity of metabolic reactions in the cell. It has been shown that addition of nicotinamide to rats inhibits the rate of lipogenesis by approximately 50% (Mclean and Greenbaum, 1970), by artificially inducing a low energetic state. This ratio greatly affects the activity of the three isoforms of IDH (IDH1, IDH2 and IDH3). IDH1 catalyses the reversible reaction of isocitrate to α-ketoglutarate in the cytosol and IDH2 catalyses the same reaction in the mitochondrion. IDH3 is directly related to the forward TCA cycle as it catalyses the irreversible reaction of isocitrate to α-ketoglutarate (Khallaf, 2017).

A low NAD^+/NADH ratio will prevent the forward direction of the mitochondrial TCA cycle by inhibiting IDH3. Increased NADH, indicating a more positive energy balance, favours the reductive carboxylation of α-ketoglutarate to isocitrate by the reverse reactions of IDH1/2 (Wise et al., 2011). Citrate accumulated in the mitochondrion from IDH2 is transported to the cytosol and together with cytosolic citrate already present from IDH1, they participate in anabolic processes, such as DNL. Overexpression of cytosolic IDH1 leads to increased lipogenesis in liver and adipose tissue (Koh et al., 2004). The conversion of glutamate to α-ketoglutarate, via glutamate dehydrogenase, decreases the NAD^+/NADH ratio by generating NADH (Botman et al., 2014), increasing the mitochondrial energy balance. Therefore, glutamate might participate in the synthetic pathways of IDH1 and 2, by inhibiting IDH3, to shuttle citrate out of the mitochondrion and induce an anabolic effect rather than being used by the TCA cycle (Figure 2).

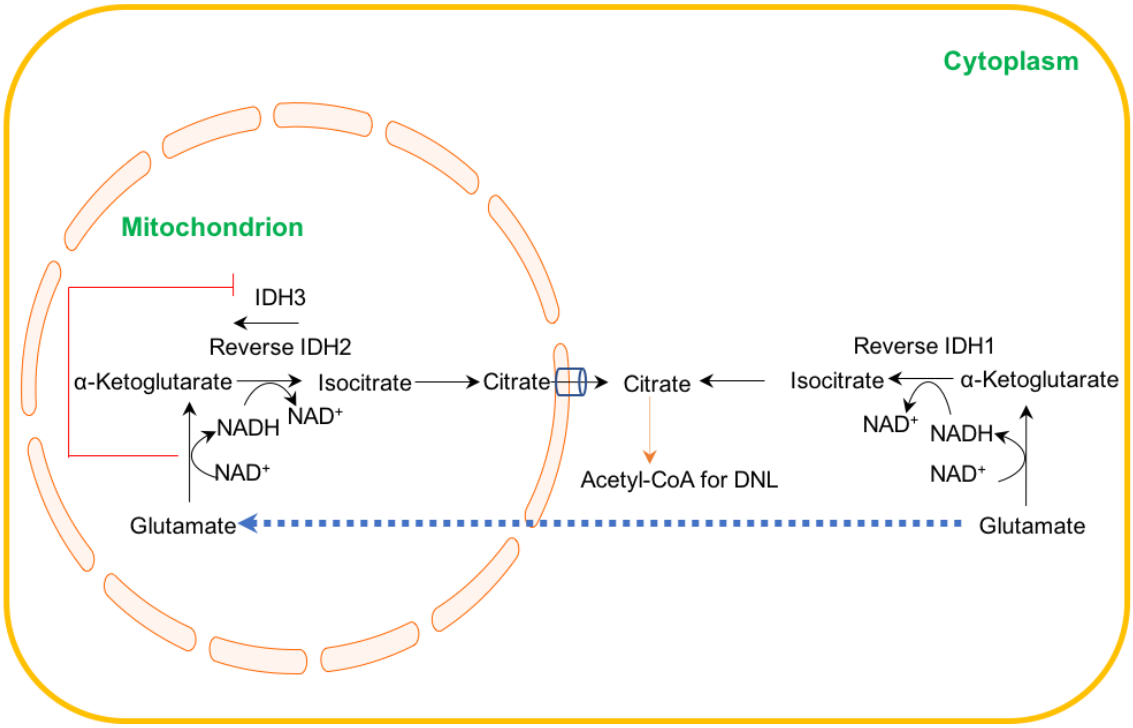

Figure 2. The role of the three isocitrate dehydrogenase isoforms during periods of anabolism. Once glutamate is in the cell, glutamate dehydrogenase oxidises glutamate to α-ketoglutarate using NAD^+ as a cofactor. Under reduced conditions (low NAD^+/NADH), IDH1 and IDH2 synthesise citrate in the mitochondrion and cytosol, respectively, by reducing α-ketoglutarate through the use of increased NADH. IDH3 is inhibited and therefore, citrate is not oxidised in the TCA cycle. Citrate that has accumulated in the mitochondrion by IDH2 is exported to the cytosol. Build-up of citrate in the cytosol, from IDH1 and 2, induces DNL as the lysis of citrate produces the DNL's substrate acetyl-CoA.

4.1.5 mTOR and DNL

DNL takes place in the cytosol and in order to obtain cytosolic acetyl-CoA (the primary substrate), citrate is exported from the mitochondrion to the cytosol. Once in the cytosol, citrate is lysed by ACL to generate cytosolic acetyl-CoA. Acetyl-CoA is then carboxylated to malonyl-CoA by ACC. Malonyl-CoA is the working substrate of FAS, which generates fatty acids. Further molecules of acetyl-CoA are used to generate malonyl-CoA, transferred to FAS and added to the lengthening carbon chain to generate palmitate (Donnelly et al., 2005). Palmitate is the primary product of DNL, and it can be further desaturated by SCD1, and/or elongated, by ELOVL6. The resulting fatty acids may then be incorporated into TAGs and VLDLs for export. A subset of TAGs containing short chain saturated fatty acids, typically palmitate, have been previously correlated with DNL and hepatic steatosis (Sanders et al., 2018).

The expression of genes that encode for the proteins mentioned above as being central to DNL (ACLY, ACACA, FASN, SCD1 and ELOVL6) is under the control of mainly two transcription factors; ChREBP1 and SREBP-1c. Glucose activates ChREBP1 (Tong et al., 2009) whilst insulin activates SREBP-1c (Ferré and Foufelle, 2007). Activation of the insulin receptor results in the activation of the IRS that recruits PI3K to the membrane, where it phosphorylates PIP_2 to PIP_3. PIP_3 acts as a docking site for the kinases mTORC2 and PDK1. Both mTORC2 and PDK1 phosphorylate and therefore activate PKB/AKT2. PhosphoAKT2 then activates mTORC1, which stimulates $p70^{S6K1}$. This induces the nuclear translocation of LXRα, where it heterodimerises with RXR (Kawano and Cohen, 2013). The heterodimer then induces the expression of lipogenic genes including that of SREBP-1c. Once SREBP-1c is expressed, it matures via a series of reactions, to also induce the expression of lipogenic genes. In general, amino acids are regulators of the mTOR complexes (Tato et al., 2011) and glutamate may therefore induce DNL via the PI3K/PKB/AKT2 signalling cascade.

4.2 Chapter aims

After identifying that a high protein meal, rich in glutamate, increases scTAG content in blood plasma that have been previously correlated with increased DNL, it is hypothesised that glutamate may induce DNL or may itself be used to synthesise lipids. In this chapter, hepatocytes are supplemented with labelled glutamate to determine whether carbon from glutamate can be incorporated into fatty acids and intact lipids under physiological glucose concentrations. In addition, hepatocytes are treated with increasing doses of glutamate to characterise whether glutamate can induce DNL in terms of gene expression, protein function and at the metabolic level, using the scTAG cluster as a proxy.

4.3 Materials and methods

4.3.1 Cell culture

Growth of AML 12 hepatocytes

AML 12 cells were purchased from American Type Culture Collection (ATCC) and cultured in 1:1 (v/v) Dulbecco's modified Eagle's medium and Ham's F12 medium (Thermo), supplemented with 10% fetal bovine serum (FBS), 1% penicillin/streptomycin (100 units/mL and 100 µg/mL, respectively), 1% insulin-transferrin-selenium (ITS; 10 mg/L, 5.5 mg/L and 6.7 µg/L respectively) and dexamethasone (100 µmol/L) at 37°C in 5% CO_2. Cells were removed from liquid nitrogen, thawed rapidly and initially cultured in a T25 flask (Cat. # 690175, Greiner). Medium was changed every two days, and upon reaching confluence, cells were sub-cultured in T75 flasks (Cat. # 7340290, Corning) at a ratio of 1:3. Cells were plated at a density of 50,000 cells/well in collagen 1-coated 12-well plates (Cat. # 7340295, Corning) and grown to confluence in maintenance medium. Cells were then supplemented with low glucose (7.60 mmol/L) with unlabelled L-glutamate (2.4 mmol/L) and dialysed FBS (Thermo) for 2 days. After switching medium, cells were serum-starved for 20 h in low glucose medium.

AML 12 $^{13}C_5$-^{15}N-L-glutamate labelling procedure

Cells were supplemented with glucose (7.60 mmol/L) with unlabelled-L-glutamate (4 mmol/L, n=3) or glucose (7.60 mmol/L) with $^{13}C_5{}^{15}N$-L-glutamate (4 mmol/L, n=3). Based on previous experiments, the cells were allowed 3 h such that the $^{13}C_5$-^{15}N-L-glutamate could reach an isotopic steady state in the TCA cycle. Cells and media were harvested at 0, 3 and 24 h (Figure 3). Table 1 summarises the composition of growth and treatment media used.

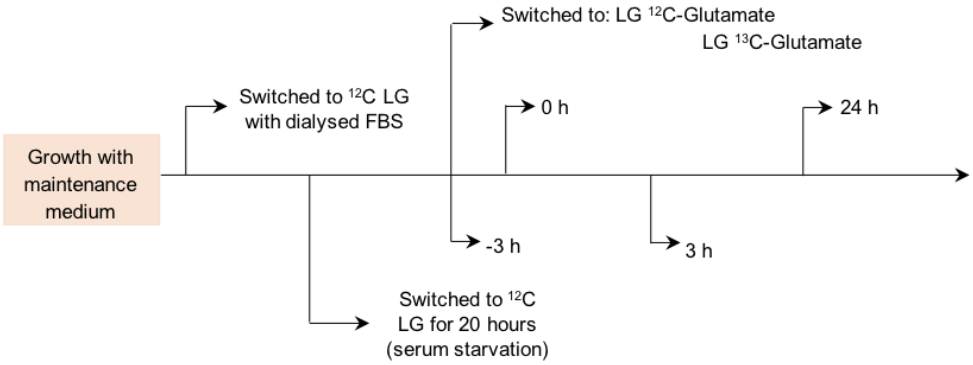

Figure 3. Schematic representation of growth and $^{13}C_5{}^{15}N$-L-glutamate treatment of AML 12 hepatocytes. Hepatocytes were switched to low-glucose (LG) for 2 days, serum starved for a day and then treated with either labelled or unlabelled L-glutamate. Cells were collected at 0, 3, 24 h.

Table 1. Medium components used for growth and treatment of AML 12 hepatocytes.

Medium	Components	[Glucose] & [Glutamate]	Manufacturer
Maintenance	90% 1:1 DMEM/F12 [a] 10% FBS[b] ITS [c] 0.10 mol/L Dexamethasone[d] Penicillin/Streptomycin [e]	17.50 mmol/L Glucose 2.44 mmol/L L-Glutamine	Cat. # 11330-032, Thermo [a] Cat. # F7524, Sigma [b] Cat. # 41400045, Thermo [c] Cat. # D4902, Sigma [d] Cat. # P4333, Sigma [e]
Unlabelled glutamate	90% 1:1 DMEM/F12 [f] 10% dialysed FBS [g] ITS [c] 0.10 mol/L Dexamethasone [d] Penicillin/Streptomycin [e]	7.60 mmol/L Glucose 4 mmol/ L ^{12}C-L-glutamic acid [h]	Cat. # D5921:N4888, Sigma [f] Cat. # A3382001, Thermo [g] Cat. # 49450, Fluka [h]
Labelled glutamate	100% DMEM/F12 [f] ITS [c] 0.10 mol/L Dexamethasone [d] Penicillin/Streptomycin [e]	7.60 mmol/L Glucose 4 mmol/L ^{13}C-L-glutamic acid [i]	Cat. # CNLM-7812-0.25, Cambridge Isotope Laboratories [i]
Increasing dose of glutamate	90% 1:1 DMEM/F12 [f] 10% dialysed FBS [g] ITS [c] 0.10 mol/L Dexamethasone [d] Penicillin/Streptomycin [e]	7.60 mmol/L Glucose 0,2,4 and 10 mmol/ L ^{12}C-L-glutamic acid [h]	Cat. # D5921:N4888, Sigma [f] Cat. # A3382001, Thermo [g] Cat. # 49450, Fluka [h]

[a-i] Components lettered a-i and corresponding catalogue number and manufacturers

Dose response of glutamate in insulin sufficient AML 12 hepatocytes

Cells were supplemented with low glucose (7.60 mmol/L) and 1% ITS without glutamate (0 mmol/L, n=3) or with increasing levels of glutamate (2, 4, 10 mmol/L, n=3/amino acid concentration). Cells and media were harvested after 24 h (Figure 4).

Dose response of glutamate in insulin depleted AML 12 hepatocytes

Cells were supplemented with low glucose (7.60 mmol/L, *n* = 3), 5.5 mg/L transferrin and 6.7 µg/L selenium without insulin. Cells were treated without glutamate (0 mmol/L) or with increasing levels of glutamate (2, 4, 10 mmol/L, *n* = 3/amino acid concentration). Cells and media were harvested after 24h (Figure 4).

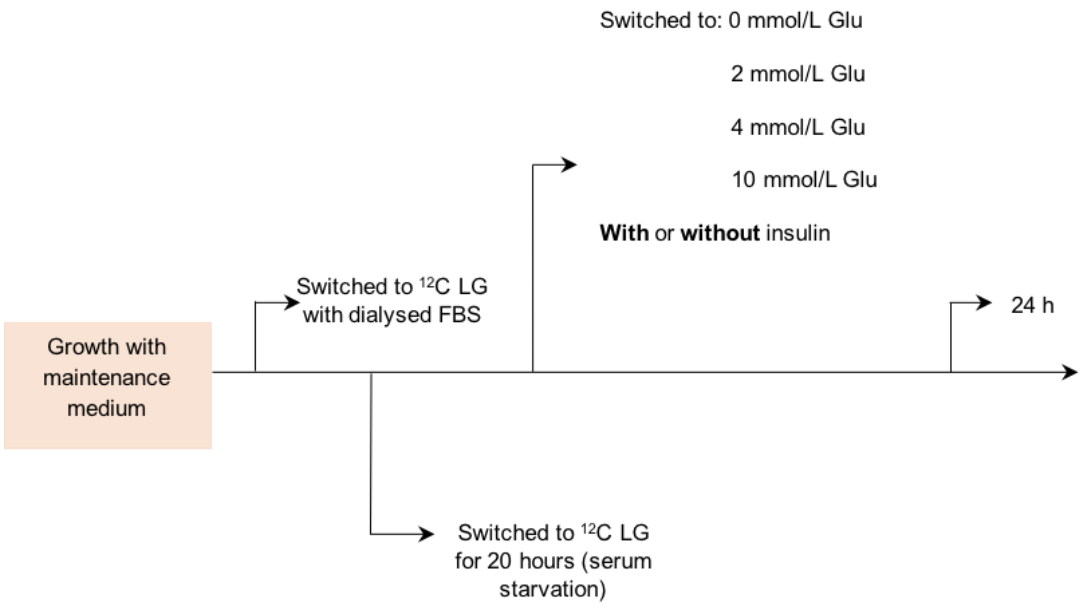

Figure 4. Schematic representation of growth and dose response of glutamate in AML 12 hepatocytes. Hepatocytes were switched to LG for 2 days, serum starved for a day and then treated with 0, 2, 4 or 10 mmol/L glutamate with or without insulin. Cells were collected at 24 h.

Harvesting of AML 12 cells for metabolomics

For cells and media undergoing metabolomic analyses, 900 µL of medium was taken from each well and stored at -80°C. Each well was then washed with 1 mL of 0.9% saline (9 g/L NaCl) and cells were lifted from the plates by adding 0.5 mL trypsin (10X trypsin-EDTA, Cat. # 25300045, Invitrogen). Each well was re-washed with 0.5 mL of 0.9% sterile-filtered saline and the resulting solution was transferred into a 2 mL microcentrifuge tube and centrifuged at 13,000 x g for 10 min to pellet the cells. The supernatant was removed and the pellet was resuspended in 750 µL of a 2:1 (v:v) chloroform:methanol solution to prevent enzymatic degradation of metabolites, and frozen at -80°C.

Metabolite extractions

Metabolites were extracted as described in Chapter 2, Section 2.1.1.

4.3.2 LC-MS of aqueous and organic fractions

Analysis of aqueous metabolites by triple quadrupole-mass spectrometry

Metabolites were extracted as described above and aqueous extracts were reconstituted in 50 µL of 10 mmol/L ammonium acetate in water before TCA cycle intermediates were separated using reversed phase liquid chromatography using a Vanquish UHPLC attached to a TSQ Quantiva triple quadrupole mass spectrometer (Thermo Scientific). Multiple reaction monitoring was used in conjunction with positive/negative ion mode switching utilising the optimised mass transitions detailed in Table 3. A C18-PFP column (150 mm x 2.1 mm, 2.0 µm; ACE) was utilised at a flow rate of 0.5 mL/min, with a 3.5 µL injection volume. For chromatography on the UHPLC system, mobile phase A was 0.1% formic acid in water and mobile phase B was 0.1% formic acid in ACN. The gradient started at 30% B, increased to 90% B at 4.5 min for 0.5 min and returned to the starting conditions for a further 1.5 min to re-equilibrate the column. Mass transitions of each species were as follows (precursor > product): D5-L-proline 121.2 > 74.2; D8-L-valine 126.1 > 80.2; D10-L-leucine 142.0 > 96.2; L-glutamate

[M] 148.0 > 84.2; L-glutamate [M+1] 149.0 > 85.2; L-glutamate [M+6] 154.1 > 89.1; Citrate 191.0 > 111.0; Citrate [M+1] 192.0 > 112.0; Citrate [M+2] 193.0 > 113.0; Citrate [M+3] 194.0 > 114.0; Citrate [M+4] 195.0 > 114.0; Citrate [M+5] 196.0 > 115.0; Citrate [M+6] 197.0 > 116.0. Collision energies and RF lens voltages were generated for each species using the TSQ Quantiva optimisation function. Instrument optimisation parameters are detailed in Table 2. Xcalibur Software (Thermo Scientific) was used to identify peaks, process mass spectra and normalise data to the closest-eluting internal standard.

Table 2. Mass spectrometer optimised settings for aqueous LC-MS

Instrument Optimisation Parameters	
Method Duration (min)	6.5
Ion Source Type	H-ESI
Ion Spray Voltage: Positive Ion (V)	3500
Ion Spray Voltage: Negative Ion (V)	2500
Sheath Gas (Arb)	16
Sweep Gas (Arb)	2
Ion Transfer Tube Temperature (°C)	356
Vaporiser Temperature (°C)	420
Column Temperature (°C)	30
Needle Wash	1:1 (v:v) water:ACN
Seal Wash	4:1 (v:v) IPA:Water with 0.1% formic acid

A TIC of aqueous metabolites in hepatocytes obtained by the above method is shown in Figure 5A. From the TIC, unlabelled and labelled glutamate (Figure 5B) as well as unlabelled and labelled citrate (Figure 5C) were extracted.

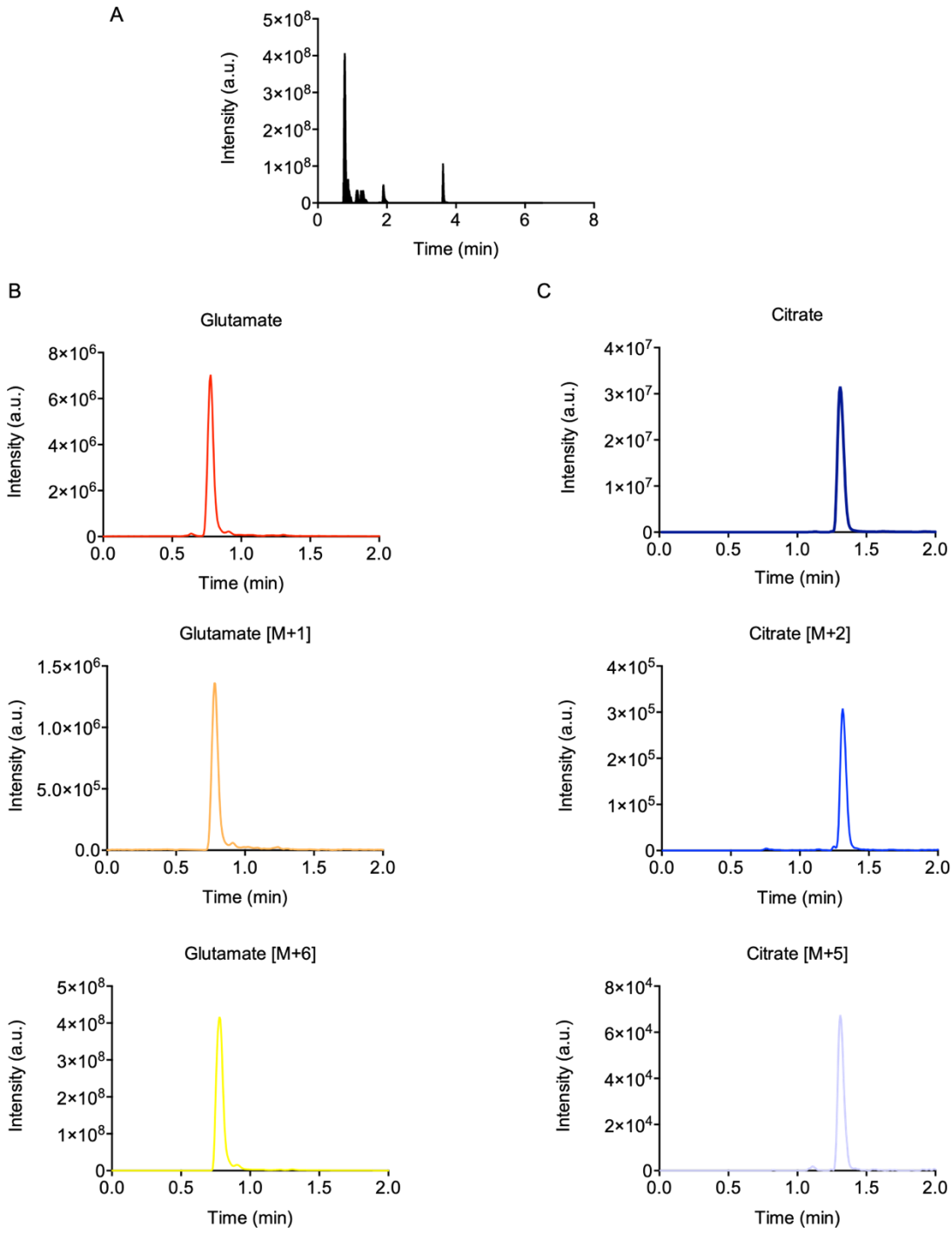

Figure 5. TIC and EIC for glutamate and citrate. (**A**) The TIC of aqueous metabolites in hepatocytes detected by LC-MS. (**B**) The EIC for glutamate M, glutamate M+1 and glutamate M+6 ions. (**C**) The EIC for citrate M, citrate M+2 and citrate M+5 ions.

Picolinyl esters of fatty acids (PEFA) derivatisation of organic fractions for LC-MS and analysis of total fatty acids by triple quadruple mass spectrometry

Each dried organic extract was derivatised by the method described in Chapter 2, Section 2.1.3 and analysed by the method described in Chapter 2, Section 2.1.4.

Analysis of intact lipids using orbitrap mass spectrometry

The organic fraction was analysed by the method described in Chapter 2, Section 2.1.2.

4.3.3 NAD^+/NADH quantification assay

NAD^+/NADH was measured according to the manufacturer's protocol (Abcam, ab65348). Briefly, cells were lysed using the NAD^+/NADH extraction buffer and enzymes that consumed NADH were removed by filtration through a 10 kDa spin column (Abcam, ab93349). For NADH detection, NAD^+ was decomposed by heating samples at 60°C for 30 min. Samples [NADH with decomposed NAD^+ and total NAD(H)] and standards were incubated with 100 µL NAD cycling reaction mix to convert NAD^+ to NADH. After 5 min, 10 µL of NADH developer was added and the reaction was allowed to cycle for 2 h. The OD was measured at 450 nm after stopping the reaction with 10 µL stop solution.

4.3.4 Staining

Oil red O staining

Media were aspirated, and cells were washed with sterile phosphate-buffered saline (PBS). After aspirating PBS, the cells were fixed with 1 mL of 10% formalin for 30 min at 37°C. A stock oil red O solution was prepared by dissolving 0.6 g of oil red O powder in 200 mL of 99% isopropanol. In the fume hood, 3 parts of oil red O stock solution were mixed with 2 parts deionised water and filtered through a 45 µm filter to remove precipitates. After formalin was removed from the plates, cells were washed with deionised water and 1 mL of 60% isopropanol was added to each well for 5 min. To the fixed cells, 1 mL of oil red O solution was added for

10 min. Oil red O was removed from the wells and the plates were rinsed with deionised water before adding 1 mL haematoxylin counterstain into each well for 2 min. Haematoxylin was poured off and the plates were gently rinsed with warm water. Plates were viewed on a phase contrast microscope. Intact lipids were stained red and nuclei blue.

4.3.5 Gene expression analysis

Ribonucleic acid (RNA) extraction and purification from AML12 hepatocytes

Total RNA was extracted and purified from hepatocytes using a RNeasy Mini Kit (QIAgen) according to the manufacturer's specifications. After aspirating the media, 350 µL of buffer RLT and 70% ethanol were added to each well to lyse the cells. After mixing, the solution was transferred to a RNeasy spin column and centrifuged at 8,000 x g for 15 s to bind RNA to the membrane. The flow-through was discarded and the membrane was washed with 700 µL RW1 wash buffer by centrifuging at 8,000 x g for 15 s. The flow-through was discarded and the washing step was repeated. Subsequently, 500 µL of Buffer RPE (working ethanol buffer) was added to the RNeasy spin column and centrifuged at 8,000 x g for 15 s. The flow-through was discarded and the process repeated, before centrifugation at 8,000 x g for 15 s. The RNeasy spin column was placed in a new 2 mL collection tube and centrifuged at maximum speed for 2 min to dry the membrane and prevent carryover of ethanol. To elute pure RNA, the column was placed in a new 1.5 mL collection tube and 30 µL RNase-free water was added directly to the membrane before centrifuging at 8,000 x g for 1 min. Purified RNA concentration was quantified at 260 nm using a NanoDrop 100 (Thermo Fisher Scientific).

Complimentary DNA production by reverse transcription

Each purified RNA sample was diluted with RNase-free water to a final concentration of 100 ng/µL. Complimentary DNA (cDNA) synthesis and genomic DNA elimination in RNA samples was performed using an RT^2 First Strand Synthesis kit (QIAgen) according to the manufacturer's specifications. Genomic DNA elimination was performed by mixing each RNA

sample with 2 µL of genomic elimination buffer (buffer GE) and incubating on a thermocycler (Techne) at 42°C for 5 min and then immediately placed on ice for 1 min. The reverse transcription mix was prepared by adding 4 µL 5X Buffer BC3, 1 µL Control P2 (random hexamers), 2 µL RE3 Reverse Transcriptase Mix and 3 µL RNase-free water. To each reaction tube, 10 µL reverse-transcription mix were added and mixed gently. The samples were then reverse transcribed by incubating on a thermocycler at 42°C for exactly 15 min and then immediately terminating the reaction by incubating at 95°C for 5 min. The reactions were stored at -20°C prior to real time quantitative PCR analysis.

Quantitative Polymerase Chain Reaction (qPCR)

The relative abundance of transcripts of interest was measured by qPCR in RT^2 SYBR Green Mastermix (QIAgen) with a StepOnePlus detection system (Applied Biosystems). The SYBR Green qPCR Mastermix contained HotStart DNA Taq Polymerase, PCR Buffer, dNTP mix (dATP, dCTP, dGTP, dTTP) and SYBR Green dye. Before adding cDNA to each well of the 96-well plate, cDNA was diluted in RNase-free water to a final concentration of 8 ng/µL. PCR component mix was prepared by mixing 10 µL SYBR Green qPCR Mastermix with 0.6 µL of 10 µmol/L target primers (forward and reverse; 6 pmoles/reaction) and 4.4 µL RNase-free water. To each well of a 96-well plate, 5 µL cDNA (total amount 40 ng) and 15 µL PCR components mix were added. The plate was centrifuged at 1000 x g for 30 s to ensure that the contents were mixed and to remove any bubbles present in the wells. The plate was placed in the real-time cycler with the following cycling conditions: 10 min at 95°C for 1 cycle to activate HotStart DNA Taq Polymerase; 15 s at 95°C and 1 min at 60°C to perform elongation and cooling for 40 cycles. RT^2 qPCR Primer Assays for mouse *Rn18s*, *Fasn*, *Acaca*, *Acly*, *Elvol6*, *Scd1*, *Dgat2*, *Mttp* and *Apoc3* were purchased from QIAgen. Expression levels were normalised to the endogenous control, *Rn18s*, using the ΔΔCt method and fold changes reported were relative to the control group in the dose response (0 mmol/L 'amino acid').

4.3.6 Protein quantification and activity analysis

Preparation of cell lysates

Cell pellets were lysed in 100 µL Cell Extraction Buffer (10 mmol/L Tris, 100 mmol/L NaCl, 1 mmol/L EDTA, 1 mmol/L EGTA, 10 mmol/L NaF, 20 mmol/L $Na_4P_2O_7$, 20 mmol/L Na_3VO_4, 1% Triton X-100, 10% glycerol, 0.1% sodium dodecyl sulfate, 0.5% deoxycholate, 1 mmol/L phenylmethylsulfonyl fluoride, complete protease inhibitor tablet and 1% of each phosphatase cocktail inhibitor 2 and 3) for 30 min, vortexing at 10-min intervals. The lysate was centrifuged at 13,000 x g for 10 min at 4°C and the supernatant was collected and stored at -80°C.

AKTpS473 and AKT [total] quantification by enzyme-linked immunosorbent assay

PKB/AKT concentrations were measured using commercial assay kits (Invitrogen). The protocol was followed according to the manufacturer's specifications. Briefly, cells were collected by centrifugation and washed with cold PBS. After diluting samples and standards with standard diluent buffer, they were incubated on a 96-well plate containing an immobilised antibody to AKTpS473 or AKT [Total] for 2 h at room temperature with gentle shaking. Unbound constituents were washed off and then an AKT [Total] biotin conjugate or AKTpS473 detection antibody was added to each well for 1 h at room temperature with gentle shaking. After washing off unbound conjugates, streptavidin-HRP solution (AKT [Total]) or anti-rabbit IgG HRP solution (AKTpS473) was added to each well and incubated for 30 min at room temperature with gentle shaking. Following washing, a stabilised chromogen was added to each well and incubated for 30 min in the dark without shaking. Stop solution was added to each well to stop the enzymatic reaction and the absorbance was read at 450 nm. The background absorbance was subtracted from all data points, including standards, and a standard curve was generated. The unknown concentrations were read from the standard curve and the concentrations were multiplied by the appropriate dilution factor. Values were normalised to protein concentration using a reducing-agent compatible bicinchoninic acid (BCA) protein assay and values of AKT [pS473] were normalised to AKT [Total].

p70^{S6K1} activity assay

The activity of p70^{S6K1} was measured according to the manufacturer's protocol (Abcam ab139438). A 96-well plate was incubated with 50 µL of kinase assay dilution buffer at room temperature for 10 min. Cells were lysed as detailed above, and each sample was loaded into the appropriate well. The reaction was initiated by addition of 10 µL of diluted ATP and incubating at 30°C for 1 h. The kinase reaction was stopped by emptying the contents of each well. The phosphospecific substrate antibody was then added to each well and incubated at room temperature for 1 h. The contents of the well were emptied again and washed 4 times. After drying, the diluted Anti-Rabbit IgG: HRP Conjugate was added to each well for 30 min at room temperature. Following washing the TMB substrate was added to each well and incubated for 30 min at room temperature. Stop solution was added to each well to stop the enzymatic reaction and the absorbance was read at 450 nm. The background absorbance was subtracted from all data points, including standards, and a standard curve was generated. The unknown kinase activity was read from the standard curve and the activities were multiplied by the appropriate dilution factor. Values were normalised to protein concentration using a reducing-agent compatible bicinchoninic acid protein assay.

Bicinchoninic acid protein (BCA) assay - reducing agent compatible

Protein concentrations were measured using a commercial assay kit by Pierce™ Thermo Scientific. The protocol was followed according to the manufacturer's specifications. Briefly, samples were diluted in Compatibility Reagent Stock solution (1:1, v:v) and incubated at 37°C for 15 min. Samples were cooled at room temperature for at least 5 min. After samples and Bovine serum albumin (BSA) standards were added to a 96-well plate, BCA working reagent was added to each well (1:3, v:v, sample/standard: BCA working reagent). The absorbance was measured at 562 nm and the average absorbance of the blank replicates was subtracted from each standard and sample replicate. A standard curve was generated by plotting the average blank corrected absorbance measurements for each BSA standard versus the known

concentration. An equation in the form y=mx+c was generated for the protein standards from which the unknown concentrations were calculated.

4.3.7 Statistical analysis

Univariate statistics

Data were visualised using GraphPad (GraphPad Prism 5.2; GraphPad Software, San Diego, CA, USA). All data are expressed as means ± SEM. In GraphPad, one-, two-way ANOVA or two-tailed Student's t-Test were performed where appropriate to determine significant differences between experimental groups. For one-way ANOVA, Tukey's *post-hoc* multiple comparison test was performed, whilst for two-way ANOVA, Sidak's *post-hoc* multiple comparison test was used. Differences between experimental groups were considered to be statistically significant when $p \leq 0.05$.

4.4 Results

4.4.1 Glutamate acts as a substrate for the synthesis of TAGs, via the TCA cycle and DNL-derived palmitate in AML 12 hepatocytes

Labelling of palmitate from glutamate via reductive carboxylation

Under normal physiological conditions carbohydrates act as the canonical source of substrate for DNL. However, the contribution of amino acids, which could be derived from protein-rich diets, is less well understood beyond the context of oncometabolism. To determine whether glutamate acts as substrate for DNL under conditions of typical carbohydrate supply (approximately 5 mmol/L), AML 12 hepatocytes were supplemented with $^{13}C_5$-labelled glutamate, one of the most abundant dietary amino acids, to trace its metabolic fate. Glutamate may enter the TCA cycle via deamination to α-ketoglutarate. Analysis of subsequent TCA cycle intermediates using mass spectrometry showed that, compared with unlabelled samples, the levels of labelled TCA cycle intermediate citrate $[M+2]^+$and $[M+5]^+$ (mass of the unlabelled compound plus 2 and 5 Da for the labelled carbons) were markedly increased in labelled samples over 24 h (Figure 6). Interestingly, the $[M+4]^+$ citrate generated by the addition of unlabelled acetyl-CoA to $[M+4]^+$ oxaloacetate cannot supply $[M+2]^+$ labelled acetyl-CoA for the synthesis of fatty acids (Marietta et al., 1981). Whilst citrate is chemically symmetrical, the enzymes CS and ACL are regiospecific, such that the acetyl-CoA cleaved by ACL is the same as that added by CS (Berwick et al., 2002; Gottschalk, 1968). The ^{13}C label from glutamate was detected in the $[M+4]^+$ ion of palmitate, which was found to be significantly increased in labelled samples 3 h post-supplementation (Figure 7A). Once fatty acids are synthesised, they are packaged into TAGs and exported from the liver as VLDL. We further detected the label in the scTAG 48:0 both intracellularly and in the cell culture media (Figure 7B).

As such, we suggest the most likely process by which carbon from glutamate was incorporated into FAs was via reductive carboxylation in the TCA cycle. This reverse flow through the TCA cycle typically occurs during periods of decreased NAD^+ to NADH ratio, corresponding to high

energy balance, which was detected in glutamate-supplemented samples compared to control (Figure 7C).

Taken together, these data suggest that not only do amino acids provide carbon for use in DNL, the levels of incorporation of amino acid-derived carbon are appreciable even under physiological glucose concentrations.

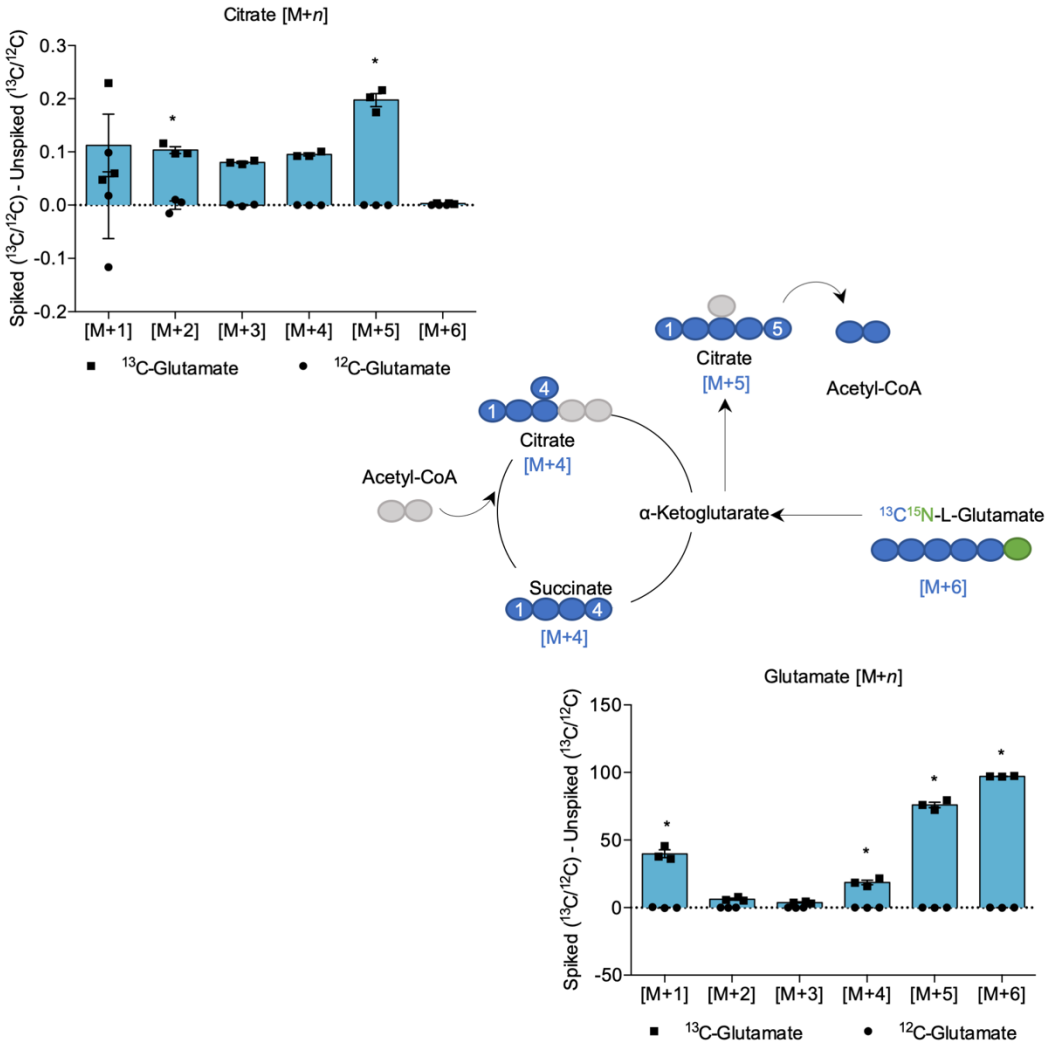

Figure 6. Carbon from 13C5-labelled glutamate is incorporated into the TCA cycle in AML 12 hepatocytes. Labelling in glutamate and citrate, detected by LC-MS over 24 h post-supplementation. Data are presented as mean ± SEM and analysed by two-way ANOVA with post-hoc Sidak's multiple comparisons test; * = $p \leq 0.05$, n = 3/group.

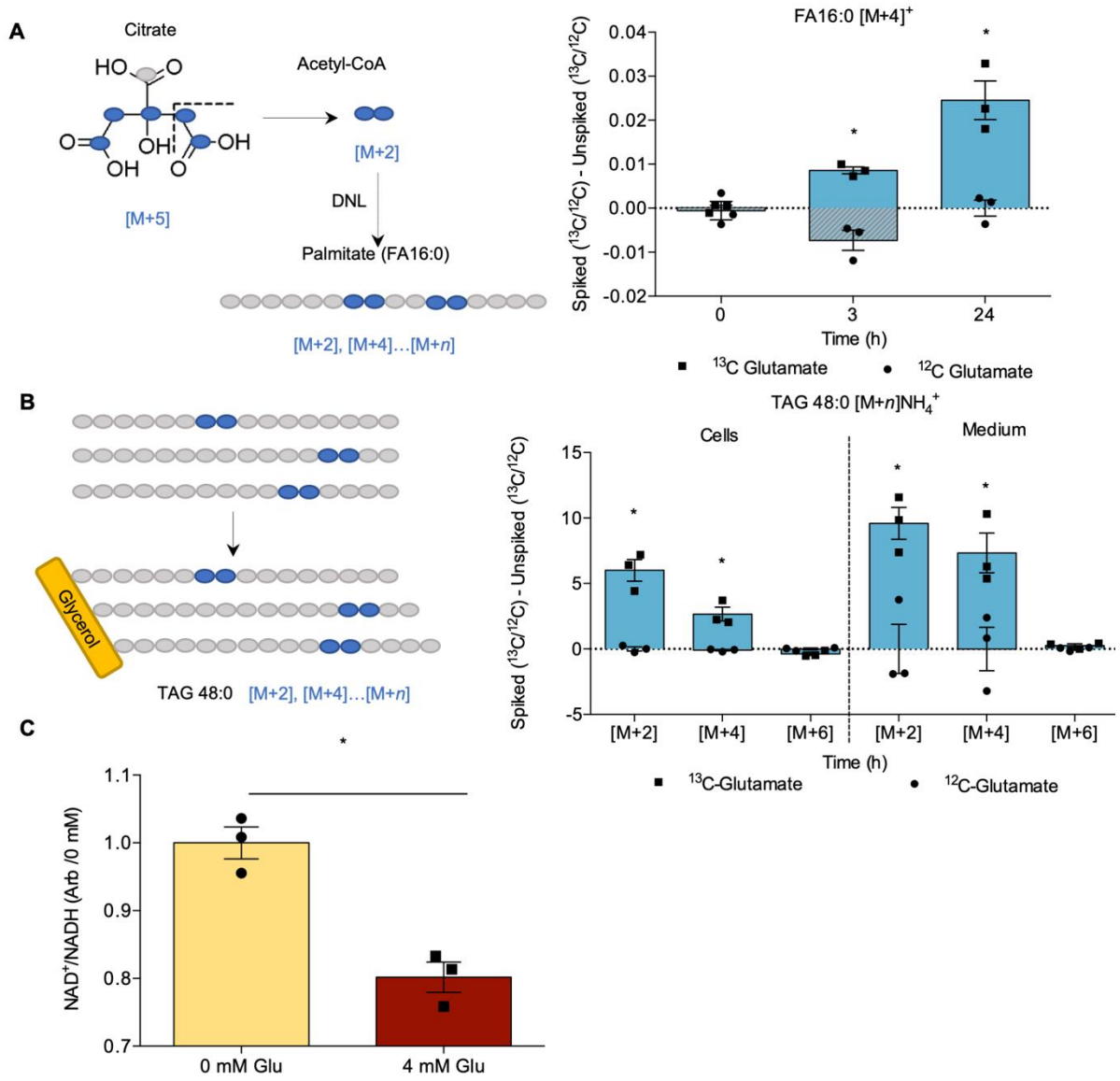

Figure 7. Carbon from $^{13}C_5$-labelled glutamate is incorporated into DNL-derived palmitate and triacylglycerols in AML 12 hepatocytes. (A) Labelling derived from glutamate in the $[M+4]^+$ ion of the picolynyl-ester of palmitate (FA16:0) generated by DNL, detected by LC-MS over 24 h post-supplementation. **(B)** Labelling derived from glutamate in the $[M+2]NH_4^+$, $[M+4]NH_4^+$ and $[M+6]NH_4^+$ ions of glyceryl tripalmitate (TAG 48:0) produced from DNL-derived palmitate in both cells and medium, detected by LC-MS after 24 h. **(C)** NAD^+/NADH at 0 mmol/L and 4 mmol/L glutamate after 24 h. Data are presented as mean ± SEM and analysed by two-way ANOVA with post-hoc Sidak's multiple comparisons test (**A**-**B**) or unpaired t-Test (**C**); * = $p \leq 0.05$, n = 3/group.

4.4.2 Glutamate induces DNL in AML 12 hepatocytes

Glutamate increased scTAGs in AML 12 hepatocytes

To determine whether the glucogenic amino acid, glutamate, can also increase DNL, AML 12 hepatocytes were supplemented with increasing concentrations of glutamate. As expected, intracellular glutamate levels increased dose dependently in response to glutamate increases in media (Figure 8A). Total scTAG levels also increased dose-dependently in response to glutamate concentrations, with a significant change at 10 mmol/L glutamate (Figure 8B). The total amount of TAGs did not change (Figure 8C).

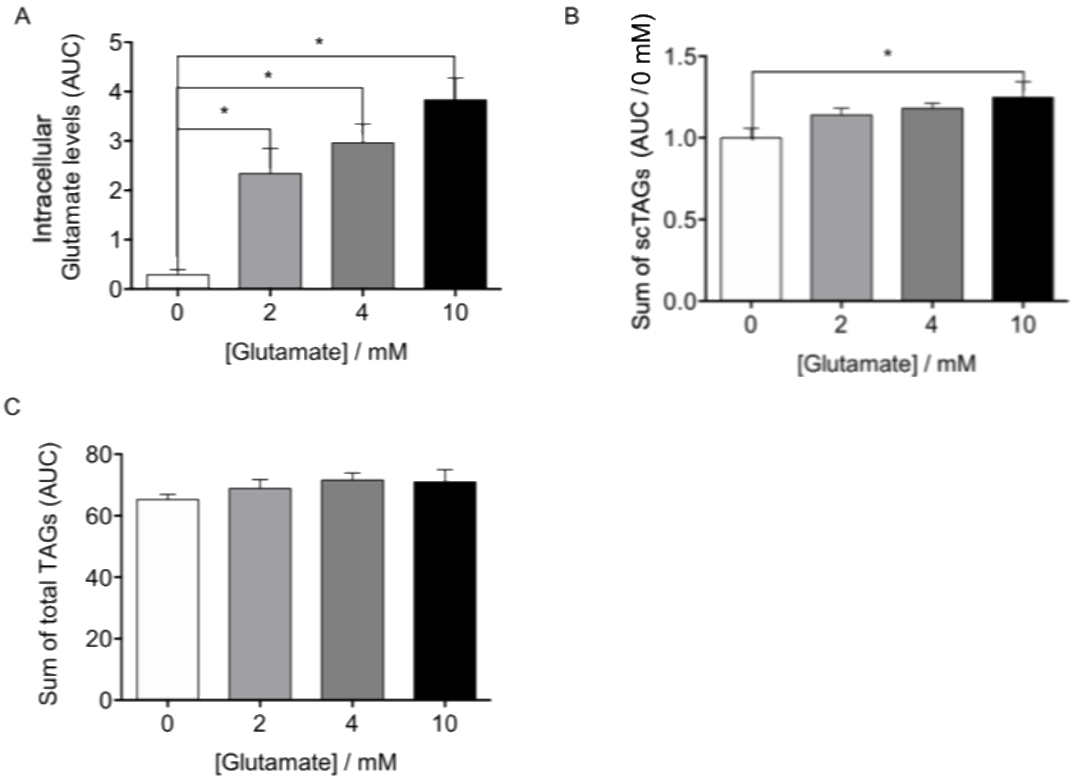

Figure 8. Intracellular scTAGs levels increased dose-dependently in response to glutamate concentrations in AML 12 hepatocytes. (**A**) Glutamate levels in cells in response to glutamate treatment at 0, 2, 4 and 10 mmol/L concentrations measured by LC-MS after 24 h. (**B**) Sum of scTAG content in cells in response to glutamate treatment at 0, 2, 4 and 10 mmol/L concentrations measured by LC-MS after 24 h. (**C**) Sum of total TAG content in cells in response to glutamate treatment at 0, 2, 4 and 10 mmol/L concentrations measured by LC-MS after 24 h. Data are presented as mean ± SEM and analysed by one-way ANOVA with *post-hoc* Dunnett's multiple comparisons test; * = $p \leq 0.05$, n = 3/group.

Total intact lipid content was not changed in response to glutamate concentrations

To determine whether glutamate changes the total lipid content, AML12 hepatocytes were treated with increasing glutamate concentrations and stained with oil red O. Oil red O is a fat-soluble diazol dye that stains neutral lipids red (TAGs and cholesteryl esters). The cell nuclei were stained blue with haematoxylin to normalise for cell count. The total neutral lipid content between cells treated with different concentrations of glutamate was not significantly different (Figure 9).

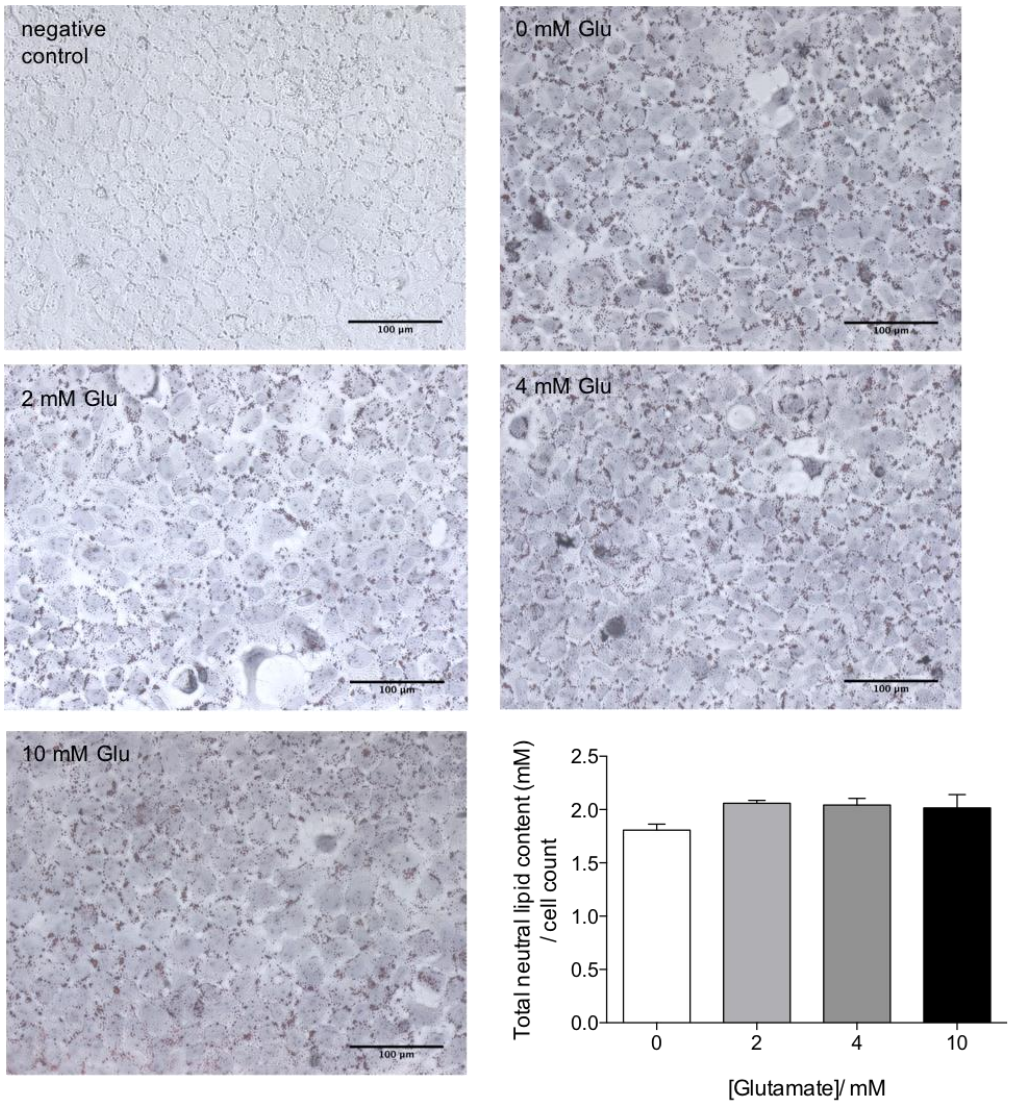

Figure 9. Intracellular total neutral lipid content was not affected by glutamate in AML 12 hepatocytes. Visualisation and quantification of neutral lipids by oil red O (red) and nuclei by haematoxylin (blue) in AML 12 hepatocytes treated with 0, 2, 4 and 10 mmol/L glutamate after 24 h. Scale bars, 100 µm; magnification is × 40. Data are presented as mean ± SEM and analysed by one-way ANOVA with *post-hoc* Dunnett's multiple comparisons test; *n* = 3/group.

Glutamate increased the expression of DNL genes

The synthesis of VLDL particles may be separated into 3 main processes (Figure 10 inset): synthesis of fatty acids (1), elongation and desaturation of fatty acids (2) and packing of fatty acids into triacylglycerols and VLDL (3). Synthesis of fatty acids is initiated by ATP-citrate lyase (*Acly*), responsible for lysing citrate to acetyl-CoA. Acetyl-CoA is then carboxylated to malonyl-CoA, via acetyl-CoA carboxylase (*Acaca*), which is subsequently utilised by a multifunctional enzyme, fatty acid synthase (*Fasn*), to synthesise fatty acids.

Increasing levels of glutamate elevated the expression of *Acly* and *Fasn* dose-dependently, with a significant increase at 10 mmol/L glutamate after 24 h (Figure 10A). However, there were no changes in the expression of *Acaca*. Once synthesised, palmitate may be desaturated and/or elongated to palmitoleate and stearate by stearoyl-CoA desaturase 1 (*Scd1*) and elongation of very long fatty acids protein 6 (*Elovl6*), respectively. Glutamate increased the expression of *Scd1* (10 mmol/L glutamate) and Elovl6 (4 and 10 mmol/L glutamate; Figure 10B). Fatty acids are then sequentially esterified to glycerol to form triacylglycerides, with the terminal step catalysed by diacylglycerol O-acyltransferase 2 (*Dgat2*). The microsomal triglyceride transfer protein (*Mttp*) is then responsible for shuttling triacylglycerides through membranes such that they may associate with apolipoprotein B100 and apolipoprotein C-III (*Apoc3*). Glutamate at 10 mmol/L increased the expression of *Dgat2* and *Apoc3* but not *Mttp* (Figure 10C).

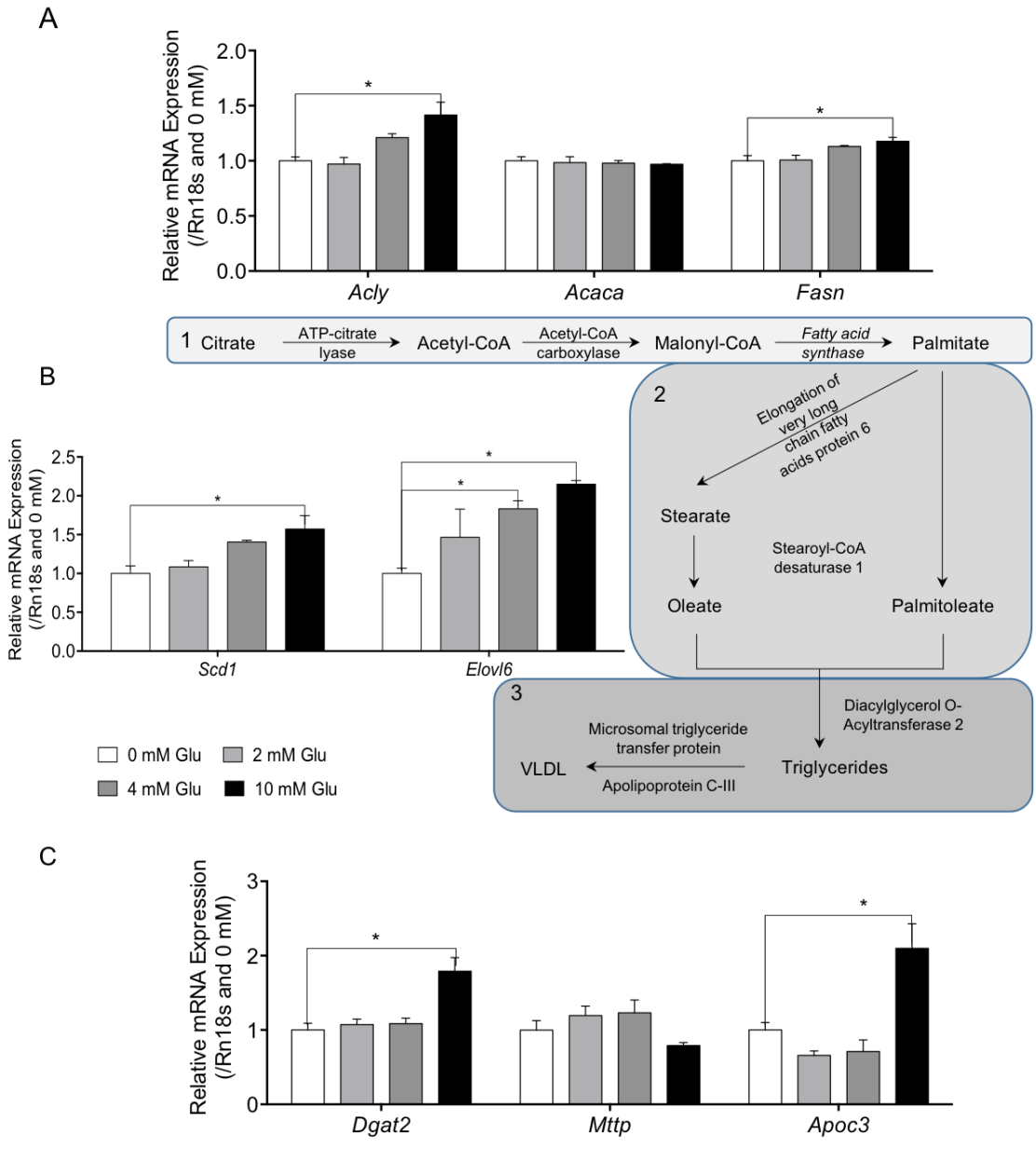

Figure 10. Increasing glutamate concentration increased DNL synthesis, processing and VLDL packaging gene expression for fatty acids in AML 12 hepatocytes. (**A**) qPCR analysis of expression of DNL synthesis genes *Acly*, *Acaca* and *Fasn* after 24 h. (**B**) qPCR analysis of expression of processing genes *Scd1* and *Elovl6* after 24 h. (**C**) qPCR analysis of expression of packaging genes *Dgat2*, *Mttp* and *Apoc3* after 24 h. Inset: Schematic representation of (1) cytosolic palmitate synthesis from citrate via acetyl- and malonyl-CoA, (2) processing by desaturation and/or elongation of palmitate to stearate, oleate and palmitoleate, (3) packaging of DNL-derived fatty acids into triacylglycerols and subsequently VLDL for export. Data are presented as mean ± SEM and analysed by one-way ANOVA with *post-hoc* Dunnett's multiple comparisons test; * = $p \leq 0.05$, n = 3/group.

Glutamate increased phosphorylation of AKT

Through a partially characterised mechanism, insulin activates the transcription factor SREBP-1c to induce the expression of genes required for hepatic DNL. A key node in this signalling cascade is PKB/AKT2, a protein kinase that transduces the signal to downstream effectors, such mTORC1. It is known that amino acids activate mTORC1, however, it has only recently been reported that mTORC1 activation in the absence of PKB/AKT2 is not sufficient to stimulate SREBP1c and thus DNL (Yecies et al., 2011). To characterise whether glutamate can act upstream of mTORC1 and activate PKB/AKT2, the levels of the active kinase, phosphorylated PKB/AKT2 (pPKB/AKT2), were measured. In particular, phosphorylation at Ser 473 of the protein was quantified as a ratio of total PKB/AKT2. In AML12 hepatocytes, intracellular pPKB/AKT2 levels increased dose-dependently in response to glutamate (4 and 10 mmol/L) (Figure 11).

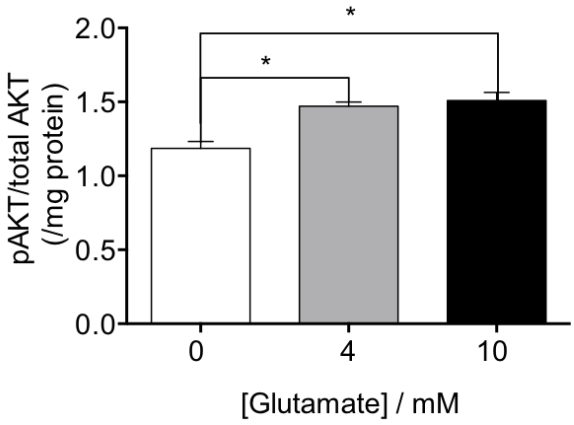

Figure 11. Intracellular pAKT levels increased dose-dependently in response to glutamate concentrations in AML 12 hepatocytes. Analysis of AKT activation as a function of AKTpS473 levels detected by ELISA after 24 h of glutamate supplementation. Data are presented as mean ± SEM and analysed by one-way ANOVA with *post-hoc* Dunnett's multiple comparisons test; * = $p \leq 0.05$, n = 3/group.

Glutamate increased the activity of p70^{S6K1}

A downstream effector of mTORC1 is p70^{S6K1}, which induces the nuclear localisation of the LXRα and heterodimerises with RXR to induce the transcription of DNL genes, including SREBP-1C (Hwahng et al., 2009). To examine whether glutamate treatment can also propagate signals from PKB/AKT downstream to p70^{S6K1}, AML 12 cells were treated with glutamate and the activity of p70^{S6K1} was measured. The intracellular activity of p70^{S6K1} increased significantly in response to glutamate (Figure 12).

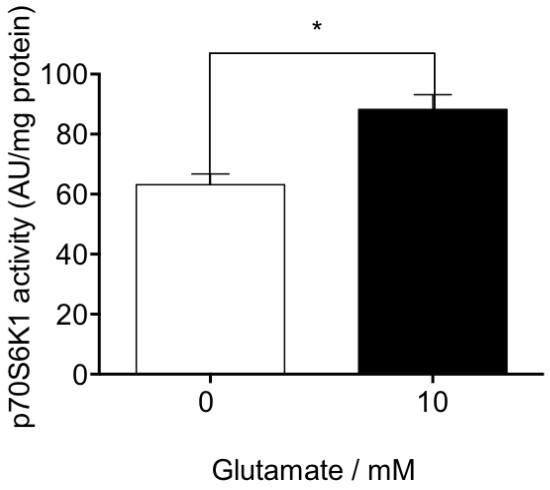

Figure 12. Intracellular activity of p70^{S6K1} increased in response to glutamate concentrations in AML 12 hepatocytes. Quantification of p70^{S6K1} activity by an ELISA based activity kit after 24 h of glutamate supplementation. Data are presented as mean ± SEM and analysed by an unpaired t-Test; * = $p \leq 0.05$, n = 3/group.

4.4.3 Induction of DNL by glutamate is insulin-dependent in AML 12 hepatocytes

Glutamate did not increase scTAGs in the absence of insulin

Recent advances in the understanding of mTOR regulation have demonstrated that both hormonal and nutrient signals are required for full activation of this pathway. In particular, amino acids have been shown to increase the activity of $p70^{S6K1}$ and insulin has been proven to further increase its activity to maximal levels (Hara et al., 1998). To examine whether insulin is required for glutamate to induce DNL, AML 12 hepatocytes were supplemented with increasing concentrations of glutamate, but insulin starved. The intracellular levels of scTAGs did not increase without insulin. The amount of scTAGs at 2, 4 and 10 mmol/L glutamate was significantly greater in the presence of insulin compared with insulin-starved cells (Figure 13).

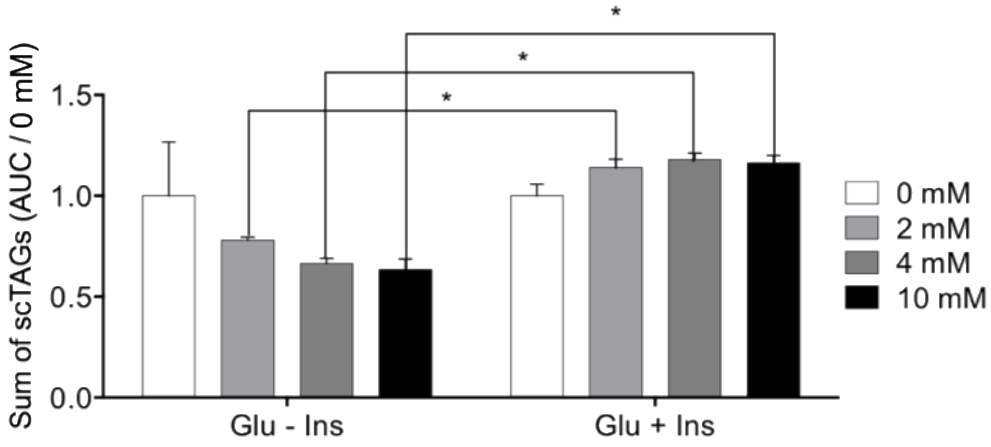

Figure 13. Intracellular levels of scTAGs were decreased in the absence of insulin in AML 12 hepatocytes supplemented with glutamate. Sum of scTAG content in cells in response to glutamate treatment at 0, 2, 4 and 10 mmol/L concentrations ± insulin measured by LC-MS after 24 h. Data are presented as mean ± SEM and analysed by two-way ANOVA with *post-hoc* Sidak's multiple comparisons test; * = $p \leq 0.05$, n = 3/group.

Glutamate did not increase the expression fatty acid synthesis genes in the absence of insulin

To examine whether the absence of insulin affects the expression of DNL genes, the expression of DNL genes in insulin starved cells was measured by qPCR. The relative expression of fatty acid synthesis genes, *Acly*, *Acaca* and *Fasn*, did not increase in the absence of insulin. The expression of *Acly* and *Fasn* at 4 and 10 mmol/L glutamate was significantly greater in the presence of insulin compared with insulin starved cells (Figure 14A and 14C). The expression of *Acaca* at 4 mmol/L glutamate was significantly higher in insulin sufficient cells than insulin starved cells (Figure 14B).

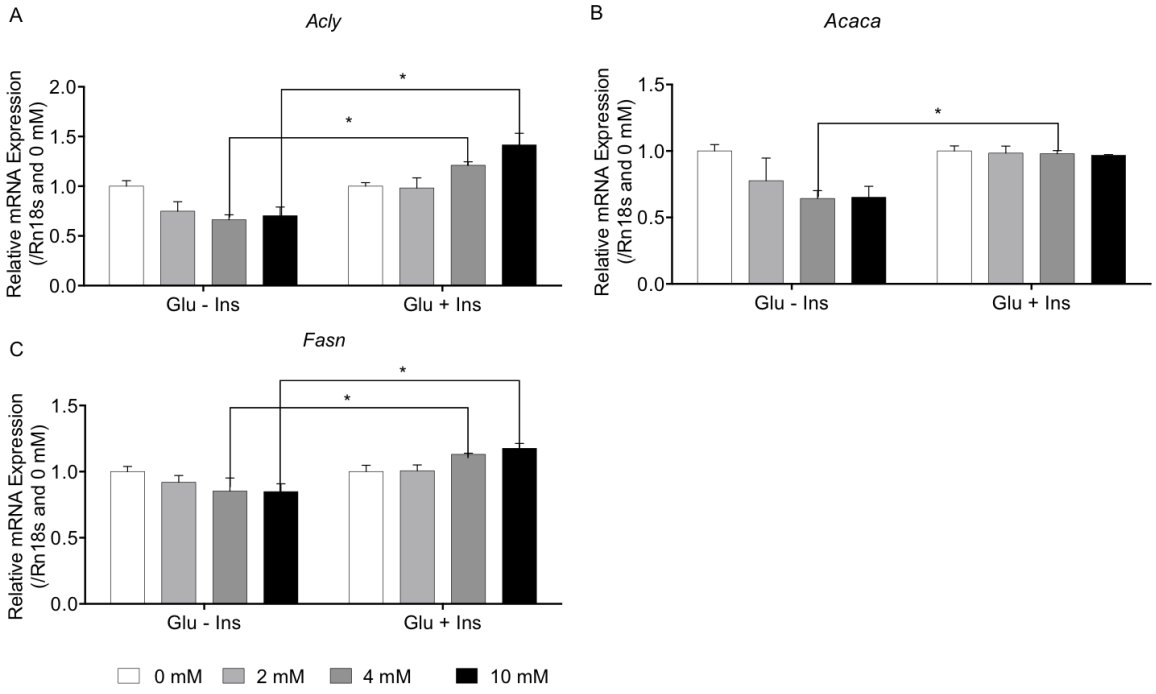

Figure 14. The expression levels of fatty acid synthesis genes were decreased in insulin starved AML 12 hepatocytes supplemented with glutamate. (**A**) qPCR analysis of expression of fatty acid synthesis gene *Acly* after a 24 h treatment with glutamate at 0, 2, 4 and 10 mmol/L ± insulin. (**B**) qPCR analysis of expression of fatty acid synthesis gene *Acaca* after a 24 h treatment with glutamate at 0, 2, 4 and 10 mmol/L ± insulin. (**C**) qPCR analysis of expression of fatty acid synthesis gene *Fasn* after a 24 h treatment with glutamate at 0, 2, 4 and 10 mmol/L ± insulin. Data are presented as mean ± SEM and analysed by two-way ANOVA with *post-hoc* Sidak's multiple comparisons test; * = $p \leq 0.05$, n = 3/group.

Glutamate did not increase the expression of fatty acid processing genes in the absence of insulin in AML 12 hepatocytes

The relative expression of fatty acid processing genes, measured by qPCR, was not changed in insulin starved cells. The expression of the desaturase, *Scd1*, at 4 and 10 mmol/L glutamate was higher in insulin sufficient cells than insulin starved cells (Figure 15A). The expression of the elongase, *Elovl6*, at 2, 4 and 10 mmol/L glutamate was higher in insulin sufficient cells than insulin starved cells (Figure 15B).

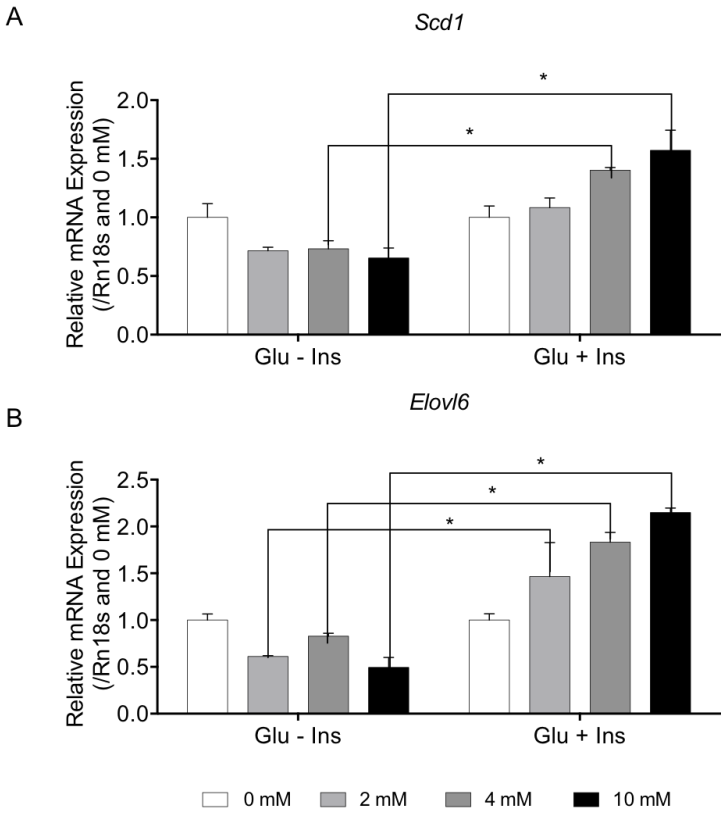

Figure 15. The expression levels of fatty acid processing genes were decreased in insulin starved AML 12 hepatocytes supplemented with glutamate. (**A**) qPCR analysis of expression of fatty acid processing gene *Scd1* after a 24 h treatment with glutamate at 0, 2, 4 and 10 mmol/L ± insulin. (**B**) qPCR analysis of expression of fatty acid processing gene *Elvol6* after a 24 h treatment with glutamate at 0, 2, 4 and 10 mmol/L ± insulin. Data are presented as mean ± SEM and analysed by two-way ANOVA with *post-hoc* Sidak's multiple comparisons test; * = $p \leq 0.05$, n = 3/group.

4.5 Discussion

The nutritional transition from traditional to western-style diets (rich in sugar, fat and protein from red meat) has led to a growing prevalence of NAFLD and T2DM (Bhat et al., 2012). Hepatic lipid accumulation, via upregulated levels of DNL, is mutual to both disorders. Whilst it is well-established that glucose and fructose are lipogenic precursors (Moore et al., 2014; Tappy and Lê, 2012), studies of other lipogenic precursors are limited. It has been reported that glutamate is the main carbon source for lipid synthesis in cancer tissue demonstrating that it can be an important substrate for DNL under certain conditions (Yin et al., 2012). However, the contribution of glutamate, one of the most common amino acids in foods, to fat synthesis under physiological conditions has been understudied. In the previous chapter, a high protein meal rich in glutamate increased the levels of triacylglycerides associated with DNL in plasma and liver-derived lipoproteins. This study investigated the underlying mechanism of the increase in lipogenic triacylglycerides caused by a high glutamate meal.

In the present chapter, carbon from glutamate was incorporated into palmitate and palmitate-containing triacylglycerides under physiological glucose concentrations in wild-type hepatocytes. Glutamate can be incorporated into the TCA cycle via glutaminolysis or reductive carboxylation. Both pathways have been proven to be active in cancer (Fendt et al., 2013), however, studies using physiological conditions are limited. In glutaminolysis, α-ketoglutarate from glutamate is oxidised to malate, which can exit the mitochondrion and be converted to pyruvate. In this study, labelled pyruvate was not detected suggesting that glutamate was not incorporated into lipids via glutaminolysis under physiological conditions. During reductive carboxylation, α-ketoglutarate is reduced to isocitrate and then citrate. Citrate [M+5] was the most abundant label in the labelled samples, suggesting that citrate was derived from reduction of α-ketoglutarate (rather than oxidation). Reductive carboxylation is induced by an increase in the cellular energy balance, reflected by a low NAD^+/NADH ratio (Wise et al., 2011). High NADH concentrations inhibit the oxidation of isocitrate to α-ketoglutarate (inhibition of IDH3) and stimulate the reduction of α-ketoglutarate to isocitrate by the reverse reactions of IDH1/2

(Wise et al., 2011). Isocitrate from both reverse reactions is then converted to citrate, which accumulates in the cytosol. The ratio of NAD^+/NADH was lower when cells were supplemented with glutamate compared with cells without glutamate. This is because, once glutamate is in the cell, glutamate dehydrogenase catalyses the oxidative deamination of glutamate to α-ketoglutarate by using NAD^+ to form NADH. Accumulated citrate in the cytosol is used to synthesise fatty acids by DNL (Giudetti et al., 2016). Levels of labelled palmitate, the primary product of DNL, and glyceryl tripalmitate (TAG 16:0/16:0/16:0) were significantly higher in samples supplemented with labelled glutamate compared with samples with unlabelled glutamate. Together, these data demonstrate that labelled glutamate was incorporated into lipids via reductive carboxylation.

Besides demonstrating that glutamate is incorporated into lipids under physiological conditions, it is also demonstrated that glutamate induces the process of DNL. In support to the finding that a meal rich in glutamate increases scTAGs, glutamate supplementation of hepatocytes increased scTAGs. Glutamate supplementation also increased the expression of fatty acid synthesis genes, *Acly* and *Fasn*, processing and packaging genes. However, glutamate did not affect the expression of the synthetic gene, *Acaca*. *Acaca* encodes ACC, the enzyme that catalyses the formation of malonyl-CoA, the working unit of FAS. Glutamate directly increases the activity of pure ACC by inducing its polymerisation (Boone et al., 2000). Despite the fact that the activity of ACC is increased by glutamate, its expression was not affected. The expression of fatty acid synthesis and processing genes is under the control of the transcription factor SREBP-1c (Benhamed et al., 2012), however, *Acaca* did not exhibit the expected response of SREBP-1c controlled genes. This might suggest the *Acaca* has an additional level of transcriptional regulation. It has been reported that *Acaca* has CpG signatures that delineate the 5' ends housekeeping genes (Travers et al., 2005), suggesting that it is not acutely regulated.

A plausible mechanism to account for these changes induced by glutamate is the mTOR signalling cascade. The mTORC1 is responsible for sensing amino acid signals as well as

integrating insulin signals via its phosphorylation by PI3-kinase/AKT2 (Yoon and Choi, 2016). AKT2 is activated by mTORC2 and in turn it stimulates mTORC1 (Vinod and Venkatesh, 2009). The mTORC1 activates $p70^{S6K1}$, leading to the nuclear translocation of LXRα and its heterodimerisation with RXR. This protein dimer induces the expression of lipogenic genes, including that of the transcription factor SREBP-1c (Hwahng et al., 2009). Full maturation of SREBP-1c is also mediated by mTORC1. SREBP-1c is also required for the expression of lipogenic genes. In this study, glutamate increased the activity of AKT2, suggesting that glutamate acts upstream of mTORC1. This is supported by the recent finding that mTORC1 activation in the absence of AKT2 is not sufficient to stimulate SREBP-1c, and thus DNL. In addition, glutamate increased the activity of $p70^{S6K1}$, indicating that the signal propagates to one of the last effectors of the pathway to induce the expression of DNL genes.

As mentioned above, mTORC1 governs and integrates signals from multiple pathways, including energy status, stress, amino acids, and insulin (Saxton and Sabatini, 2017). It has recently been demonstrated that both hormonal and nutritional signals are required to fully activate this pathway (Tremblay and Marette, 2001). The activation of the kinase $p70^{S6K1}$ has been shown to be maximal in the presence of amino acids and insulin together (Patti et al., 1998). In this study, the absence of insulin impairs the action of glutamate to increase DNL in hepatocytes. This indicates that both stimuli, insulin and glutamate, are required to induce DNL.

Amino acids in general are sensed by mTOR, particularly the BCAA leucine (Lynch, 2001). Elevated BCAA levels have been correlated with insulin resistance and type 2 diabetes (Würtz et al., 2012). Hyperactivation of the mTOR pathway by excessive amino acid concentrations leads to the phosphorylation of multiple serine residues within, and subsequent inactivation of, IRS-1 (Tremblay et al., 2007). This results in a weakened response to insulin, progressing to persistent insulin resistance. Despite this, high protein/low carbohydrate diets are popular regimes for weight loss in humans and dietary protein has been shown to decrease hepatic lipid accumulation in rodents (Schwarz et al., 2012). Presently, the precise amino acid

components that are responsible for these effects, and the extent to which amino acids are able to induce DNL and VLDL secretion are not known. In the next chapter, a variety of amino acids (representatives of glucogenic, ketogenic and BCAA) will be used to study their effects on DNL and glucose uptake.

4.6 Conclusions

This chapter investigated the mechanism underlying the increase in lipogenic triacylglycerides caused by a high protein meal rich in glutamate. Carbon from glutamate was incorporated into palmitate and palmitate-containing triacylglycerides, via reductive carboxylation. This suggests that glutamate, besides glucose and fructose, can also act as a lipogenic precursor under physiological conditions. In addition, glutamate increased scTAG content and the expression DNL genes, indicating that this amino acid not only provides a carbon source for fats but also induces DNL. Glutamate increased the activity of hepatic AKT2 and $p70^{S6K1}$, downstream effectors of the insulin signalling cascade, that activate the SREBP-1c to promote hepatic lipogenesis. The effect of glutamate on hepatic DNL was abrogated in insulin deprived cells, indicating that both hormonal and nutritional signals are required to fully activate this lipogenic pathway. The extent to whether this induction in DNL is a response of a general amino acid increase or amino acid specific will be investigated in the next chapter.

Chapter 5. Select amino acids induce *de novo* lipogenesis and decrease glucose uptake in hepatocytes

Abstract

Dietary changes have led to the growing prevalence of type 2 diabetes and non-alcoholic fatty liver disease. A hallmark of both disorders is hepatic lipid accumulation, derived in part from increased *de novo* lipogenesis. Despite high protein diets being popular for weight loss in patients with these metabolic disorders, the effect of dietary protein on *de novo* lipogenesis is poorly studied and the precise amino acid composition of high protein diets is not yet determined. In the previous chapters, high protein feeding, rich in glutamate, increased *de novo* lipogenesis-associated triacylglycerides in plasma and liver-derived very low-density lipoprotein particles in samples from human subjects. In hepatocytes, glutamate was incorporated into palmitate and in turn into triacylglycerides. In this chapter, it is demonstrated that specific amino acids provide carbon for fatty acid synthesis, through a change in energy balance. The same amino acids were able to induce *de novo* lipogenesis, through increasing the activation of protein kinase B, and in turn decrease glucose uptake in hepatocytes. In addition, their effects on lipogenesis were dependent on insulin, suggesting that these amino acids induce *de novo* lipogenesis via the insulin signalling cascade. These findings provide mechanistic insight into how select amino acids may induce *de novo* lipogenesis and insulin resistance, suggesting that utilising high protein feeding to tackle diabetes and obesity requires greater consideration.

5.1 Introduction

5.1.1 DNL and the metabolic syndrome

Both NAFLD and T2DM have been associated with increased hepatic lipid production via DNL (Bhat et al., 2012). This pathway synthesises “new” fat, utilising acetyl-CoA as a carbon source, derived from a number of metabolic reactions including glycolysis and the deamination of amino acids. Fatty-acyl chains can then be incorporated into a variety of lipid species, including TAG and phospholipids. To obtain cytosolic acetyl-CoA, citrate is exported to the cytosol where is lysed by ACL to acetyl-CoA. The pathway of DNL commences by carboxylation of acetyl-CoA to malonyl-CoA by ACC. Malonyl-CoA is then transferred to a complex multifunctional enzyme, FAS. Multiple rounds of activation of acetyl-CoA to malonyl-CoA, transferral to FAS and addition to the lengthening carbon chain generate palmitate (Donnelly et al., 2005). DNL is regulated at a transcriptional level by both glucose and insulin. It has previously been established that hyperinsulinaemia and high carbohydrate diets “prime” DNL by providing a large substrate pool (Marques-lopes et al., 2001; Schwarz et al., 2003). Glucose also stimulates the expression of anabolic DNL genes, including those encoding ACL, ACC and FAS (*ACLY*, *ACACA* and *FASN*, respectively) by the action of the transcription factor, ChREBP (Kim et al., 2016). In turn, insulin activates the same genes, via protein kinase B/AKT2 (Titchenell et al., 2016), by the action of SREBP-1c, one of two transcripts produced from the sterol response element-binding protein gene. Once FAs are synthesised, they are subsequently desaturated via the action of SCD1, and/or elongated, by ELOVL6. Finally, fatty acids may be incorporated into TAGs and packaged into VLDLs for export.

Accumulation of a subset of scTAGs and VLDL-associated TAGs in the liver and blood, respectively, has been associated with hepatic steatosis (Sanders et al., 2018). In healthy humans, the amount of *de novo*-produced TAG incorporated in VLDL is minimal (below 5%; (Timlin and Parks, 2005). However, in hyperinsulinaemic individuals with NALFD, TAG content increases to 26% (Donnelly et al., 2005). Furthermore, in healthy human subjects, feeding with a high carbohydrate meal is sufficient to increase TAG content to 23% (Timlin and Parks,

2005). Whilst numerous studies have shown that high carbohydrate feeding increases DNL (Hudgins et al., 1996), studies of the effect of high protein feeding in relation to DNL in humans are limited.

In previous chapters, a high protein meal, rich in glutamate, increased scTAGs and VLDL-associated scTAGs. Moreover, glutamate induced DNL and is itself incorporated in fatty acids via the TCA cycle in hepatocytes, indicating that amino acids can be potential precursors for DNL substrates.

5.1.2 The fates of carbon skeletons of amino acids

Amino acids can be classified as 'ketogenic' or 'glucogenic' based on intermediates they form during their catabolism. Ketogenic amino acids break down directly to acetoacetate (leucine, lysine, phenylalanine, tryptophan and tyrosine) or to acetyl-CoA (isoleucine, leucine and tryptophan) to form ketone bodies (Figure 1). Ketone bodies are used as energy sources, particularly by the brain, during low blood glucose concentrations (Nehlig, 2004). On the other hand, glucogenic amino acids may be converted to glucose via pyruvate (alanine, cysteine, serine and tryptophan), α-ketoglutarate (arginine, glutamate, glutamine, histidine and proline), succinyl-CoA (isoleucine, methionine, threonine and valine), fumarate (phenylalanine and tyrosine) or oxaloacetate (asparagine and aspartate). This occurs during starvation, to synthesise 'new glucose' from amino acids through gluconeogenesis (Felig et al., 1969). Out of the 20 proteinogenic amino acids, only leucine and lysine are exclusively ketogenic. During high energy balance, the carbon of amino acids may be used for fatty acid synthesis, via the formation of acetyl-CoA (Whereat et al., 1967). The extent to which amino acids can provide carbon for fatty acid synthesis under physiological conditions has not been studied.

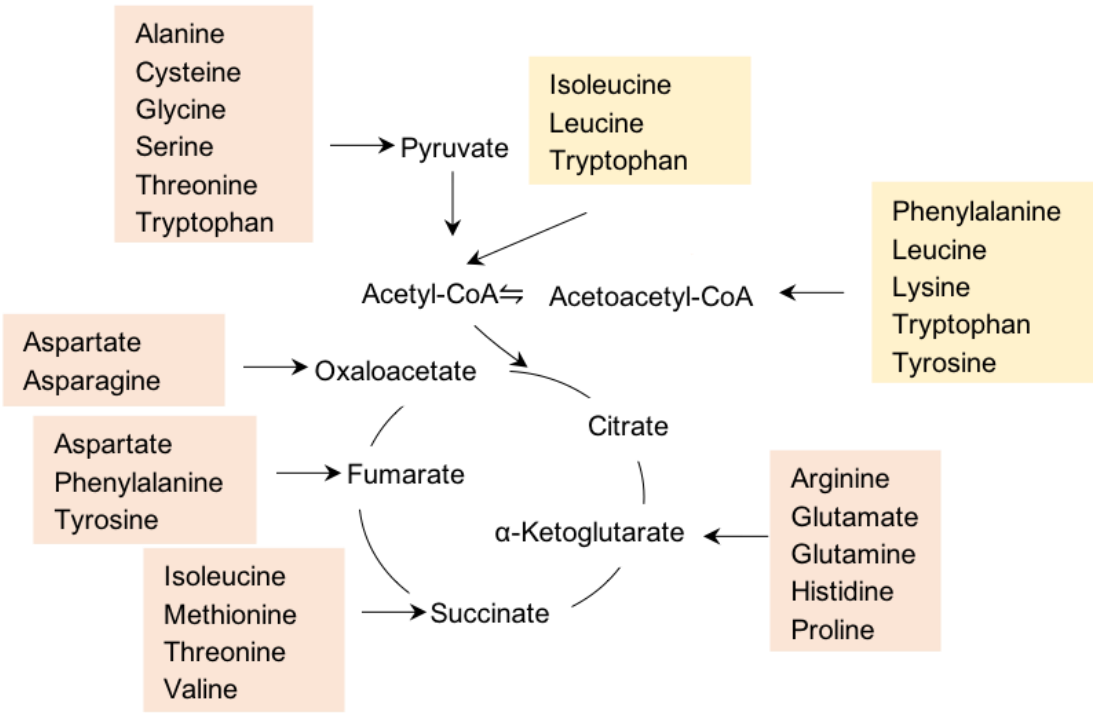

Figure 1. Amino acid entry in the TCA cycle. Ketogenic amino acids (yellow) break down to acetoacetate (leucine, lysine, phenylalanine, tryptophan and tyrosine) or to acetyl-CoA (isoleucine, leucine and tryptophan). Whilst glucogenic amino acids (orange) may be converted to glucose via pyruvate (alanine, cysteine, serine and tryptophan), α-ketoglutarate (arginine, glutamate, glutamine, histidine and proline), succinyl-CoA (isoleucine, methionine, threonine and valine), fumarate (phenylalanine and tyrosine) and oxaloacetate (asparagine and aspartate)

5.1.3 Branched-chain amino acids and insulin resistance

The BCAAs, leucine, isoleucine and valine, are essential amino acids that have an aliphatic side-chain with a methyl group as a branch. BCAAs account for 20% of protein intake and are known to correlate with insulin resistance and T2DM in humans (Würtz et al., 2012). Studies have demonstrated that deprivation of BCAAs from the diet whilst maintaining levels of other amino acids is sufficient to improve glycaemic control (Xiao et al., 2014). Circulating BCAAs are sensed by mTOR, a protein kinase which is a critical node of the insulin signalling cascade, and subsequently promote DNL (Figure 2). Activation of the insulin receptor results in the recruitment and phosphorylation of the IRS at multiple tyrosine residues. These phosphorylated sites act as docking motifs for PI3K (Shaw, 2011). PI3K phosphorylates PIP_2

to PIP_3, where PKB/AKT2 can bind and get phosphorylated at threonine 308 by PDK1 (Sarbassov et al., 2005). AKT2 is also phosphorylated by mTORC2 at serine 473 (Sarbassov et al., 2005). The kinase AKT2 regulates the TSC1/2 by phosphorylating TSC2 at multiple sites. This phosphorylation relieves the inhibitory effect of the TSC1/2 complex on Rheb allowing it to activate mTORC1 (Harrington et al., 2004).

A downstream effector of mTORC1 is the $p70^{S6K1}$, which induces the nuclear translocation of the LXRα and its heterodimerisation with the RXR. The LXRα-RXR complex increases the expression of lipogenic genes (*ACLY*, *ACACA*, *FASN*, *SCD1* and *ELOVL6*) and SREBP-1c (Yoshikawa et al., 2001).

Activated mTORC1 and $p70^{S6K1}$ phosphorylate the insulin receptor substrate at multiple serine residues, which leads to its degradation and therefore inhibits any further activation of the aforementioned signalling pathway (Carlson et al., 2004). This inhibition works as a negative feedback loop (Yu et al., 2011). However, hyperactivation of the mTOR pathway by excessive amino acid concentrations leads to the phosphorylation of multiple serine residues and subsequent inactivation of IRS-1 (Tremblay et al., 2007). This results in a weakened response to insulin, progressing to persistent insulin resistance (Yoon, 2016).

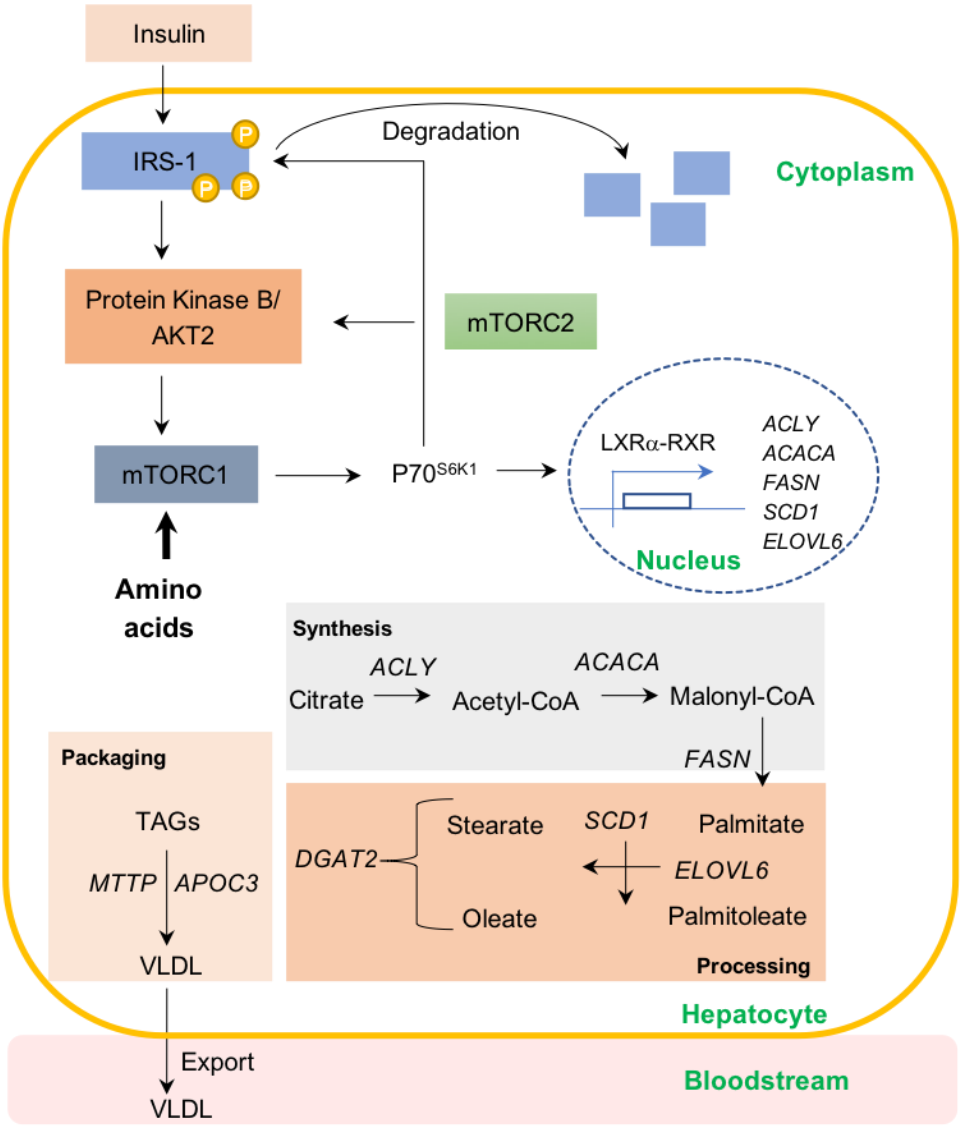

Figure 2. Schematic representation of mTOR activation by amino acids. Amino acids may activate mTORC1 and mTORC2. The mTOR complexes activate the insulin signalling cascade at different nodes. The mTORC2 activates PKB/AKT2, which activates mTORC1. Whilst mTORC1 activates $p70^{S6K1}$ and results in the activation of the LXRα-RXR complex. The pathway induces DNL by stimulating the expression of genes required for the process of fatty acid synthesis. Once DNL genes are expressed and translated into proteins, they activate the synthesis (*ACLY*, *ACACA* and *FASN*) and processing (*SCD1* and *ELOVL6*) of fatty acids as well as the esterification of fatty acid with glycerol to synthesise TAGs (*DGAT2*) and subsequent packaging (*MTTP* and *APOC3*) of TAGs in VLDL particles for export. Activation of $p70^{S6K1}$ results in the phosphorylation of IRS-1 at multiple serine residues, leading to its subsequent degradation.

5.2 Chapter aims

In the previous chapters, a meal rich in glutamate increased the levels of a subset of TAGs that have been correlated with DNL. Carbon from glutamate was detected in palmitate and palmitate-containing triacylglycerols. Glutamate also induced DNL, through activation of the AKT2 pathway, and induced the expression of genes required for DNL. To examine whether these effects are due to a general increase in amino acid levels or specific to amino acids, hepatocytes are treated with glucogenic, ketogenic and BCAAs to investigate whether they can induce DNL at a genomic, proteomic and metabolic level, using the scTAG cluster.

5.3 Materials and methods

5.3.1 Cell culture

Growth of AML 12 hepatocytes

AML 12 cells were purchased from ATCC and cultured in 1:1 (v:v) Dulbecco's modified Eagle's medium and Ham's F12 medium (Thermo), supplemented with 10% FBS, 1% penicillin/streptomycin (100 units/mL and 100 µg/mL, respectively), 1% ITS (10 mg/L, 5.5 mg/L and 6.7 µg/L, respectively) and dexamethasone (100 µmol/L) at 37°C in 5% CO_2. Cells were removed from liquid nitrogen, thawed rapidly and initially cultured in a T25 flask (Cat. # 690175, Greiner). Medium was changed every two days, and upon reaching confluence, cells were sub-cultured in T75 flasks (Cat. # 7340290, Corning) at a ratio of 1:3. Cells were plated at a density of 50,000 cells/well in collagen 1-coated 12-well plates (Cat. # 7340295, Corning) and grown to confluence in maintenance medium. Cells were then supplemented with low glucose (7.60 mmol/L) with unlabelled L-glutamine, L-leucine or L-lysine (2.4 mmol/L) and dialysed FBS (Thermo) for 2 days. After switching medium, cells were serum-starved for 20 h in low glucose medium.

Dose response of glutamine, leucine and lysine in insulin sufficient AML 12 hepatocytes

Cells were supplemented with low glucose (7.60 mmol/L) and 1% ITS without the specific amino acid (0 mmol/L, n = 3) or with increasing levels of amino acid (2, 4, 10 mmol/L, n = 3/amino acid). Cells and media were harvested after 24 h (Figure 3).

Dose response of glutamine, leucine and lysine in insulin-depleted AML 12 hepatocytes

Cells were supplemented with low glucose (7.60 mmol/L), 5.5 mg/L transferrin and 6.7 µg/L selenium without any insulin. Cells were treated without the specific amino acid (0 mmol/L, n = 3) or with increasing levels of amino acid (2, 4, 10 mmol/L, n = 3/amino acid). Cells and media were harvested after 24 h (Figure 3).

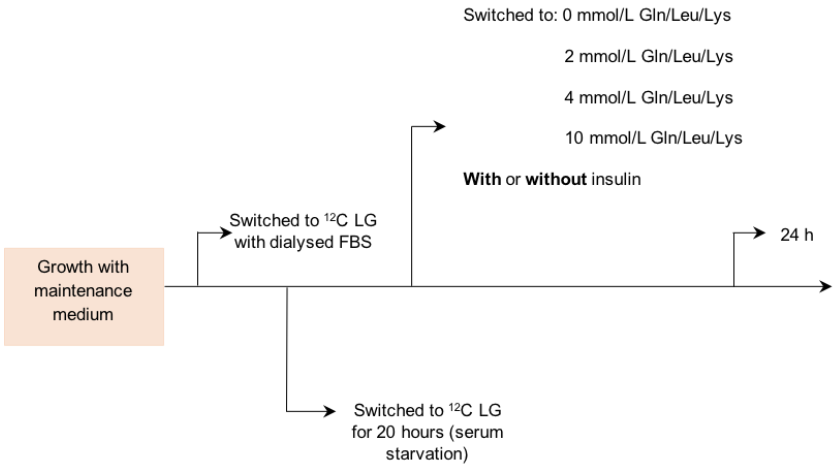

Figure 3. Schematic representation of dose response with glutamine, leucine and lysine in AML 12 hepatocytes. Hepatocytes were switched to LG for 2 days, then serum starved for a day and then treated with 0, 2, 4 or 10 mmol/L amino acid with or without insulin. Cells were collected at 24 h.

AML 12 cell $^{13}C_6$-L-lysine labelling procedure

Cells were supplemented with glucose (7.60 mmol/L, *n* = 3) with unlabelled-L-lysine (4 mmol/L) or glucose (7.60 mmol/L, *n* = 3) with $^{13}C_6$-L-lysine (4 mmol/L, *n* = 3). Based on previous experiments, the cells were allowed 3 h such that the $^{13}C_6$-L-lysine could reach an isotopic steady state in the TCA cycle. Cells and media were harvested at 0 and 24 h (Figure 4). Table 1 summarises the media used for growth and treatment.

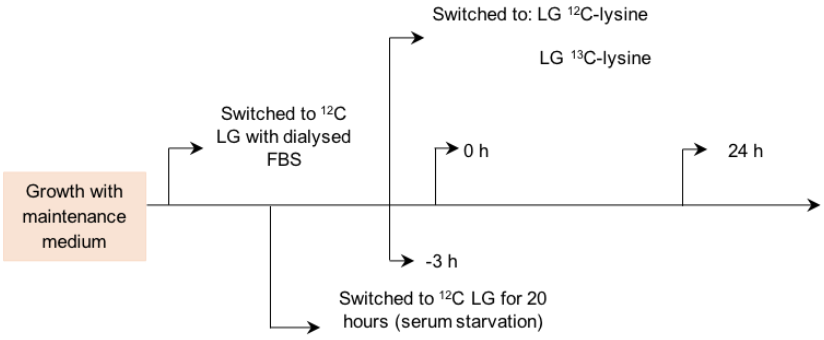

Figure 4. Schematic representation of growth and $^{13}C_6$-L-lysine treatment of AML 12 hepatocytes. Hepatocytes were switched to LG for 2 days, then serum starved for a day and then treated with either labelled or unlabelled L-lysine. Cells were collected at 0, and 24 h.

Table 1. Medium components used for growth and treatment of AML 12 hepatocytes.

Medium	Components	[Glucose] & [Amino acid]	Manufacturer
Maintenance	90% 1:1 DMEM/F12 [a] 10% FBS [b] ITS [c] 0.10 mol/L Dexamethasone [d] Penicillin/Streptomycin [e]	17.50 mmol/L Glucose 2.44 mmol/L L-Glutamine	Cat. # 11330-032, Thermo [a] Cat. # F7524, Sigma [b] Cat. # 41400045, Thermo [c] Cat. # D4902, Sigma [d] Cat. # P4333, Sigma [e]
Increasing dose of glutamine	90% 1:1 DMEM/F12 [f] 10% dialysed FBS [g] ITS [c] 0.10 mol/L Dexamethasone [d] Penicillin/Streptomycin [e]	7.60 mmol/L Glucose 0,2,4 and 10 mmol/ L ^{12}C-L-glutamine [h]	Cat. # D9443:N4888, Sigma[f] Cat. # A3382001, Thermo [g] Cat. # 25030081, Thermo [h]
Increasing dose of leucine	90% 1:1 DMEM/F12 [f] 10% dialysed FBS [g] ITS [c] 0.10 mol/L Dexamethasone [d] Penicillin/Streptomycin [e]	7.60 mmol/L Glucose 0,2,4 and 10 mmol/ L ^{12}C-L-leucine [i]	Cat. # D9443:N4888, Sigma[f] Cat. # A3382001, Thermo [g] Cat. # L8000, Sigma [i]
Increasing dose of lysine	90% 1:1 DMEM/F12 [f] 10% dialysed FBS [g] ITS [c] 0.10 mol/L Dexamethasone [d] Penicillin/Streptomycin [e]	7.60 mmol/L Glucose 0,2,4 and 10 mmol/ L ^{12}C-L-lysine [j]	Cat. # D9443:N4888, Sigma[f] Cat. # A3382001, Thermo [g] Cat. # L5751, Sigma [j]
Unlabelled lysine	90% 1:1 DMEM/F12 [f] 10% dialysed FBS [g] ITS [c] 0.10 mol/L Dexamethasone [d] Penicillin/Streptomycin [e]	7.60 mmol/L Glucose 4 mmol/ L ^{12}C-L-lysine [j]	Cat. # D9443:N4888, Sigma[f] Cat. # A3382001, Thermo g Cat. # L5751, Sigma [j]
Labelled lysine	100% DMEM/F12 [f] ITS [c] 0.10 mol/L Dexamethasone [d] Penicillin/Streptomycin [e]	7.60 mmol/L Glucose 4 mmol/L ^{13}C-L-lysine [k]	Cat. # CLM-2247-H-0.05, Cambridge Isotope Laboratories [k]

[a-k] Components lettered a-k and corresponding catalogue number and manufacturers

Harvesting of AML12 cells for metabolomics

For cells and media undergoing metabolomic analyses, 900 µL of medium was taken from each well and stored at -80°C. Each well was then washed with 1 mL of 0.9% saline and cells were lifted from the plates by adding 0.5 mL trypsin (10X trypsin-EDTA, Cat. # 25300045, Invitrogen). Each well was re-washed with 0.5 mL of 0.9% sterile-filtered saline and the resulting solution was transferred into a 2 mL microcentrifuge tube and centrifuged at 13,000

x g for 10 min to pellet the cells. The supernatant was removed and the pellet was resuspended in 750 µL of a 2:1 (v:v) chloroform:methanol solution to prevent enzymatic degradation of metabolites, and frozen at -80°C.

Metabolite extractions

Metabolites were extracted as described in Chapter 2, Section 2.1.1.

5.3.2 LC-MS of organic fractions

PEFA derivatisation of organic fractions for LC-MS and analysis of total fatty acids by triple quadrupole mass spectrometry

Each dried organic extract was derivatised by the method described in Chapter 2, Section 2.1.3 and analysed by the method described in Chapter 2, Section 2.1.4

Analysis of intact lipids using orbitrap mass spectrometry

The organic fraction was analysed by the method described in Chapter 2, Section 2.1.2.

5.3.3 Oxidising/Reducing agent quantification

NAD^+/NADH assay

NAD^+/NADH was measured according to the manufacturer's protocol (Abcam, ab65348). Briefly, cells were lysed using NAD^+/NADH extraction buffer and enzymes that consumed NADH were removed by filtration through a 10 kDa spin column (Abcam, ab93349). For NADH detection, NAD^+ was decomposed by heating samples at 60°C for 30 min. Samples [NADH with decomposed NAD^+ and total NAD(H)] and standards were incubated with 100 µL NAD cycling reaction mix to convert NAD^+ to NADH. After 5 min, 10 µL of NADH developer was added and the reaction was allowed to cycle for 2 h. The optical density (OD) was measured at 450 nm after stopping the reaction with 10 µL stop solution.

5.3.4 Gene expression analysis

RNA extraction and purification from AML 12 hepatocytes

Total RNA was extracted and purified from hepatocytes using a RNeasy Mini Kit (QIAgen) according to the manufacturer's specifications. After aspirating the media, 350 µL of buffer RLT and 70% ethanol were added to each well to lyse the cells. After mixing, the solution was transferred to an RNeasy spin column and centrifuged at 8,000 x g for 15 s to bind RNA to the membrane. The flow-through was discarded and the membrane was washed with 700 µL RW1 wash buffer by centrifuging at 8,000 x g for 15 s. The flow-through was discarded and the washing step was repeated. Subsequently, 500 µL of Buffer RPE (working ethanol buffer) was added to the RNeasy spin column and centrifuged at 8,000 x g for 15 s. The flow-through was discarded and the process repeated, before centrifugation at 8,000 x g for 15 s. The RNeasy spin column was placed in a new 2 mL collection tube and centrifuged at maximum speed for 2 min to dry the membrane and prevent carryover of ethanol. To elute pure RNA, the column was placed in a new 1.5 mL collection tube and 30 µL RNase-free water was added directly to the membrane before centrifuging at 8,000 x g for 1 min. Purified RNA concentration was quantified at 260 nm using a NanoDrop 100 (Thermo Fisher Scientific).

cDNA production by reverse transcription

Each purified RNA sample was diluted with RNase-free water to a final concentration of 100 ng/µL. cDNA synthesis and genomic DNA elimination in RNA samples was performed using an RT^2 First Strand Synthesis kit (QIAgen) according to the manufacturer's specifications. Genomic DNA elimination was performed by mixing each RNA sample with 2 µL of genomic elimination buffer (buffer GE) and incubating on a thermocycler (Techne) at 42°C for 5 min before being rapidly cooled to 4°C for 1 min. The reverse transcription mix was prepared by adding 4 µL 5X Buffer BC3, 1 µL Control P2 (random hexamers), 2 µL RE3 Reverse Transcriptase Mix and 3 µL RNase-free water. To each reaction tube, 10 µL reverse-transcription mix were added and mixed gently. The samples were then reverse transcribed

by incubating them on a thermocycler (Techne) at 42°C for exactly 15 min and then immediately terminating the reaction by incubating at 95°C for 5 min. The reactions were stored at -20°C prior to real time PCR analysis.

qPCR

The relative abundance of transcripts of interest was measured by qPCR in RT^2 SYBR Green Mastermix (QIAgen) with a StepOnePlus detection system (Applied Biosystems). The SYBR Green qPCR Mastermix contained HotStart DNA Taq Polymerase, PCR Buffer, dNTP mix (dATP, dCTP, dGTP, dTTP) and SYBR Green dye. Before adding cDNA to each well of the 96-well plate, cDNA was diluted in RNase-free water to a final concentration of 8 ng/µL. PCR component mix was prepared by mixing 10 µL SYBR Green qPCR Mastermix with 0.6 µL of 10 µmol/L target primers (forward and reverse; 6 pmoles/reaction) and 4.4 µL RNase-free water. To each well of a 96-well plate, 5 µL cDNA (total amount 40 ng) and 15 µL PCR components mix were added. The plate was centrifuged at 1000 x g for 30 s to ensure that the contents were mixed and to remove any bubbles present in the wells. The plate was placed in the real-time cycler with the following cycling conditions: 10 min at 95°C for 1 cycle to activate HotStart DNA Taq Polymerase; 15 s at 95°C and 1 min at 60°C to perform elongation and cooling for 40 cycles. RT^2 qPCR Primer Assays for mouse *Rn18s*, *Fasn*, *Acaca*, *Acly*, *Elvol6*, *Scd1*, *Dgat2*, *Mttp* and *Apoc3* were purchased from QIAgen. Expression levels were normalised to the endogenous control, *Rn18s*, using the ΔΔCt method and fold changes reported were relative to the control group in the dose response (0 mmol/L 'amino acid').

5.3.5 Protein quantification and glucose uptake analysis

Preparation of cell lysates

Cell pellets were lysed in 100 µL Cell Extraction Buffer (10 mmol/L Tris, 100 mmol/L NaCl, 1 mmol/L EDTA, 1 mmol/L EGTA, 10 mmol/L NaF, 20 mmol/L $Na_4P_2O_7$, 20 mmol/L Na_3VO_4, 1% Triton X-100, 10% glycerol, 0.1% sodium dodecyl sulfate, 0.5% deoxycholate, 1 mmol/L phenylmethylsulfonyl fluoride, complete protease inhibitor tablet and 1% of each phosphatase cocktail inhibitor 2 and 3) for 30 min, vortexing at 10-min intervals. The lysate was centrifuged at 13,000 x g for 10 min at 4°C and the supernatant was collected and stored at -80°C.

Cell AKTpS473 and AKT [total] quantification by enzyme-linked immunosorbent assay

PKB/AKT concentrations were measured using commercial assay kits (Invitrogen). The protocol was followed according to the manufacturer's specifications. Briefly, cells were collected by centrifugation and washed with cold PBS. After diluting samples and standards with standard diluent buffer, they were incubated on a 96-well plate containing an immobilised antibody to AKTpS473 or AKT [Total] for 2 h at room temperature with gentle shaking. Unbound constituents were washed off and then an AKT [Total] biotin conjugate or AKTpS473 detection antibody was added to each well for 1 h at room temperature with gentle shaking. After washing off unbound conjugates, streptavidin-HRP solution (AKT [Total]) or anti-rabbit IgG HRP solution (AKTpS473) was added to each well and incubated for 30 min at room temperature with gentle shaking. Following washing, a stabilised chromogen was added to each well and incubated for 30 min in the dark without shaking. Stop solution was added to each well to stop the enzymatic reaction and the absorbance was read at 450 nm. The background absorbance was subtracted from all data points, including standards, and a standard curve was generated. The unknown concentrations were read from the standard curve and the concentrations were multiplied by the appropriate dilution factor. Values were normalised to protein concentration using a reducing-agent compatible bicinchoninic acid protein assay and values of AKT [pS473] were normalised to AKT [Total].

BCA Protein assay- reducing agent compatible

Protein concentrations were measured using a commercial assay kit by Pierce™ Thermo Scientific. The protocol was followed according to the manufacturer's specifications. Briefly, samples were diluted in Compatibility Reagent Stock solution (1:1) and incubated at 37°C for 15 min. Samples were cooled at room temperature for at least 5 min. After cooling, samples and BSA standards were added to a 96-well plate, BCA working reagent was added to each well (1:3 sample/standard: BCA working reagent). The absorbance was measured at 562 nm and the average absorbance of the blank replicates was subtracted from each standard and sample replicate. A standard curve was generated by plotting the average blank corrected absorbance measurements for each BSA standard vs. known concentration. An equation in the form $y = mx + c$ was generated for the protein standards from which the unknown concentrations were calculated.

2-Deoxyglucose uptake assay

2-Deoxyglucose uptake was measured using a commercial assay kit (Abcam, ab136955). The protocol was followed according to the manufacturer's instructions. In brief, cells were washed 3 times with PBS and starved of glucose by pre-incubating with Krebs-Ringer phosphate buffer (KRPH) with 2% BSA for 40 min. Cells were subsequently washed with PBS (background), stimulated or not stimulated with 1 µmol/L insulin for 20 min. Insulin and non-insulin stimulated (control) cells were incubated with the glucose analogue 2-deoxyglucose for 20 min. Cells were then washed and lysed with extraction buffer by freeze/thawing and vortex mixing. Endogenous NAD(P) was subsequently degraded by heating at 85°C for 40 min. After diluting samples and standards with assay buffer, NADPH was generated from 2-deoxyglucose oxidation. Any unused NADP left in the sample was degraded by heating to 90°C for 40 min. This resulted in the oxidation of the substrate which was detected at 412 nm in kinetic mode.

5.3.6 Statistical analysis

Univariate statistics

Data were visualised using GraphPad (GraphPad Prism 5.2; GraphPad Software, San Diego, CA, USA). All data are expressed as means ± SEM. In GraphPad, one- or two-way ANOVA was performed where appropriate to determine significant differences between experimental groups. For one-way ANOVA, Tukey's *post-hoc* multiple comparison test was performed, whilst for two-way ANOVA, Sidak's *post-hoc* multiple comparison test was used. Differences between experimental groups were considered to be statistically significant when $p \leq 0.05$.

5.4 Results

5.4.1 Select amino acids induce DNL in AML 12 hepatocytes

Glutamine and leucine but not lysine increased scTAGs in AML 12 hepatocytes

After demonstrating that glutamate induces DNL in Chapter 4, the effect of other amino acids on DNL was examined. AML 12 hepatocytes were supplemented with increasing concentrations of representatives of glucogenic (glutamine) and ketogenic (leucine and lysine) amino acids. As expected, intracellular amino acid levels increased dose dependently in response to the corresponding amino acid increases in media (Figure 5A). Total scTAG levels increased dose-dependently in response to glutamine and leucine but not lysine concentrations (Figure 5B), with the greatest effect achieved via supplementation with leucine. The amount of total TAGs did not change in response to any amino acid (Figure 5C).

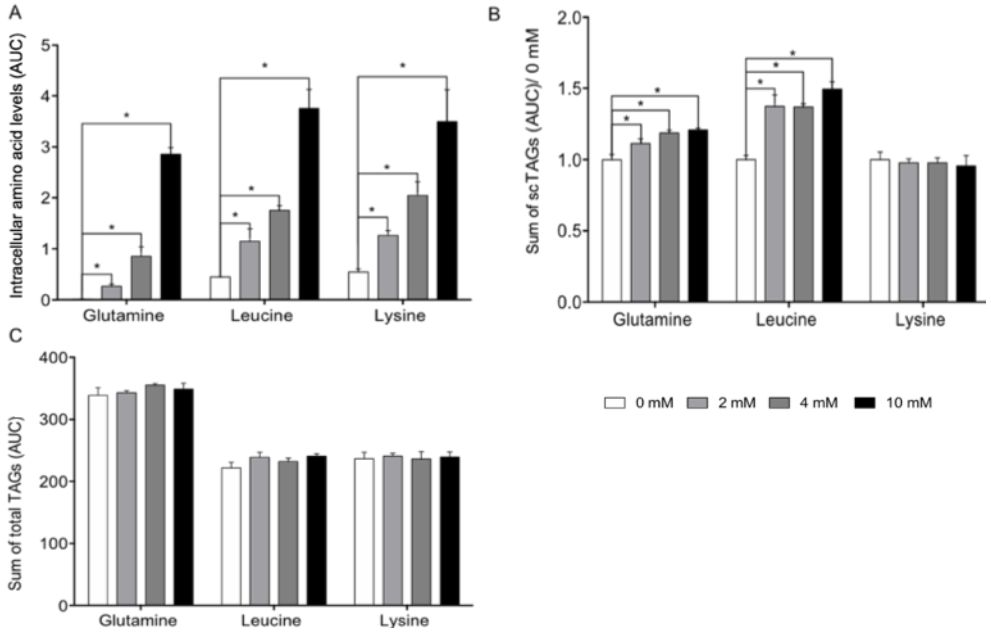

Figure 5. Intracellular scTAGs levels increased dose-dependently in response to glutamine and leucine but not lysine concentrations in AML 12 hepatocytes. (**A**) Amino acid levels in cells in response to specific amino acid treatment at 0, 2, 4 and 10 mmol/L concentrations measured by LC-MS after 24 h. (**B**) Sum of scTAG content in cells in response to specific amino acid treatment at 0, 2, 4 and 10 mmol/L concentrations measured by LC-MS after 24 h. (**C**) Sum of total TAG content in cells in response to amino acid treatment at 0, 2, 4 and 10 mmol/L concentrations measured by LC-MS after 24 h. Data are presented as mean ± SEM and analysed by one-way ANOVA with *post-hoc* Dunnett's multiple comparisons test; * = $p \leq 0.05$, n = 3/group.

Glutamine and leucine but not lysine increased the energy balance of AML 12 hepatocytes

As previously mentioned, lipogenesis commences with the export of citrate from the mitochondrion to the cytosol. This is achieved by the low NAD^+/NADH ratio. Supplementation of glutamine and leucine significantly decreased the NAD^+/NADH ratio. However, lysine supplementation did not change the energy balance within the cell. In support to the previous finding that leucine had the greatest increase in scTAGs, it also increased the energy balance the most (biggest decrease in NAD^+/NADH ratio). Moreover, lysine did not affect scTAG content nor the energy balance of cells (Figure 6).

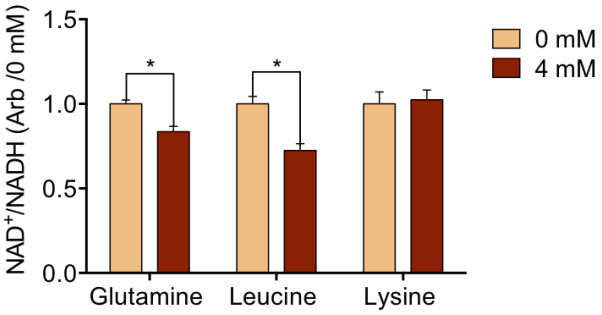

Figure 6. Glutamine and leucine but not lysine decreased the NAD^+/NADH ratio in AML 12 hepatocytes. NAD^+/NADH at 0 mmol/L and 4 mmol/L glutamine, leucine and lysine after 24 h. Data are presented as mean ± SEM and analysed by two-way ANOVA with *post-hoc* Sidak's multiple comparisons test; * = $p \leq 0.05$, n = 3/group

Carbon from labelled lysine was not incorporated in palmitate and palmitate-containing triacylglycerides

As shown above, lysine did not affect the scTAG content but also did not change the NAD^+/NADH ratio, suggesting that this amino acid did not affect DNL. Even though catabolism of lysine generates acetyl-CoA, label from $^{13}C_6$-lysine was not detected in palmitate or palmitate-containing triacylglycerides (Figure 7A & 7B respectively), suggesting that lysine cannot provide sufficient amounts of substrate for DNL.

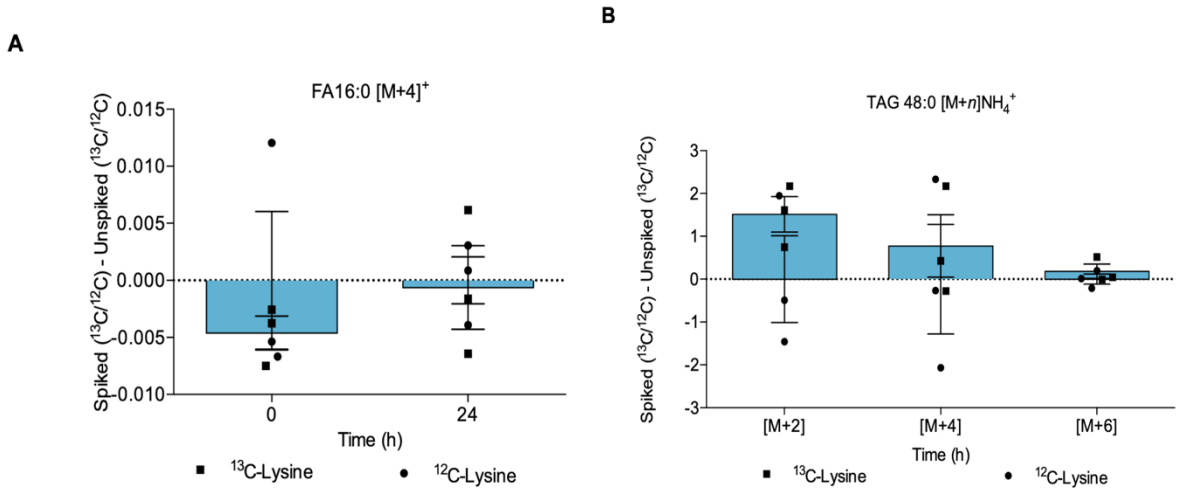

Figure 7. Carbon from $^{13}C_6$-labelled lysine was not incorporated into DNL-derived palmitate or triacylglycerols in AML 12 hepatocytes. (**A**) The $[M+4]^+$ ion of the picolynyl-ester of palmitate (FA16:0) detected by LC-MS was not labelled by lysine over 24 h post-supplementation. (**B**) The $[M+2]NH_4^+$, $[M+4]NH_4^+$ and $[M+6]NH_4^+$ ions of glyceryl tripalmitate (TAG 48:0) in cells detected by LC-MS were not labelled by lysine after 24 h. Data are presented as mean ± SEM and analysed by two-way ANOVA with *post-hoc* Sidak's multiple comparisons test; * = $p \leq 0.05$, n = 3/group.

Glutamine increased the expression of DNL genes

To determine whether these changes in DNL were because of changes in the expression of genes required for DNL, the expression levels of key genes in the synthesis of VLDL particles were quantified by qPCR. The synthesis of VLDL particles may be separated into 3 main processes: **synthesis** of fatty acids, elongation and desaturation of fatty acids (**processing**) and **packaging** of fatty acids into triacylglycerols and VLDL. Glutamine at 2 and 4 mmol/L increased the expression of the fatty acid synthesis genes (*Acly* and *Fasn,* but not *Acaca*), as well as the processing and packaging genes. However, at 10 mmol/L glutamine, the expression of *Fasn* and *Elovl6* was no longer significantly increased (Figure 8).

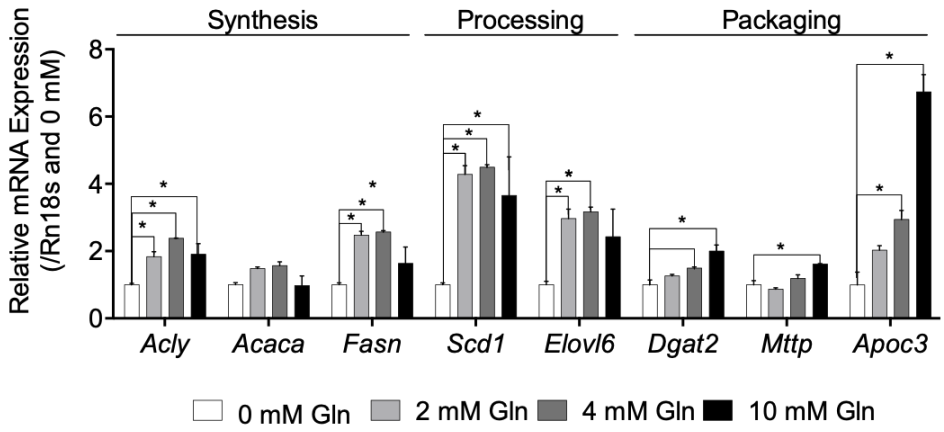

Figure 8. Glutamine concentrations increased the expression of DNL synthesis, processing and VLDL packaging gene expression in AML 12 hepatocytes. qPCR analysis of expression of *Acly*, *Acaca*, *Fasn*, *Scd1*, *Elovl6*, *Dgat2*, *Mttp* and *Apoc3* in response to 0, 2, 4 and 10 mmol/L glutamine after 24 h. Data are presented as mean ± SEM and analysed by one-way ANOVA with *post-hoc* Dunnett's multiple comparisons test; * = $p \leq 0.05$, n = 3/group.

Leucine decreased the expression of fatty acid synthesis and processing genes but increases the expression of packaging genes

Despite leucine resulting in the greatest increase in scTAGs in hepatocytes, it decreased the expression of fatty acid synthesis (except *Acaca*) and processing genes, with significant changes at 10 mmol/L leucine. However, it increased the expression of packaging genes dose-dependently (Figure 9).

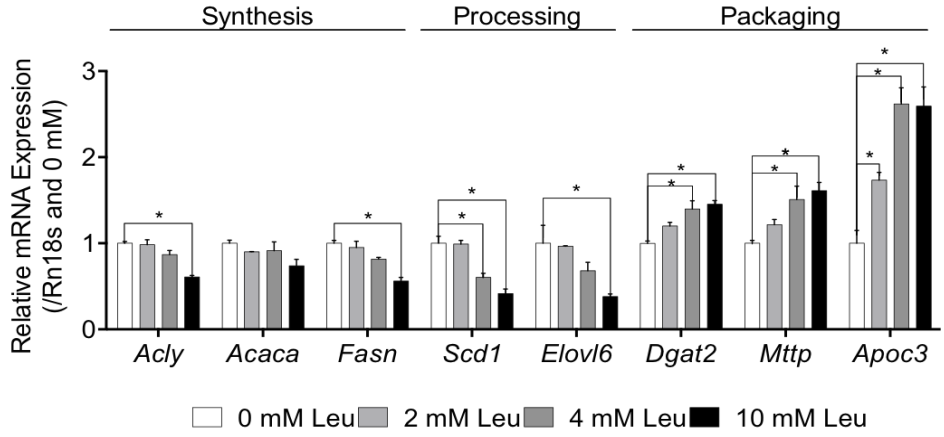

Figure 9. Leucine concentrations decreased the expression of DNL synthesis and processing genes but increases VLDL packaging gene expression in AML 12 hepatocytes. qPCR analysis of expression of *Acly*, *Acaca*, *Fasn*, *Scd1*, *Elovl6*, *Dgat2*, *Mttp* and *Apoc3* in response to 0, 2, 4 and 10 mmol/L leucine after 24 h. Data are presented as mean ± SEM and analysed by one-way ANOVA with *post-hoc* Dunnett's multiple comparisons test; * = $p \leq 0.05$, n = 3/group.

Lysine did not affect the expression of DNL genes

Lysine did not change the expression of any genes significantly. This is in agreement with the finding that lysine did not affect scTAG content nor the NAD^+/NADH ratio in hepatocytes (Figure 10).

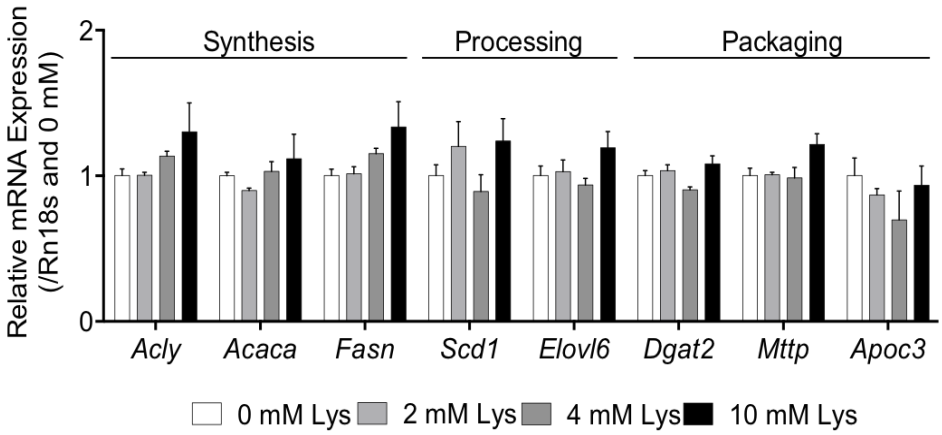

Figure 10. Lysine concentrations did not affect the expression of DNL synthesis, processing and VLDL packaging gene expression in AML 12 hepatocytes. qPCR analysis of expression of *Acly*, *Acaca*, *Fasn*, *Scd1*, *Elovl6*, *Dgat2*, *Mttp* and *Apoc3* in response to 0, 2, 4 and 10 mmol/L lysine after 24 h. Data are presented as mean ± SEM and analysed by one-way ANOVA with *post-hoc* Dunnett's multiple comparisons test; * = p≤0.05, *n* = 3/group.

Glutamine and leucine increased phosphorylation of AKT

Insulin induces the expression of genes required for hepatic DNL, by activating SREBP-1c. PKB/AKT2 transduces the signal to mTORC1. It is well characterised that mTORC1 responds to amino acids stimuli, however, it has only recently been reported that mTORC1 activation in the absence of PKB/AKT2 is not sufficient to stimulate SREBP1c and thus DNL (Yecies et al., 2011). To investigate whether amino acids act upstream of mTORC1, the levels of the active PKB/AKT2, were quantified. The levels of the active kinase were expressed as a ratio to total PKB/AKT2, via measuring phosphorylation at Ser 473. In AML12 hepatocytes, intracellular pPKB/AKT2 levels increased dose-dependently in response to glutamine (10 mmol/L) and leucine (4 and 10 mmol/L). Lysine concentrations did not affect pPKB/AKT2 levels (Figure 11).

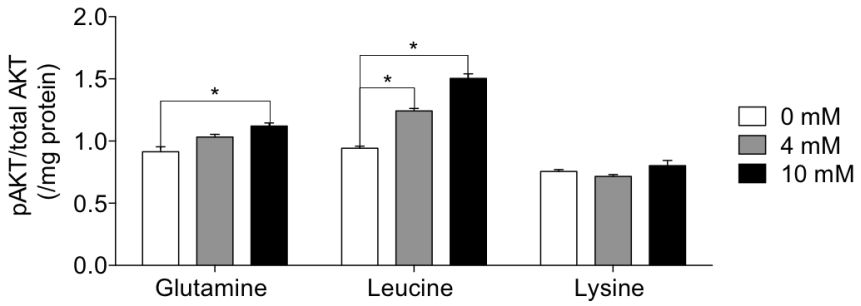

Figure 11. Intracellular pAKT levels increased dose-dependently in response to glutamine and leucine but not lysine concentrations in AML 12 hepatocytes. Analysis of AKT activation as a function of AKTpS473 levels detected by ELISA after 24 h of amino acid supplementation. Data are presented as mean ± SEM and analysed by one-way ANOVA with *post-hoc* Dunnett's multiple comparisons test; * = $p \leq 0.05$, n = 3/group.

5.4.2 Select amino acids decrease glucose uptake in AML 12 hepatocytes

Glutamine and leucine decreased glucose uptake in AML 12 hepatocytes

As insulin resistance is thought, at least in part, to result from the hyperactivation of mTOR and the subsequent phosphorylation of IRS-1 (Tremblay and Marette, 2001), the acute effects of amino acid supplementation on the uptake of the glucose analogue, 2-deoxyglucose, were examined. This molecule is recognised by glucose transporters, phosphorylated within the cell by glucokinase but cannot be further metabolised and is thus sequestered within the cell. Upon addition of 2-deoxyglucose, insulin-stimulated uptake was significantly lower in both glutamine- and leucine-supplemented cells (Figure 12A and 12B, respectively), but not with lysine (Figure 12C).

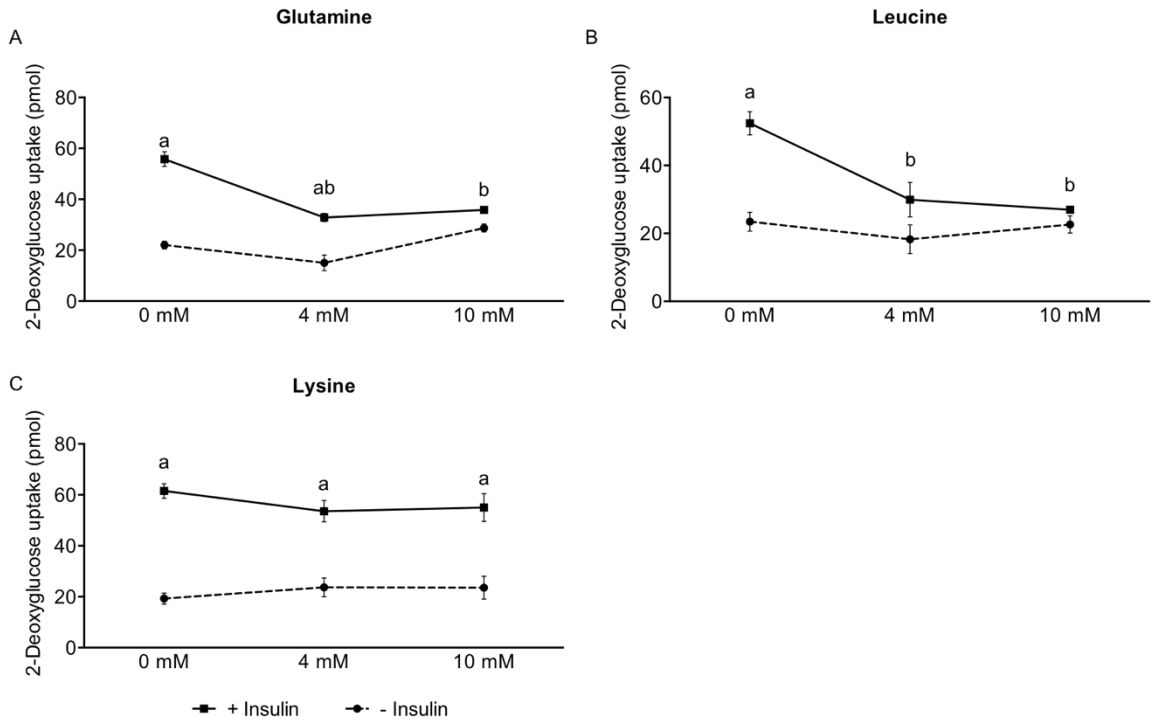

Figure 12. 2-deoxyglucose uptake decreased in response to glutamine and leucine but not lysine in AML 12 hepatocytes. (**A**) 2-deoxyglucose uptake assay on AML12 cells exposed to 0, 4 and 10 mmol/L glutamine for 24 h. (**B**) 2-deoxyglucose uptake assay on AML12 cells exposed to 0, 4 and 10 mmol/L leucine for 24 h. (**C**) 2-deoxyglucose uptake assay on AML12 cells exposed to 0, 4 and 10 mmol/L lysine for 24 h. Data are presented as mean ± SEM and analysed by two-way ANOVA with *post-hoc* Sidak's multiple comparisons test; a,b = $p \leq 0.05$, n = 3/group. a = comparisons between ± insulin within same amino acid concentration; b = comparisons between different amino acid concentrations within insulin treatment versus 0 mmol/L.

5.4.3 Induction of DNL by glutamine is lessened in the absence of insulin in AML 12 hepatocytes

Glutamine did not increase scTAGs in the absence of insulin in AML 12 hepatocytes

Full activation of the mTOR signalling pathway requires both hormonal and nutritional signals (Hara et al., 1998). As shown in the previous chapter, glutamate induced DNL was dependent on insulin. To examine whether insulin is required for glutamine to induce DNL, AML 12 hepatocytes were supplemented with increasing concentrations of glutamine, but insulin starved. The intracellular levels of scTAGs did not increase without insulin. The amount of scTAGs at 2, 4 and 10 mmol/L glutamine was significantly more in the presence of insulin compared with insulin starved cells (Figure 13).

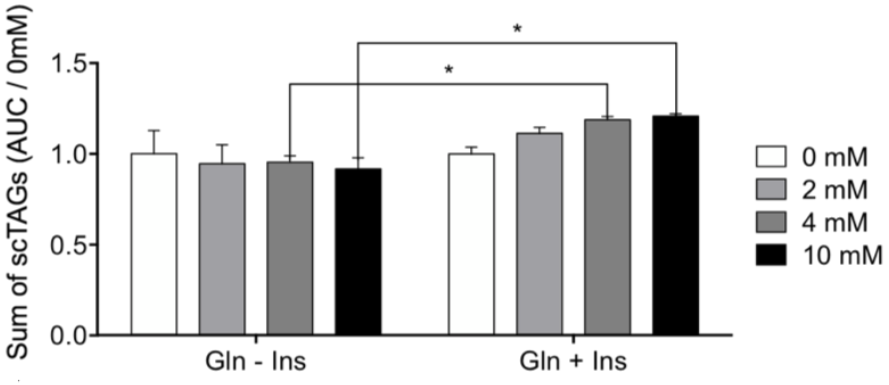

Figure 13. Intracellular levels of scTAGs did not increase in the absence of insulin in glutamine supplemented AML 12 hepatocytes. Sum of scTAG content in cells in response to glutamine treatment at 0, 2, 4 and 10 mmol/L concentrations with insulin or without insulin measured by LC-MS after 24 h. Data are presented as mean ± SEM and analysed by two-way ANOVA with *post-hoc* Sidak's multiple comparisons test; * = $p \leq 0.05$, n = 3/group.

Insulin deprivation decreased the expression of fatty acid synthesis genes in cells supplemented with glutamine

To examine whether the absence of insulin affects the expression of DNL genes, the expression of DNL genes in insulin starved cells was measured by qPCR. The expression of *Acly* and *Fasn* at 2, 4 and 10 mmol/L glutamine was significantly more in the presence of insulin compared with insulin starved cells (Figure 14A and 14C). The expression of *Acaca* at 2 mmol/L glutamine was significantly higher in insulin sufficient cells than insulin starved cells (Figure 14B).

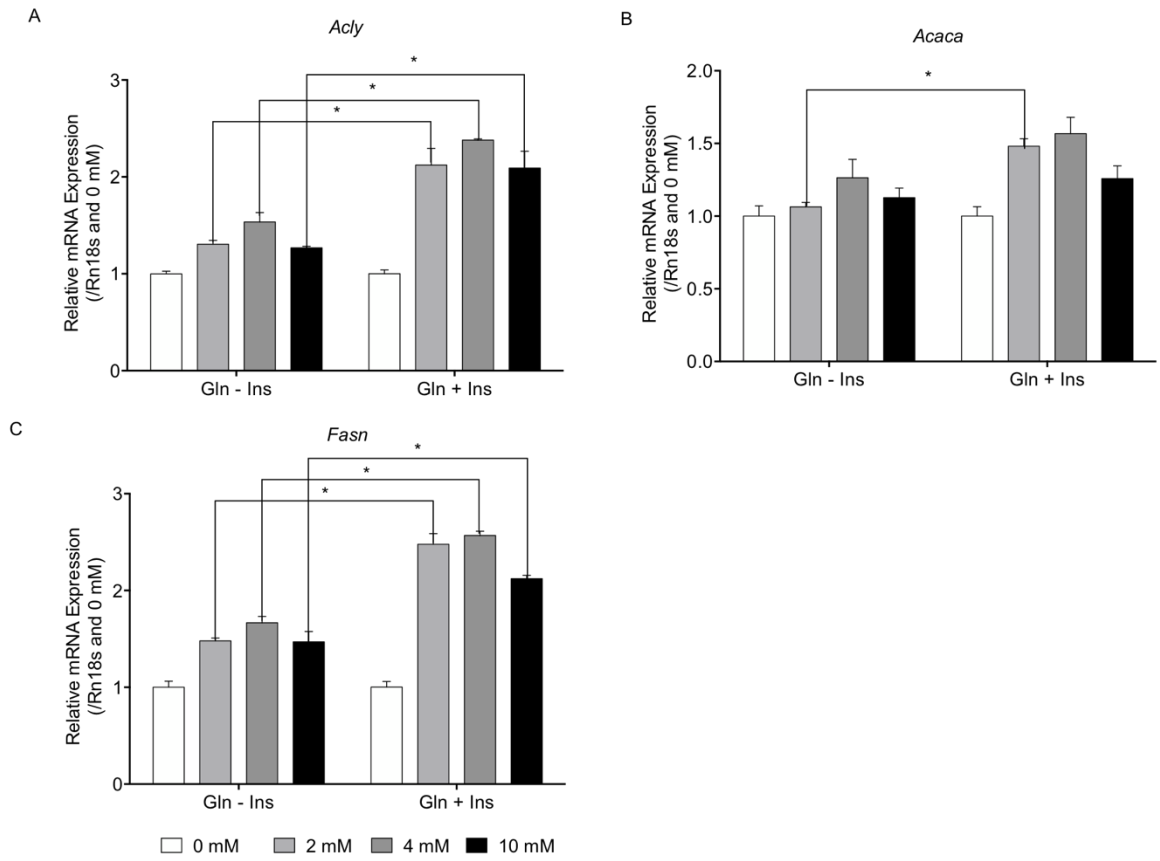

Figure 14. The expression of fatty acid synthesis genes decreased in insulin starved AML 12 hepatocytes supplemented with glutamine. (**A**) qPCR analysis of expression of fatty acid synthesis gene *Acly* after a 24 h treatment with glutamine at 0, 2, 4 and 10 mmol/L with insulin or without insulin. (**B**) qPCR analysis of expression of fatty acid synthesis gene *Acaca* after a 24 h treatment with glutamine at 0, 2, 4 and 10 mmol/L with insulin or without insulin (**C**) qPCR analysis of expression of fatty acid synthesis gene *Fasn* after a 24 h treatment with glutamine at 0, 2, 4 and 10 mmol/L with insulin or without insulin. Data are presented as mean ± SEM and analysed by two-way ANOVA with *post-hoc* Sidak's multiple comparisons test; * = $p \leq 0.05$, n = 3/group.

Insulin deprivation decreased the expression of fatty acid processing genes in cells supplemented with glutamine

The relative expression of fatty acid processing genes, measured by qPCR, decreased in the absence of insulin. The expression of the desaturase, *Scd1*, at 2, 4 and 10 mmol/L glutamine was significantly higher in insulin sufficient cells than insulin starved cells (Figure 15A). The expression of the elongase, *Elovl6*, at 2 mmol/L glutamine was higher in insulin sufficient cells than insulin starved cells (Figure 15B).

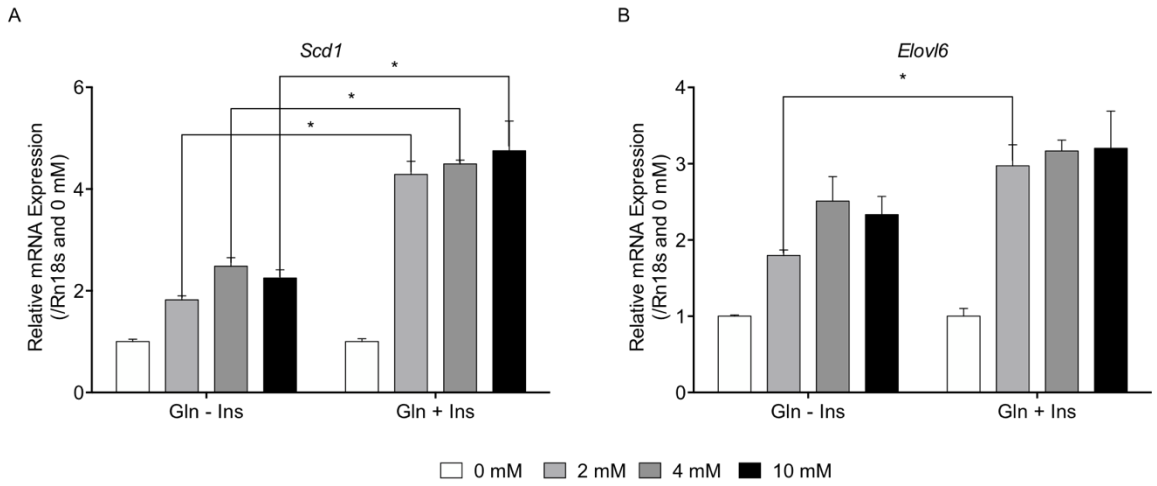

Figure 15. The expression of fatty acid processing genes decreased in insulin starved AML 12 hepatocytes supplemented with glutamine. (**A**) qPCR analysis of expression of fatty acid processing gene *Scd1* after a 24 h treatment with glutamine at 0, 2, 4 and 10 mmol/L with insulin or without insulin. (**B**) qPCR analysis of expression of fatty acid processing gene *Elvol6* after a 24 h treatment with glutamine at 0, 2, 4 and 10 mmol/L with insulin or without insulin. Data are presented as mean ± SEM and analysed by two-way ANOVA with *post-hoc* Sidak's multiple comparisons test; * = $p \leq 0.05$, n = 3/group.

5.4.4 Induction of DNL by leucine is lessened is the absence of insulin in AML 12 hepatocytes

The absence of insulin decreased the scTAG content of leucine-supplemented cells

To examine whether insulin is required for leucine to induce DNL, AML 12 hepatocytes were supplemented with increasing concentrations of leucine, but insulin starved. The amount of scTAGs at 10 mmol/L leucine was significantly higher in insulin sufficient cell than insulin starved cells (Figure 16).

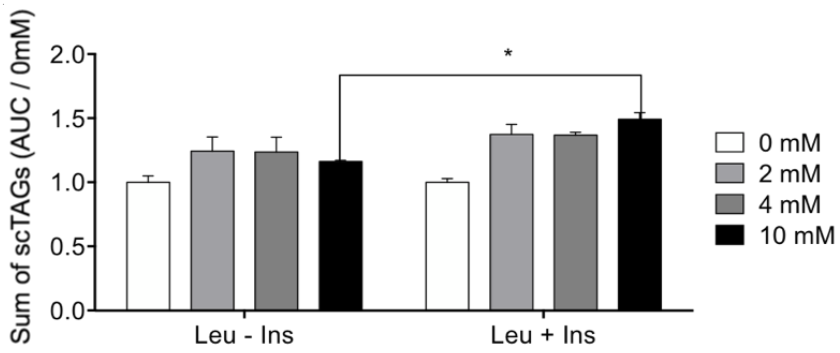

Figure 16. Intracellular levels of scTAGs were decreased in the absence of insulin in AML 12 hepatocytes supplemented with leucine. Sum of scTAG content in cells in response to leucine treatment at 0, 2, 4 and 10 mmol/L concentrations with insulin or without insulin measured by LC-MS after 24 h. Data are presented as mean ± SEM and analysed by two-way ANOVA with *post-hoc* Sidak's multiple comparisons test; * = $p \leq 0.05$, n = 3/group.

The absence of insulin increased the expression of fatty acid synthesis genes in leucine-supplemented cells

Even though leucine induced the biggest increase in scTAG content, it decreased the expression of DNL genes in the presence of insulin. The absence of insulin increased the expression of fatty acid synthesis genes at 10 mmol/L leucine. The expression of *Acly* and *Fasn* at 10 mmol/L leucine was significantly less in the presence of insulin compared with insulin starved cells (Figure 17A and 17C). The expression of *Acaca* was not changed between the two treatments (Figure 17B).

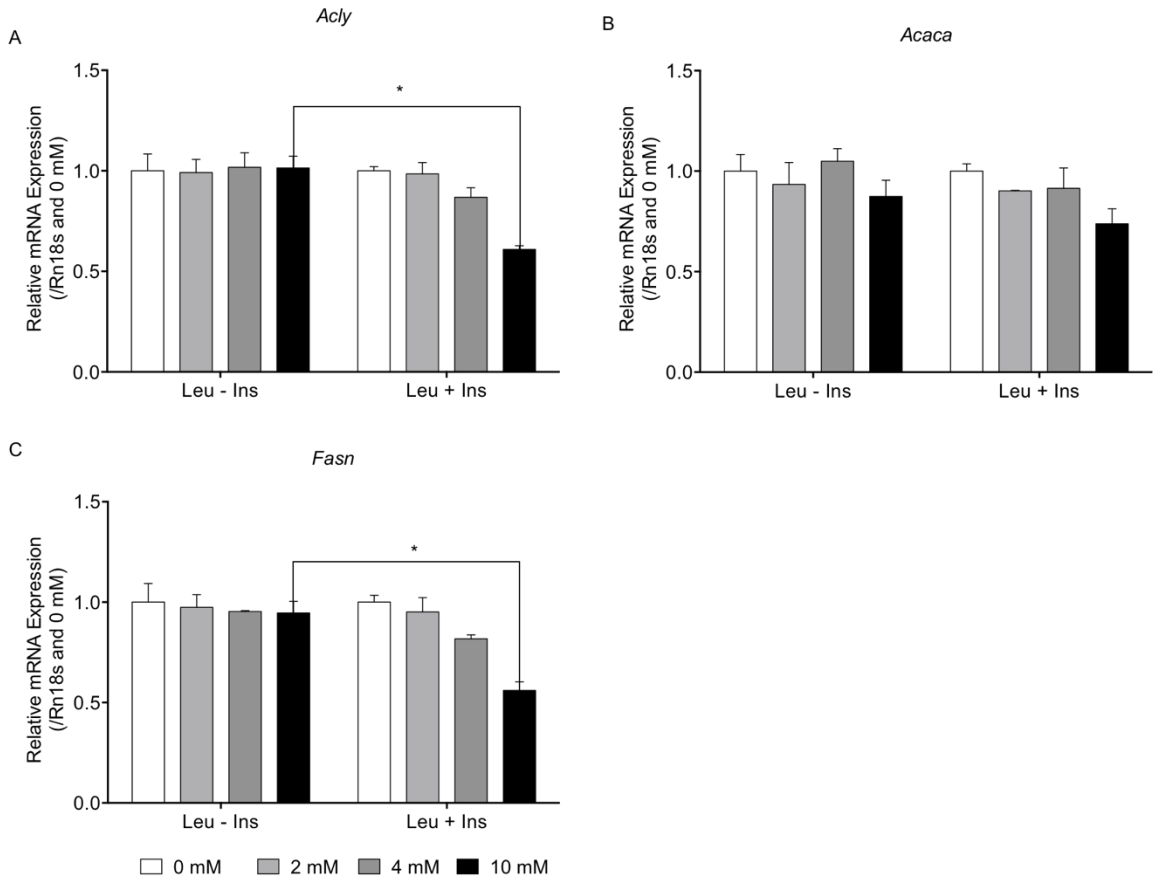

Figure 17. The expression of fatty acid synthesis genes increased in insulin starved AML 12 hepatocytes supplemented with leucine. (**A**) qPCR analysis of expression of fatty acid synthesis gene *Acly* after a 24 h treatment with leucine at 0, 2, 4 and 10 mmol/L with insulin or without insulin. (**B**) qPCR analysis of expression of fatty acid synthesis gene *Acaca* after a 24 h treatment with leucine at 0, 2, 4 and 10 mmol/L with insulin or without insulin (**C**) qPCR analysis of expression of fatty acid synthesis gene *Fasn* after a 24 h treatment with leucine at 0, 2, 4 and 10 mmol/L with insulin or without insulin. Data are presented as mean ± SEM and analysed by two-way ANOVA with *post-hoc* Sidak's multiple comparisons test; * = $p \leq 0.05$, n = 3/group.

The absence of insulin increased the expression of fatty acid processing genes in leucine-supplemented cells

The relative expression of fatty acid processing genes, measured by qPCR, increased in the absence of insulin. The expression of the desaturase, *Scd1*, and the elongase *Elovl6* at 10 mmol/L leucine were lower in insulin sufficient cells than insulin starved cells (Figure 18A&B).

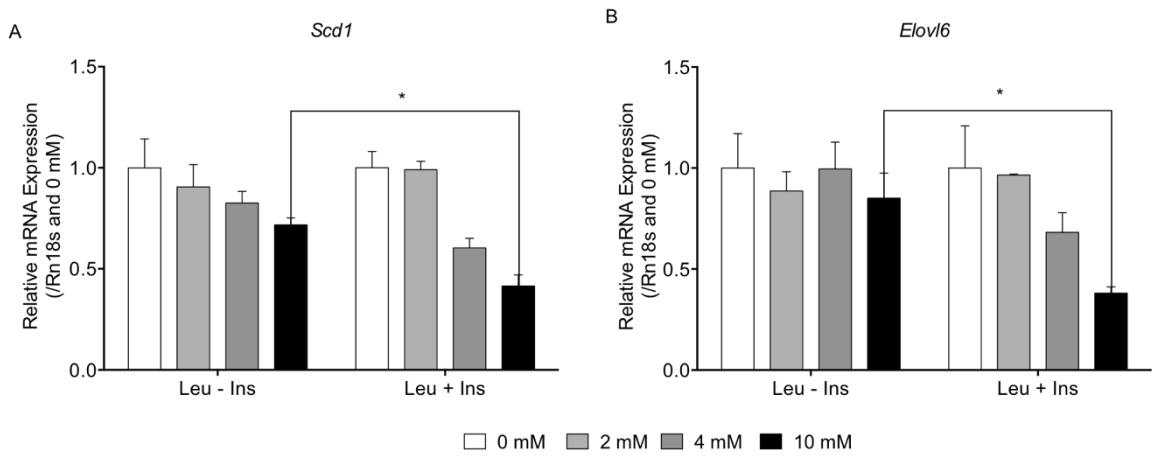

Figure 18. The expression of fatty acid processing genes increased in insulin starved AML 12 hepatocytes supplemented with leucine. (**A**) qPCR analysis of expression of fatty acid processing gene *Scd1* after a 24 h treatment with leucine at 0, 2, 4 and 10 mmol/L with insulin or without insulin. (**B**) qPCR analysis of expression of fatty acid processing gene *Elvol6* after a 24 h treatment with leucine at 0, 2, 4 and 10 mmol/L with insulin or without insulin. Data are presented as mean ± SEM and analysed by two-way ANOVA with *post-hoc* Sidak's multiple comparisons test; * = $p \leq 0.05$, n = 3/group.

5.4.5 Lysine supplementation does not affect DNL in the absence of insulin

Lysine supplementation did not affect the content of scTAGs in the absence of insulin

The amounts of scTAGs detected at 2, 4 and 10 mmol/L lysine were not different between insulin sufficient and starved cells (Figure 19).

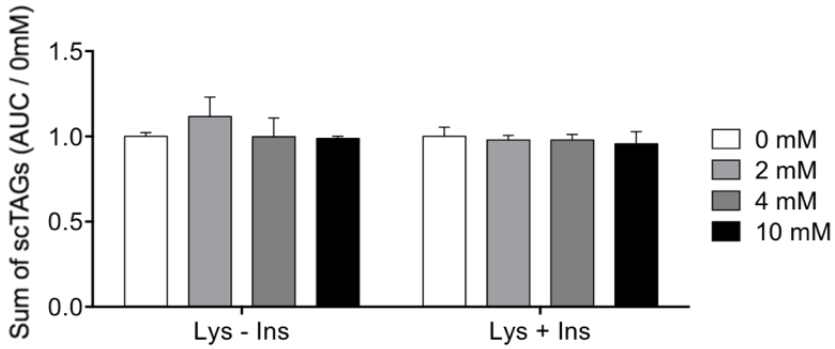

Figure 19. Intracellular levels of scTAGs were not affected by the absence of insulin in AML 12 hepatocytes supplemented with lysine. Sum of scTAG content in cells in response to lysine treatment at 0, 2, 4 and 10 mmol/L concentrations with or without insulin measured by LC-MS after 24 h. Data are presented as mean ± SEM and analysed by two-way ANOVA with *post-hoc* Sidak's multiple comparisons test; * = $p \leq 0.05$, n = 3/group.

Lysine supplementation did not alter the expression of fatty acid genes in the absence of insulin

The relative expression of fatty acid synthesis genes, measure by qPCR, did not change between the two treatment groups (Figure 20A-C).

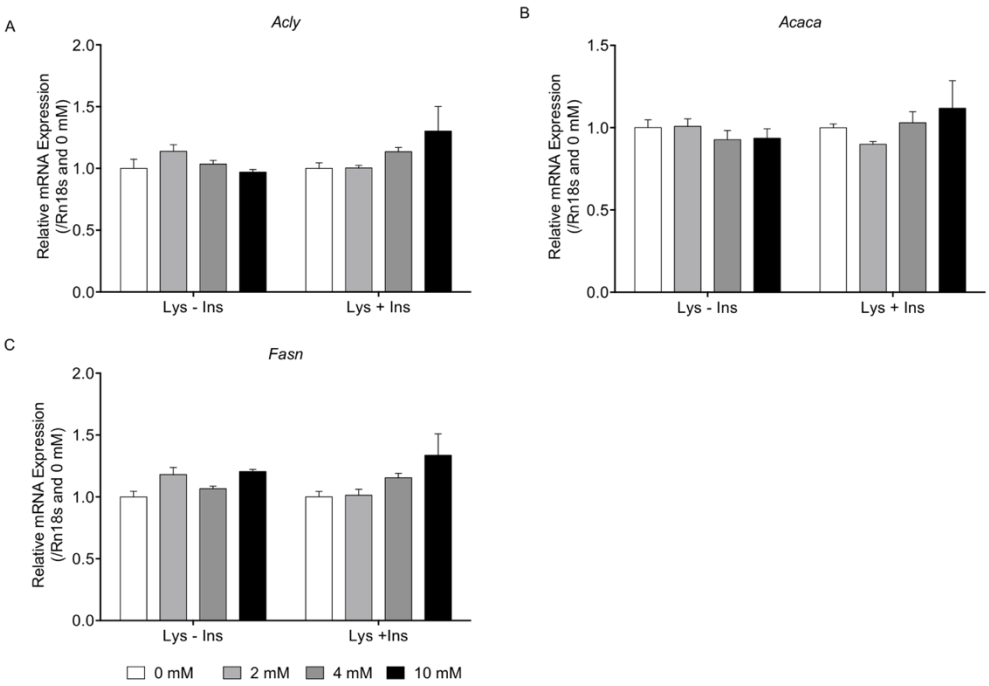

Figure 20. The expression of fatty acid synthesis genes was not changed between insulin starved and insulin sufficient AML 12 hepatocytes supplemented with lysine. (**A**) qPCR analysis of expression of fatty acid synthesis gene *Acly* after a 24 h treatment with lysine at 0, 2, 4 and 10 mmol/L with or without insulin. (**B**) qPCR analysis of expression of fatty acid synthesis gene *Acaca* after a 24 h treatment with lysine at 0, 2, 4 and 10 mmol/L with or without insulin (**C**) qPCR analysis of expression of fatty acid synthesis gene *Fasn* after a 24 h treatment with lysine at 0, 2, 4 and 10 mmol/L with or without insulin. Data are presented as mean ± SEM and analysed by two-way ANOVA with *post-hoc* Sidak's multiple comparisons test; * = $p \leq 0.05$, n = 3/group.

Lysine supplementation decreased the expression of fatty acid genes in the absence of insulin

The relative expression of fatty acid processing genes, measured by qPCR, decreased in the absence of insulin. The expression of the desaturase, *Scd1*, and the elongase *Elovl6* at 10 mmol/L lysine were higher in insulin sufficient cells than insulin starved cells (Figure 21A&B).

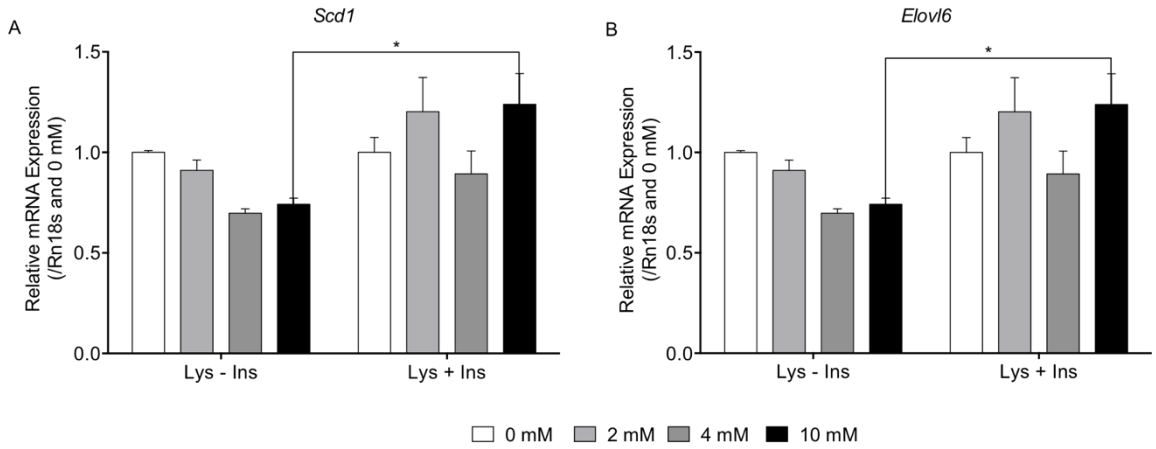

Figure 21. The expression of fatty acid processing genes decreased in insulin starved AML 12 hepatocytes supplemented with lysine. (**A**) qPCR analysis of expression of fatty acid processing gene *Scd1* after a 24 h treatment with lysine at 0, 2, 4 and 10 mmol/L with or without insulin. (**B**) qPCR analysis of expression of fatty acid processing gene *Elvol6* after a 24 h treatment with lysine at 0, 2, 4 and 10 mmol/L with or without insulin. Data are presented as mean ± SEM and analysed by two-way ANOVA with *post-hoc* Sidak's multiple comparisons test; * = $p \leq 0.05$, n = 3/group.

5.5 Discussion

The latest nutritional transition from traditional to western-style diets (rich in sugar, fat and protein from red meat) has led to a growing prevalence of NAFLD and T2DM (Bhat et al., 2012). Hepatic lipid accumulation, via upregulated levels of DNL, is mutual to both disorders. Whilst it is well established that high carbohydrate feeding increases DNL (Hudgins et al., 1996), studies of the effect of high protein feeding in relation to DNL in humans, are limited. Despite high protein/low carbohydrate diets being popular regimes for weight loss in humans to prevent obesity and diabetes, recent studies correlated elevated BCAA levels with insulin resistance and T2DM (Würtz et al., 2012). Studies have previously demonstrated that a higher protein/lower carbohydrate diet downregulates DNL (Garcia-Caraballo et al., 2013; Margolis et al., 2016), typically in longer-term dietary interventions. However, the precise amino acid composition of the high protein diet is not determined. In the previous chapters, dietary amino acids increased scTAGs in healthy human subjects. Carbon from glutamate was incorporated into palmitate via DNL, suggesting that amino acids may provide carbon as a substrate for this process under physiological substrate concentrations. In this chapter, amino acids had differential effects on scTAGs as well as the expression of genes required for synthesis, processing and packaging of fatty acids, likely involving the action of AKT2 in hepatocytes.

Citrate is found at a cross-road between catabolism and anabolism. An increase in the energy balance (decreased NAD^+/NADH ratio) inhibits catabolic pathways and drives the anabolic reactions within a cell, such as fatty acid synthesis (Whereat et al., 1967). During anabolism, citrate is withdrawn from the TCA cycle and exported from the mitochondrion to the cytosol, via the mitochondrial citrate carrier (Gnoni et al., 2009). In the cytosol, citrate is lysed to acetyl-CoA, which may then be used for fatty acid synthesis (Williams and O'Neill, 2018). These synthetic processes are tightly regulated by the high energy balance; high NADH levels inhibit β-oxidation and promote the synthesis of cytosolic acetyl-CoA, via citrate, which in turn inhibits the activity of glycolytic enzymes (Williams and O'Neill, 2018). Cytosolic acetyl-CoA is then carboxylated by ACC to malonyl-CoA, which inhibits CPT1, the enzyme which facilitates the

entry of fatty acids into the mitochondrion to undergo β-oxidation. In theory all amino acids may provide acetyl-CoA for fatty acid synthesis. Ketogenic amino acids break down in the mitochondrion to acetyl-CoA, which condenses with oxaloacetate to synthesise citrate by citrate synthase, whilst glucogenic amino acids break down to a variety of TCA cycle intermediates that eventually generate citrate (Andrea, 1998). The data herein demonstrate that glutamine and leucine but not lysine supplementation increased the energy balance in hepatocytes. This agrees with the result that carbon from lysine was not incorporated in fatty acids. In contrast, glutamate supplementation was sufficient to induce DNL and provide carbon for fatty acids synthesis (Chapter 4). Carbon from glutamine and leucine has also been shown to be incorporated into fatty acids in differentiated 3T3-L1 adipocytes (Crown et al., 2015). The data suggest that glutamate, glutamine, leucine but not lysine supplementation is sufficient to export citrate in the cytosol and generate cytosolic acetyl-CoA for fatty acid synthesis. Once citrate is in the cytosol, a variety of enzymes are required to synthesise fatty acids (Ducheix et al., 2017). The expression of genes that translate to these enzymes is under the control of the insulin signalling cascade and mTOR (Zhou et al., 2018).

A master regulator of cell growth, mTORC1, is responsible for sensing nutrient signals, particularly amino acids (Yoon and Choi, 2016). The mTORC1 signalling pathway integrates insulin signals, through its phosphorylation by PI3-kinase/AKT2 (Vinod and Venkatesh, 2009). Activation of mTORC1 leads to the nuclear localisation of LXRα, whereupon it heterodimerises with the RXR to induce the expression of lipogenic genes as well as SREBP1c (Hwahng et al., 2009). The mTORC1 also mediates the nuclear translocation of SREBP1c, where it induces the transcription of genes required for DNL (Peterson et al., 2011). However, it has recently been reported that mTORC1 activation in the absence of AKT2 is not sufficient to stimulate SREBP1c, and thus DNL (Yecies et al., 2011), suggesting that amino acids regulate an upstream node in the pathway, or act in an, as yet, undetermined manner. The data of this chapter show that select amino acids, glutamine and leucine but not lysine, activated AKT2. This may also indicate that specific amino acids may regulate mTORC2, responsible for the activation of AKT2 and subsequent induction in the expression of genes required for DNL, in

support of a signalling pathway proposed by Tato et al (Tato et al., 2011). Amino acids, branched-chain in particular, have been linked with insulin resistance. The molecular basis is the activation $p70^{S6K1}$ by amino acids (Iiboshi et al., 1999), a downstream kinase of mTORC1. This in turn phosphorylates the insulin receptor substrate at multiple serine/threonine residues and directs it to degradation. This acts as a negative feedback loop, whereby active $p70^{S6K1}$ attenuates any further activation of the insulin signalling pathway, reducing glucose uptake. Persistent activation of $p70^{S6K1}$ by excessive amino acid concentrations may therefore lead to insulin resistance (Tremblay and Marette, 2001). Herein, it is demonstrated that glutamine and leucine decrease insulin-dependent glucose uptake, whilst lysine does not.

In support of the finding that specific amino acids activated PKB/AKT2 (glutamate, glutamine and leucine but not lysine), the same amino acids increased scTAG content and decreased glucose uptake in hepatocytes. In addition, the same amino acids increased the energy balance, as measured by the reducing potential of the cell, and have been shown to provide carbon for fatty acid synthesis. These differential effects of amino acids on DNL are not specific to an amino acid class (ketogenic, glucogenic or BCAAs) as glutamate, glutamine and leucine that affect DNL belong to different amino acid classes. The data suggest that specific amino acids are able to change the energy balance, activate the mTOR complexes and subsequently induce DNL.

Leucine resulted in the greatest increase in scTAG content followed by glutamine and lastly, glutamate (Chapter 4). Both glutamate and glutamine increased the expression of genes required for the synthesis, processing as well as packaging of fatty acids. Perhaps surprisingly, leucine and the highest concentration of glutamine decreased the expression of genes required for synthesis and processing of fatty acids but increased the expression of genes required for packaging. This suggests a possible negative feedback mechanism, whereby accumulation of high levels of scTAGs or other intermediate species (such as fatty acyl-CoAs or diacylglycerides) in the liver inhibit the expression of these genes, but not the expression of genes required for subsequent processing and packaging. Indeed, studies demonstrate that

unsaturated fatty acids lower the levels of mRNA for SREBP1c by accelerating its degradation (Ou et al., 2001), whilst longer chain polyunsaturated fatty acids are potent inhibitors of ACC (Brim et al., 1997). The findings presented in this chapter also suggest that fatty acid synthesis and processing genes are differentially regulated to packaging genes. SREBP1c induces the expression of genes required for the synthesis (*Acly*, *Acaca* and *Fasn*) and processing (*Scd1* and *Elovl6*) of fatty acids (Ducheix et al., 2017). On the other hand, packaging genes (*Mttp* and *Apoc3*) have been shown to be regulated by the Forkhead box O1 (FoxO1) transcription factor (Sparks and Dongb, 2009). FoxO1 is responsible for the expression of the gene encoding functional MTP, a protein responsible for the packaging of lipids with nascent apoB (only present in VLDL) in the endoplasmic reticulum. The action of MTP upon the growing VLDL particles is a rate limiting step in their formation and release into the blood. Elevated levels of MTP increase the secretion of VLDL by the liver and correlate with the pathophysiology of insulin resistance and T2DM (Higuchi et al., 2011). FoxO1 is itself negatively regulated by insulin, which causes its phosphorylation and nuclear exclusion (Altomonte et al., 2004). In cases of impaired insulin regulation, this may result in uncontrollable levels of MTP (Higuchi et al., 2011) expression. The production of hepatic, but not intestinal apoCIII is also controlled by FoxO1 via the -498/-403 element in the apoC3 promoter (Altomonte et al., 2004; West et al., 2017). Two separate insulin signalling axes, PI3-kinase/PKB/AKT2 and MAPK(erk), may be responsible for this inhibition. While there is evidence supporting a role for both axes (Brunet et al., 1999; Liang et al., 2016), data herein suggest that PI3-kinase/PKB/AKT2 is not involved in this inhibition, as the expression of *Mttp* and *apoC3* are increased in the presence of increased PKB/AKT2. This is consistent with the work of Au et al, 2003 that demonstrated that insulin inhibits the transcription of *Mttp* via the MAPK(erk) signalling cascade, but not that of PI-3 kinase (Au et al., 2003). In the context of insulin resistance and the development of fatty liver via dysregulated rates of DNL, it might be considered hepato-protective to increase the rate at which liver-derived lipoproteins are exported, at least in the shorter term. However, it is unlikely that prolonged

hypertriglyceridaemia, brought about by chronic insulin resistance, has equally beneficial effects on long-term cardiovascular health.

It has been reported that both hormonal and nutritional stimuli are required to fully activate the mTOR signalling pathway (Drummond et al., 2008; Saxton and Sabatini, 2017). The data herein show that insulin is required for the induction of DNL by glutamine and leucine. The induction of DNL by glutamine is diminished in the absence of insulin. The amount of scTAGs and the expression of lipogenic genes in insulin-deprived cells supplemented with glutamine were lower compared with insulin-sufficient cells. In addition, the levels of scTAGs in insulin deprived cells supplemented with leucine were lower than insulin sufficient cells. The expression of genes required for DNL in leucine supplemented cells did not decrease in the absence of insulin. As mentioned above, leucine had the biggest increase in scTAGs and therefore this induced a negative regulation in the gene expression required for DNL. In the absence of insulin, the expression of genes required for DNL did not decrease, suggesting that the expression of genes required for DNL is not negatively regulated as less scTAGs are accumulating in the liver.

5.6 Conclusions

In the previous chapters, a meal rich in glutamate increased scTAGs in healthy males. Carbon from glutamate was incorporated into palmitate via DNL and glutamate induced DNL at a protein, genomic and metabolic level. Studies have previously demonstrated that a higher protein/lower carbohydrate diet downregulates DNL, typically in longer-term dietary interventions. However, the precise amino acid composition of the high protein diets in these studies were not determined. In this chapter, it is demonstrated that specific amino acids provide carbon for fatty acid synthesis, through a change in the energy balance of the cell. In addition, the same amino acids were responsible for inducing DNL, via the AKT2 pathway, as well as decreasing the glucose uptake in hepatocytes by reducing insulin sensitivity. The precise metabolic parameters of other amino acids and time-frame of these effects on DNL remain to be fully elucidated. As dietary trends have shifted towards high carbohydrate/high fat consumption, and high-protein diets are popularised as healthier alternatives, the data herein suggest that this is a more complex consideration. Therefore, advocating the consumption of protein in the treatment of diabetes and obesity requires a more profound understanding of the roles of amino acids in the context of hepatic DNL.

Chapter 6. Conclusion

6.1 Summary of findings

The work contained in this thesis examined the role of changing the solid/liquid ratio as well as macronutrient composition of meals on the rates of gastric emptying and DNL. The thought processes and hypotheses of this thesis are shown in Appendix V. In Chapter 3, liquid carbohydrate delayed gastric emptying of healthy subjects. The delay caused by carbohydrate in the liquid phase occurred only up to a liquid carbohydrate content of 50%, after which, increasing levels of liquid carbohydrate no longer affected gastric emptying rates. Though liquid carbohydrate emptied the stomach faster and delayed the emptying of the solid phase, it was not sufficient to induce DNL. Interestingly, HP meal, rich in glutamate, increased the levels of DNL-derived metabolites, suggestive of an increase in rates of DNL.

In Chapter 4, the role of glutamate on DNL was investigated. Glutamate supplementation in liver cells was sufficient to increase the energy balance and provide carbon for fatty acid synthesis. In addition, glutamate induced DNL at a gene expression, protein function and metabolic level. In Chapter 5, the effects of specific amino acids (glucogenic, ketogenic and branch-chain amino acids) on DNL were examined. Glutamine and leucine but not lysine induced a change in the energy balance and stimulated DNL. The same amino acids decreased glucose uptake by liver cells, and this might provide a possible link between lipogenesis and insulin resistance (Figure 1).

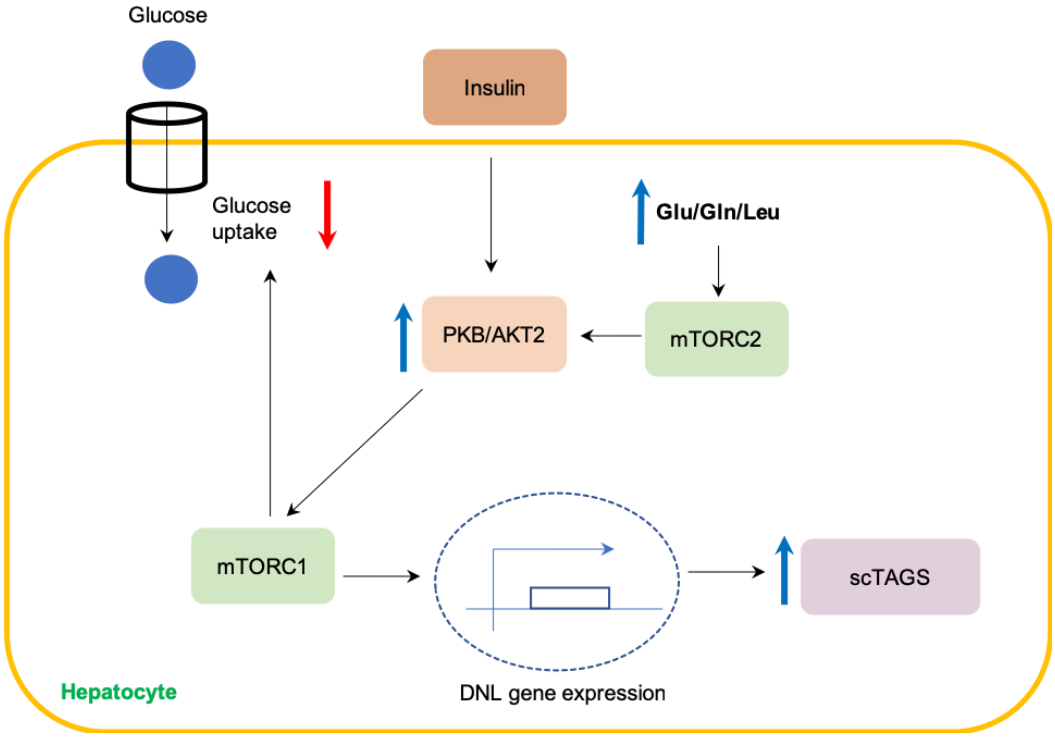

Figure 1. Summary of findings. Supplementation of hepatocytes with glutamate (Glu), glutamine (Gln) and leucine (Leu) increased the levels of activated AKT2, which is induced by mTORC2. This increased the expression of DNL genes, via mTORC1 resulting in increased scTAGs and decreased glucose uptake by hepatocytes. Red arrows represent a decrease and blue arrows an increase.

6.2 The effect of liquid carbohydrate on gastric emptying and DNL

The results of this thesis indicate that liquid carbohydrate was the primary determinant of gastric emptying rather than macronutrient compositions. The delay caused by carbohydrate in the liquid phase occurred only up to a liquid carbohydrate content of 50%, after which, increasing levels of liquid carbohydrate no longer affected gastric emptying rates. This agrees with the hypothesis that early delivery of carbohydrate to the duodenum is sensed by receptors in the small intestine to delay the emptying of the solid portion, where the supplied ^{13}C-octanoic acid is bound. The rate of gastric emptying is crucial for maintaining blood glucose homeostasis as there is bidirectional communication between gastric emptying and glucose (Phillips et al., 2015). The delay observed in this study is the physiological response of the gastrointestinal tract when exposed to nutrients (known as the ileal brake; Maljaars et al., 2008). This is only an acute response to nutrient exposure in healthy subjects, it is unknown

how prolonged exposure to carbohydrates affects gastric emptying. It has been postulated that the reaction of the stomach to nutrients could be adaptive to dietary habits, thus affecting gastric emptying of subsequent meals (Karen M. Cunningham et al., 1991). This adaptation could be protective to control glycaemia; however, it could also be maladaptive and result in uncontrolled glycaemia. It would be interesting to discover at a population level, using epidemiological studies, how liquid carbohydrate affects gastric emptying, glycaemic control and insulin sensitivity.

Liquid carbohydrate empties the stomach faster: approximately 80% of the liquid fraction is emptied before the solid fraction (Phillips et al., 2015) and this might provide substrate to support increased rates of DNL. However, in this study a 2 MJ high carbohydrate meal was not sufficient in this case to induce DNL, which may be a consequence of it being used to replenish glycogen stores depleted by the preceding fast. In previous studies demonstrating an increase in DNL after high carbohydrate feeding, the meals were above 3 MJ (Marques-lopes et al., 2001) and in some other studies, subjects were fed twice rather than once (Timlin and Parks, 2005). Interestingly, the HP meal increased the levels of scTAGs, that have been correlated with insulin resistance and steatosis, at 4 hours after feeding, agreeing with the time that DNL peaks after eating (Timlin and Parks, 2005). Even though amino acids are not typically viewed as lipogenic precursors, the data of Chapter 3 suggested that amino acids may induce DNL.

6.3 The role of amino acids on DNL

In this thesis a high protein meal, rich in glutamate (5.7g), induced DNL in humans. This is above the acceptable daily intake (ADI) of dietary glutamate and glutamate food additives such as monosodium glutamate, potassium glutamate, ammonium glutamate, calcium glutamate and magnesium glutamate. The EFSA established an ADI of 30 mg/kg body weight per day for all glutamate and glutamate additives (EFSA Panel on Food Additives and Nutrient Sources added to Food, 2017). This safety level of intake is based on the highest dose of these

additives at which adverse effects are seen on animals. This is alarming as meat/fish eaters, vegetarians consume on average 15 g/day of glutamate from natural foods (Tennant, 2018). This obvious exceedance of the proposed acceptable daily intake creates uncertainties about the potential effects of glutamate from natural sources as well as glutamate additives. The adverse effect seen in this thesis is the induction of DNL by glutamate. Therefore, a more mechanistic understanding of how glutamate and other amino acids induce DNL is required.

Biochemical mechanisms of DNL activation by amino acids

Oscillations of the cellular redox NAD^+/NADH and oxidised nicotinamide phosphate ($NADP^+$)/reduced nicotinamide phosphate (NADPH) determine the cellular metabolic phenotype (Mclean and Greenbaum, 1970). The reduced cofactors, NADH and NADPH are used for biosynthesis, whilst, NAD^+ and $NADP^+$, have been found to inhibit synthesis and promote catabolism (Mclean and Greenbaum, 1970). An increase in the energy balance, reflected by increased levels of reduced cofactors, induces the export of citrate from the mitochondrion to the cytosol, where it is lysed to generate cytosolic acetyl-CoA for fatty acid synthesis. It has recently been reported that high protein intake is associated with low plasma NAD^+ levels in healthy humans (Seyedsadjadi et al., 2018). NAD^+ supplementation decreases lipogenesis (Mclean and Greenbaum, 1970), supported by findings in this thesis, where acute protein feeding (which decreased NAD^+ compared to NADH) increased DNL in healthy subjects. Together, the data support that protein feeding modulates the NAD^+/NADH redox. Indeed, select amino acids (glutamate, glutamine and leucine but not lysine) affected the energy balance in liver cells by decreasing the NAD^+/NADH redox ratio, suggesting that these amino acids may activate fatty acid synthesis. It has been demonstrated in this thesis that carbon from glutamate is incorporated into fatty acids whilst carbon from lysine is not. In addition, glutamine and leucine have been previously shown to provide carbon for fatty acid synthesis (Crown et al., 2015).

Once citrate is in the cytosol a variety of enzymes are required to synthesise and process fatty acids. The expression of the genes that encode these enzymes is under the control of the

transcription factor SREBP-1c, which responds to insulin stimuli (Zhou et al., 2018). Engagement of insulin to the insulin receptor activates the insulin receptor substrate that recruits PI3K to the membrane, where it phosphorylates PIP_2 to PIP_3. The PIP_3 acts as a docking site for the kinases mTORC2 and PDK1. Both mTORC2 and PDK1 phosphorylate and thereby activate PKB/AKT2. Activated AKT2 relieves the inhibitory effect of TSC1/2 on the mTORC1 by phosphorylating TSC2 at multiple sites (Huang and Manning, 2010). The kinase mTORC1 has multiple downstream effectors, one of which is $p70^{S6K1}$, that induces the nuclear translocation of LXRα, where it may heterodimerise with RXR (Kawano and Cohen, 2013). The heterodimer then induces the expression of lipogenic genes including SREBP-1c. The kinase mTORC1 is responsible for sensing nutrient signals, particularly amino acids (Yoon and Choi, 2016) and therefore it integrates nutrient and insulin signals, through its phosphorylation by PI3-kinase/AKT2 (Vinod and Venkatesh, 2009). The activation of mTORC1 in the absence of AKT2 is not sufficient to induce SREBP1c, and thus DNL (Yecies et al., 2011), suggesting that amino acids regulate an upstream node in the pathway, or act in an, as yet, undetermined pathway. AKT2 activation was amino acid specific, agreeing with the finding of this thesis that glutamate, glutamine and leucine but not lysine, increased scTAG levels. This may also indicate that specific amino acids may regulate mTORC2, responsible for the activation of AKT2 and subsequent induction in the expression of genes required for DNL, in support of the signalling pathway proposed by Tato et al., 2011.

Increased levels of BCAAs correlate with insulin resistance (Würtz et al., 2012). The activation of $p70^{S6K1}$ by BCAAs has been described as the molecular basis of insulin resistance by amino acids (Iiboshi et al., 1999). Activated $p70^{S6K1}$ phosphorylates IRS at multiple serine/threonine residues, which leads to its degradation. This negative feedback loop attenuates any further activation of the insulin signalling pathway. It is suggested that excess amino acids result in the persistent activation of $p70^{S6K1}$ and may therefore lead to insulin resistance (Tremblay and Marette, 2001).

The extent to which specific amino acids can shift the energy balance within cells and induce DNL is as yet unknown. A plausible explanation might be the net gain of reducing agents produced by amino acid catabolism. Once glutamine is within the cell, it is hydrolysed to glutamate by a glutaminase. Glutamate is further metabolised to α-ketoglutarate by glutamate dehydrogenase, which uses NAD^+ and generates NADH. This shift in the energy balance activates IDH1/2, which convert α-ketoglutarate to citrate in the cytosol and mitochondrion respectively. In addition, high NADH concentrations prevent the unnecessary oxidation of isocitrate to α-ketoglutarate via inhibition of IDH3 (Wise et al., 2011). Accumulated citrate in the cytosol is used to synthesise fatty acids by DNL (Giudetti et al., 2016). In theory the degradation of all amino acids should result in a net gain of reducing equivalents as amino acids are oxidised to generate TCA cycle intermediates, pyruvate or acetyl-CoA. However, in practise, as shown in this thesis, only specific amino acids changed the cellular energy balance. This might be because some amino acids may be preferentially used in other metabolic pathways, for instance protein synthesis or just not metabolised to the same extent, for example because of differences in activities of their associated amino transferases.

The amino acid specificity of mTORC1 and mTORC2 is also unclear. Although amino acids in general promote the lysosomal localisation and activation of mTORC1, the identity of amino acid sensor/sites of recognition are yet unclear. The branched-chain amino acids, leucine and isoleucine, have been found to be potent activators of mTORC1 (Yoon, 2016). Wolfson et al. identified a biochemical sensor of leucine, Sestrin2, which has recently been implicated in the lysosomal localisation and activation of mTORC1 (Wolfson et al., 2016). In addition, glutamine has also been found to activate mTORC1 indirectly by increasing the uptake of leucine (Nicklin et al., 2009) or directly by a different mechanism to that of leucine that does not require a GTPase (Jewell et al., 2015). Another amino acid that has been shown to activate mTORC1 is arginine (Rebsamen et al., 2015). It has also been reported that for some amino acids to activate mTORC1, they require priming by another amino acid. Cysteine has been reported to inhibit this priming step in mTORC1 activation (Dyachok et al., 2016). In addition, amino acids have been shown to activate mTORC2, however the amino acid specificity of

mTORC2 is still unknown. As mentioned, AKT2, which is activated by mTORC2, was activated by glutamine, glutamate and leucine but not lysine. This indicates that mTORC2 also has some amino acid specificity. Research is focussed on mTORC1 but as seen in this thesis and by other work (Tato et al., 2011), specific amino acids activate mTORC2. Therefore, more studies are required to understand how amino acids activate mTORC2.

The work in this thesis has introduced novel effects of dietary amino acid supplementation on DNL. Though it remains unclear as to how specific amino acids can activate the mTOR complexes, the increase in energy balance caused by specific amino acids might change the activity of amino acid sensors that are responsible for activating mTORC2 (Figure 2) and thus DNL. It would be interesting to characterise the effect of all 20 proteinogenic (and possibly non-proteinogenic) amino acids on mTORC1 and mTORC2 activation as well as identify the amino acid sensors responsible for these effects. This will enable us to characterise whether a group of amino acids are sensed by the same sensor or different ones.

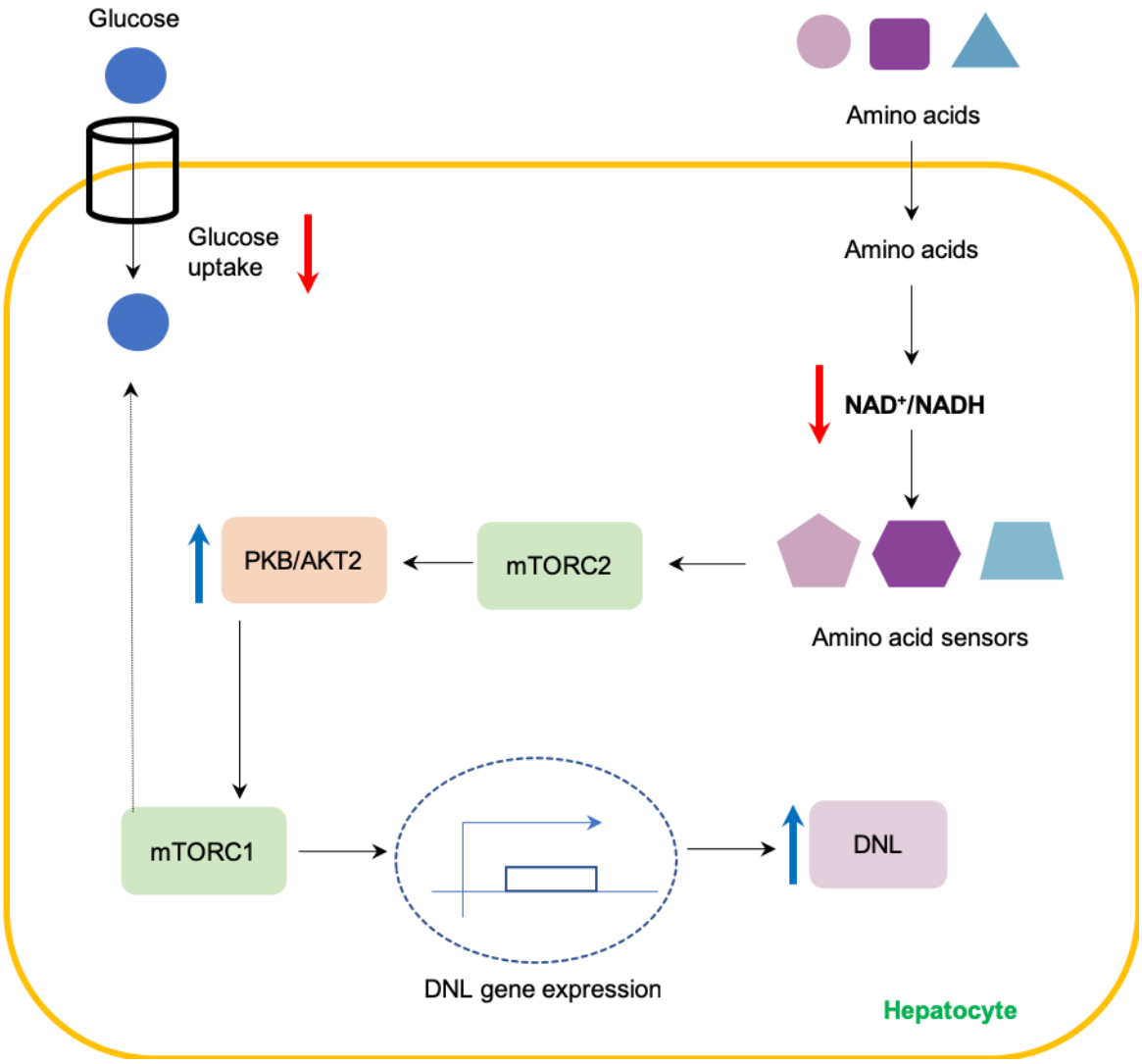

Figure 2. Proposed mechanism by which specific amino acids activate DNL. Specific amino acids may activate mTORC2, via an increase in the energy balance (decreased NAD^+/NADH). Activated mTORC2 may then induce DNL, via AKT2/mTORC1, and decrease glucose uptake by liver cells. Red arrows represent a decrease and blue arrows an increase.

All the studies in this thesis are focussed on the acute effects of amino acids on DNL. The next step will be to study the long-term effects of amino acids on DNL. Studies have previously demonstrated that a higher protein/lower carbohydrate diet downregulates DNL (Garcia-Caraballo et al., 2013; Margolis et al., 2016), typically in longer-term dietary interventions. However, the precise amino acid composition of high protein diets used in research is not determined and as shown herein the induction of DNL is amino acid specific. Therefore, future studies on how protein affects DNL should be more specific as to which amino acid is increased in the meal. In addition, it would be interesting to see whether the effects that are seen in cell

culture can be translated *in vivo*, initially into an animal model, in both short-term and long-term settings.

It is important to characterise the effects of amino acids on DNL as insulin resistance Is correlated with dysregulated hepatic lipid metabolism (Brown and Goldstein, 2008), that entails increased levels of DNL. The proposed mechanism behind hepatic insulin is the activation of protein kinase C isoforms (PKCλ/ζ), by increased diacylglycerol levels synthesised by DNL, inhibiting the activation of the IRS (Taniguchi et al., 2006). Expression of PKC in fatty liver is also elevated (Samuel et al., 2010). Yet again, amino acids might also be contributing to the inhibition of the IRS, both via mTORC1 activation and by inducing lipogenesis. As dietary trends have shifted towards high carbohydrate/high fat consumption, and high protein diets are popularised as healthier alternatives, the data herein suggest that this is a more complex consideration. Therefore, advocating the consumption of protein in the treatment of diabetes and obesity requires a more profound understanding of the roles of amino acids in the context of hepatic DNL.

References

Aarsland, A., Chinkes, D., Wolfe, R.R., 1996. Contributions of de novo synthesis of fatty acids to total VLDL-triglyceride secretion during prolonged hyperglycemia hyperinsulinemia in normal man. *J. Clin. Invest.* 98, 2008–2017.
Adiels, M., Olofsson, S.O., Taskinen, M.R., Borén, J., 2008. Overproduction of very low-density lipoproteins is the hallmark of the dyslipidemia in the metabolic syndrome. *Arterioscler. Thromb. Vasc. Biol.* 28, 1225–1236.
Alberti, K.G., Zimmet, P., Shaw, J., 2006. Metabolic syndrome-a new world-wide definition. A Consensus Statement from the International Diabetes Federation. *Diabet. Med.* 23, 469–480.
Altomonte, J., Cong, L., Harbaran, S., Richter, A., Xu, J., Meseck, M., Dong, H.H., 2004. Foxo1 mediates insulin action on apoC-III and triglyceride metabolism. *J. Clin. Invest.* 114, 1493–1503.
Ameer, F., Scandiuzzi, L., Hasnain, S., Kalbacher, H., Zaidi, N., 2014. De novo lipogenesis in health and disease. *Metabolism*. 63, 895–902.
Andrea, G.D., 1998. Classifying amino acids as gluco(glyco)genic, ketogenic, or both. *Biochem. Educ.* 28, 27–28.
Aronson, D., Rayfield, E.J., 2002. How hyperglycemia promotes atherosclerosis: Molecular mechanisms. *Cardiovasc. Diabetol*. 1, 1–10.
Au, W., Kung, H., Lin, M.C., 2003. Regulation of Microsomal Triglyceride Transfer Protein Gene by Insulin in HepG2 Cells. *Diabetes*. 52, 1073–1080.
Baggio, L.L., Drucker, D.J., 2007. Biology of Incretins: GLP-1 and GIP. *Gastroenterology* 132, 2131–2157.
Bar-Peled, L., Sabatini, D.M., 2014. Regulation of mTORC1 by amino acids. *Trends Cell Biol.* 24, 400–406.
Bar-Peled, L., Schweitzer, L.D., Zoncu, R., Sabatini, D.M., 2012. An expanded Ragulator is a GEF for the Rag GTPases that signal amino acid levels to mTORC1. *Cell*. 150, 1196–1208.
Benhamed, F., Denechaud, P.D., Lemoine, M., Robichon, C., Moldes, M., Bertrand-Michel, J., Ratziu, V., Serfaty, L., Housset, C., Capeau, J., Girard, J., Guillou, H., Postic, C., 2012. The lipogenic transcription factor ChREBP dissociates hepatic steatosis from insulin resistance in mice and humans. *J. Clin. Invest.* 122, 2176–2194.
Berg, J., Tymoczko, J., Stryer, L., 2002. *Biochemistry*, 7th ed, New York.
Berwick, D.C., Hers, I., Heesom, K.J., Moule, S.K., Tavare, J.M., 2002. The Identification of ATP-citrate Lyase as a Protein Kinase B (Akt) Substrate in Primary Adipocytes. *J. Biol. Chem*. 277, 33895–33900.
Bhat, G., Baba, C.S., Pandey, A., Kumari, N., Choudhuri, G., 2012. Life style modification improves insulin resistance and liver histology in patients with non-alcoholic fatty liver disease. *World J. Hepatol*. 4, 209–217.
Bianchi, A., Evans, J.L., Iverson, A.J., Nordlung, A.C., Watts, T.D., Witters, L.A., 1990. Identification of an isozymic form of acetyl-CoA carboxylase. *J. Biol. Chem*. 265, 1502–1509.
Boden, G., Salehi, S., Cheung, P., Homko, C., Song, W., Loveland-Jones, C., Jayarajan, S., 2013. Comparison of in vivo effects of insulin on SREBP-1c activation and INSIG-1/2 in rat liver and human and rat adipose tissue. *Obesity* 21, 1208–1214.
Bonaz, B., Bazin, T., Pellissier, S., 2018. The vagus nerve at the interface of the microbiota-gut-brain axis. *Front. Neurosci*. 12, 49.
Boone, A.N., Chan, A., Kulpa, J.E., Brownsey, R.W., 2000. Bimodal activation of acetyl-CoA carboxylase by glutamate. *J. Biol. Chem*. 275, 10819–10825.
Botman, D., Tigchelaar, W., Van Noorden, C.J.F., 2014. Determination of Glutamate Dehydrogenase Activity and Its Kinetics in Mouse Tissues using Metabolic Mapping (Quantitative Enzyme Histochemistry). *J. Histochem. Cytochem*. 62, 802–812.
Brener, W., Hendrix, T.R., McHugh, P.R., 1983. Regulation of the gastric emptying of glucose. *Gastroenterology* 85, 76–82.
Brim, T., Assimacopoulos-jeannet, F., Corkey, B.E., Prentki, M., 1997. Long-Chain Fatty Acids Inhibit Acetyl-CoA Carboxylase Gene Expression in the Pancreatic β-Cell Line INS-1. *Diabetes* 46, 393–400.

Brose, S.A., Marquardt, A.L., Golovko, M.Y., 2015. Fatty acid biosynthesis from glutamate and glutamine is specifically induced in neuronal cells under hypoxia. *J. Neurochem*. 129, 400–412.
Brown, M.S., Goldstein, J.L., 2008. Selective versus Total Insulin Resistance: A Pathogenic Paradox. *Cell Metab.* 7, 95–96.
Brownlee, M., Vlassara, H., Cerami, A., 1985. Nonenzymatic glycosylation products on collagen covalently trap low-density lipoprotein. *Diabetes* 34, 938–941.
Brownlee, Vlassara, Kooney, Ulrich, Cerami, 1986. Aminoguanidine prevents diabetes-induced arterial wall protein cross-linking. *Science*. 232, 1629–1623.
Brunet, A., Bonni, A., Zigmond, M.J., Lin, M.Z., Juo, P., Hu, L.S., Anderson, M.J., Arden, K.C., Blenis, J., Greenberg, M.E., 1999. Akt Promotes Cell Survival by Phosphorylating and Inhibiting a Forkhead Transcription Factor. *Cell* 96, 857–868.
Byrne, C.D., Targher, G., 2015. NAFLD: A multisystem disease. J. Hepatol. 62, S47–S64.
Calbet, J.A., MacLean, D.A., 1997. Role of caloric content on gastric emptying in humans. *J. Physiol.* 498 (Pt 2), 553–559.
Carlson, C.J., White, M.F., Rondinone, C.M., 2004. Mammalian target of rapamycin regulates IRS-1 serine 307 phosphorylation. *Biochem. Biophys. Res. Commun.* 316, 533–539.
Chakravarty, B., Gu, Z., Chirala, S.S., Wakil, S.J., Quiocho, F.A., 2004. Human fatty acid synthase: Structure and substrate selectivity of the thioesterase domain. *Proc. Natl. Acad. Sci.* 101, 15567–15572.
Chang, S.I., Hammes, G.G., 1990. Structure and Mechanism of Action of a Multifunctional Enzyme: Fatty Acid Synthase. *Acc. Chem. Res.* 23, 363–369.
Chaw, C.S., Yazaki, E., Evans, D.F., 2001. The effect of pH change on the gastric emptying of liquids measured by electrical impedance tomography and pH-sensitive radiotelemetry capsule. *Int. J. Pharm*. 227, 167–175.
Clambey, E.T., McNamee, E.N., Westrich, J.A., Glover, L.E., Campbell, E.L., Jedlicka, P., de Zoeten, E.F., Cambier, J.C., Stenmark, K.R., Colgan, S.P., Eltzschig, H.K., 2012. Hypoxia-inducible factor-1 alpha – dependent induction of FoxP3 drives regulatory T-cell abundance and function during inflammatory hypoxia of the mucosa. *PNAS* 109, E2784–E2793.
Clegg, M., Shafat, A., 2010. Energy and macronutrient composition of breakfast affect gastric emptying of lunch and subsequent food intake, satiety and satiation. *Appetite* 54, 517–523.
Coleman, R.A., Lee, D.P., 2004. Enzymes of triacylglycerol synthesis and their regulation. *Prog. Lipid Res.* 43, 134–176.
Collins, P.J., Houghton, L.A., Read, N.W., Horowitz, M., Chatterton, B.E., Heddle, R., Dent, J., 1991. Role of the proximal and distal stomach in mixed solid and liquid meal emptying. *Gut* 32, 615–619.
Crown, S.B., Marze, N., Antoniewicz, M.R., 2015. Catabolism of branched chain amino acids contributes significantly to synthesis of odd-chain and even-chain fatty acids in 3T3-L1 adipocytes. *PLoS One* 10, e0145850.
Dekker, M.J., Su, Q., Baker, C., Rutledge, A.C., Adeli, K., 2010. Fructose: a highly lipogenic nutrient implicated in insulin resistance, hepatic steatosis, and the metabolic syndrome. AJP Endocrinol. *Metab.* 299, E685–E694.
Dentin, R., Benhamed, F., Hainault, I., Fauveau, V., Foufelle, F., Dyck, J.R.B., Girard, J., Postic, C., 2006. Liver-specific inhibition of ChREBP improves hepatic steatosis and insulin resistance in ob/ob mice. *Diabetes* 55, 2159–2170.
Diraison, F., Yankah, V., Letexier, D., Dusserre, E., Jones, P., Beylot, M., 2003. Differences in the regulation of adipose tissue and liver lipogenesis by carbohydrates in humans. *J. Lipid Res.* 44, 846–853.
Donnelly, K.L., Smith, C.I., Schwarzenberg, S.J., Jessurun, J., Boldt, M.D., Parks, E.J., 2005. Sources of fatty acids stored in liver and secreted via lipoproteins in patients with nonalcoholic fatty liver disease. *J Clin Invest* 115, 1343–1351.
Drummond, M.J., Bell, J.A., Fujita, S., Dreyer, H.C., Glynn, E.L., Volpi, E., Rasmussen, B.B., 2008. Amino Acids are Necessary for the Insulin-Induced Activation of mTOR/S6K1

Signaling and Protein Synthesis in Healthy and Insulin Resistant Human Skeletal Muscle. *Clin. Nutr.* 27, 447–456.
Ducheix, S., Montagner, A., Polizzi, A., Lasserre, F., Régnier, M., Marmugi, A., Benhamed, F., Bertrand-Michel, J., Mselli-Lakhal, L., Loiseau, N., Martin, P.G., Lobaccaro, J.-M., Ferrier, L., Postic, C., Guillou, H., 2017. Dietary oleic acid regulates hepatic lipogenesis through a liver X receptor- dependent signaling. *PLoS One* 12, e0181393.
Duh, E.J., Sun, J.K., Stitt, A.W., 2017. Diabetic retinopathy: current understanding, mechanisms, and treatment strategies. *JCI Insight* 2, pii: 93751.
Dunn, W.B., Broadhurst, D., Begley, P., Zelena, E., Francis-McIntyre, S., Anderson, N., Brown, M., Knowles, J.D., Halsall, A., Haselden, J.N., Nicholls, A.W., Wilson, I.D., Kell, D.B., Goodacre, R., The Human Serum Metabolome (HUSERMET) Consortium, 2011. Procedures for large-scale metabolic profiling of serum and plasma using gas chromatography and liquid chromatography coupled to mass spectrometry. *Nat. Protoc.* 6, 1060–1083.
Dyachok, J., Earnest, S., Iturraran, E.N., Cobb, M.H., Ross, E.M., 2016. Amino acids regulate mTORC1 by an obligate two-step mechanism. *J. Biol. Chem*. 291, 22414–22426.
Eales, K.L., Hollinshead, K.E.R., Tennant, D.A., 2016. Hypoxia and metabolic adaptation of cancer cells. *Oncogenesis* 5, e190-8.
Eberlé, D., Hegarty, B., Bossard, P., Ferré, P., Foufelle, F., 2004. SREBP transcription factors: Master regulators of lipid homeostasis. *Biochimie* 86, 839–848.
EFSA Panel on Food Additives and Nutrient Sources added to Food (ANS), 2017. Re-evaluation of glutamic acid (E 620), sodium glutamate (E 621), potassium glutamate (E 622), calcium glutamate (E 623), ammonium glutamate (E 624) and magnesium glutamate (E 625) as food additives. *EFSA supporting publication*. 15(7):4910.
EFSA, 2017. Dietary Reference Values for nutrients Summary Report. EFSA supporting publication. e15121, 92.
Eiden, M., Koulman, A., Hatunic, M., West, J.A., Murfitt, S., Osei, M., Adams, C., Wang, X., Chu, Y., Marney, L., Roberts, L.D., O'Rahilly, S., Semple, R.K., Savage, D.B., Griffin, J.L., 2015. Mechanistic insights revealed by lipid profiling in monogenic insulin resistance syndromes. *Genome Med*. 7, 63.
Eng, K., Kay, M., 2012. Gastrointestinal bezoars: History and current treatment paradigms. *Gastroenterol. Hepatol.* 8, 776–778.
Felig, P., Owen, O.E., Wahren, J., Jr., G.F.C., 1969. Amino acid metabolism during prolonged starvation. *J. Clin. Invest.* 48, 574–583.
Fendt, S.-M., Bell, E.L., Keibler, M.A., Olenchock, B.A., Mayers, J.R., Wasylenko, T.M., Vokes, N.I., Guarente, L., Vander Heiden, M.G., Stephanopoulos, G., 2013. Reductive glutamine metabolism is a function of the α-ketoglutarate to citrate ratio in cells. *Nat. Commun.* 4, 2236.
Ferramosca, A., Zara, V., 2014. Dietary fat and hepatic lipogenesis: mitochondrial citrate carrier as a sensor of metabolic changes. *Adv. Nutr*. 5, 217–225.
Ferré, P., Foufelle, F., 2007. SREBP-1c Transcription Factor and Lipid Homeostasis: *Clinical Perspective. Horm. Res*. 6, 72–82.
Foodworks, 2015. High Gate Hill, *Qld: Xyris Software*. Version 08. 2015.
Folch, J., Lees, M., Sloane, G.H., 1957. A simple method for isolation and purification of total lipides from animal tissue. *J. Biol. Chem*. 226, 497–509.
Foster, K.G., Fingar, D.C., 2010. Mammalian target of rapamycin (mTOR): Conducting the cellular signaling symphony. *J. Biol. Chem*. 285, 14071–14077.
Gaggini, M., Morelli, M., Buzzigoli, E., DeFronzo, R.A., Bugianesi, E., Gastaldelli, A., 2013. Non-alcoholic fatty liver disease (NAFLD) and its connection with insulin resistance, dyslipidemia, atherosclerosis and coronary heart disease. *Nutrients* 5, 1544–1560.
Garcia-Caraballo, S.C., Comhair, T.M., Verheyen, F., Gaemers, I., Schaap, F.G., Houten, S.M., Hakvoort, T.B.M., Dejong, C.H.C., Lamers, W.H., Koehler, S.E., 2013. Prevention and reversal of hepatic steatosis with a high-protein diet in mice. *Biochim. Biophys. Acta* 1832, 685–695.
Castiglione K.E., Read N.W., French S.J., 2002. Adaptation to high-fat diet accelerates

emptying of fat but not carbohydrate test meals in humans. *Am J Physiol Regul Integr Comp Physiol*;282:R366-71.
Gentilcore, D., Chaikomin, R., Jones, K.L., Russo, A., Feinle-Bisset, C., Wishart, J.M., Rayner, C.K., Horowitz, M., 2006. Effects of fat on gastric emptying of and the glycemic, insulin, and incretin responses to a carbohydrate meal in type 2 diabetes. *J. Clin. Endocrinol. Metab.* 91, 2062–2067.
Ghoos, Y.F., Maes, B.D., Geypens, B.J., Mys, G., Hiele, M.I., Rutgeerts, P.J., Vantrappen, G., 1993. Measurement of gastric emptying rate of solids by means of a carbon-labeled octanoic acid breath test. *Gastroenterology* 104, 1640–1647.
Giudetti, A.M., Stanca, E., Siculella, L., Gnoni, G. V., Damiano, F., 2016. Nutritional and hormonal regulation of citrate and carnitine/acylcarnitine transporters: Two mitochondrial carriers involved in fatty acid metabolism. *Int. J. Mol. Sci.* 17, 817.
Gnoni, G. V., Priore, P., Geelen, M.J.H., Siculella, L., 2009. The mitochondrial citrate carrier: Metabolic role and regulation of its activity and expression. *IUBMB Life* 61, 987–994.
Goldberg, I.J., 2001. Diabetic Dyslipidemia: Causes and Consequences. *J. Clin. Endocrinol. Metab.* 86, 965–971.
Gottschalk, G., 1968. The Stereospecificity of the Citrate Synthase in Sulfate-Reducing and Photosynthetic Bacteria. *Eur. J. Biochem*. 5, 346–351.
Grundy, S.M., 2016. Overnutrition, ectopic lipid and the metabolic syndrome. *J. Investig. Med*. 64, 1082–1086.
Grundy, S.M., 2004. Obesity, metabolic syndrome, and cardiovascular disease. *J. Clin. Endocrinol. Metab*. 89, 2595–2600.
Guo, X., Li, H., Xu, H., Woo, S., Dong, H., Lu, F., Lange, A.J., Wu, C., 2012. Glycolysis in the control of blood glucose homeostasis. *Acta Pharm. Sin.* B 2, 358–367.
Halland, M., Bharucha, A.E., 2016. Relationship Between Control of Glycemia and Gastric Emptying Disturbances in Diabetes Mellitus. *Clin. Gastroenterol. Hepatol.* 14, 929–936.
Hara, K., Yonezawa, K., Weng, Q.-P., Kozlowski, M.T., Belham, C., Avruch, J., 1998. Amino Acid Sufficiency and mTOR Regulate p70 S6 Kinase and eIF-4E BP1 through a Common Effector Mechanism. *J. Biol. Chem* 273, 14484–14494.
Harrington, L.S., Findlay, G.M., Gray, A., Tolkacheva, T., Wigfield, S., Rebholz, H., Barnett, J., Leslie, N.R., Cheng, S., Shepherd, P.R., Gout, I., Downes, C.P., Lamb, R.F., 2004. The TSC1-2 tumor suppressor controls insulin-PI3K signaling via regulation of IRS proteins. *J. Cell Biol*. 166, 213–223.
Hellström, P.M., Samuelsson, B., Al-Ani, A.N., Hedström, M., 2017. Normal gastric emptying time of a carbohydrate-rich drink in elderly patients with acute hip fracture: A pilot study. *BMC Anesthesiol*. 17, 23.
Higuchi, N., Kato, M., Tanaka, M., Miyazaki, M., Takao, S., Kohjima, M., Kotoh, K., Enjoji, M., Nakamuta, M., Takayanagi, R., 2011. Effects of insulin resistance and hepatic lipid accumulation on hepatic mRNA expression levels of apoB, MTP and L-FABP in non-alcoholic fatty liver disease. *Exp. Ther. Med*. 2, 1077–1081.
Holman, J.D., Tabb, D.L., Mallick, P., 2014. Employing ProteoWizard to convert raw mass spectrometry data. *Curr. Protoc. Bioinforma*. 17, 1–9.
Horowitz, M., O'Donovan, D., Jones, K.L., Feinle, C., Rayner, C.K., Samsom, M., 2002. Gastric emptying in diabetes: clinical significance and treatment. *Diabet. Med*. 19, 177–194.
Houghton, L.A., Mangnall, Y.F., Read, N.W., 1990. Effect of incorporating fat into a liquid test meal on the relation between intragastric distribution and gastric emptying in human volunteers. *Gut* 31, 1226–1229.
Hruby, A., Hu, F.B., 2015. The Epidemiology of Obesity: A Big Picture. *Pharmacoeconomics* 33, 673–689.
Huang, J., Manning, B., 2010. A complex interplay between Akt,TSC2 and the two mTOR complexes. Biochem. *Soc. Trans*. 37, 217–222.
Hudgins, L.C., Hellerstein, M., Seidman, C., Neese, R., Diakun, J., Hirsch, J., 1996. Human Fatty Acid Synthesis Is Stimulated by a Eucaloric Low Fat , High Carbohydrate Diet. *J. Clin. Invest*. 97, 2081–2091.
Hwahng, S.H., Ki, S.H., Bae, E.J., Kim, H.E., Kim, S.G., 2009. Role of adenosine

monophosphate-activated protein kinase-p70 ribosomal S6 kinase-1 pathway in repression of liver X receptor-alpha-dependent lipogenic gene induction and hepatic steatosis by a novel class of dithiolethiones. *Hepatology* 49, 1913–1925.
Iiboshi, Y., Papst, P.J., Kawasome, H., Hosoi, H., Abraham, R.T., Houghton, P.J., Terada, N., 1999. Amino Acid-dependent Control of p70 s6k. *J. Biol. Chem*. 274, 1092–1099.
Iizuka, K., Bruick, R.K., Liang, G., Horton, J.D., Uyeda, K., 2004. Deficiency of carbohydrate response element-binding protein (ChREBP) reduces lipogenesis as well as glycolysis. *Proc. Natl. Acad*. Sci. U. S. A. 101, 7281–6.
Iizuka, K., Horikawa, Y., 2008. ChREBP: A Glucose-activated Transcription Factor Involved in the Development of Metabolic Syndrome. *Endocr. J*. 55, 617–624.
Jewell, J.L., Kim, Y.C., Russell, R.C., Yu, F.X., Park, H.W., Plouffe, S.W., Tagliabracci, V.S., Guan, K.-L., 2015. Metabolism. Differential regulation ofmTORC1 by leucine and glutamine. *Science* 347, 194–198.
Jones, J.G., 2016. Hepatic glucose and lipid metabolism. *Diabetologia* 59, 1098–1103.
Jones, J.G., Solomon, M.A., Cole, S.M., Sherry, A.D., Malloy, C.R., 2001. An integrated (2)H and (13)C NMR study of gluconeogenesis and TCA cycle flux in humans. *Am. J. Physiol. Endocrinol*. Metab. 281, E848–E856.
Kabashima, T., Kawaguchi, T., Wadzinski, B.E., Uyeda, K., 2003. Xylulose 5-phosphate mediates glucose-induced lipogenesis by xylulose 5-phosphate-activated protein phosphatase in rat liver. *Proc. Natl. Acad. Sci.* 100, 5107–5112.
Kamagate, A., Qu, S., Perdomo, G., Su, D., Kim, D.H., Slusher, S., Meseck, M., Dong, H.H., 2008. FoxO1 mediates insulin-dependent regulation of hepatic VLDL production in mice. *J Clin Invest* 118, 2347–2364.
Kampmann, U., Christensen, B., Nielsen, T.S., Pedersen, S.B., Ørskov, L., Lund, S., Møller, N., Jessen, N., 2011. GLUT4 and UBC9 protein expression is reduced in muscle from type 2 diabetic patients with severe insulin resistance. *PLoS One* 6, e27854.
Karen M. Cunningham, Horowitz, M., Read, N.W., 1991. The effect of short-term dietary supplementation with glucose on gastric emptying in humans. *Br. J. Nutr.* 65, 15–19.
Kaur, J., 2014. A comprehensive review on metabolic syndrome. *Cardiol. Res. Pract*. 2014, 943162.
Kawaguchi, T., Osatomi, K., Yamashita, H., Kabashima, T., Uyeda, K., 2002. Mechanism for fatty acid “sparing” effect on glucose-induced transcription: Regulation of carbohydrate-responsive element-binding protein by AMP-activated protein kinase. *J. Biol. Chem*. 277, 3829–3835.
Kawaguchi, T., Takenoshita, M., Kabashima, T., Uyeda, K., 2001. Glucose and cAMP regulate the L-type pyruvate kinase gene by phosphorylation/dephosphorylation of the carbohydrate response element binding protein. *Proc. Natl. Acad. Sci*. 98, 13710–13715.
Kawano, Y., Cohen, D.E., 2013. Mechanisms of hepatic triglyceride accumulation in non-alcoholic fatty liver disease. *J. Gastroenterol*. 48, 434–441.
Kessner, D., Chambers, M., Burke, R., Agus, D., Mallick, P., 2008. ProteoWizard: Open source software for rapid proteomics tools development. Bioinformatics 24, 2534–2536.
Khallaf, H. Al, 2017. Isocitrate dehydrogenases in physiology and cancer: biochemical and molecular insight. *Cell Biosci*. 7, 37.
Kim, B., Li, J., Jang, C., Arany, Z., 2017. Glutamine fuels proliferation but not migration of endothelial cells. *EMBO J*. 36, 2321–2333.
Kim, M., Krawczyk, S.A., Doridot, L., Fowler, A.J., Wang, J.X., Trauger, S.A., Noh, H., Kang, H.J., Meissen, J.K., Blatnik, M., Kim, J.K., Lai, M., Herman, M.A., 2016. ChREBP regulates fructose-induced glucose production independently of insulin signaling. *J Clin Invest*. 126, 4372–4386.
Kirby, B.S., Crecelius, A.R., Voyles, W.F., Dinenno, F.A., 2012. Impaired skeletal muscle blood flow control with advancing age in humans: attenuated ATP release and local vasodilation during erythrocyte deoxygenation. *Circ. Res.* 111, 220–230.
Koh, H.J., Lee, S.M., Son, B.G., Lee, S.H., Ryoo, Z.Y., Chang, K.T., Park, J.W., Park, D.C., Song, B.J., Veech, R.L., Song, H., Huh, T.L., 2004. Cytosolic NADP+-dependent Isocitrate Dehydrogenase Plays a Key Role in Lipid Metabolism. *J. Biol. Chem*. 279,

39968–39974.
Kuhl, C., Tautenhahn, R., Böttcher, C., Larson, T.R., Neumann, S., 2012. CAMERA: An integrated strategy for compound spectra extraction and annotation of liquid chromatography/mass spectrometry data sets. *Anal. Chem*. 84, 283–289.
Kylin, E., 1923. On clinical determination of capillary tension. *J. Intern. Med*. 57, 566–586.
Lee, J.J., Lambert, J.E., Hovhannisyan, Y., Ramos-Roman, M.A., Trombold, J.R., Wagner, D.A., Parks, E.J., 2015. Palmitoleic acid is elevated in fatty liver disease and reflects hepatic lipogenesis. *Am. J. Clin. Nutr*. 101, 34–43.
Leiper, J.B., 2015. Fate of ingested fluids: factors affecting gastric emptying and intestinal absorption of beverages in humans. *Nutr. Rev.* 73, 57–72.
Li, S., Brown, M.S., Goldstein, J.L., 2010. Bifurcation of insulin signaling pathway in rat liver: mTORC1 required for stimulation of lipogenesis, but not inhibition of gluconeogenesis. *Proc. Natl. Acad. Sci.* 107, 3441–3446.
Li, X., Franke, A.A., 2011. Improved LC–MS Method for the Determination of Fatty Acids in Red Blood Cells by LC–Orbitrap MS. *Anal Chem* 83, 3192–3198.
Liang, R., Rimmelé, P., Bigarella, C.L., Yalcin, S., Ghaffari, S., 2016. Evidence for AKT-independent regulation of FOXO1 and FOXO3 in haematopoietic stem and progenitor cells. *Cell Cycle* 15, 861–867.
Libiseller, G., Dvorzak, M., Kleb, U., Gander, E., Eisenberg, T., Madeo, F., Neumann, S., Trausinger, G., Sinner, F., Pieber, T., Magnes, C., 2015. IPO: A tool for automated optimization of XCMS parameters. *BMC Bioinformatics* 16.
Liggi, S., Hinz, C., Hall, Z., Laura, M., Simone, S., John, P., Atzori, L., Griffin, J.L., 2018. KniMet : a pipeline for the processing of chromatography – mass spectrometry metabolomics data. *Metabolomics* 14, 52.
Lynch, C.J., 2001. Role of Leucine in the Regulation of mTOR by Amino Acids: Revelations from Structure – Activity Studies. *J. Nutr*. 131, 861S–865S.
Ma, L., Tsatsos, N.G., Towle, H.C., 2005. Direct role of ChREBP·Mlx in regulating hepatic glucose-responsive genes. *J. Biol. Chem*. 280, 12019–12027.
Maier, T., Jenni, S., Ban, N., 2006. Architecture of Mammalian Fatty Acid Synthase at 4.5 Å Resolution. *Science* 311, 1258–1263.
Maier, T., Leibundgut, M., Ban, N., 2008. The crystal structure of a mammalian fatty acid synthase. *Science* 321, 1315–1322.
Maljaars, P.W., Peters, H.P., Mela, D.J., Masclee, A.A., 2008. Ileal brake: A sensible food target for appetite control. A review. *Physiol. Behav*. 95, 271–281.
Marathe, C.S., Rayner, C.K., Jones, K.L., Horowitz, M., 2013. Relationships between gastric emptying, postprandial glycemia, and incretin hormones. *Diabetes Care* 36, 1396–1405.
Marchesini, G., Bugianesi, E., Forlani, G., Cerrelli, F., Lenzi, M., Manini, R., Natale, S., Vanni, E., Villanova, N., Melchionda, N., Rizzetto, M., 2003. Nonalcoholic fatty liver, steatohepatitis, and the metabolic syndrome. *Hepatology* 37, 917–923.
Marciani, L., Cox, E.F., Pritchard, S.E., Major, G., Hoad, C.L., Mellows, M., Hussein, M.O., Costigan, C., Fox, M., Gowland, P.A., Spiller, R.C., 2015. Additive effects of gastric volumes and macronutrient composition on the sensation of postprandial fullness in humans. *Eur. J. Clin. Nutr*. 69, 380–384.
Margolis, L.M., Rivas, D.A., Ezzyat, Y., Gaffney-Stomberg, E., Young, A.J., McClung, J.P., Fielding, R.A., Pasiakos, S.M., 2016. Calorie Restricted High Protein Diets Downregulate Lipogenesis and Lower Intrahepatic Triglyceride Concentrations in Male Rats. *Nutrients* 8, 571.
Marietta, M.A., Srere, P.A., Walsh, C., 1981. Stereochemical Outcome of Processing of Fluorinated Substrates by ATP Citrate Lyase and Malate Synthase. *Biochemistry* 20, 3719–3723.
Marques-lopes, I., Ansorena, D., Astiasaran, I., Forga, L., Martínez, J.A., 2001. Postprandial de novo lipogenesis and metabolic changes induced by a high-carbohydrate, low-fat meal in lean and overweight men. *Am J Clin Nutr* 73, 253–61.
Martín-Timón, I., Collantes, C.S., Galindo, A.S., del Cañizo-Gómez, F.J., 2014. Type 2 diabetes and cardiovascular disease: Have all risk factors the same strength? *World J. Diabetes* 5, 444–470.

Mclean, P., Greenbaum, A.L., 1970. The Effect of Raising the NAD+ Content on the Pathways of Carbohydrate Metabolism and Lipogenesis in Rat Liver. *Eur. J. Biochem.* 15, 179–190.
Metallo, C.M., Gameiro, P.A., Bell, E.L., Mattaini, K.R., Yang, J., Hiller, K., Jewell, C.M., Johnson, Z.R., Irvine, D.J., Guarente, L., Kelleher, J.K., Heiden, M.G. Vander, Iliopoulos, O., Stephanopoulos, G., 2011. Reductive glutamine metabolism by IDH1 mediates lipogenesis under hypoxia. *Nature* 481, 380–384.
Mikkelsen, H.B., 2010. Interstitial cells of Cajal, macrophages and mast cells in the gut musculature: Morphology, distribution, spatial and possible functional interactions. *J. Cell. Mol. Med*. 14, 818–832.
Mikkelsen, J., Hojrup, P., Rasmussen, M.M., Roepstorff, P., Knudsen, J., 1985. Amino acid sequence around the active-site serine residue in the acyltransferase domain of goat mammary fatty acid synthetase. *Biochem. J.* 227, 21–27.
Misra, A., Khurana, L., 2008. Obesity and the Metabolic Syndrome in Developing Countries. *J Clin Endocrinol Metab* 93, 9–30.
Moore, J.B., Gunn, P.J., Fielding, B.A., 2014. The role of dietary sugars and de novo lipogenesis in non-alcoholic fatty liver disease. *Nutrients* 6, 5679–5703.
Mushref, M. Al, Srinivasan, S., 2013. Effect of high fat-diet and obesity on gastrointestinal motility. *Ann. Transl. Med*. 1, 14.
Muz, B., Azab, A.K., 2015. The role of hypoxia in cancer progression , angiogenesis, metastasis, and resistance to therapy. Hypoxia 3, 83–92.
Nehlig, A., 2004. Brain uptake and metabolism of ketone bodies in animal models. *Prostaglandins Leukot. Essent. Fat. Acids* 70, 265–275.
Nicklin, P., Bergman, P., Zhang, B., Triantafellow, E., Wang, H., Nyfeler, B., Yang, H., Hild, M., Kung, C., Wilson, C., Myer, V.E., MacKeigan, J.P., Porter, J.A., Wang, Y.K., Cantley, L.C., Finan, P.M., Murphy, L.O., 2009. Bidirectional Transport of Amino Acids Regulates mTOR and Autophagy. *Cell* 136, 521–534.
Nieminen, P., Rouvinen-Watt, K., Harris, L., Huitu, O., Henttonen, H., Mustonen, A., 2016. De novo lipogenesis is suppressed during fasting but upregulated at population decline in cyclic voles. *Exp. Biol. Med.* 241, 882–887.
Nishimura, M., Uyeda, K., 1995. Purification and characterization of a novel xylulose 5-phosphate- activated protein phosphatase catalyzing dephosphorylation of fructose- 6-phosphate,2-kinase:fructose-2,6-bisphosphatase. *J. Biol. Chem.* 270, 26341–26346.
Ordog, T., Ward, S.M., Sanders, K.M., 1999. Interstitial cells of Cajal generate electricial slow waves in the murine stomach. *J. Physiol*. 518, 257–269.
Otero, Y.F., Stafford, J.M., McGuinness, O.P., 2014. Pathway-selective insulin resistance and metabolic disease: The importance of nutrient flux. *J. Biol. Chem*. 289, 20462–20469.
Ou, J., Tu, H., Shan, B., Luk, A., Debose-boyd, R.A., Bashmakov, Y., Goldstein, J.L., Brown, M.S., 2001. Unsaturated fatty acids inhibit transcription of the sterol regulatory element-binding protein-1c (SREBP-1c) gene by antagonizing ligand- dependent activation of the LXR. *PNAS* 98, 6027–6032.
Paglialunga, S., Dehn, C.A., 2016. Clinical assessment of hepatic de novo lipogenesis in non-alcoholic fatty liver disease. *Lipids Health Dis*. 15, 1–10.
Pais, R., Pascale, A., Fedchuck, L., Charlotte, F., Poynard, T., Ratziu, V., 2011. Progression from isolated steatosis to steatohepatitis and fibrosis in nonalcoholic fatty liver disease. *Clin. Res. Hepatol. Gastroenterol.* 35, 23–28.
Pan, M., Liang, J.S., Fisher, E.A., Ginsberg, H.N., 2002. The late addition of core lipids to nascent apolipoprotein B100, resulting in the assembly and secretion of triglyceride-rich lipoproteins, is independent of both microsomal triglyceride transfer protein activity and new triglyceride synthesis. *J. Biol. Chem*. 277, 4413–4421.
Parks, E.J., Skokan, L.E., Timlin, M.T., Dingfelder, C.S., 2008. Dietary Sugars Stimulate Fatty Acid Synthesis in Adults. *J. Nutr*. 138, 1039–1046.
Paschos, P., Paletas, K., 2009. Non alcoholic fatty liver disease and metabolic syndrome. *Hippokratia* 13, 9–19.
Patti, M.E., Brambilla, E., Luzi, L., Landaker, E.J., Kahn, C.R., 1998. Bidirectional modulation

of insulin action by amino acids. *J. Clin. Invest.* 101, 1519–1529.
Peterson, T.R., Sengupta, S.S., Harris, T.E., Carmack, A.E., Kang, S.A., Balderas, E., Guertin, D.A., Madden, K.L., Carpenter, A.E., Finck, B.N., Sabatini, D.M., 2011. mTOR Complex 1 Regulates Lipin 1 Localization to Control the SREBP Pathway. *Cell* 146, 408–420.
Phillips, L.K., Deane, A.M., Jones, K.L., Rayner, C.K., Horowitz, M., 2015. Gastric emptying and glycaemia in health and diabetes mellitus. *Nat. Rev. Endocrinol.* 11, 112–128.
Popkin, B.M., 2006. Global nutrition dynamics: the world is shifting rapidly toward a diet linked with noncommunicable diseases. *Am J Clin Nutr* 84, 289–98.
Qin, W., Sundaram, M., Wang, Y., Zhou, H., Zhong, S., Chang, C.C., Manhas, S., Yao, E.F., Parks, R.J., McFie, P.J., Stone, S.J., Jiang, Z.G., Wang, C., Figeys, D., Jia, W., Yao, Z., 2011. results in impaired assembly and secretion of triacylglycerol-rich very low density lipoproteins: evidence that ApoC-III plays a major role in the formation of lipid precursors within the microsomal lumen. *J. Biol. Chem.* 286, 27769–27780.
R Core Team, 2017. R: A language and environment for statistical computing. R Foundation for Statistical Computing.
Raymond, M., Li, P., Mangin, J., Huntsman, M., Gallo, V., 2011. Chronic Perinatal Hypoxia Reduces Glutamate – Aspartate Transporter Function in Astrocytes through the Janus Kinase / Signal Transducer and Activator of Transcription Pathway. *J. Neurosci.* 31, 17864–17871.
Reaven, G.M., 2001. Syndrome X: A Short History. *Ochsner J.* 3, 124–5.
Rebsamen, M., Pochini, L., Stasyk, T., De Araújo, M.E.G., Galluccio, M., Kandasamy, R.K., Snijder, B., Fauster, A., Rudashevskaya, E.L., Bruckner, M., Scorzoni, S., Filipek, P.A., Huber, K.V.M., Bigenzahn, J.W., Heinz, L.X., Kraft, C., Bennett, K.L., Indiveri, C., Huber, L.A., Superti-Furga, G., 2015. SLC38A9 is a component of the lysosomal amino acid sensing machinery that controls mTORC1. *Nature* 519, 477–481.
Reddy, S., Ramsubeik, K., Vega, K.J., Federico, J., Palacio, C., 2010. Do HbA1C Levels Correlate With Delayed Gastric Emptying in Diabetic Patients? *J. Neurogastroenterol. Motil.* 16, 414–417.
Reddymasu, S.C., McCallum, R.W., 2010. Small Intestinal Bacterial Overgrowth in Gastroparesis. *J. Clin. Gastroenterol.* 44, e8–e13.
Ress, C., Kaser, S., 2016. Mechanisms of intrahepatic triglyceride accumulation. *World J. Gastroenterol.* 22, 1664–1673.
Rhee, E.P., Cheng, S., Larson, M.G., Walford, G.A., Lewis, G.D., McCabe, E., Yang, E., Farrell, L., Fox, C.S., O'Donnell, C.J., Carr, S.A., Vasan, R.S., Florez, J.C., Clish, C.B., Wang, T.J., Gerszten, R.E., 2011. Lipid profiling identifies a triacylglycerol signature of insulin resistance and improves diabetes prediction in humans. *J. Clin. Invest.* 121, 1402–1411.
Ronveaux, C.C., Tome, D., Raybould, H.E., 2015. Glucagon-Like Peptide 1 Interacts with Ghrelin and Leptin to Regulate Glucose Metabolism and Food Intake through Vagal Afferent Neuron Signaling. *J. Nutr*. 145, 672–680.
Rui, L., 2014. Energy Metabolism in the Liver. Compr. Physiol. 4, 177–197.
Rustaeus, S., Lindberg, K., Stillemark, P., Claesson, C., Asp, L., Larsson, T., Bore, J., Olofsson, S.O., 1999. Assembly of Very Low Density Lipoprotein: A Two-Step Process of Apolipoprotein B Core Lipidation. *J. Nutr*. 129, 467S–472S.
Samsom, M., Bharucha, A., Gerich, J.E., Herrmann, K., Limmer, J., Linke, R., Maggs, D., Schirra, J., Vella, A., Worle, H.J., Goke, B., 2009. Diabetes mellitus and gastric emptying: questions and issues in clinical practice. *Diabetes Metab. Res. Rev*. 25, 502–514.
Samson, C.E., Galia, A.L.B., Llave, K.I.C., Zacarias, M.B., Mercado-Asis, L.B., 2012. Postprandial Peaking and Plateauing of Triglycerides and VLDL in Patients with Underlying Cardiovascular Diseases Despite Treatment. *Int J Endocrinol Metab* 10, 587–593.
Samuel, V.T., Petersen, K.F., Shulman, G.I., 2010. Lipid-induced insulin resistance: unravelling the mechanism. *Lancet* 375, 2267–2277.
Sanders, F.W.B., Acharjee, A., Walker, C., Marney, L., Roberts, L.D., Imamura, F., Jenkins,

B., Case, J., Ray, S., Virtue, S., Vidal-puig, A., Kuh, D., Hardy, R., Allison, M., Forouhi, N., Murray, A.J., Wareham, N., Vacca, M., Koulman, A., Griffin, J.L., 2018. Hepatic steatosis risk is partly driven by increased de novo lipogenesis following carbohydrate consumption. *Genome Biol.* 19, 79.
Sanders, F.W.B., Griffin, J.L., 2016. De novo lipogenesis in the liver in health and disease: More than just a shunting yard for glucose. *Biol. Rev.* 91, 452–468.
Sarbassov, D.D., Ali, S.M., Sabatini, D.M., 2005. Growing roles for the mTOR pathway. *Curr. Opin. Cell Biol*. 17, 596–603.
Sartorius, B., Sartorius, K., Aldous, C., Madiba, T.E., Stefan, C., Noakes, T., 2016. Carbohydrate intake, obesity, metabolic syndrome and cancer risk? A two-part systematic review and meta-analysis protocol to estimate attributability. *BMJ Open* 6, 1–6.
Saxton, R.A., Sabatini, D.M., 2017. mTOR Signaling in Growth, Metabolism, and Disease. *Cell* 168, 960–976.
Schwarz, J., Linfoot, P., Dare, D., Aghajanian, K., 2003. Hepatic de novo lipogenesis in normoinsulinemic and hyperinsulinemic subjects consuming high-fat, low-carbohydrate and low-fat, high-carbohydrate isoenergetic diets. *Am J Clin Nutr* 77, 43–50.
Schwarz, J., Tomé, D., Baars, A., Hooiveld, G.J., Müller, M., 2012. Dietary Protein Affects Gene Expression and Prevents Lipid Accumulation in the Liver in Mice. *PLoS One* 7, e47303.
Semple, R.K., Sleigh, A., Murgatroyd, P.R., Adams, C.A., Bluck, L., Jackson, S., Vottero, A., Kanabar, D., Charlton-Menys, V., Durrington, P., Soos, M.A., Carpenter, T.A., Lomas, D.J., Cochran, E.K., Gorden, P., O'Rahilly, S., Savage, D.B., 2009. Postreceptor insulin resistance contributes to human dyslipidemia and hepatic steatosis. *J. Clin. Invest*. 119, 315–322.
Seyedsadjadi, N., Berg, J., Bilgin, A.A., Braidy, N., Salonikas, C., Grant, R., 2018. High protein intake is associated with low plasma NAD+ levels in a healthy human cohort. *PLoS One* 13, e0201968.
Shaw, L.M., 2011. The insulin receptor substrate (IRS) proteins: At the intersection of metabolism and cancer. *Cell Cycle* 10, 1750–1756.
Shi, L., Tu, B.P., 2015. Acetyl-CoA and the Regulation of Metabolism: Mechanisms and Consequences. *Curr. Opin. Cell Biol*. 33, 125–131.
Shi, Y., Cheng, D., 2009. Beyond triglyceride synthesis: the dynamic functional roles of MGAT and DGAT enzymes in energy metabolism. *AJP Endocrinol*. Metab. 297, E10–E18.
Smith, C.A., Want, E.J., O'Maille, G., Abagyan, R., Siuzdak, G., 2006. XCMS: Processing mass spectrometry data for metabolite profiling using nonlinear peak alignment, matching, and identification. *Anal. Chem*. 78, 779–787.
Smith, S., Witkowski, A., Joshi, A.K., 2003. Structural and functional organization of the animal fatty acid synthase. *Prog. Lipid Res*. 42, 289–317.
Snel, M., Jonker, J.T., Schoones, J., Lamb, H., De Roos, A., Pijl, H., Smit, J.W., Meinders, A.E., Jazet, I.M., 2012. Ectopic fat and insulin resistance: Pathophysiology and effect of diet and lifestyle interventions. *Int. J. Endocrinol*. 2012, 1–18.
Sparks, J.D., Dongb, H.H., 2009. FoxO1 and hepatic lipid metabolism. *Curr Opin Lipidol* 20, 217–226.
Srinivasan, S., 2016. Macrophages: The Missing Link in Diabetic Gastroparesis? *Cell. Mol. Gastroenterol. Hepatol.* 2, 5–6.
Stegemann, C., Pechlaner, R., Willeit, P., Langley, S.R., Mangino, M., Mayr, U., Menni, C., Moayyeri, A., Santer, P., Rungger, G., Spector, T.D., Willeit, J., Kiechl, S., Mayr, M., 2014. Lipidomics profiling and risk of cardiovascular disease in the prospective population-based bruneck study. *Circulation* 129, 1821–1831.
Strable, M.S., Ntambi, J.M., 2010. Genetic control of de novo lipogenesis: role in diet-induced obesity. *Crit. Rev. Biochem. Mol. Biol*. 45, 199–214.
Sud, M., Fahy, E., Subramaniam, S., 2012. Template-based combinatorial enumeration of virtual compound libraries for lipids. *J. Cheminform*. 25, 23.
Sundaram, M., Yao, Z., 2010. Recent progress in understanding protein and lipid factors

affecting hepatic VLDL assembly and secretion. *Nutr. Metab*. 7, 35.
Swift, L.L., 1996. Role of the Golgi apparatus in the phosphorylation of apolipoprotein B. *J. Biol. Chem.* 271, 31491–31495.
Taniguchi, C.M., Kondo, T., Sajan, M., Luo, J., Bronson, R., Asano, T., Farese, R., Cantley, L.C., Kahn, C.R., 2006. Divergent regulation of hepatic glucose and lipid metabolism by phosphoinositide 3-kinase via Akt and PKCλ/ζ. *Cell Metab*. 3, 343–353.
Tappy, L., Lê, K.A., 2012. Does fructose consumption contribute to non-alcoholic fatty liver disease? *Clin. Res. Hepatol. Gastroenterol*. 36, 554–560.
Tato, I., Bartrons, R., Ventura, F., Rosa, J.L., 2011. Amino Acids Activate Mammalian Target of Rapamycin Complex 2 (mTORC2) via PI3K/Akt Signaling. *J. Biol. Chem*. 286, 6128–6142.
Tennant D.R., 2018.Review of Glutamate Intake from Both Food Additive and Non-Additive Sources in the European Union. *Ann Nutr Metab*. 73(suppl 5):21-28.
Timlin, M.T., Parks, E.J., 2005. Temporal pattern of de novo lipogenesis in the postprandial state in healthy men. *Am. J. Clin. Nutr*. 81, 35–42.
Titchenell, P.M., Quinn, W.J., Lu, M., Chu, Q., Lu, W., Li, C., Chen, H., Monks, B.R., Chen, J., Rabinowitz, J.D., Birnbaum, M.J., 2016. Direct Hepatocyte Insulin Signaling Is Required for Lipogenesis but Is Dispensable for the Suppression of Glucose Production. *Cell Metab*. 23, 1154–1166.
Tong, X., Zhao, F., Mancuso, A., Gruber, J.J., Thompson, C.B., 2009. The glucose-responsive transcription factor ChREBP contributes to glucose-dependent anabolic synthesis and cell proliferation. *PNAS* 106, 21660–21665.
Torchon, E., Ray, R., Hulver, M.W., McMillan, R.P., Voy, B.H., 2017. Fasting rapidly increases fatty acid oxidation in white adipose tissue of young broiler chickens. *Adipocyte* 6, 33–39.
Towle, H.C., Kaytor, E.N., Shih, H.M., 1997. Regulation of the expression of lipogenic enzyme gene. *Annu. Rev. Nutr*. 17, 405–433.
Travers, M.T., Cambot, M., Kennedy, H.T., Lenoir, G.M., Barber, M.C., Joulin, V., 2005. Asymmetric expression of transcripts derived from the shared promoter between the divergently oriented ACACA and TADA2L genes. *Genomics* 85, 71–84.
Tremblay, F., Brûlé, S., Hee Um, S., L, Y., Masuda, K., Roden, M., Sun, X.J., Krebs, M., Polakiewicz, R.D., Thomas, G., Marette, A., 2007. Identification of IRS-1 Ser-1101 as a target of S6K1 in nutrient- and obesity-induced insulin resistance. *PNAS* 104, 14056–14061.
Tremblay, F., Krebs, M., Dombrowski, L., Brehm, A., Bernroider, E., Roth, E., Nowotny, P., Waldhäusl, W., Marette, A., Roden, M., 2005. Overactivation of S6 Kinase 1 as a Cause of Human Insulin Resistance During Increased Amino Acid Availability. *Diabetes* 54, 2674–2684.
Tremblay, F., Marette, A., 2001. Amino acids and insulin signaling via the mTOR/p70 S6 kinase pathway: a negative feedback mechanism leading to insulin resistance in skeletal muscle cells. *J. Biol. Chem*. 276, 38052–38060.
United Kigndom Department of Health, 1991. Dietary reference values for food energy and nutrients for the United Kigndom. Report of the Panel on Dietary Reference Values of the Committee on Medical Aspects of Food Policy. *Rep Health Soc Subj (Lond)*. 41: 1-210.
Varlamov, O., Bethea, C.L., Roberts, C.T., 2015. Sex-specific differences in lipid and glucose metabolism. *Front. Endocrinol. (Lausanne)*. 5, 241.
Verges, B., 2015. Pathophysiology of diabetic dyslipidaemia: where are we? *Diabetologia* 58, 886–899.
Vinod, P.K.U., Venkatesh, K.V., 2009. Quantification of the effect of amino acids on an integrated mTOR and insulin signaling pathway. *Mol. BioSyst*. 5, 1163–1173.
West, G., Rodia, C., Li, D., Johnson, Z., Dong, H., Kohan, A.B., 2017. Key differences between apoC-III regulation and expression in intestine and liver. *Biochem. Biophys. Res. Commun*. 491, 747–753.
Whereat, A.F., Hull, F.E., Orishimo, M.W., Rabinowitz, J.L., 1967. The Role of Succinate in the Regulation og Fatty Acis Synthesis by Heart Mitochondria. *J. Biol. Chem*. 242,

4023–4028.
Wilcox, G., 2005. Insulin and insulin resistance. *Clin. Biochem. Rev*. 26, 19–39.
Williams, E.K., Chang, R.B., Strochlic, D.E., Umans, B.D., Lowell, B.B., Liberles, S.D., 2016. Sensory neurons that detect stretch and nutrients in the digestive system. *Cell* 166, 209–221.
Williams, N.C., O'Neill, L.A.J., 2018. A role for the krebs cycle intermediate citrate in metabolic reprogramming in innate immunity and inflammation. Front. Immunol. 9, 141.
Wise, D.R., Ward, P.S., Shay, J.E., Cross, J.R., Gruber, J.J., Sachdeva, U.M., Platt, J.M., DeMatteo, R.G., Simon, M.C., Thompson, C.B., 2011. Hypoxia promotes isocitrate dehydrogenase- dependent carboxylation of α -ketoglutarate to citrate to support cell growth and viability. *PNAS* 108, 19611–19616.
Witkowski, A., Joshi, A.K., Smith, S., 1997. Characterization of the interthiol acyltransferase reaction catalyzed by the β-ketoacyl synthase domain of the animal fatty acid synthase. *Biochemistry* 36, 16338–16344.
Wolfson, R.L., Chantranupong, L., Saxton, R.A., Shen, K., Scaria, S.M., Cantor, J.R., Sabatini, D.M., 2016. Sestrin2 is a leucine sensor for the mTORC1 pathway. *Science*. 351, 43–48.
Wong, G., Barlow, C.K., Weir, J.M., Jowett, J.B., Magliano, D.J., Zimmet, P., Shaw, J., Meikle, P.J., 2013. Inclusion of Plasma Lipid Species Improves Classification of Individuals at Risk of Type 2 Diabetes. *PLoS One* 8, e76577.
Wu, Y., Ding, Y., Tanaka, Y., Zhang, W., 2014. Risk factors contributing to type 2 diabetes and recent advances in the treatment and prevention. *Int. J. Med. Sci*. 11, 1185–1200.
Würtz, P., Mäkinen, V.-P., Soininen, P., Kangas, A.J., Tukiainen, T., Kettunen, J., Savolainen, M.J., Tammelin, T., Viikari, J.S., Rönnemaa, T., Kähönen, M., Lehtimäki, T., Ripatti, S., Raitakari, O.T., Järvelin, M.-R., Ala-Korpela, M., 2012. Metabolic Signatures of Insulin Resistance in 7,098 Young Adults. *Diabetes* 61, 1371–1380.
Xiao, F., Yu, J., Guo, Y., Deng, J., Li, K., Du, Y., Chen, S., Zhu, J., Sheng, H., Guo, F., 2014. Effects of individual branched-chain amino acids deprivation on insulin sensitivity and glucose metabolism in mice. *Metabolism* 63, 841–850.
Xing, J., Chen, J.D.Z., 2004. Alterations of gastrointestinal motility in obesity. *Obes. Res.* 12, 1723–1732.
Xu, X., So, J.S., Park, J.G., Lee, A.H., 2013. Transcriptional control of hepatic lipid metabolism by SREBP and ChREBP. *Semin. Liver Dis.* 33, 301–311.
Yagihashi, S., Mizukami, H., Sugimoto, K., 2011. Mechanism of diabetic neuropathy: Where are we now and where to go? *J. Diabetes Investig*. 2, 18–32.
Yao, Y., Jones, E., Inoki, K., 2017. Lysosomal regulation of mTORC1 by amino acids in mammalian cells. *Biomolecules* 7, 51.
Yecies, J.L., Zhang, H.H., Menon, S., Liu, S., Yecies, D., Lipovsky, A.I., Gorgun, C., Kwiatkowski, D.J., Hotamisligil, G.S., Lee, C.-H., Manning, B.D., 2011. Akt stimulates hepatic SREBP1c and lipogenesis through parallel mTORC1-dependent and independent pathways. *Cell Metab*. 14, 21–32.
Yin, C., Qie, S., Sang, N., 2012. Carbon source metabolism and its regulation in cancer cells. *Crit. Rev. Eukaryot. Gene Expr.* 22, 17–35.
Yoo, H., Antoniewicz, M.R., Stephanopoulos, G., Kelleher, J.K., 2008. Quantifying reductive carboxylation flux of glutamine to lipid in a brown adipocyte cell line. *J. Biol. Chem*. 283, 20621–20627.
Yoon, M.S., 2016. The Emerging Role of Branched-Chain Amino Acids in Insulin Resistance and Metabolism. *Nutrients* 8, E405.
Yoon, M.S., Choi, C.S., 2016. The role of amino acid-induced mammalian target of rapamycin complex 1 (mTORC1) signaling in insulin resistance. *Exp. Mol. Med*. 48, e201-6.
Yoshikawa, T., Shimano, H., Amemiya-kudo, M., Yahagi, N., Hasty, A.H., Matsuzaka, T., Okazaki, H., Tamura, Y., Iizuka, Y., Ohashi, K.E., Osuga, J.I., Harada, K., Gotoda, T., Kimura, S., Ishibashi, S., Yamada, N., 2001. Identification of Liver X Receptor-Retinoid X Receptor as an Activator of the Sterol Regulatory Element-Binding Protein 1c Gene Promoter. *Mol. Cell. Biol.* 21, 2991–3000.

Yu, Y., Yoon, S.-O., Poulogiannis, G., Yang, Q., Ma, X.M., Villen, J., Kubica, N., Hoffman, G.R., Cantley, L.C., Gygi, S.P., Blenis, J., 2011. Phosphoproteomic Analysis Identifies Grb10 as an mTORC1 Substrate That Negatively Regulates Insulin Signaling. *Science*. 332, 1322–1326.

Zhou, Y., Yu, S., Cai, C., Zhong, L., Yu, H., Shen, W., 2018. LXRα participates in the mTOR/S6K1/SREBP-1c signaling pathway during sodium palmitate-induced lipogenesis in HepG2 cells. *Nutr. Metab*. 15, 31.

Zoncu, R., Bar-Peled, L., Efeyan, A., Wang, S., Sancak, Y., Sabatini, D.M., 2011. mTORC1 Senses Lysosomal Amino Acids Through an Inside-Out Mechanism That Requires the Vacuolar H+-ATPase. *Science*. 334, 678–683.

Publications

Published papers

Charidemou E., Ashmore T., Griffin J.L., 2017. The use of stable isotopes in human pathophysiology. Int J Biochem Cell Biol. 93, 102-109.

Submitted papers

Charidemou E., Ashmore T., Li X., McNally B.D., West J.A., Liggi S., Harvey M., Orford E., Griffin J.L, 2018. High protein feeding induced de novo lipogenesis in healthy humans. JCI Insight. Accepted.

In preparation

The effects of changing the liquid/solid content of an isoenergetic test meal on gastric emptying. Li et al.

Born to think or to run? The fate of ketones as a metabolic fuel and their effects on human performance. Cox et al.

Rora is a complex regulator of immune response. Haim-Vilmovsky et al.

Metabolic remodelling in liver regeneration and carcinogenesis. Hall et al.

Conferences

Oral presentation at the 14th Annual Conference of the Metabolomics Society, Seattle 2018

Poster presentation at the 39th European Society for Clinical Nutrition and Metabolism (ESPEN) Congress, The Hague 2017

2nd Metabolomics Sardinian Scientific School - Won a Conference Poster Competition and invited to present and write an article for The International Journal of Biochemistry & Cell Biology, Sardinia 2016

Poster presentation at the 12th Annual Conference of the Metabolomics Society, Dublin 2016

Appendices

Appendix I

A) Sample size calculation

To calculate the sample size of the human study, the following equation was used:

$$n = 2\left[\frac{(Z\alpha - Z\pi)^2}{(\frac{\mu ac - \mu con}{\sigma})^2}\right]$$

Z comes from the standardised normal distribution table. The type I error (significance level) was set at 5%, $Z\alpha = 1.645$. The type II error was set at $\beta = 20\%$, resulting to 80% study power (π), therefore $Z\pi = -0.842$. The effect size of the control group (μcon) was set at 100% and a 40% difference between groups (in gastric emptying rates and lipid levels), resulting to $\mu_{ac} = 140\%$. The expected standard deviation was set at $\sigma = 35\%$. This gave rise to n = 9/group.

B) Exclusion and inclusion criteria of the human study

Exclusion criteria	**Inclusion criteria**
Smokers	Non-smoker males
BMI ≤18.5 and ≥ 27.5kg/m^2	BMI 18.5-27.5
Allergy or intolerance to any component of test meals	No allergy or intolerance to any component of the meals
Known history of cardiovascular disease	No history of cardiovascular disease
Impaired fasting glucose (fasting glucose ≥ 6.1 mmol/L)	Fasting glucose ≤ 6.1 mmol/L
Cholesterol ≥ 7.7 mmol/L	Cholesterol ≤ 7.7 mmol/L
Triacylglycerides ≥ 2.3 mmol/L	Triacylglycerides ≤ 2.3 mmol/L
Weight reduction medicines, anti-dyslipidemic agents	No weight reduction medicines or anti-dyslipidemic agents
Chronic, acute or active metabolic (including type 1 and type 2 diabetes mellitus) and inflammatory condition, haematological disorders, or any other systemic illness of renal, hepatic or gastrointestinal origin	No chronic, acute or active metabolic (including type 1 and type 2 diabetes mellitus) and inflammatory condition, haematological disorders, or any other systemic illness of renal, hepatic or gastrointestinal origin
Acute and chronic conditions affecting gastrointestinal motility	No acute and chronic conditions affecting gastrointestinal motility
Fat maldigestion and malabsorption	No fat maldigestion and malabsorption
The use of medication known to affect gastrointestinal motility (such as antiemetic, cathartics, antidiarrheal, anticholinergic and narcotic medication)	No use of medication known to affect gastrointestinal motility (such as antiemetic, cathartics, antidiarrheal, anticholinergic and narcotic medication)
History of mental illness	No history of mental illness
History of substance abuse or alcoholism	No history of substance abuse or alcoholism
Current self-reported weekly alcohol intake exceeding 14 units per week	Current self-reported weekly alcohol intake less than 14 units per week

Appendix II

A) Table 1. Amount of foods used to prepare meals.

	Control (C)	High Fat (HF)	High Protein (HP)	Control with Bread (CB)	High Carbohydrate (HC)
Orange Juice (g)	556	271	414	367	681
Whole egg (g)	100	100	50	100	50
Egg white (g)	26	30	100	0	64
Butter (g)	13	26	15	12	9
Soy protein powder (g)	0	0	21	0	0
White bread (g)	0	0	0	41	0

B) Method of food preparation

In order to be able to prepare the meals a food and safety course was required beforehand. An apron and gloves were worn, and the hair was tied up. The ingredients (Table 1) were measured on the black salter scales. 100 µl ^{13}C-octanoic acid were added straight into the egg yolk when raw. For the High Protein meal, the soy protein powder was mixed with the eggs. The butter was first melted in the pan (on highest heat) and subsequently the eggs were added. The eggs were then scrambled. The meal was served on a tray.

C) Table 2. Fatty acid composition of meals. The fatty acid compositions were calculated using the FoodWorks database (FoodWorks, 2015), which performed a nutrient analysis of the meals.

Fatty acid (grams)	Control (C)	High Fat (HF)	High Protein (HP)	Control with Bread (CB)	High Carbohydrate (HC)
FA 4:0	0.342	0.684	0.395	0.316	0.237
FA 6:0	0.202	0.405	0.234	0.187	0.140
FA 8:0	0.120	0.238	0.137	0.111	0.083
FA 10:0	0.267	0.531	0.306	0.246	0.184
FA 12:0	0.298	0.594	0.343	0.276	0.206
FA 13:0	0.000	0.000	0.000	0.000	0.000
FA 14:0	1.095	2.155	1.241	1.013	0.751
FA 15:0	0.005	0.005	0.002	0.005	0.002
FA 16:0	4.994	7.763	4.308	4.936	3.030
FA 17:0	0.016	0.016	0.008	0.016	0.008
FA 18:0	2.062	3.340	1.866	2.102	1.277
FA 20:0	0.009	0.009	0.005	0.009	0.005
FA 22:0	0.011	0.011	0.006	0.011	0.006
FA 24:0	0.002	0.002	0.001	0.002	0.001
FA 14:1	0.009	0.009	0.005	0.009	0.005
FA 15:1	0.000	0.000	0.000	0.000	0.000
FA 16:1	0.534	0.770	0.421	0.516	0.312
FA 17:1	0.000	0.000	0.000	0.000	0.000
FA 18:1	6.125	8.777	4.796	5.978	3.572
FA 20:1	0.027	0.027	0.014	0.027	0.014
FA 22:1	0.002	0.002	0.001	0.002	0.001
FA 18:2	1.386	1.624	0.849	1.866	0.739
FA 20:2	0.000	0.000	0.000	0.000	0.000
FA 18:3	0.187	0.341	0.194	0.176	0.123
FA 18:4	0.000	0.000	0.000	0.000	0.000
FA 20:4	0.141	0.141	0.070	0.141	0.070
FA 20:5	0.005	0.005	0.002	0.005	0.002
FA 22:5	0.000	0.000	0.000	0.000	0.000
FA 22:6	0.036	0.036	0.018	0.036	0.018

D) Table 3. Amino acid composition of meals. The amino acid compositions were calculated using the FoodWorks database (FoodWorks, 2015), which performed a nutrient analysis of the meals.

Amino acid (grams)	Control (C)	High Fat (HF)	High Protein (HP)	Control with Bread (CB)	High carbohydrate (HC
Alanine	0.858	0.886	1.738	0.807	0.740
Arginine	0.903	0.930	2.317	0.869	0.744
Aspartic acid	1.541	1.592	3.807	1.410	1.318
Cystine	0.363	0.375	0.650	0.358	0.321
Glutamic acid	2.020	2.099	5.685	2.668	1.727
Glycine	0.519	0.536	1.339	0.534	0.448
Histidine	0.360	0.372	0.850	0.366	0.301
Isoleucine	0.843	0.873	1.824	0.810	0.726
Leucine	1.308	1.354	2.924	1.294	1.109
Lysine	1.092	1.130	2.308	0.989	0.913
Methionine	0.487	0.505	0.790	0.449	0.428
Phenylalanine	0.829	0.859	1.898	0.821	0.729
Proline	0.615	0.642	1.594	0.845	0.518
Serine	1.125	1.160	2.144	1.086	0.934
Threonine	0.729	0.754	1.477	0.697	0.610
Tryptophan	0.188	0.194	0.439	0.190	0.161
Tyrosine	0.621	0.642	1.363	0.604	0.520
Valine	0.943	0.977	1.983	0.906	0.814

E) Table 4. Comparison of meal compositions (of this thesis) with DRVs for UK adults and the literature. There is no fixed definition of what is High Fat, High Carbohydrate and High protein meal. These compositions were chosen based on the literature and DRVs. All the meals used were isocaloric, therefore the macronutrient compositions were adjusted accordingly to maintain the same caloric content.

Source	Control (with or without bread)			High Fat			High Carbohydrate			High Protein		
%	CHO	FAT	PRO	CHO	FAT	PRO	CHO	FAT	PRO	CHO	FAT	PRO
this thesis	45	40	15	24	62	14	60	26	14	35	33	32
DRVs[a]	50	35	15[b]									
DRVs[c]	45-60	20-35	~12[d]									
Castiglione et al				32	55	13	62	25	13			
Hudgins et al				45	40	15	75	10	15			
Margolis et al										46	22	32

[a] United Kingdom Department of Health, 1991
[b] 0.75 g of protein per kilogram bodyweight per day for adults or 56 g/day reference nutrient intake (RNI)
[c] EFSA, 2017
[d] 0.83 g of protein per kilogram bodyweight per day for adults as the population reference intake (PRI)

Appendix III

Quality assurance

Periodical injections of QC samples, obtained as pool of all samples in the study, were used for quality control and assurance for each metabolic feature detected, following the procedure designed by Dunn and co-workers (Dunn et al., 2011). First, they were used for intra batch processing, namely normalisation and removal of all features present in less than 50% of the QCs and having a relative standard deviation (RSD) or coefficient of variation (CV) higher than 20%. This step corrects for signal variation across the run and removes peaks with low repeatability. Second, a quality assurance (QA) step was performed on the merged dataset containing both batches, to remove features poorly repeatable in terms of intensity, *m/z* and retention time. This step consisted of:

1. Match metabolic features detected in the 2 analytical blocks, constructing a reference database. The reference database is built by matching features from the two blocks if their m/z difference is less than 5 ppm and retention time difference is less than 10 seconds.
2. Remove features with a QC Median peak area (MPA) tolerance (ζ) higher than 4, using the formula:

$$\zeta_i = \left| \frac{(MPA_{b,i} - MPA_{ref,i})}{MPA_{ref,i}} \right|$$

Where *b* is the batch, *i* is the feature, and *ref* is the reference database.

The results of the quality assurance feature matching process are summarised in Table 1. scTAGs used in this thesis are used as an example to show how repeatability is preserved for all molecular classes (Table 2).

Table 1: The total number of features detected in each batch in the two ionization modes, the number of peaks passing the first intra-batch QC filtering and their percentage compared to the total number of features detected, the number of features detected and their percentage compared to the features passing intra-batch QC filtering, the number of features passing the MPA test and their percentage compared to those matched to the reference database.

Batch	No of peaks passing QA	Peaks passing QA %	Unique matches	Unique matches %	Pass MPA test	Pass MPA test %
1 positive mode	7827	77%	1584	93%	1360	86%
2 positive mode	5337	64%	1482	87%	1360	92%
1 negative mode	5197	79%	645	99%	587	91%
2 negative mode	3375	72%	631	97%	587	93%

Table 2: scTAG masses and their corresponding inter-batch and intra-batch CVs. These TAGs are associated with the main fatty acid products from DNL including palmitate, palmitoleic acid, stearic acid and oleic acid. These TAGs have been shown to increase when DNL is raised in humans (9, 19 & 20). Samples across this study were run in two batches of roughly equal size. The technical replicates were pool samples from batch 1, the inter-batch CV was calculated as STDEV (all pools for batch X)/Mean of all pools across batch X *100%. The inter-batch CV is calculated across the two batches.

Triglyceride	***Product ion ([M+NH4]1+)***	***Intra-batch RSD/CV (%) Batch 1; Batch2***	***Inter-batch RSD/CV (%)***
TAG 46:2	*792.7076*	*9.65; 6.31*	*23.6*
TAG 46:1	*794.7232*	*13.1; 11.4*	*19.2*
TAG 46:0	*796.7389*	*12.7; 14.5*	*15.5*
TAG 48:2	*820.7389*	*12.0; 7.80*	*26.5*
TAG 48:1	*822.7545*	*9.68; 9.55*	*15.9*
TAG 48:0	*824.7702*	*34.3; 12.0*	*33.8*
TAG 49:2	*834.7545*	*9.38; 9.25*	*22.1*
TAG 49:1	*836.7702*	*12.7; 12.6*	*31.3*
TAG 49:0	*838.7858*	*5.48; 12.3*	*34.0*

Appendix IV

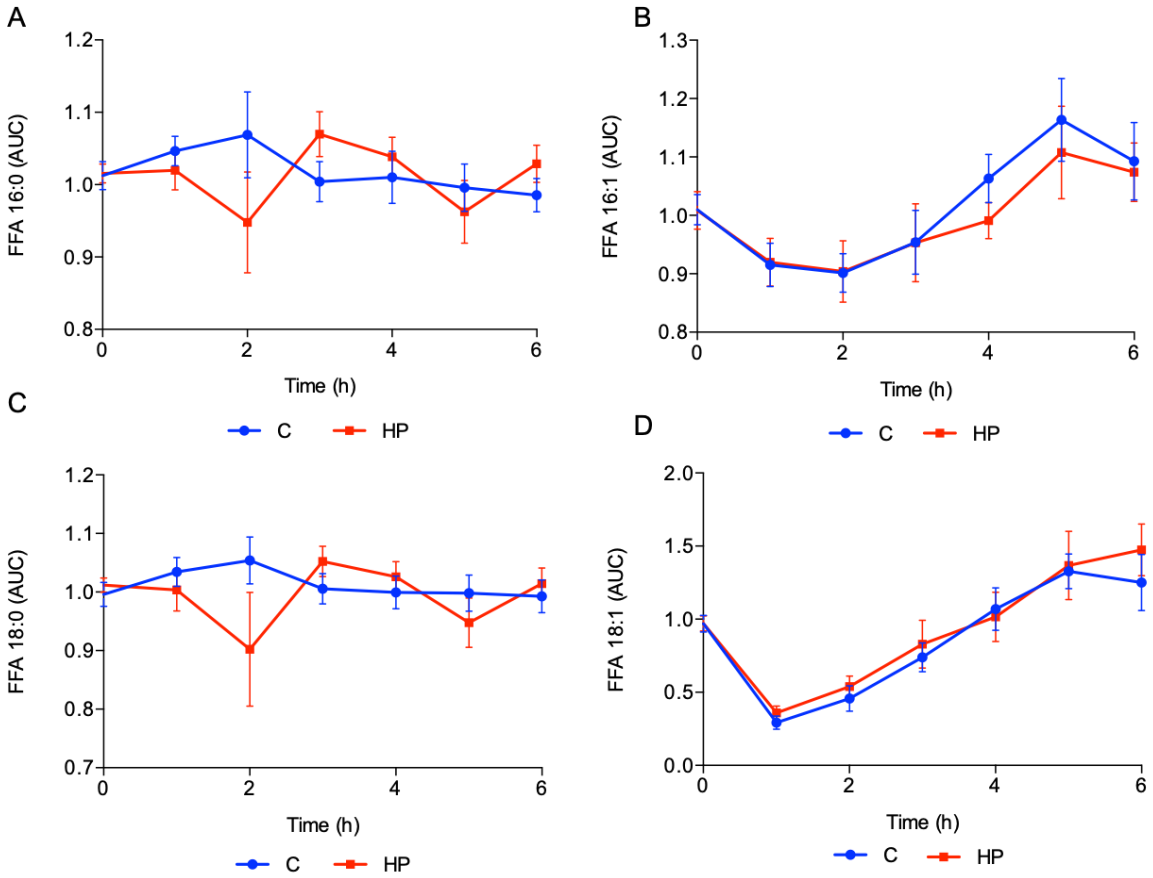

Figure 1. Plasma FFA content is not different between C and HP. (A) FFA 16:0 levels measured by LC-MS over 6 hours. **(B)** FFA 18:0 levels measured by LC-MS over 6 hours. **(C)** FFA 16:1 levels measured by LC-MS over 6 hours. **(D)** FFA 18:1 levels measured by LC-MS over 6 hours. Data are presented as mean ± SEM and analysed by two-way repeated measures ANOVA with post-hoc Sidak's multiple comparisons test; * = $p \leq 0.05$, n = 9/group.

Appendix V

Flow diagram of the thought processes and hypotheses of the thesis.